The roles of parent material, climate, and geomorphology in soil organic carbon response to short-term climate change in moist boreal forests

By

Mackenzie E. Patrick

A thesis submitted to the school of
graduate studies in partial fulfillment of
the requirements for the degree of

Doctor of Philosophy

Department of Earth Sciences

Memorial University of Newfoundland and Labrador

November 2023

St. John’s, Newfoundland and Labrador, Canada

Abstract

Boreal forests store significant soil organic carbon (SOC) where increasing temperature and extreme precipitation are expected with climate change. Yet, the impact on subsoil SOC is unclear. Dissolved organic matter (DOM) facilitates Al weathering to precipitate Al organo-metal complexes (Al_{OMC}) that stabilize mineral horizon SOC. An enhanced DOM input is expected with climate change, however, a high water-flux associated with extreme precipitation may limit Al_{OMC} precipitation. This thesis investigates the roles of parent material composition, climate and geomorphology in boreal SOC dynamics using climate and hillslope transects to enhance: (1) subsoil SOC predictions and (2) its response to short-term climate change.

A SOC content predictive model was developed using soils from four climate regions with varying parent material. Unsurprisingly, Al_{OMC} content was the main predictor, with greater SOC in regions with high Al availability. Further interactions with depth-dependent factors, C saturation of Al_{OMC} ($C:Al_{OMC}$) and their proportion of SOC, suggested infiltration depth is key within a region. As such, greater SOC is supported on gentle slopes via deeper infiltration.

Controls on SOC response to extreme precipitation were evaluated experimentally with increasing soil moisture to emulate events occurring on dry summer soils to wet late autumn soils. Antecedent soil moisture and $C:Al_{OMC}$ controlled SOC response under high water flux regardless of parent material or climate. I present a simple predictive model demonstrating shallow SOC loss but deeper storage potential, with greater potential on gentle slopes. Further, enhanced loss from dry soils indicates late summer SOC is most vulnerable to loss (~1‰). Therefore, event timing and infiltration depth are key for SOC response to extreme precipitation. Weathering profiles (mass transfer coefficients), Al_{OMC} and SOC distributions suggest that Al availability sets the water

flux threshold for Al_{OMC} precipitation. Extreme events surpass this threshold, limiting new SOC storage. Enhanced SOC storage is expected with an increasing DOM flux with climate change in Al-rich regions supporting higher Al_{OMC} precipitation thresholds, while Al-poor regions may experience SOC loss. These results find regional parent material overrides climate controls on boreal SOC, and this will inform carbon feedbacks to improve Earth Systems models.

General Summary

Boreal regions hold almost a third of carbon stored in forest soils globally where we expect significant increases in temperature and extreme precipitation. However, our ability to predict the carbon content of deep soils and it's response to climate change is poor. Carbon dissolved in soil water can become sequestered in the soil via interact with minerals. I investigated soils from across a moist boreal forest region spanning a temperature and precipitation range in line with predicted changes for the region in the next several decades. Using soil observations and experiments from across study sites I assessed: (1) the roles of regional rock mineral composition, climate, and soil water movement in stabilization of carbon in boreal forest mineral soils, and (2) how these stores of soil carbon may respond to an enhanced supply of dissolved carbon, soil drying, and the extreme precipitation events expected with climate change.

Modeling of soil carbon content found that mineral contributions controlled regional differences, but water infiltration depth-controlled variation within a region. Greater carbon content occurs on gentle slopes where deeper infiltration is exhibited. Experimental measurements of soil carbon response to extreme precipitation demonstrated that shallow soils lose carbon while deeper soils have potential to store carbon. Further, shallow carbon loss is greatest in dry soils and therefore carbon is most vulnerable during events on dry late summer soils. Therefore, event timing and water infiltration depths are key for predicting soil carbon response to extreme precipitation. Yet, the rock composition controlled the maximum size event to which carbon storage can occur via stabilization with minerals. As such, regions rich in reactive minerals should exhibit enhanced carbon storage with short-term climate change as the dissolved carbon supply increases. However, soils with poor mineral sources may exhibit carbon losses as extreme

precipitation events remove more than is stabilized. These results indicate that regional geology overrides climate controls on soil carbon content and storage with climate change, while water infiltration and event timing are key for extreme precipitation events. The insights and models presented here will aid in carbon accounting and mitigation efforts.

Acknowledgements

First and foremost, I want to express my sincere gratitude to my supervisor, Dr. Susan Ziegler. Thank you for your unwavering support, trust and understanding. I have learned much more than just science from you, and I hope that someday I am given the opportunity to show the same kindness to others that you have shown me. I want to thank my supervisory committee members, Kate Edwards, Penny Morrill, and Karen Prestegaard, for your knowledge, support, realism, and guidance. You have all went above and beyond what I had ever imagined a committee was for.

To the BBERG members, officemates, and Earth Science students who I have learned so much from over the years, thank you for the laughs and kind words. Thank you, Christian Gaviria, for assistance with the final formatting of this dissertation. To all the brilliant scientists I have collaborated with, thank you for sharing your time and knowledge with me.

To my family: thank you for always believing in me, watching Allie and sending food during those last grueling months of little sleep. Thank you, Angela Norman, for being the first audience for all my talks and cheering me on, Shane Hickey, for understanding me like no other and supporting me during those late nights, and Ryan Stanley, for checking up on me constantly. Thank you for all the unexpected support from so many people along the way.

I also would never have made it through this thesis without the classical album "Recomposed by Max Richter: Vivaldi, the Four Seasons", which I have listened to thousands of times. Max Richter, thank for this exceptional album that has helped me focus and think outside the box to produce the best ideas in this thesis.

Thank you to the Canada Research Chairs and National Sciences and Engineering Research Council of Canada Discovery Grant (DG#2018-05383), Strategic Partnerships Grants Program (SPG#479224) and Canadian Graduate Scholarship (Doctoral) for funding to make thus research possible.

Finally, thank you to the reviewers of my thesis for the kind and helpful reviews: Julia Perdrial, Shawn Leroux, and Chad Cuss.

Table of Contents

List of Tables

List of Figures

Appendix

Chapter 1: Introduction

1.1 Scientific Context

1.1.1 Climate change and the carbon cycle

Climate change is one of the greatest crises of our time. Increases in the intensity and frequency of extreme weather events such as drought, heat waves, and atmospheric rivers threaten our food supply, shelter, and livelihood. Similarly, wildlife must adapt to rapid shifts in ecosystems, and some are at risk of complete habitat loss.

Humans have been releasing CO_2 more rapidly than occurs naturally since the industrial era, mainly through fossil fuel burning and land change. This has increased atmospheric CO_2 from 280 ppmv in 1850 to 424 ppmv as of May 2023 (National Oceanic and Atmospheric Administration, Mauna Loa Observatory, Hawaii). As a result, Earth has experienced an increase in global mean air surface temperature of ~1.1 °C in the same time period, with greater decadal increases since the 1970s (IPCC, 2021). Further, this has intensified the hydrological cycle. Yet, the impact can be even further reaching as a result of feedbacks within the C cycle.

The flux of CO_2 to the atmosphere is one component of the global C cycle. Here, C fluxes among a network of large C reservoirs at various rates from slow geological processes to faster biological mechanisms of C transfer. A shift in one flux induces changes elsewhere as C is retained within the system. Such is the case for anthropogenic climate

change which can impact a wide range of C mechanisms to further increase or decrease atmospheric CO_2 through positive or negative feedback loops, respectively. Therefore, the implications of such impacts on the C cycle beyond direct anthropogenic emissions must also be considered to fully understand the effects of climate change and make predictions of future climate. One such aspect of the C cycle is soil organic carbon (SOC) loss from soils via enhancement of the dissolved organic carbon (DOC) terrestrial-to-aquatic flux (Drake et al., 2018; Tank et al., 2018; Webb et al., 2019).

River "browning" has been recognized to be increasing globally (i.e., increasing river DOC concentration) and is attributed to SOC loss (Freeman et al., 2001; Roulet and Moore, 2006; Drake et al., 2018; Finstad et al., 2016; Huntington et al., 2016). This mobile and reactive form of C is more vulnerable to CO_2 mineralization than C that is stabilized within soils. Since globally, soils store about three times more C than the atmosphere (Schmidt et al., 2011), this potential positive feedback risks further enhancing atmospheric CO_2 and exacerbating climate change. Understanding the mechanisms of SOC stability and how these may be impacted by climate change are key to reconciling carbon balance.

1.1.2 Mechanisms of soil organic carbon storage

Soils are at the interface of the critical zone, integrating chemical, physical and biological processes. The five factors of soil formation presented by Jenny (1941) more than 80 years ago still stand true: climate, parent material, time, topography, and organisms. These cover a range of spatial and time scales impacting the relative roles of each factor in the development of the different soil types with time and horizons with depth. Interactions

among these factors further contribute to the balance of inputs and losses determining SOC content.

Litterfall inputs support organic horizon SOC via organic matter which progresses through stages of increasing decomposition with depth. In the hot and humid tropics, organic matter decomposition is rapid, and more C is held in the vegetation, while slower overturn in colder high latitude biomes promotes greater SOC accumulation (Scharlemann et al 2014).

Organic matter is transported vertically with the soil solution as dissolved organic matter (DOM). In the underlying mineral horizon, microbial mineralization of DOM to CO_2 is slowed by a variety of mineral-organic associations with soil weathering products or by physical occlusion such as within aggregates or pore space (Baldock and Skjemstad, 2000; Eusterhues et al., 2003; Feng et al., 2005; Hassink, 1997; Kleber et al., 2015). Hydrophobic and highly aromatic DOM offer greater adsorption potential than hydrophilic compounds (Kaiser and Kalbitz, 2012). Therefore, hydrophilic compounds are more mobile and easily distributed with soil solution, while hydrophobic and highly aromatic DOM have longer retention times (Shen et al., 2015). While the proportion of clay-sized content had been considered a main control on SOC content stabilization because of the large surface area, recent work suggests that the mineral composition is of greater importance (Rasmussen et al., 2018).

Water plays a key role in weathering, soil development and SOC storage. Soils progress through defined weathering stages, starting from primary minerals which weather

to organo-metal complexes (OMCs) and poorly crystalline metal oxyhydroxides, and further, to more stable clays and crystalline metal oxyhydroxides (Torn et al., 1997). Storage of SOC is greatest in young- to middle-aged soils but is most stable with crystalline metal weathering products in older soils. Global-scale water balance determines the proportion of SOC stored in total metal weathering products which increases in water replete biomes to a maximum threshold of ~65% (Kramer and Chadwick, 2018).

The metals of weathering products are supplied by the underlying geological parent material upon which the soils develop. At the continental scale, parent material and climate govern their formation through weathering rates. As such, SOC is greatest in "enhanced weathering zones" where young parent material with significant weatherable primary minerals and excess water occur together (Slessarev et al., 2022).

Soil organic carbon can also become destabilized, thereby becoming vulnerable to microbial decomposition. This may occur from disruption of the structures physically occluding SOC from degradation via bioturbation or break down of aggregates during freeze-thaw cycles. Changes in the soil solution such as shifts in pH or redox potential can impact the solubility of minerally-associated organic matter and changes in surface charges can lead to organic matter desorption (Bailey et al., 2019).

At the global scale, soils are expected to largely exhibit SOC reductions with climate change (Wang et al., 2022). This study found that the most important controls of SOC loss in response to warming at the global scale are current SOC content and mean annual precipitation. They suggest loss should be greater in shallow soils and high-latitude

systems, with the greatest SOC reductions expected in boreal forests (Wang et al., 2022). The contrasting role of water availability in supporting greater SOC content via enhanced weathering but also driving SOC loss with climate change suggests a closer look at its contribution to the mechanisms and timescales of storage and loss, particularly in vulnerable boreal forests. Therefore, water availability may support greater SOC stabilization via enhanced weathering yet is also a driver of SOC loss with climate change. This suggests a closer look at the role of water availability in SOC storage and loss mechanisms, such as weathering, particularly in vulnerable boreal forests.

1.1.3 Boreal forests

Boreal soil organic carbon dynamics are linked with podzolization

Boreal forest soils make up about 30% of the global forest SOC stock where approximately half is estimated to reside in the subsoil (Pan et al., 2011; Scharlemann et al., 2014). Mean annual temperature in boreal regions is increasing twice as fast as the global average, thereby enhancing evapotranspiration and soil drying (IPCC 2013). These regions are further projected to experience increasing frequency and intensity of extreme precipitation events and shifts in precipitation form and timing (Lee et al. 2021). However, our predictive understanding of this large C reservoir at depth is poor and likely contributes significantly to the large uncertainty in Earth system models of atmosphere-land C exchange (Friedlingstein et al., 2014).

Water replete boreal biomes should fall within the enhanced weathering zone supporting greater SOC as young soils in recently deglaciated regions still contain ample minimally weathered primary minerals (Slessarev et al., 2022). Comparisons of model predictions and measured SOC suggest climate factors are overemphasized in models at the biome scale while geological parent material may be of greater relative importance (Georgiou et al., 2021).

Podzolization links chemical weathering and carbon dynamics in these moist, acidic soils. Organic acids percolate down from the organic horizon as dissolved organic matter (DOM) to facilitate chemical weathering by chelating metals to form dissolved complexes which are transported with the solution (Lundstrom et al., 2000a, 2000b). These dissolved complexes can precipitate as Al or Fe organo-metal complexes (OMCs) to stabilize organic matter as SOC in the underlying mineral horizon via increasing pH and at solution metal to carbon ratios >0.03 (Nierop et al., 2002). Thus, OMCs should be a main control on shallow mineral horizon SOC content in boreal forests. The podzolization process results in the development of the characteristic bleached Ae horizon of podzols where metals are eluviated and the darker Bh illuvial horizon below where OMCs accumulate. These horizons progressively deepen with time via dissolution of formerly precipitated OMCs in low pH soil solutions to transport OMCs vertically (Ferro-Vázquez et al., 2014). Additional SOC can be stabilized within microaggregates as OMCs glue together to occlude OM (Shimada et al., 2020; Wagai et al., 2020).

Spatiotemporal variation in controls on SOC dynamics and potential impact of climate change

At the regional scale, the availability of water, DOM and metals for SOC stabilization via OMC formation is controlled by climate and parent material input. Precipitation intensity controls the soil water residence time for weathering reactions at the event scale. High water-fluxes may limit OMC coprecipitation by reducing the time to reach metal concentrations via weathering. Parent material composition and soil age controls metal availability as only primary minerals are chelated with DOM, therefore older weathered clay-rich soils have limited Al for this reaction despite a high-Al composition (Slessarev et al., 2022). The DOM flux provides the mineral horizon C source and storage mechanism, increasing with annual temperature and snowpack length (Bowering et al., 2022). This flux varies seasonally, with the greatest contributions occurring in autumn and snowmelt, followed by summer, and winter (Bowering et al., 2023). Winter and spring DOM consists of more degraded organic matter relative to the higher molecular weight and C:N source during summer and autumn seasons (Bowering et al., 2023).

At the hillslope scale, spatial variations in hydrological processes and soil properties influence DOM delivery and soil water residence times relevant for OMC formation (Bachmair and Weiler, 2012; Hopp and McDonnell, 2009). The fate of DOM and its contribution to SOC stores is regulated by soil water flow paths, weathering and residence time (Hunter et al., 2023; Tank et al., 2018). The majority exported to rivers is modern, aromatic, and high-molecular weight DOM suggesting loss from shallow flow

paths (Barnes et al., 2018). Activation of preferential flow paths during high-water flux events promotes rapid runoff via shallow lateral flow paths (Anderson et al., 2009; Beiter et al., 2020). Increasing Al concentration as DOM flows laterally downslope during high water flux events suggests the formation of dissolved Al OMC but lack of coprecipitation for SOC storage (Cory et al., 2007, 2006; Löfgren and Cory, 2010). Observations of stream DOM indicate significant runoff from shallow organic and mineral horizons with snow melt (Ågren et al., 2010) and large autumn precipitation events (Roebuck et al. submitted). Yet, others have found vertical infiltration to also be greatest during such events despite the large proportion of runoff (Schaetzl et al. 2015; Schaetzl and Rothstein 2016), providing deeper mineral soils with a C source where less weathered soils should promote storage.

The most abundant OMCs, Al and Fe, may exhibit contrasting spatial distributions with hydrology and soil solution as Fe OMCs are soluble under reducing conditions but Al mobilization is limited to mobilization at low pH (Jansen et al., 2005, 2004, 2003; Nierop et al., 2002). Beyond wetlands, reducing conditions may arise temporarily in seasonally saturated soils when the water table rises for an extended time, in shallower soils during snow melt, or under the snowpack as oxygen is depleted by microbes (Wang and Bettany, 1995; Yin et al., 2019). While the physical breakdown of microaggregates occurs on millennial-scales (Shimada et al., 2020), soils can change rapidly in response to chemical shifts in the system. For example, within the span of just 30 years, podzols have been observed to exhibit very different metal weathering profiles with depth in response to

reduced acid rain input (Armfield et al., 2019). This suggests that weathering and OMCs can respond to external forcings on timescales relevant to short-term climate change.

In boreal regions, climate change will likely result in diminishing spring melt water flux, increasing summer evapotranspiration rates and extent of soil drying, and increasing frequency and precipitation intensity of autumn storms, including formation of atmospheric rivers (Finnis and Daraio 2018; Laudon et al. 2013; Helbig et al. 2020; Hsu and Chen 2020; Wang et al. 2021). Enhanced mobilization of DOM from organic horizons may occur during warmer winters with shorter snowpack seasons, producing higher DOM inputs to the mineral soil in moist boreal forests (Bowering et al. 2022).

Short water residence times associated with high water flux events may limit shallow Al OMC precipitation and SOC storage as metal concentrations conducive to coprecipitation are unlikely to be reached (Nierop et al., 2002). However, deeper infiltration during such events could enhance deep storage. Enhanced extent of soil drying with increasing evapotranspiration could make SOC vulnerable to desorption during dry periods in late summer (Helbig et al., 2020; Wang et al., 2021). Finally, an enhanced DOM flux is also expected with warming in moist boreal forests (Bowering et al., 2022). While this will increase the mineral horizon C input and weathering rates, the potential for storage depends on interactions of factors in OMC coprecipitation. Thus, one of the most important gaps to resolve in our predictive understanding of SOC response to climate change are the relative roles of parent material and short-term climate change on SOC dynamics.

1.2 Objectives, Study Design and Thesis Outline

1.2.1 The gaps in our understanding and relevant spatial scales to evaluate the impact of climate change on boreal forest soil organic carbon

In this thesis, I investigated controls on mineral horizon soil organic carbon (SOC) storage and its response to climate change in wet boreal forests. These soils store significant SOC in regions vulnerable to climate change, but have remained poorly understood, particularly in the subsoil. Large-scale studies have highlighted water availability and weathering links with SOC storage mechanisms and indicate this biome is vulnerable to water balance shifts (Kramer and Chadwick, 2018; Slessarev et al., 2022). This indicates the need for regional scale studies within a biome with a range of parent material compositions to elucidate the relative roles of parent material and short-term climate change impacts on SOC. Further, studies evaluating variation with depth and slope are needed to examine the potential impact of climate change on infiltration depth and other hydrological processes with space. I considered factors involved in weathering and SOC dynamics within the wet boreal biome at the regional, hillslope and depth scales.

Regional studies within a biome are best suited to evaluate the relative roles of parent material and climate on SOC content and its response to climate change for several reasons. (1) This spatial scale can capture variations in regional parent material whose importance was found to be underestimated in within-biome models (Georgiou et al., 2021). (2) It offers better predictability by limiting the range of water availability and vegetation to better focus on the operating mechanisms. (3) Further, regional climate

transect studies within a biome are most relevant for short-term climate change (20–100 years) as shifts in climate can be observed across space without dominant vegetation shifts.

The depth and hillslope scales further evaluated the distribution of water and DOM inputs via geomorphological controls on flow path distribution. Since climate and parent material are constant, it is the spatial variations in hydrology that are of interest, both in the direct mechanisms within the soil water but also in the long-term development of characteristics that also influence SOC content.

1.2.2 Objectives and study design

The broad goal of this thesis was to enhance our predictive understanding of wet boreal forest mineral horizon SOC content and response to projected climate change. This was addressed in four chapters that evaluate the relative roles of factors controlling SOC dynamics. Here, SOC response at event, season, and long-term time scales was investigated via experimental and observational studies. The results were further interpreted within the context of expected climate change (Table 1.1).

It is important to note that the predictors may operate at very different time scales than that of the SOC response timescale of interest. For example, at the event scale many solid soil characteristics like Al OMC content can be considered fixed as they are a result of many years of accumulation. However, adsorption of DOC to Al OMC surfaces, or coprecipitation of Al OMC from the soil solution during an event, are measurable at the event scale.

Table 1.1 Soil organic carbon (SOC) response method of evaluation.

Study design showing approach to evaluate soil organic carbon (SOC) response to short-term climate change for a range of spatial scales (Chapters 2–5). Bold chapters indicate where SOC controls or response were directly evaluated, plain text indicates where these were interpreted from observations made across additional time and spatial scales. For the purposes of this research long-term refers to 100–1000s of years and short-term climate change is 20–100 yrs. Dissolved organic carbon (DOC).

SOC variable	Timescale	Approach	Spatial scale (Chapter)		
			Depth	Hillslope	Regional
SOC content	100-1000s yrs	Observational/ Statistic Analysis: Controls on SOC content	**5**	**3**	**2 + 5**
Short-term climate change response	20-100 yrs	Interpreted via SOC content and precipitation event response with anticipated climate change impacts on hydrology	4 + 5	3	4 + 5
Seasonal Response	Months	Experimental: Impact of soil moisture and soil solution composition on DOC uptake or loss	**3** + 4	**3**	**4**
Extreme event response	Hours - Day(s)	Experimental: Controls on DOC uptake/loss	**3** + 4	**3**	**4**

Soil organic carbon content is the net result of stabilization and loss mechanisms over 100–1000s of years leading to accumulation. This history is recorded in soil characteristics. Evaluating controls on SOC content provides insights about the mechanisms that dominated their stabilization on average over many events. The goal of Chapter 2 was to identify these dominant control(s) to use in the design of the following chapters. Specifically, I was interested in determining if Fe or Al OMCs exhibited greater control on SOC content as different soil conditions govern their stability. Further, I aimed to determine if there were further interactions of OMCs with other soil characteristics or ecosystem parameters that may be related to climate or vulnerable to climate change. To

this end, I used the information theoretic approach to rank models rather than p-values with hypothesis testing to identify the best model from many similar models.

The results of Chapter 2 indicated that Al OMCs were the dominant control on SOC in shallow soils, with negligible influence from climate or other physicochemical properties. From here, Chapters 3–5 focused on the role of Al OMCs in SOC dynamics. Each chapter employs a different spatial scale to evaluate specific roles of climate, geological parent material, or geomorphology. Parent material and climate contributions to Al OMCs dynamics were evaluated at the regional scale via a climate transect which trades space for time to interpret short-term climate change. The role of hydrology in the distribution of water and thus DOM via geomorphological controls on flow paths was considered at depth and hillslope scales. The objectives of each chapter are presented in Table 1.2 and discussed below.

Climate change will likely subject boreal soils to a range of new conditions including enhanced summer drying, extreme precipitation, increasing DOM flux, and a reduction in the volume of water during the spring melt. The response of SOC to events with such conditions was evaluated experimentally in Chapters 3 and 4 by manipulating event factors in soils from a range of spatial locations and soil characteristics. The main objectives of these experiments were to identify controls on SOC response to high precipitation events and the impact of antecedent dry conditions or DOM concentration which is indicative of event timing. The hillslope and regional scales were further used (Chapters 3 and 4, respectively) to evaluate spatial variations in the response to these events and in the trajectory of SOC change with climate change.

Table 1.2 Chapter spatial scales and research goals.

Objectives of each chapter with spatiotemporal scales involved in evaluation of soil organic carbon (SOC) response to climate change (CC), and including role of organometal complexes OMCs), dissolved organic matter (DOM) flux or concentration, and parent material (PM).

Ch.	Spatial scale	SOC Timescale	Research Question/ Goals
2	Regional + Shallow	Long-term	What are the main controls on SOC content that direct next steps including relative role of Fe vs Al OMCs? Any interactions with other soil characteristics or ecosystem parameters?
3	Hillslope + Depth	Event	Controls on SOC response to high water flux: soil characteristics or space in hillslope?
		Season	Soil moisture and DOM characteristics impact on SOC response to high water flux?
		Long-term	What does distribution of SOC tell us about the impact of hillslope hydrology and slope on SOC content?
		Short-term CC	Does direction of change associated with the large precipitation events predicted with CC vary spatially?
4	Regional Shallow	Event	Does SOC response to high water flux vary with region?
	Depth	Event + season	How does infiltration depth and event timing impact SOC response to high water flux?
5	Regional + Depth	Long-term	What are relative roles of climate, PM and depth in soil characteristics on SOC content and the stabilization of SOC via Al OMC precipitation?
		Event + Short -term CC	What is the impact of the large precipitation events predicted with CC on these mechanisms controlling SOC?

In Chapter 5, I developed a multiple linear regression model to predict SOC content and uncovered the relative roles of parent material, climate and depth in SOC dynamics and the formation of important predictive soil characteristics. Relationships among Al, DOM and water availability to Al OMC coprecipitation were investigated via SOC and weathering depth profiles, weathering rates, carbon ages, organic matter decomposition and observed current Al OMC content relative to regional inputs. The response of SOC to climate change was further considered based on anticipated changes in the contributions of these factors to OMC coprecipitation in light of threshold controls set by parent material weathering.

1.2.3 Study area

The Newfoundland and Labrador Boreal Ecosystem Latitudinal Transect (NL-BELT) is a climate transect spanning 5.5º latitude along the eastern coast of Labrador and western coast of the island of Newfoundland. The transect spans a 5 ºC gradient in mean annual temperature and a range of 1073 to 1505 mm in mean annual precipitation (Environment and Climate Change Canada 30-year normal for 1980-2010). The NL-BELT exhibits a water availability (mean annual precipitation less potential evapotranspiration) of 641–832 mm, placing the transect in the zone of high sensitivity to changing moisture at the global scale. This further suggests that approximately 60% of SOC in the mineral horizon occurs in total metal weathering products (Kramer and Chadwick, 2018).

Regional scale work within this transect focuses on three of the four established regions, Eagle River (North; 53° latitude), Salmon River (Mid; 51° latitude) and Grand Codroy (South; 48° latitude) (Figure 1.1). Within each region are three established forest stand sites approximately 80m x 80m, within which three soil sampling plots (10m diameter) were randomly chosen per site (Table 1.3). All sites are dominated by mature stands of balsam fir (*Abies balsamea*), with mesic, well-drained humo-ferric podzolic soils (Canadian System of Soil Classification). Organic horizon SOC increases with warming across the transect, as do litterfall inputs and losses via soil respiration and DOC flux (Ziegler et al., 2017; Bowering et al., 2022).

Soils are of young to intermediate maturity, formed in a post-glacial area from till after glacial retreat 10 – 12.5 thousand years ago (Brookes, 1977; Ricketts and Vatcher, 1996; Putt et al. 2010; King, 1985). The till varies among regions with parent material in the South mainly composed of Al-poor quartz-rich sedimentary till, while the North region offers greater Al-availability via granitoids and mafic amphibolites. The Mid region is highly variable, composed of fresh and weathered granite, slightly-to-moderately weathered sandstone, and fresh limestone, shale and phyllite (Ricketts and Vatcher, 1996).

The Pynn's Brook Experimental Watershed Area (PBEWA) is located within the Humber River region in western Newfoundland and Labrador (Canada). This area experiences a mean annual temperature of 3.6°C and receives approximately 1095mm of precipitation annually (Environment Canada Climate Normals, Deer Lake Airport 1981–2010).

The PBEWA study site is divided into eight roughly 50 × 50 m plots dominated by black spruce (*Picea mariana*) and humo-ferric podzolic soils (Moroni et al. 2009). In this study, two neighboring plots oriented parallel to the slope are employed. The upslope plot is gently sloped, well-drained, and exhibits shallow SOC enrichment, while the footslope is moderately sloped and situated just upslope from wetlands. The study region was completely glaciated during the Quaternary, with ice retreating at ~13 thousand and soils started pedogenesis from fresh glacial till deposits of granite and sedimentary rocks (Batterson & Catto 2001).

Table 1.3. Region and site information.

Region	Name	Site	Site ID	Latitude	Longitude	Elevation (m)
North	Eagle River	Muddy Pond	ER-MP	53.5503	-56.9869	145
		Sheppard's Ridge	ER-SR	53.5568	-56.934	170
		Harry's Pond	ER-HP	53.5868	-56.8891	136
Mid	Salmon River	Hare Bay	SR-HB	51.2559	-56.1369	31
		Tuckamore	SR-TM	51.1641	-56.0042	16
		Catch-a-Feeder	SR-CF	51.0892	-56.2042	38
South	Grand Codroy	O'Regan's	GC-OR	47.8934	-59.1745	100
		Maple Ridge	GC-MR	48.0078	-58.9207	165
		Slug Hill	GC-SH	48.0107	-58.9045	215

Chapters 2 and 4 employed all three regions of the NL-BELT, while Chapter 5 did not include the mid-latitude region as the parent material contributions were too variable across the region. A large range in SOC content and associated soil characteristics was captured in the mid-region, which was attributed, at least in part, to the diverse parent material contributing to soil development. However, parent material samples could not be collected and associated with individual soil profiles. Therefore, only end-member regions were used in Chapter 5 to evaluate the role of parent material as here it was considered relatively consistent across the region. The PBEWA was employed to evaluate hillslope scale controls in Chapter 3, and also in the development of the predictive SOC model in Chapter 5 to create a more robust model.

1.2.4 Thesis outline

This thesis is presented in manuscript format. It is comprised of six chapters. Chapter 1 introduces the scientific context surrounding climate change, weathering and SOC storage and the gaps in our understanding in vulnerable boreal forests. The objectives and study design of this research are also presented in this chapter.

Chapters 2–5 are stand-alone manuscripts that are published or are intended to be submitted for publication after editing. Chapter 2 is published in Geoderma (2022) and differs only in format and minor edits from the publication. Chapters 3–5 will be revised further prior to publication. Each chapter includes an introduction, methods, results, discussion and conclusions section with the exception of Chapter 4 for which the results

and discussion sections have been combined. Finally, Chapter 6 synthesizes the overall findings and conclusions.

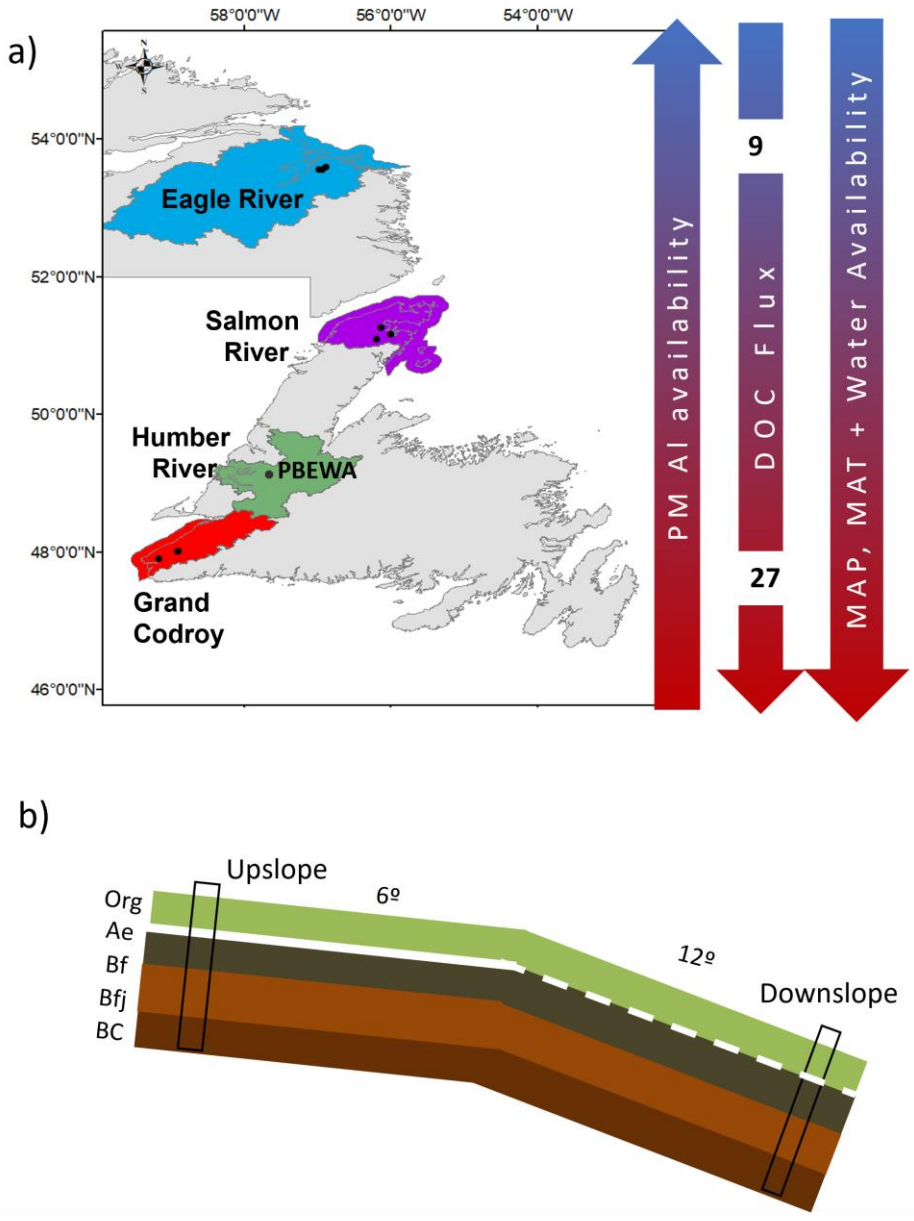

Figure 1.1.

a) Regions of study with site locations within the Newfoundland and Labrador Boreal Ecosystem Latitudinal Transect (NL-BELT). Eagle River (North region), Salmon River (Mid region), and Grand Codroy (South region) are part of the regional scale transect study, and the (b) Pynn's Brook Experimental Watershed Area

(PBEWA) within the Humber River region is employed for hillslope scale studies. The trajectories of mean annual temperature (MAT), mean annual precipitation (MAP), and the soil dissolved organic carbon (DOC) flux across the NL-BELT regions is provided on the right side.b) An illustration depicting major features of the boreal forest hillslope located in PBEWA showing horizons and pit locations

1.3 References

Ågren, A., Haei, M., Köhler, S.J., Bishop, K., Laudon, H., 2010. Regulation of stream water dissolved organic carbon (DOC) concentrations during snowmelt, The role of discharge, winter climate and memory effects. Biogeosciences 7, 2901–2913. https://doi.org/10.5194/bg-7-2901-2010

Anderson, A.E., Weiler, M., Alila, Y., Hudson, R.O., 2009. Dye staining and excavation of a lateral preferential flow network. Hydrol Earth Syst Sci 13. https://doi.org/10.5194/hess-13-935-2009

Armfield, J.R., Perdrial, J.N., Gagnon, A., Ehrenkranz, J., Perdrial, N., Cincotta, M., Ross, D., Shanley, J.B., Underwood, K.L., Ryan, P., 2019. Does stream water composition at sleepers river in vermont reflect dynamic changes in soils during recovery from acidification? Front Earth Sci (Lausanne) 6. https://doi.org/10.3389/feart.2018.00246

Bachmair, S., Weiler, M., 2012. Hillslope characteristics as controls of subsurface flow variability. Hydrol Earth Syst Sci 16, 3699–3715. https://doi.org/10.5194/hess-16-3699-2012

Bailey, V.L., Pries, C.H., Lajtha, K., 2019. What do we know about soil carbon destabilization? Environmental Research Letters. https://doi.org/10.1088/1748-9326/ab2c11

Baldock, J.A., Skjemstad, J.O., 2000. Role of the soil matrix and minerals in protecting natural organic materials against biological attack. Org Geochem 31, 697–710. https://doi.org/10.1016/S0146-6380(00)00049-8

Batterson, M.J., Catto, N.R., 2001. Topographically-controlled deglacial history of the Humber River basin, western Newfoundland. Geographie Physique et Quaternaire 55, 213–228, https://doi.org/10.7202/006851ar

Barnes, R.T., Butman, D.E., Wilson, H.F. and Raymond, P.A., 2018. Riverine export of aged carbon driven by flow path depth and residence time. En Sci & Tech, *52*(3), pp.1028-1035

Beiter, D., Weiler, M., Blume, T., 2020. Characterising hillslope–stream connectivity with a joint event analysis of stream and groundwater levels. Hydrol Earth Syst Sci 24, 5713–5744, https://doi.org/10.5194/hess-24-5713-2020

Bowering, K.L., Edwards, K.A., Wiersma, Y.F., Billings, S.A., Warren, J., Skinner, A., Ziegler, S.E., 2022. Dissolved Organic Carbon Mobilization Across a Climate Transect of Mesic Boreal Forests Is Explained by Air Temperature and Snowpack Duration, https://doi.org/10.1007/s10021-022-0074

Bowering, K. L., Edwards, K. A., and Ziegler, S. E.2023. Seasonal controls override forest harvesting effects on the composition of dissolved organic matter mobilized from boreal forest soil organic horizons, Biogeosciences, 20, 2189–2206, https://doi.org/10.5194/bg-20-2189-2023

Climate Change 2021: The Physical Science Basis. Contribution of Working Group I to the Sixth Assessment Report of the Intergovernmental Panel on Climate Change [Canadell, J.G., P.M.S. Monteiro, M.H. Costa, L. Cotrim da Cunha, P.M. Cox, A.V. Eliseev, S. Henson, M. Ishii, S. Jaccard, C. Koven, A. Lohila, P.K. Patra, S. Piao, J. Rogelj, S. Syampungani, S. Zaehle, and K. Zickfeld, 2021: Global Carbon and other Biogeochemical Cycles and Feedbacks. In Climate Change 2021: The Physical Science Basis. Contribution of Working Group I to the Sixth Assessment Report of the Intergovernmental Panel on Climate Change [Masson-Delmotte, V., P. Zhai, A. Pirani, S.L. Connors, C. Péan, S. Berger, N. Caud, Y. Chen, L. Goldfarb, M.I. Gomis, M. Huang, K. Leitzell, E. Lonnoy, J.B.R. Matthews, T.K. Maycock, T. Waterfield, O. Yelekçi, R. Yu, and B. Zhou (eds.)]. Cambridge University Press, Cambridge, United Kingdom and New York, NY, USA, pp. 673–816, https://doi.org/10.1017/9781009157896.007

Cory, N., Buffam, I., Laudon, H., Köhler, S., Bishop, K., 2006. Landscape control of stream water aluminum in a boreal catchment during spring flood. Environ Sci Technol 40, 3494–3500, https://doi.org/10.1021/es0523183

Cory, N., Laudon, H., Köhler, S., Seibert, J., Bishop, K., 2007. Evolution of soil solution aluminum during transport along a forested boreal hillslope. J Geophys Res Biogeosci 112. https://doi.org/10.1029/2006JG000387

Cotrufo, M.F., Ranalli, M.G., Haddix, M.L., Six, J., Lugato, E., 2019. Soil carbon storage informed by particulate and mineral-associated organic matter. Nat Geosci 12, 989–994. https://doi.org/10.1038/s41561-019-0484-6

Drake, T.W., Raymond, P.A., Spencer, R.G.M., 2018. Terrestrial carbon inputs to inland waters: A current synthesis of estimates and uncertainty. Limnol Oceanogr Lett. https://doi.org/10.1002/lol2.10055

Eusterhues, K., Rumpel, C., Kleber, M., Kögel-Knabner, I., 2003. Stabilisation of soil organic matter by interactions with minerals as revealed by mineral dissolution and oxidative degradation. Org Geochem 34, 1591–1600, https://doi.org/10.1016/j.orggeochem.2003.08.007

Feng, X., Simpson, A.J., Simpson, M.J., 2005. Chemical and mineralogical controls on humic acid sorption to clay mineral surfaces. Org Geochem 36, 1553–1566, https://doi.org/10.1016/j.orggeochem.2005.06.008

Ferro-Vázquez, C., Nóvoa-Muñoz, J.C., Costa-Casais, M., Klaminder, J., Martínez-Cortizas, A., 2014. Metal and organic matter immobilization in temperate podzols: A high resolution study. Geoderma 217–218, 225–234, https://doi.org/10.1016/j.geoderma.2013.10.006

Finnis J, and Daraio, J, (2018) Projected Impacts of Climate Change for the Province of Newfoundland & Labrador: 2018 Update. Memorial University of Newfoundland, St. John's, NL.

Finstad, A.G., Andersen, T., Larsen, S., Tominaga, K., Blumentrath, S., De Wit, H.A., Tømmervik, H., Hessen, D.O., 2016. From greening to browning: Catchment vegetation development and reduced S-deposition promote organic carbon load on decadal time scales in Nordic lakes. Sci Rep 6. https://doi.org/10.1038/srep31944

Freeman, C., Evans, C. D., Monteith, D. T., Reynolds, B., & Fenner, N., 2001. Export of organic carbon from peat soils. Nature, 412(6849), 785-785.

Friedlingstein, P., Meinshausen, M., Arora, V.K., Jones, C.D., Anav, A., Liddicoat, S.K., Knutti, R., 2014. Uncertainties in CMIP5 climate projections due to carbon cycle feedbacks. J Clim 27, 511–526. https://doi.org/10.1175/JCLI-D-12-00579.1

Georgiou, K., Malhotra, A., Wieder, W.R., Ennis, J.H., Hartman, M.D., Sulman, B.N., Berhe, A.A., Grandy, A.S., Kyker-Snowman, E., Lajtha, K., Moore, J.A.M., Pierson, D., Jackson, R.B., 2021. Divergent controls of soil organic carbon between observations and process-based models. Biogeochemistry 156, 5–17. https://doi.org/10.1007/s10533-021-00819-2

Gimeno, L., Nieto, R., Vázquez, M., Lavers, D.A., 2014. Atmospheric rivers: A mini-review. Front Earth Sci (Lausanne). https://doi.org/10.3389/feart.2014.00002

Hassink, J., 1997. The capacity of soils to preserve organic C and N by their association with clay and silt particles, Plant and Soil. Kluwer Academic Publishers.

Helbig, M., Waddington, J.M., Alekseychik, P., Amiro, B.D., Aurela, M., Barr, A.G., Black, T.A., Blanken, P.D., Carey, S.K., Chen, J., Chi, J., Desai, A.R., Dunn, A., Euskirchen, E.S., Flanagan, L.B., Forbrich, I., Friborg, T., Grelle, A., Harder, S., Heliasz, M., Humphreys, E.R., Ikawa, H., Isabelle, P.E., Iwata, H., Jassal, R., Korkiakoski, M., Kurbatova, J., Kutzbach, L., Lindroth, A., Löfvenius, M.O., Lohila, A., Mammarella, I., Marsh, P., Maximov, T., Melton, J.R., Moore, P.A., Nadeau, D.F., Nicholls, E.M., Nilsson, M.B., Ohta, T., Peichl, M., Petrone, R.M., Petrov, R., Prokushkin, A., Quinton, W.L., Reed, D.E., Roulet, N.T., Runkle, B.R.K., Sonnentag, O., Strachan, I.B., Taillardat, P., Tuittila, E.S., Tuovinen, J.P., Turner, J., Ueyama, M., Varlagin, A., Wilmking, M., Wofsy, S.C., Zyrianov, V., 2020. Increasing contribution of peatlands to boreal evapotranspiration in a warming climate. Nat Clim Chang 10. https://doi.org/10.1038/s41558-020-0763-7

Holz, M., Augustin, J., 2021. Erosion effects on soil carbon and nitrogen dynamics on cultivated slopes: A meta-analysis. Geoderma 397. https://doi.org/10.1016/j.geoderma.2021.115045

Hopp, L., McDonnell, J.J., 2009. Connectivity at the hillslope scale: Identifying interactions between storm size, bedrock permeability, slope angle and soil depth. J Hydrol (Amst) 376. https://doi.org/10.1016/j.jhydrol.2009.07.047

Hsu, H.-H., Chen, Y.-T., 2020. Simulation and Projection of Circulations Associated with Atmospheric Rivers along the North American Northeast Coast. J Clim 33, 5673–5695. https://doi.org/10.1175/jcli-d-19-0104.1

Hu, Y., Berhe, A.A., Fogel, M.L., Heckrath, G.J., Kuhn, N.J., 2016. Transport-distance specific SOC distribution: Does it skew erosion induced C fluxes? Biogeochemistry 128, 339–351. https://doi.org/10.1007/s10533-016-0211-y

Hunter, B.D., Roering, J.J., Almond, P.C., Chadwick, O.A., Polizzotto, M.L., Silva, L.C.R., 2023. Pedogenic pathways and deep weathering controls on soil organic carbon in Pacific Northwest forest soils. Geoderma 436, 116531. https://doi.org/10.1016/j.geoderma.2023.116531

Huntington, T.G., Balch, W.M., Aiken, G.R., Sheffield, J., Luo, L., Roesler, C.S., Camill, P., 2016. Climate change and dissolved organic carbon export to the Gulf of Maine. J Geophys Res Biogeosci 121, 2700–2716. https://doi.org/10.1002/2015JG003314

IPCC, 2021: *Climate Change 2021: The Physical Science Basis. Contribution of Working Group I to the Sixth Assessment Report of the Intergovernmental Panel on Climate Change*[Masson-Delmotte, V., P. Zhai, A. Pirani, S.L. Connors, C. Péan, S. Berger, N. Caud, Y. Chen, L. Goldfarb, M.I. Gomis, M. Huang, K. Leitzell, E. Lonnoy, J.B.R. Matthews, T.K. Maycock, T. Waterfield, O. Yelekçi, R. Yu, and B. Zhou (eds.)]. Cambridge University Press, Cambridge, United Kingdom and New York, NY, USA, In press, doi:10.1017/9781009157896.

Jansen, B., Nierop, K.G.J., Verstraten, J.M., 2005. Mechanisms controlling the mobility of dissolved organic matter, aluminium and iron in podzol B horizons. Eur J Soil Sci 56, 537–550. https://doi.org/10.1111/j.1365-2389.2004.00686.x

Jansen, B., Nierop, K.G.J., Verstraten, J.M., 2004. Mobilization of dissolved organic matter, aluminium and iron in podzol eluvial horizons as affected by formation of metal-organic complexes and interactions with solid soil material. Eur J Soil Sci 55. https://doi.org/10.1111/j.1365-2389.2004.00598.x

Jansen, B., Nierop, K.G.J., Verstraet, J.M., 2003. Mobility of Fe(II), Fe(III) and Al in acidic forest soils mediated by dissolved organic matter: Influence of solution pH and metal/organic carbon ratios, in: Geoderma. Elsevier, pp. 323–340. https://doi.org/10.1016/S0016-7061(02)00368-3

Jenny, H., 1941. Factors of soil formation. 281 pp. *New York, 801*.

Kleber, M., Eusterhues, K., Keiluweit, M., Mikutta, C., Mikutta, R., Nico, P.S., 2015. Mineral-Organic Associations: Formation, Properties, and Relevance in Soil Environments. Advances in Agronomy 130, 1–140. https://doi.org/10.1016/bs.agron.2014.10.005

Kothawala, D.N., Moore, T.R., Hendershot, W.H., 2009. Soil Properties Controlling the Adsorption of Dissolved Organic Carbon to Mineral Soils. Soil Science Society of America Journal 73, 1831–1842. https://doi.org/10.2136/sssaj2008.0254

Kothawala, D.N., Roehm, C., Blodau, C., Moore, T.R., 2012. Selective adsorption of dissolved organic matter to mineral soils. Geoderma 189–190, 334–342. https://doi.org/10.1016/j.geoderma.2012.07.001

Kramer, M.G., Chadwick, O.A., 2018. Climate-driven thresholds in reactive mineral retention of soil carbon at the global scale. Nat Clim Chang 8, 1104–1108. https://doi.org/10.1038/s41558-018-0341-4

Laudon, H., Tetzlaff, D., Soulsby, C., Carey, S., Seibert, J., Buttle, J., Shanley, J., Mcdonnell, J.J., Mcguire, K., 2013. Change in winter climate will affect dissolved organic carbon and water fluxes in mid-to-high latitude catchments. Hydrol Process 27. https://doi.org/10.1002/hyp.9686

Lee, J.-Y., Marotzke, Jochem, Bala, Govindasamy, Milinski, S., Yun, K.-S., Ribes, A., Ruane, A.C., Kumar Kanikicharla Qatar, K., Kattsov, V., Kimoto, M., Marotzke, J, Bala, G, Cao, L., Corti, S., Dunne, J., Engelbrecht, F., Fischer, E., Fyfe, J., Jones, C., Maycock, A., Mutemi, J., Ndiaye, O., Panickal, S., Zhou, T., Pirani, A., Connors, S., Péan, C., Berger, S., Caud, N., Chen, Y., Goldfarb, L., Gomis, M., Huang, M., Leitzell, K., Lonnoy, E., Matthews, J., Maycock, T., Waterfield, T., Yelekçi, O., Yu, R., Zhou, B., n.d. Chapter 4: Future Global Climate: Scenario-based Projections and Near-term Information 553–672. https://doi.org/10.1017/9781009157896.006

Löfgren, S., Cory, N., 2010. Groundwater Al dynamics in boreal hillslopes at three integrated monitoring sites along a sulphur deposition gradient in Sweden. J Hydrol (Amst) 380, 289–297. https://doi.org/10.1016/j.jhydrol.2009.11.004

Lundstrom, U.S., Van Breemen, N., Bain, D., 2000a. The podzolization process. A review, Geoderma.

Lundstrom, U.S., Van Breemen, N., Bain, D.C., Van Hees, P.A.W., Giesler, R., Gustafsson, J.P., Ilvesniemi, H., Karltun, E., Melkerud, P.-A., Olsson, M., Riise, G., Wahlberg, O., Bergelin, A., Bishop, K., Finlay, R., Jongmans, A.G., Magnusson, T., Mannerkoski, H., Nordgren, A., Nyberg, L., Starr, M., Strand, L.T., 2000b. Advances in understanding the podzolization process resulting from a multidisciplinary study of three coniferous forest soils in the Nordic Countries, Geoderma.

Moroni, M.T., Carter, P.Q., J Ryan, D.A., T, M.M., n.d. Harvesting and slash piling affect soil respiration, soil temperature, and soil moisture regimes in Newfoundland boreal forests.

Nierop, K.G.J., Jansen, B., Verstraten, J.M., 2002. Dissolved organic matter, aluminium and iron interactions: precipitation induced by metalycarbon ratio, pH and competition, The Science of the Total Environment.

Pan, Y., Birdsey, R.A., Fang, J., Houghton, R., Kauppi, P.E., Kurz, W.A., Phillips, O.L., Shvidenko, A., Lewis, S.L., Canadell, J.G., Ciais, P., Jackson, R.B., Pacala, S.W., McGuire, A.D., Piao, S., Rautiainen, A., Sitch, S., Hayes, D., 2011. A large and persistent carbon sink in the world's forests. Science (1979) 333, 988–993. https://doi.org/10.1126/science.1201609

Putt, M.M., Bell, T., Batterson, M.J., Smith, J.S., 2010. LATE WISCONSINAN ICE-FLOW HISTORY ON THE TIP OF THE NORTHERN PENINSULA, NORTHWESTERN NEWFOUNDLAND, Current Research.

Rasmussen, C., Heckman, K., Wieder, W.R., Keiluweit, M., Lawrence, C.R., Berhe, A.A., Blankinship, J.C., Crow, S.E., Druhan, J.L., Hicks Pries, C.E., Marin-Spiotta, E., Plante, A.F., Schädel, C., Schimel, J.P., Sierra, C.A., Thompson, A., Wagai, R., 2018. Beyond clay: towards an improved set of variables for predicting soil organic matter content. Biogeochemistry 137, 297–306. https://doi.org/10.1007/s10533-018-0424-3

Ricketts and vatcher, 1996. Granuler aggregate resource mapping in the roddickton-main brook area, great northern peninsula, newfoundland.

Roulet, N., Moore, T., 2006. Browning the waters. Nature 444, 283–284. https://doi-org.qe2a-proxy.mun.ca/10.1038/444283a

Schaetzl, R.J., Luehmann, M.D., Rothstein, D., 2015. Pulses of Podzolization: The Relative Importance of Spring Snowmelt, Summer Storms, and Fall Rains on Spodosol Development. Soil Science Society of America Journal 79, 117–131. https://doi.org/10.2136/sssaj2014.06.0239

Schaetzl, R.J., Rothstein, D.E., 2016. Temporal variation in the strength of podzolization as indicated by lysimeter data. Geoderma 282, 26–36. https://doi.org/10.1016/j.geoderma.2016.07.005

Scharlemann, J.P.W., Tanner, E.V.J., Hiederer, R., Kapos, V., 2014. Global soil carbon: Understanding and managing the largest terrestrial carbon pool. Carbon Manag. https://doi.org/10.4155/cmt.13.77

Schmidt, M.W.I., Torn, M.S., Abiven, S., Dittmar, T., Guggenberger, G., Janssens, I.A., Kleber, M., Kögel-Knabner, I., Lehmann, J., Manning, D.A.C., Nannipieri, P., Rasse, D.P., Weiner, S., Trumbore, S.E., 2011. Persistence of soil organic matter as an ecosystem property. Nature. https://doi.org/10.1038/nature10386

Shimada 2022 millenium timescale C stability in andisol_ how persistent are organo metal complexes, 2020. . Geoderma 417.

Slessarev, E.W., Chadwick, O.A., Sokol, N.W., Nuccio, E.E., Pett-Ridge, J., 2022. Rock weathering controls the potential for soil carbon storage at a continental scale. Biogeochemistry 157. https://doi.org/10.1007/s10533-021-00859-8

Tank, S.E., Fellman, J.B., Hood, E., Kritzberg, E.S., 2018. Beyond respiration: Controls on lateral carbon fluxes across the terrestrial-aquatic interface. Limnol Oceanogr Lett 3, 76–88. https://doi.org/10.1002/lol2.10065

Torn, M. S., Trumbore, S. E., Chadwick, O. A., Vitousek, P. M., and Hendricks, D. M. (1997). Mineral control of soil organic carbon storage and turnover. *Nature*, 389(6647), 170-173.

Wagai, R., Kajiura, M., Asano, M., 2020. Iron and aluminum association with microbially processed organic matter via meso-density aggregate formation across soils: Organo-metallic glue hypothesis. SOIL 6, 597–627. https://doi.org/10.5194/soil-6-597-2020

Wang, F.L., Bettany, J.R., 1995. Methane emission from a usually well-drained prairie soil after snowmelt and precipitation. Canadian Journal of Soil Science, 75(2), 239-241.

Wang, T., Zhang, H., Zhao, J., Guo, X., Xiong, T., Wu, R., 2021. Shifting Contribution of Climatic Constraints on Evapotranspiration in the Boreal Forest. Earths Future 9. https://doi.org/10.1029/2021EF002104

Wang, X., Wackett, A.A., Toner, B.M., Yoo, K., 2022. Consistent mineral-associated organic carbon chemistry with variable erosion rates in a mountainous landscape. Geoderma 405. https://doi.org/10.1016/j.geoderma.2021.115448

Webb, J.R., Santos, I.R., Maher, D.T., Finlay, K., 2019. The Importance of Aquatic Carbon Fluxes in Net Ecosystem Carbon Budgets: A Catchment-Scale Review. Ecosystems 22, 508–527. https://doi.org/10.1007/s10021-018-0284-7

Wei, S., Zhang, X., McLaughlin, N.B., Chen, X., Jia, S., Liang, A., 2017. Impact of soil water erosion processes on catchment export of soil aggregates and associated SOC. Geoderma 294, 63–69. https://doi.org/10.1016/j.geoderma.2017.01.021

Yin, M., Gao, X., Tenuta, M., Gui, D., Zeng, F., 2019. Presence of spring-thaw N2O emissions are not linked to functional gene abundance in a drip-fertigated cropped soil in arid northwestern China. Science of The Total Environment, 695, 133670.

Ziegler, S. E., Benner, R., Billings, S. A., Edwards, K. A., Philben, M., Zhu, X., Laganière, J., 2017. Climate warming can accelerate carbon fluxes without changing soil carbon stocks. Frontiers in Earth Sci. 5, 2.

Chapter 2: Mineralogic controls are harbingers of hydrological controls on soil organic matter content in warmer boreal forests

Abstract

Boreal forests contain ~30% of the global forest soil organic carbon (SOC) stock within a region vulnerable to climate change, yet regional studies on the climate relevant controls of this large reservoir are lacking. The Newfoundland and Labrador Boreal Ecosystem Latitudinal Transect represents a boreal climate gradient of sites ranging in temperature and precipitation similar in extent to changes expected within the region over the next century. Though forest and soil type are similar across the transect, geological parent material upon which soils have developed vary across the region. Despite a >50% increase in litterfall and a 3-fold increase in the dissolved organic matter inputs to the mineral soil with decreasing latitude, average surface horizon mineral SOC and N content are similar among regions. To explain this, the relationships between mineral soil characteristics and other ecosystem parameters with SOC and N content were assessed using an information theoretic approach to rank models. Rankings were used to determine the most relevant variables explaining regional variance in surface mineral SOC. Unsurprisingly, organo-metal complexes (OMCs), a weathering product, were a major component of all plausible

models. However, Al complexes ranked higher than Fe, likely because of the greater solubility of reduced Fe in reducing microsites, particularly beneath the winter snowpack or within the saturated soils during the spring melt. These results highlight the potential role of seasonal hydrology on the formation of metal-stabilized C and N in boreal forests and suggest that the role of Fe OMC in C sequestration may be enhanced with warmer winters. The realization and effect of these seasonally controlled OMC mechanisms require further understanding of mineral soil characteristics and hydrology and their response to climate warming. Such efforts will improve predictions of the impact of climate change on soil C and N content in these forests.

2.1 Introduction

Forests play a major role in the global carbon (C) cycle and support a number of carbon-climate feedbacks. Boreal forests contain about 30% of the global forest soil organic carbon (SOC) stock (Pan et al., 2011; Scharlemann et al., 2014) within a region expected to undergo significant increases in temperature and precipitation over the next century (IPCC, 2013). Yet, our predictive understanding of this stock in response to climate change is poor and contributes significantly to the uncertainty in Earth system models of atmosphere-land C exchange (Friedlingstein et al., 2014). Continental and global scale studies on forest soil C stocks reveal correlations with latitude and mean annual precipitation, suggesting some large-scale climate controls (McGuire et al., 2002). Regional scale studies further indicate the potential role of soil moisture and nitrogen (N)

deposition on both the organic (O) and mineral horizon soil C stocks (Olsson et al., 2009). However, correlations among factors associated with latitude (e.g., Scandinavia where N deposition gradients with latitude are large) often make it difficult to partition climatic from atmospheric deposition influences on productivity and its associated patterns with soil C stocks. Nitrogen limitation can dictate the potential of C sequestration in forests (Oren et al., 2011), consistent with greater O horizon C stocks associated with increased N deposition (Mäkipää et al., 1999; Maaroufi et al., 2015; Geng et al., 2021) and increased N cycling in boreal forests (Philben et al., 2016; Ziegler et al., 2017). However, it is unclear if influences on the slower turnover mineral soil C and N contents are similar to those observed for overlying O horizons in boreal forests.

In the mineral soil, soil forming processes link carbon dynamics and chemical weathering, and the products of such processes serve as mechanisms for organic matter (OM) stabilization. In moist, acidic soils such as boreal podzols, organic acids formed from OM decomposition percolate downward into mineral soil horizons as dissolved organic matter (DOM) where they chelate metals to form organo-metal complexes (OMCs; Lundstrom et al., 2000). These complexes are precipitated within the mineral horizon as pH increases or as they become saturated with metals, rendering the organic material resistant to mobilization and mineralization (Nierop et al., 2002). This process plays a key role in soil organic matter (SOM) sequestration in boreal forest soils (Lundstrom et al., 2000; Masiello et al., 2004); and indicates that DOM delivery to the mineral horizon is more than just a C and N source, as it also serves to promote the maintenance of soil C and N stocks.

Positive correlations among SOC content and metal weathering products are commonly found in moist soils (Lawrence et al., 2015; Doetterl et al., 2015; Porras et al., 2017; Heckman et al., 2018; Rasmussen et al., 2018; Yu et al., 2021). At the global scale, the proportion of SOC associated with metal weathering products is related to a biome's effective moisture, defined as the difference between mean annual precipitation and potential evapotranspiration, suggesting that climate is a first order control on the formation of reactive weathering products that stabilize organic matter (Kramer and Chadwick, 2018). Moist boreal forests likely have a large proportion of SOC associated with weathering products (60–70%) and thus stocks of mineral SOC that are highly sensitive to moisture or hydrologic changes (Kramer and Chadwick, 2018).

Shifts in seasonal hydrology may impact SOC storage in boreal forests on timescales relevant to climate change as soil conditions control OMC stability. While pH affects the solubility of Al and Fe OMCs similarly in that they are both soluble under acidic conditions, Fe complexes are significantly more soluble in reducing environments (Nierop et al., 2002; Jansen et al., 2003). Consequently, Al OMCs have been found to be better predictors of SOC content locally in flooded or seasonally flooded soils where reducing conditions result in losses of Fe OMCs (Banik et al., 2014; Lacroix et al., 2019). However, the extent of this relationship may be even more widespread as reducing microsites have also been found in upland soils (Keiluweit et al., 2016 and 2017).

At the continental scale, mineral SOC is most abundant in regions where wet climates coexist with relatively fresh and weatherable parent rock generating high active weathering zones to form OMCs (Gray et al., 2016; Slessarev et al., 2021). Boreal mineral

soil should, therefore, have high active weathering and C storage potential since they are developed on relatively fresh (i.e., weatherable) minerals recently deposited during the last deglaciation (~10,000 years ago), and wet and acidic soil conditions that promote weathering. The parent material also strongly influences other soil characteristics such as bulk surface area (SA_{bulk}), pore volume (PV) and cation exchange capacity (CEC) which may also influence SOC content (Oades, 1988; Hassink, 1997; Arnarson and Keil, 2000; Baldock and Skjemstad, 2000; Marschner and Kalbitz, 2003; Eusterhues et al., 2005; Feng et al., 2005; Kleber et al., 2015; Gartzia-Bentoetxea et al., 2020). Since SOC controls depend on spatial scale (Wiesmeier et al., 2019), within-site replication is required to capture variation in soil physicochemical properties and relationships with SOC (Nave et al., 2021). Thus, detailed regional and site-specific studies of these vulnerable moist boreal forests, particularly across a range of parent rock compositions, are needed to examine the relative roles of biogeochemistry and climate on SOC content and elucidate the potential consequences of global warming on soil C stocks. Further, regional scale studies within a single biome are essential for imminent climate change predictions prior to regime shifts.

I use a boreal climate transect with variable geological parent material to identify the main controls on mineral soil C and N content and evaluate the relative roles and interactions of mineral soil characteristics and climate or climate-controlled ecosystem parameters. I employ the Newfoundland and Labrador Boreal Ecosystem Latitudinal Transect (NL-BELT), a climate transect that exhibits an increase in precipitation and temperature with decreasing latitude similar to that expected for the region over the next hundred years (IPCC, 2013). Ecosystem C fluxes (e.g., litterfall, DOC inputs to mineral

soil) increase with temperature across the transect, as does the organic horizon SOC stock; however, no such increase is observed in the surface mineral horizon SOC (Ziegler et al. 2017). The higher variability in surface mineral SOC content within climate zones than among climate zones (Ziegler et al. 2017), suggests controls beyond climate or C inputs. The widely variable parent rock contributions in the intermediate climate region provides an opportunity to test the hypothesis that mineral soil characteristics, controlled by parent material, play a relatively stronger role on SOM content than climate or climate-controlled ecosystem parameters. Since there are many variables and interactions that may contribute to SOM content, I use an "information theoretic approach" to rank models and consider the results within the context of climate change.

2.2 Methods

2.2.1 Study area

The Newfoundland and Labrador Boreal Ecosystem Latitudinal Transect (NL-BELT) is a climate transect spanning 5.5º latitude along the eastern coast of Labrador and western coast of the island of Newfoundland (see map in Ziegler et al., 2017). The transect spans a 5 ºC gradient in mean annual temperature and a range of 1073 to 1505 mm in mean annual precipitation (Table 2.1; Environment and Climate Change Canada 30-year normal for 1980-2010). This work focuses on three of four established regions, Eagle River (ER; 53° latitude), Salmon River (SR; 51° latitude) and Grand Codroy (GC; 48° latitude) which I will refer to as high, mid and low latitude regions, respectively (Figure 2.1). Within each region are three established forest stand sites approximately 80m x 80m, within which three

soil sampling plots (10m diameter) were randomly chosen per site. Three replicates were collected from each plot for a total of 81 soil samples across the transect (27 per region). All sites are dominated by mature stands of balsam fir (*Abies balsamea*), with mesic, well-drained humo-ferric podzolic soils. Soils are of young to intermediate maturity, formed in a post-glacial area from till that varies in depth and composition between regions (Figure 2.1).

Table 2.1 Average regional NL-BELT climate data, C fluxes and geology.

Mean annual temperature (MAT), precipitation (MAP) and potential evapotranspiration (PET) are based on Environment Canada climate normals for 1981–2010 from the Cartwright, Plum Point and Port Aux Basques weather stations, respectively. Effective moisture is calculated as the difference of MAP and PET. Dissolved organic carbon (DOC) flux is the flux of DOC from the organic horizon to the top of mineral soil, measured across nine plots within one site in each region (from Ziegler et al., 2017). Litterfall inputs include needles, cones, bark and twigs collected at each plot over 4 years (from Ziegler et al., 2017). Bedrock and till samples were collected at exposed areas near soil sites. Plagioclase (pl), quartz (qtz), K-feldspar (ksp), biotite, (bt), amphibole (amph), chlorite (chl) and muscovite (musc).

	High latitude	**Mid latitude**	**Low latitude**
MAT (ºC)	0	2.4	5.2
MAP (mm yr^{-1})	1073	1211	1505
PET (mm yr^{-1})	432	431	608
Effective moisture (mm yr^{-1})	641	780	897
DOC flux (gC m^2 yr^{-1})	8.5 ± 3.5	14.3 ± 7.3	29.3 ± 13.6
Litterfall (kg ha^{-1})	3.9 ± 2.1	11.7 ± 4.8	13.9 ± 4.1
Bedrock	Granitoids, mafic amphibolite	Carbonate, ophiolite, siliciclastic sedimentary, orthogneiss, granite	Siliciclastic sedimentary
Till composition	Pl, qtz, ksp, bt, amph, chl, musc	Highly variable	Qtz, ksp, pl, chl, musc

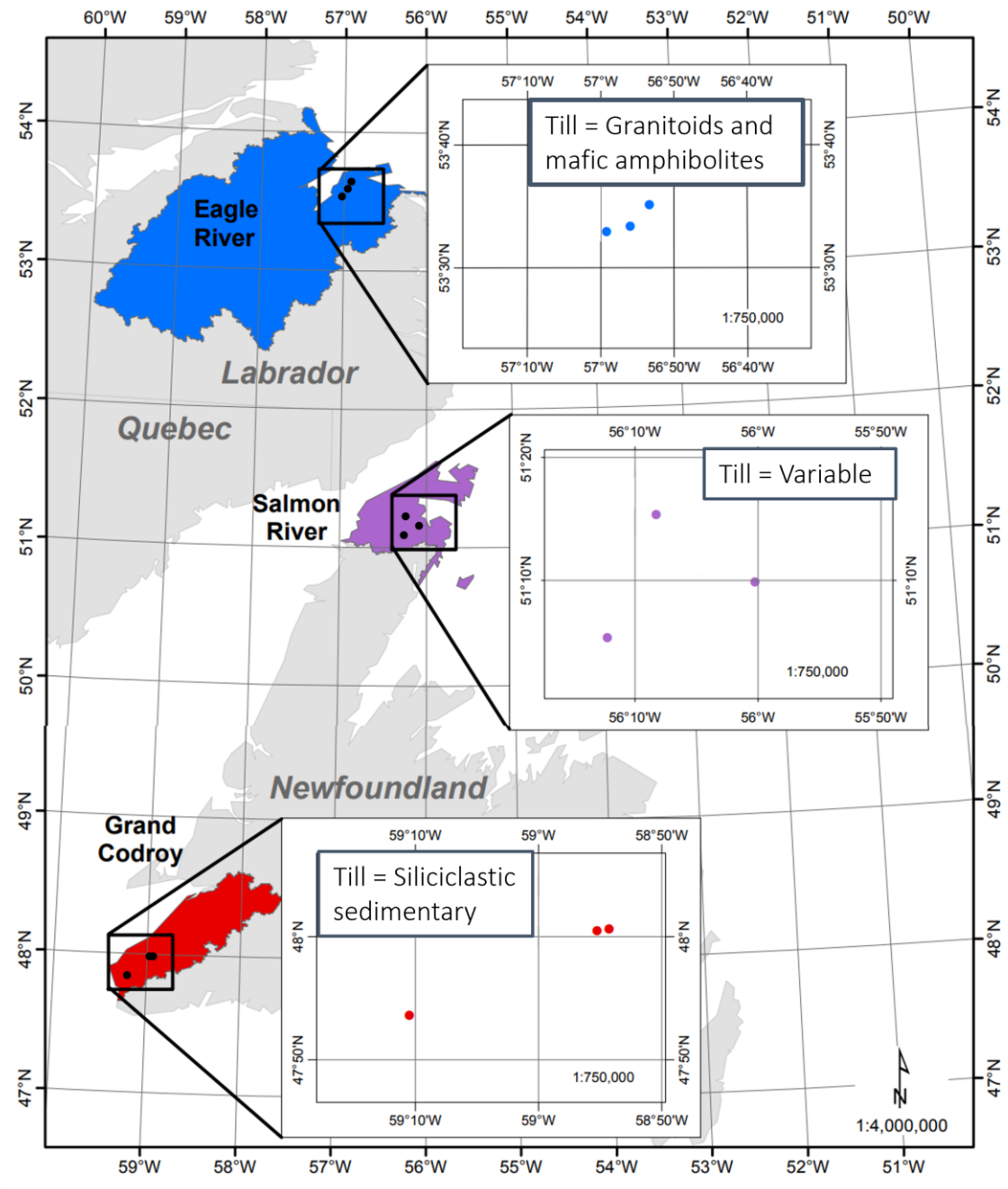

Figure 2.1.

Study area. Map of the Newfoundland and Labrador Boreal Ecosystem Latitudinal Transect (NL-BELT). Within each region are three forest sites established in 2011, the locations of which are shown in the enlarged map associated with each region. Eagle River (North region), Salmon River (Mid region), and Grand Codroy (South region). Geological inputs from till are indicated for each region. Modified after Ziegler et al. (2017).

The Laurentide Ice Sheet covered the entire research area during the Late Wisconsinan Glacial Maxima. Presumably all developed soil was removed during its retreat, leaving rock to restart pedogenesis. Glacial retreat began in the south around 14 ka, with retreat, re-advance, and a final retreat at 12.6 ka (Brookes, 1977), while the mid and high latitude regions were ice-free by 11.5 ka (Ricketts and Vatcher, 1996; Putt et al., 2010) and 10 ka (King, 1985), respectively. This places an upper limit on the age of the soil in each region.

The higher latitude region is underlain by early Proterozoic bedrock of the Grenville Province (Gower, 1998) with bedrock including granite, quartzofeldspathic and mafic amphibolites and gneisses. The local till is largely composed of gneissic or granitic clasts, potentially locally derived and is generally less than 50 cm thick, with sub-angular to very angular granule to boulder size clasts making up, on average, 35% of the till (McCuaig, 2002). The mid-latitude region is underlain by early Ordovician limestone and dolostone bedrock of the Humber Zone (Colman-Sadd et al., 2000). Bedrock found nearby includes granite, gneiss, ultramafics, and fine siliciclastic sedimentary rocks. The till is highly variable across the region, composed of fresh and weathered granite, slightly-to-moderately weathered sandstone, and fresh limestone, shale and phyllite (Ricketts and Vatcher, 1996). The lower latitude region is underlain by siliciclastic non-marine sedimentary bedrock of the Carboniferous and Devonian Codroy and Anguille Groups (Coleman-Sadd et al., 2000). Here, till is largely composed of micaceous sandstone and siltstone, granite, with lesser dolomite, diorite, gabbro, gneiss and quartz pebbles (Ricketts, 2001).

Litterfall, soil respiration, and DOC fluxes from the organic layer increase along the transect with decreasing latitude (Ziegler et al., 2017). The DOC fluxes have been found to increase as a function of increased winter temperature and reduced snowpack (Bowering et al. 2022). Similarly, organic horizon %C and %N increase with decreasing latitude (Figure 2.2; C and N weight as % of bulk soil), as well as C and N stocks; Figure S2.1; kg C m^{-2} and kg N m^{-2}). Average surface mineral SOC content is similar among regions despite high within-region variation, and younger C in the south consistent with increased SOM turnover rates from higher productivity and losses associated with the warmer climate (Ziegler et al., 2017).

Three replicates were collected from each plot over a two-week period in late June to early July of 2011 (n = 81). The organic horizon was cut to 20 x 20 cm^2 and removed with a trowel. The top of the mineral soil was identified as below the Ae horizon (bleached eluvial horizon) which was scraped off with a trowel. The mineral soil was extracted to 10 cm depth with a 5.1 cm diameter soil corer and stored at 5°C until processing. This depth was selected as I were interested in the C-rich Bf horizon (Canadian soil classification) which accumulates organic matter and metal weathering products just below the Ae. Further, this shallow depth limits the increasing variability in SOC and OMC content with depth that results from variations in infiltration from microtopography. The soils were air dried and sieved to <2 mm. From here, %C and N were analyzed for 81 samples and averaged by plot (n=27). The remaining sample was pooled by plot (n=27), and size fractionated for different analyses (see Figure 2.3 for flow chart of analyses).

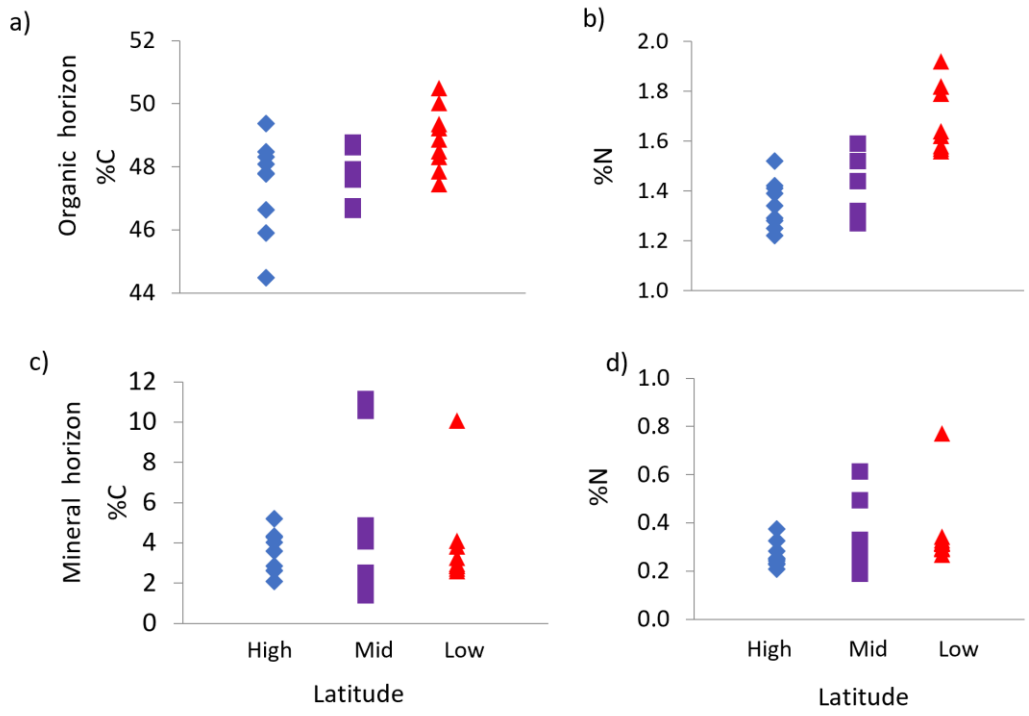

Figure 2.2.

Regional variation in soil %C and %N from the NL-BELT organic horizon (a, b) and top 10 cm of <2mm mineral soil (c, d). Collection, preparation, and analytical methods.

For C and N concentrations were determined on ground <2 mm soils with a Carlo Erba NA1500 9 1 Series II Elemental Analyser (Milan, Italy) as per methods in Ziegler et al. (2017). The CEC was evaluated by the $BaCl_2$ compulsive exchange method of Gillman and Sumpter (1986), determined at the pH and ionic strength of the soil. Here, soil was shaken with 0.1 M $BaCl_2 \cdot 2H_2O$ and then centrifuged. The higher affinity of exchangeable sites for Ba forces other ions into solution. Ions in the supernatant were measured with inductively coupled plasma optical emission spectrometry at the Geological Survey of

Newfoundland using a Thermo Fisher Scientific iCAP 6500 series Optical Emission Spectrometer.

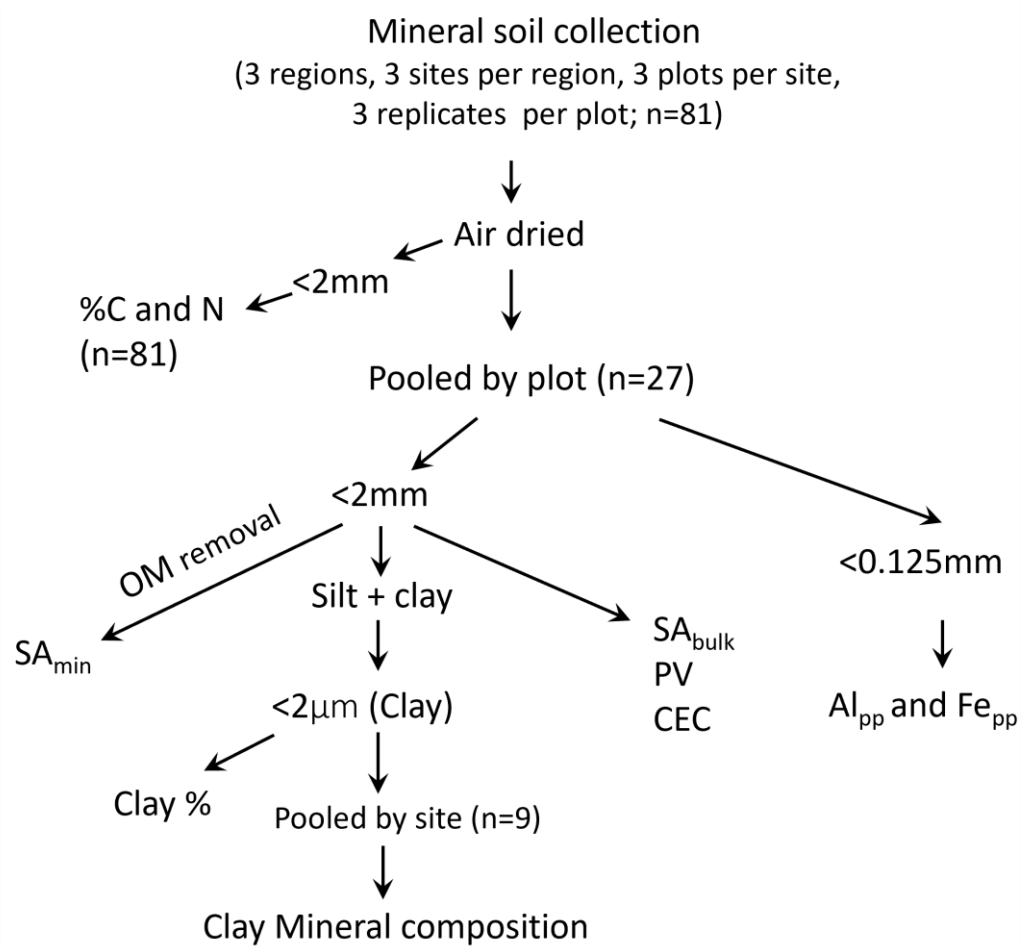

Figure 2.3.

Flow chart of methods for mineral soil samples. Soil organic C and N concentration (%C and N), cation exchange capacity (CEC), bulk and mineral surface area (SAbulk and SAmin), pore volume (PV), pyrophosphate extracted Fe and Al (Fepp and Alpp), clay size fraction (clay %), organic matter (OM).

The surface area (SA_{bulk}) and pore volume (PV) of the <2 mm fraction samples were measured at the University of Florida by N_2 sorption on a Quantachrome Autosorb 1, at 77K. Samples were de-gassed under vacuum for at least 24 h at 180 ˚C prior to analysis. SA was calculated according to Brunauer-Emmett-Teller (BET; Brunauer et al., 1938) theory using adsorption data in the 0.01 – 0.3 relative pressure range. Because N_2 is kinetically impeded from entering nanopores (<1 nm), this measure of SA represents only nanopore-enclosed surfaces (1.5 – 50 nm). Nanopore volumes were calculated using Barrett-Joyner-Halenda (BJH; Barrett et al., 1951) theory. Another potential predictor is soil SA after OM removal (Kaiser and Guggenberger, 2003; Siregar et al., 2005), which may be a better predictor than the conventionally measured SA_{bulk} of the >2 mm soil fraction (bulk soil) since it operationally quantifies mineral surfaces that may be potentially available for OM interactions. Therefore, SA was measured again on the same size fraction after the removal of organic matter, yielding what I operationally define as the mineral SA (SA_{min}).

To remove organic matter, the room temperature hypochlorite method from Kaiser and Guggenberger (2003) was chosen as it does not alter the crystalline mineral SA like high temperature methods (Kaiser and Guggenberger, 2003; Siregar et al., 2005) and alters metal weathering products least, which are of interest in this study (Wagai et al., 2009). The trade-off here is that it is not as effective in OM removal, leaving 5 – 23% OM remaining after treatment (Wagai et al., 2009). Samples were shaken for 6 hours in a 1 M NaOCl solution adjusted to a pH of 8 with concentrated HCl and supernatant was discarded over 5 cycles, and then rinsed twice with deionized water. The final air-dried pellet was

analyzed for TOC, confirming a decrease of at least 60 % compared to original mineral soil samples. Further, I found that % C and % N was strongly correlated (p-values of 0.00027 and 0.0015; Pearson correlation of 70 and 62 %, respectively) with the difference between SA_{bulk} and SA_{min} confirming OM removal from associations with minerals (Figure S2.2 in Appendix).

Metal weathering products were extracted with sodium pyrophosphate (Fe_{pp} and Al_{pp}) from the <0.125 mm fraction using the methods of Courchesne and Turmel (2008). This extraction releases Al and Fe OMCs (McKeague et al., 1971; Stumm, 1992). Silicate minerals and crystalline Al and Fe oxides, which are not of interest here, are not significantly dissolved with either of these extraction methods (Courchesne and Turmel, 2008).

To determine the size fractions, sand was separated by wet sieving sand from the fine fraction, followed by several centrifugation steps to separate clay from silt following the methods of Soukup et al., (2008). Their proportions were determined by weighing after drying at 50 ºC. X-ray diffraction on a Rigaku Ultima-IV XRD with a Cu source was used to identify and quantify minerals within the clay size fraction of the mineral soil. Two preparatory steps based on the methods of Soukup et al. (2008) were performed to focus on clay mineral peaks. First, organic matter was removed by sonication in an 80 ºC bath with sodium hypochlorite adjusted to pH 9.5 with 0.2 M HCl, centrifuging and discarding the supernatant until it was clear. Second, metal weathering products were removed with a citrate buffer solution of 0.3 M sodium citrate and 1 M sodium bicarbonate as these do not have a crystalline structure for XRD analysis. This was heated to 80ºC in a bath, sodium

dithionite was added and centrifuged, the supernatant was discarded, and the pellet set to air dry. Jade software (MDI, California) was used for mineral identification by matching peak locations using the International Centre for Diffraction Database (ICDD). Mineral proportions were quantified using reference intensity ratios as a proportion of the peak height of minerals with known proportions within the database (Zhou et al., 2018).

2.2.2 Statistical methods

Our approach to understanding the factors controlling C storage in these mineral soils was to identify the best model to predict mineral soil C and N content. However, there are many factors and interactions at play in these forest ecosystems, making it challenging to identify a singular model. Traditional null hypothesis testing is uninformative in this case as it is deterministic and does not allow for the understanding of the relative importance of multiple plausible factors and thus model selection (Anderson et al., 2000). Reactive metal weathering products have been identified as predictors of forest soil C and N content in the literature at larger scales, but it is unknown if interactions of these products with ecosystem factors or soil characteristics at the region and site scales also play a role. Further, Fe and Al organo-metal complexes are often considered together despite their differing solubilities under reducing conditions. For this reason, the information theoretic approach (Burnham and Anderson, 2002) was employed as it is useful for assessing the relative importance of specific factors and/or their interactions relevant within complex natural systems by ranking models using the Akaike Information Criterion (AIC) (Anderson et al., 2000). This measure is a bias corrected maximum log-likelihood value that estimates the deviation of the tested model from the true model, thus a smaller AIC

indicates a better performing model. However, it is a relative measure that is only comparable among models with the same response variable. Ranking allows us to identify the power of each additional term as it was added to the model, to identify terms that do not add further explanation of variation, thus enabling the identification of a combination of terms generating the most parsimonious model to describe soil C and N.

Generalized linear models were employed so that non-linear relationships could be identified by linking different error structures. Residual errors were checked to be homogeneous, independent, and normally distributed with residual versus fit, lag and quantile-quantile plots, respectively (McCullagh and Nelder, 1989; Zuur et al., 2007; Welham et al., 2007). Where these assumptions were not met because of non-linearity, Inverse Gaussian or Gamma error structures were used and found to be a better fit for the models meeting the assumptions required.

Models were selected *a priori* and based around OMC as these were expected to be important based on their role in podsolization and soil OM content. Fe and Al OMC were evaluated separately because of their differing stabilities with soil conditions (Nierop et al., 2002). In addition to the OMC weathering products, OM inputs and soil characteristics that may be important for C stabilization were also evaluated in the models. With eight factors to be tested, along with their interactions and co-correlations, it was not possible to evaluate a global model. Instead, smaller full models each with Fe_{pp} and Al_{pp}, or SA_{min}, along with other uncorrelated terms, were tested separately (list of full models in Table 2. 2).

Co-correlations with Fe_{pp}, $Al_{pp,}$ and $_{SAmin}$ were tested with Pearson correlation coefficients where >0.40 values indicate moderate to very-strong correlations (Table S2.1 in Appendix; n=27). Co-correlated factors were not evaluated within the same full model. Litterfall without wood (diameter >2 mm) was selected as an OM input parameter over litterfall including wood since the sporadic larger wood inputs from recent high windthrow events are not likely representative of soil inputs on decadal time scales. Inputs of DOC from the organic layer were excluded as a parameter as this data is only available for one site per region and found to be regionally and/or climatically controlled in these forest sites (Bowering et al., 2022); however, C and N from the overlying organic horizon (SOC and N content) were considered as a potential input. Soil characteristics chosen included CEC, SA_{bulk} (SA of <2mm soil), PV, and clay content, as each represents a measure of a surface or bonding site with potential to stabilize organic matter. The mineral SA (SA_{min}; SA measured after organic matter was removed) was considered separately from Al_{pp} and Fe_{pp} as it is co-correlated with both (models 6─7). Climate variables were not used directly in the models since the approach here was to uncover factors associated with climate that may regulate mineral soil C and N content.

Full models (Table 2.2) were broken down into their components and evaluated by sequentially adding terms to test their impact on the overall predictive power of the model. An AIC modified for small sample size (AIC_c) was employed because of the low ratio of sample size to terms (Burnham and Anderson, 1998). A smaller (or more negative) AICc is indicative of a model that better describes C or N content, determining the ranking order. Delta AIC_c (ΔAIC_c) evaluates the plausibility of the model relative to other highly

ranked models, calculated as the difference of its AIC_c from the highest ranked model. Models with $\Delta AIC_c < 2$ were equally highly plausible (Burnham and Anderson, 2002). Akaike weights (w_i) evaluates the weight of evidence in favour of the model relative to other sub-models of each full model. Finally, the best models from each full model were compared using AICc.

Table 2.2 All full models evaluated using the information theoretic approach.

Pyrophosphate-extracted Fe and Al (Fe_{pp}, Al_{pp}), litterfall (LF), C and N stocks from the organic horizon (C_{org}, N_{org}), clay size fraction as a percent (clay), pore volume (PV), cation exchange capacity (CEC), surface area of <2mm soil (SA_{bulk}), and surface area after removal of organic matter (SA_{min}). Bivariate interactions among variables were also considered. E = error. See Tables S3-4 for all sub-models that were evaluated.

Model #	Dependent Variable	Full models
1	C or %N	Fe_{pp} + LF + CEC + Interactions + E
2	C or %N	Fe_{pp} + LF + Clay + Interactions + E
3	C or %N	Al_{pp} + SA_{bulk} + LF + Interactions + E
4	C or %N	Al_{pp} + PV + LF + Interactions + E
5a	%C	Al_{pp} + C_{org} + SA_{bulk} + Interactions + E
5b	%N	Al_{pp} + N_{org} + SA_{bulk} + Interactions + E
6	C or %N	SA_{min}+ LF + LF*SA_{min} + E
7a	%C	SA_{min} + C_{org} + C_{org}*SA_{min} + E
7b	%N	SA_{min} + N_{org} + N_{org}*SA_{min} + E

All models, Pearson coefficients, p-values and ANOVAs were evaluated in RStudio version 1.4.1106. Microsoft Excel 2017 was used to construct scatter plots and

box and whisker plots, and to perform T-tests to determine if there were statistical differences in soil characteristics among regions.

2.3 Results

2.3.1 Mineral soil characteristics

Organic horizon **%** C and % N averages increased from high to low latitude while the mineral horizon exhibited no significant differences among regions (Figure 2.2). The high latitude region exhibited the lowest average values for SA_{bulk}, PV, CEC, and clay size fraction with little within region variability, while the mid latitude region had the highest averages for all characteristics except SA_{bulk} and had the highest within region variability for all characteristics (Figure 2.4; Table S2.2 in Appendix). The dominant exchangeable cation recovered by the CEC extraction was Al^{3+}, followed by Ca^{2+}, with lesser contributions from Mg^{2+}, Na^{+}, and K^{+}. Two exceptions to this were from two sites in the mid region, where the CEC was dominated by Ca^{2+} and Mg^{2+}, with negligible Al^{3+}. Average Fe_{pp} content increased with climate warming across the transect from 8.3 ± 2.9 to 14.3 ± 4.6 g kg^{-1}. Average Al_{pp} was similar across regions with higher variability in the mid latitude, 5.4 ± 3.2, 6.3 ± 7.2, and 5.4 ± 2.5 g kg^{-1}, from high to low latitude, respectively (Figure 2.4 and Figure S2.2 in Appendix).

A minimum of 60% of total C was removed with the hypochlorite method of OM removal. All samples exhibited an increase in surface area with OM removal, with SA_{min} 43 – 827 % higher than SA_{bulk}. The high latitude region had the lowest average SA_{min} of 13.8 ± 7.0 m^2 g^{-1}, while the mid and low regions had higher averages of 26.2 ± 13.0 and

25.2 ± 5.2 $m^2 g^{-1}$, respectively (Table S2.2 in in Appendix, Figure 2.5). Minerals within the clay size fraction were combined into five groups based on their structure: (1) non-clays; (2) kaolin-serpentine-group minerals; (3) chlorite-group minerals; (4) smectite-group minerals; (5) mica group minerals (S2.3 in Appendix). Non-clays made up the largest proportion of the clay size fraction within the high latitude region, where feldspars and quartz were dominant. Clay content increased at lower latitudes, where mica was the dominant clay in both mid and lower regions.

2.3.2 Model ranking results indicate Alpp is a better descriptor of C and N content than Fepp

The information theoretic approach (Burnham and Anderson, 2002) was employed to assess the relative importance of Al_{pp} and Fe_{pp} and their interactions with other soil characteristics and ecosystem factors on boreal mineral soil C and N content by model ranking. Overall, both pyrophosphate-extracted metals are good terms for explaining % C and %N variation in these soils; however, Al_{pp} models performed better than Fe_{pp} (Tables 2.3 – 2.4 in Appendix). Simpler models worked best for %C while relatively more complex models were needed to describe % N variability.

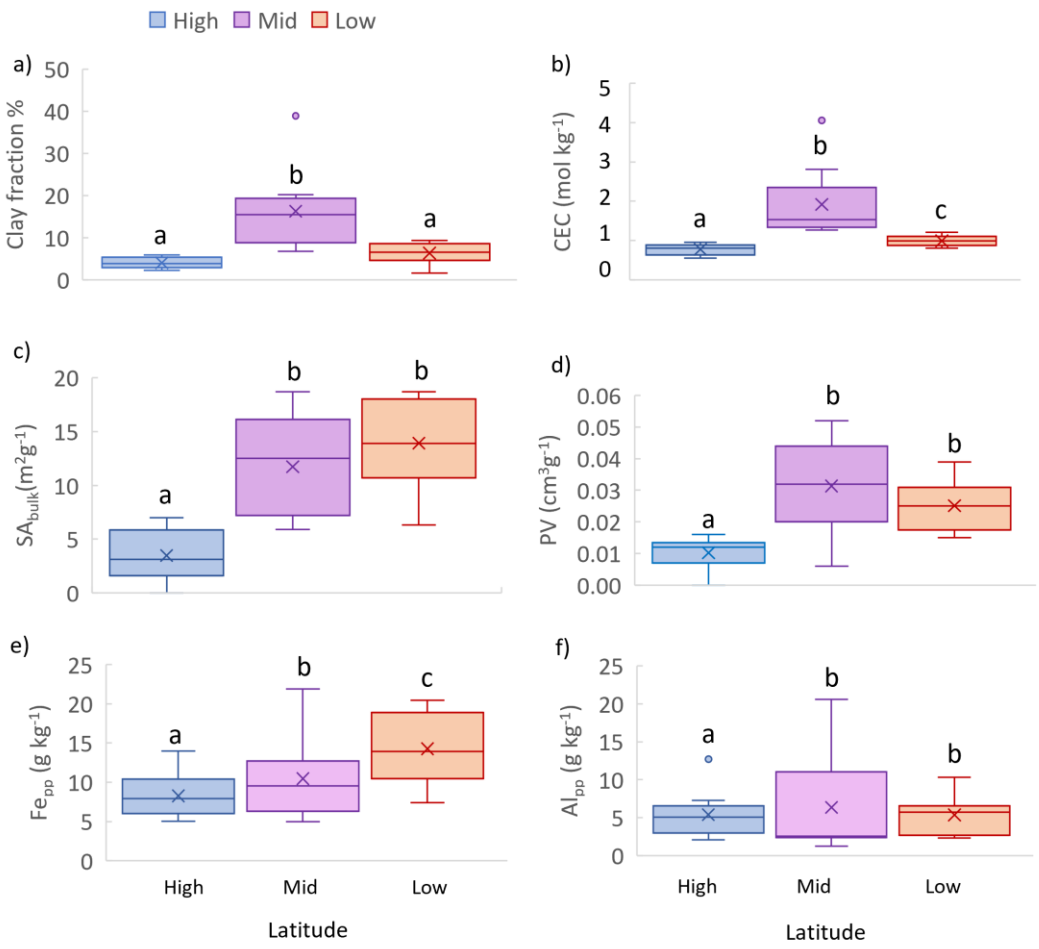

Figure 2.4.

Mineral soil characteristics. NL-BELT regional variation in <2mm mineral soil characteristics: (a) clay size fraction (%), (b) cation exchange capacity (CEC), (c) bulk soil surface area (SAbulk), (d) pore volume (PV), (e) pyrophosphate extracted Fe (Fepp, a proxy for organically complexed Fe), and (f) pyrophosphate extracted Al (Alpp, a proxy for organically complexed Al). Shown are the quartiles, mean (x) and median (middle horizontal line). Significantly different groups are indicated with lowercase letter above box.

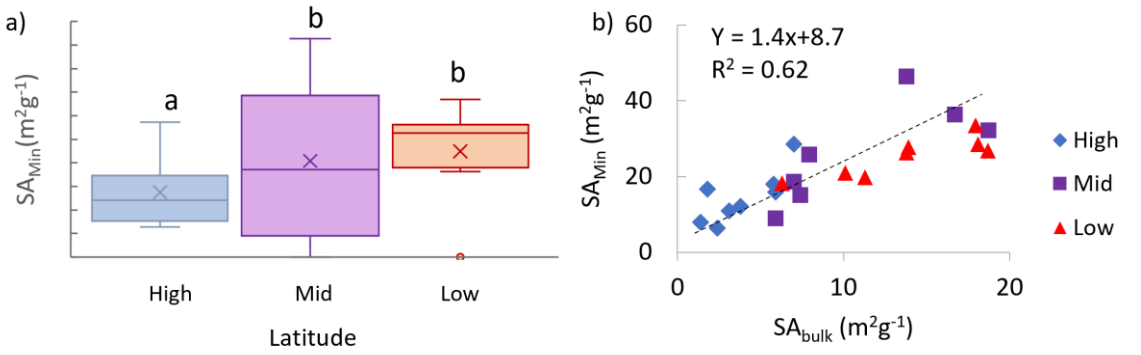

Figure 2.5.

Mineral surface area (SA_{Min}, operationally defined surface area after removal of organic matter) (a) NL-BELT regional variation and (b) relationship to bulk SA (SA_{bulk} = surface area of the >2 mm soil fraction). Significantly different groups are indicated with lowercase letter above box.

All highly plausible models for explaining C and N content are ranked in Tables 2.3 and 2.4, respectively. The full list of models considered, and their resulting statistics is available in the supplementary material (Table S2.3 – 2.4 in Appendix). Uninformative parameters are shown in italics, these terms increase the AICc when added and do not provide any additional predictive power (Arnold, 2010). For example, considering model 1, the term Fe_{pp}*Litter is identified as an uninformative parameter since adding this term increased the AICc. In other words, the highest ranked model Fe_{pp}+Fe_{pp}*CEC is simply a special case of Fe_{pp}+Fe_{pp}*CEC+Fe_{pp}*Litter, and the explanatory power comes from the better performing model rather than the added parameter (Arnold, 2010). Where a term was found to be uninformative in one model, it was also considered not useful in others and not used further in the modelling effort (e.g., Al_{pp}*Litterfall, Al_{pp}*C_{org}).

Table 2.3 Highly plausible models to describe %C variation.

The full model that each of these models is associated with is identified by number and as listed in Table 2.2. An AIC modified for small sample size (AIC_c) was employed and is based on the maximum log-likelihood with a penalty for additional terms that do not add additional predictive power. A smaller (more negative) AIC_c indicates a better model. Delta AIC_c (ΔAIC_c) is the difference in AIC_c from the highest ranked model, all models with ΔAIC_c <2 are considered highly plausible. Akaike weights (w_i) indicate the weight of evidence in favour of each model as a decimal percent. Terms in italics are uninformative parameters that add no additional predictive power to the model.

Full Model	Sub-model	ΔAICc	AICc	w_i	log-likelihood
1	Fe_{pp} + CEC*Fe_{pp} + E	0.000	99.6	0.57	-46.20
1	Fe_{pp} + CEC*Fe_{pp} + *LF***Fe_{pp}* + E	0.461	100.0	0.31	-45.40
2	Fe_{pp}+ E	0.000	103.1	0.44	-48.96
2	Fe_{pp} + *LF***Fe_{pp}* + E	1.532	104.6	0.21	-48.71
2	Fe_{pp} + *LF* + E	1.653	104.7	0.19	-48.77
3	Al_{pp} + *Al_{pp}***LF* + Al_{pp}*SA_{bulk} + E	0.000	86.8	0.27	-38.79
3	Al_{pp} + *Al_{pp}***LF* + E	0.213	87.0	0.24	-39.93
3	Al_{pp} + Al_{pp}*SA_{bulk} + E	0.888	87.7	0.17	-40.26
3	SA_{bulk}+ Al_{pp} + E	1.270	88.1	0.14	-40.46
4	Al_{pp} + PV*Al_{pp} + E	0.000	86.4	0.26	-39.61
4	Al_{pp} + PV*Al_{pp} + *Al_{pp}***LF* +E	0.424	86.8	0.21	-38.80
4	Al_{pp} + *Al_{pp}***LF* + E	0.625	87.0	0.19	-39.93
5a	Al_{pp} + Al_{pp}*SA_{bulk} + E	0.000	87.7	0.41	-40.26
5a	Al_{pp} + Al_{pp}*SA_{bulk}+ *C_{org}***Al_{pp}* + E	1.435	89.1	0.20	-39.96
5a	Al_{pp} + Al_{pp}*SA_{bulk}+ *C_{org}***Al_{pp}* + *C_{org}***SA_{bulk}*+ E	1.507	89.2	0.19	-38.96
6	SA_{min} +LF*SA_{min}+ E	0.000	88.1	0.65	-40.45
7a	SA_{min} + C_{org}*SA_{min}+ E	0.000	88.4	0.51	-40.59
7a	C_{org} + SA_{min}+ E	0.112	88.5	0.49	-40.64

Table 2.4 Highly plausible models to describe %N variation.

The full model that each of these models is associated with is identified by number and as listed in Table 2.2. An AIC modified for small sample size (AICc) was employed and is based on the maximum log-likelihood with a penalty for additional terms that do not add additional predictive power. A smaller (more negative) AICc indicates a better model. Delta AICc (ΔAICc) is the difference in AICc from the highest ranked model, all models with ΔAICc < 2 are considered highly plausible. Akaike weights (wi) indicate the weight of evidence in favour of each model as a decimal percent. Terms in italics are uninformative parameters that add no additional predictive power to the model.

Full model	Sub-model	ΔAICc	AICc	w_i	log-likelihood
1	Fe_{pp} + CEC*Fe_{pp} + E	0.000	-67.32	0.33	37.25
1	Fe_{pp} + CEC*Fe_{pp} + *LF*Fe_{pp}* + E	0.920	-66.40	0.21	37.81
1	Fe_{pp} + E	1.185	-66.14	0.19	35.63
2	Fe_{pp} + E	0.000	-66.14	0.47	35.63
2	Fe_{pp} + *LF*Fe_{pp}* + E	1.582	-64.55	0.21	35.86
3	Al_{pp} + SA*Al_{pp} + E	0.000	-67.62	0.31	37.40
3	Al_{pp} + SA_{bulk} + E	0.054	-67.57	0.30	37.37
3	Al_{pp} + Al_{pp}*LF + E	0.542	-67.08	0.23	37.13
4	Al_{pp} + Al_{pp}*LF + E	0.000	-67.08	0.50	37.13
4	Al_{pp} + LF + E	0.875	-66.20	0.32	36.69
5b	Al_{pp} + N_{org}*SA_{bulk} + N_{org}*Al_{pp} + Al_{pp} * SA_{bulk} + E	0.000	-80.47	0.35	45.88
5b	Al_{pp} + N_{org}*Al_{pp}+E	0.321	-80.15	0.30	43.66
6	SA_{min} + E	0.000	-59.03	0.38	32.08
6	SA_{min}+ *LF*SA_{min}*+ E	0.143	-58.88	0.35	33.03
7b	N_{org} + SA_{min}+ E	0.000	-60.80	0.36	33.99
7b	N_{org} +SA_{min}+ *N_{org}*SA_{min}*+ E	0.166	-60.64	0.33	34.93
7b	SA_{min}+ *N_{org}*SA_{min}*+ E	1.750	-59.05	0.15	33.11
7b	SA_{min}+ E	1.778	-59.03	0.15	32.08

Either Fe_{pp} or Al_{pp} were a component of all the best models for %C variation, usually with one or multiple interaction term(s) involving the metal and an input (litter, C_{org} or N_{org}) or mineral soil characteristic. However, most of the descriptive power comes from the metal term as the addition of further terms has little effect on AICc. Further, models with uninformative parameters perform similarly to the best models with additional terms. For example, in models 3 ─ 5 (Table 2.3), sub-models Al_{pp}+Al_{pp}*PV and Al_{pp}+Al_{pp}*SA_{bulk} have similarly low AICc values and are considered the best Al_{pp}-bearing models for describing %C. However, considering that the Al_{pp}*Litter term is uninformative (Model 4) and the sub-model Al_{pp}+Al_{pp}*Litter performs almost as well as either of these best models above, I assume that most explanatory power comes from the Al_{pp} term and the positive effect of the interactive terms Al_{pp}*PV and Al_{pp}*SA_{bulk} is negligible. Mineral surface area is also a good explanatory term for %C (Models 6 ─ 7; Table 2.3). The highest ranking SA_{min} models performed better than the top Fe_{pp} models (AICc=88.1 compared with 99.6) and were similar to Al_{pp}-bearing models (AICc = 86.4) for explaining % C with respect to AICc.

As with %C, pyrophosphate-extracted metals and SA_{min} are good explanatory terms for describing %N variation as these were components of all the plausible models (Models 1 ─ 7, Table 2.4). Here, however, the highest ranked sub-model (Model 5), including Al_{pp} and organic horizon N (N_{org}), had a significantly lower AICc than all other models.

On their own, both metals perform similarly in terms of AICc for describing %N (AICc=-63.9 compared with -66.1 for sub-models Al_{pp} and Fe_{pp}, respectively). In Fe_{pp}

models 1 ─ 2, most descriptive power likely comes from Fe_{pp}, as Fe_{pp}*Litter is an uninformative parameter, and sub-model Fe_{pp} and the top-ranking model $Fe_{pp}+Fe_{pp}$*CEC have similar AICc (-66.1 compared with -67.3).

For the highly plausible Al_{pp}-bearing models 3─4 (Table 2.4), Al_{pp} with one additional term (either SA_{bulk}, litterfall, Al_{pp}*SA_{bulk} or Al_{pp}*litter) all produced a similar AICc for describing %N. Models adding more than one of these terms did not provide a better AICc (Table S2.5 in Appendix) as the cost for the additional terms increases the AICc more than the additional explanatory power it provides. This suggested that Al_{pp} provides the majority of the explanatory power in models 3 ─ 4, and the addition of either of these terms only added slightly more power. Model 5 performed better than the next best model (AICc = -80 compared with -68 for model 3) with the addition of the term N_{org}*Al_{pp} which decreased the AICc significantly relative to model 3 (Table 2.4 and S2.5 in Appendix), suggesting that the interaction of Al_{pp} with N from the overlying organic horizon influences the mineral soil N content. The further addition of SA*N_{org} and Al_{pp}*SA had a negligible effect on AICc suggesting that the majority of explanatory power came from $Al_{pp}+Al_{pp}$*N_{org}. Therefore, the best model for describing %N was $Al_{pp}+Al_{pp}$*N_{org}+SA*N_{org}+Al_{pp}*SA, where most of the descriptive power comes from the first two terms.

As with %C, SA_{min} is also a good explanatory term for describing %N variation in models 6 ─ 7 (Table 2.4). The interactions of SA_{min} with litterfall and N_{org} were uninformative terms, and SA_{min} on its own performed almost as well as $SA_{min}+N_{org}$,

suggesting that most power came from SA_{min} alone. However, the best Fe_{pp} and Al_{pp} models from 1 ─ 5 performed better than SA_{min} models for describing % N variation. Clay content did not perform well in any models describing either % C or % N variation. It is not present in any of the best models, and significantly increases the AICc when it is added (Table S2.3 – 2.4 in Appendix).

Model ranking and AICc values do not provide a measure of the explanatory power of the factors used, therefore the direct relationships and explained variance for the most important individual terms are shown in Figure 2.6. The use of R^2 for each linear correlation, however, is limiting as does not incorporate interactions with other factors as was investigated in the ranking of models. Here, Al_{pp} and SA_{min} are better at describing variance in %C (R^2 = 0.75 and 0.48) and % N variation (R^2 = 0.54 and 0.52) than Fe_{pp} (R^2 = 0.26 and 0.48 for %C and %N, respectively), as is reflected in the ranking of the models. These relationships appear strongest in the mid region where the largest range in C and %N is accompanied by a similarly wide range in SA_{min}, Al_{pp} and Fe_{pp} (Figure 2.6). The response of %C to SA_{min} and Fe_{pp}, and % N to Al_{pp} can further be divided by region where the explained variance increases when the region is considered. Here, the response of % C or %N to these variables in the high latitude region is relatively lower than the other regions (Figure 2.6).

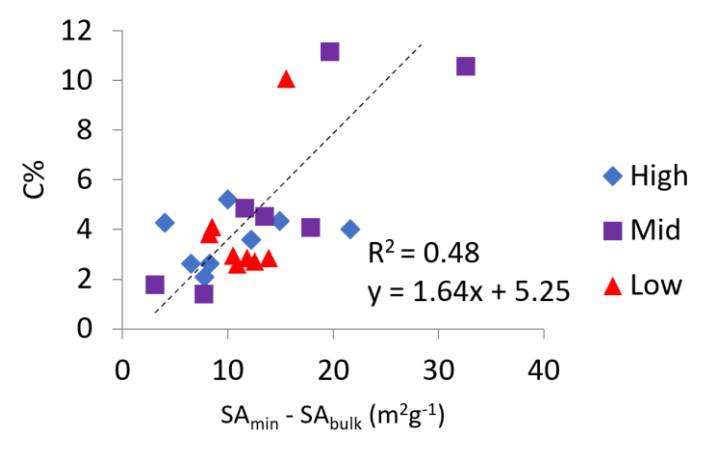

Figure 2.6.

NL-BELT surface mineral horizon soil organic matter %C and %N relationships with mineral surface area (SA_{min} is the surface area after organic matter removal), and pyrophosphate extracted Al and Fe in the mineral soil (Al_{pp} and Fe_{pp}). Black trend lines indicate no difference among regions, coloured dotted trend lines show regional trend where significant ($p < 0.05$).

2.4 Discussion

2.4.1 Organo-mineral complexes are the dominant feature explaining SOM variance

I found that both Fe and Al OMCs, as indicated by Fe_{pp} and Al_{pp} proxies, were components of the best models for describing mineral soil C and N variation. The importance of OMCs in predicting SOM was not surprising given their known role in podzolization in boreal forests (Kleber, 2015). The identification of metal weathering product controls on SOM has been demonstrated in global and continental-scale studies spanning many forest and soil types and moisture regimes (Torn et al., 1997; Doetterl et al., 2015; Rasmussen et al., 2018; Yu et al., 2021), and have highlighted the importance of

climate and geology on SOM content. Here I was able to explore these climate-geology interactions through the focus on a single ecosystem type exhibiting a large vulnerable C reservoir and at a regional spatial scale relevant for our predictive understanding of climate change impacts on SOM on decadal to century time scales (Ziegler et al. 2017).

While climate related increases in C inputs are observed across the regions of the NL-BELT (Ziegler et al. 2017), mineral soil C content is not controlled by these inputs. Regional variability in SOC content can make it difficult to attribute the role of inputs. However, the fact that soil N content was in part explained by N source or input across the transect indicates that detecting associations between inputs and SOM were feasible here. This makes sense because N is often limiting, and shallow rooting depths (Schenk and Jackson, 2002) limit the availability of soil N sources to mineral soils to a greater extent than soil C in boreal forests (Tamm, 2012). This is consistent with longer retention times of N relative to C in the organic horizons and increased N cycling with climate warming in these forest sites (Philben et al., 2016; Myers-Pigg et al., submitted; Podrebarac et al., unpublished results).

However, supporting the results of Rasmussen et al. (2018), von Fromm et al. (2021), and Yu et al. (2021), the clay size fraction was also poor at predicting SOM content in our study. This may be explained by: (1) the fact that a significant portion of the clay-size fraction in these soils is composed of minerals that are not reactive with OM such as quartz and feldspar (2) OMCs only make up a portion of the clay fraction as they sometimes form aggregates, and (3) not all clay surfaces are available for binding to OM (Schweizer et al., 2021).

Similarly, the SA_{bulk} was considered here as a SOM predictor because of the importance of available surfaces for organo-mineral interactions (Eusterhues et al., 2005; Mikutta et al., 2008). However, the bulk measure of SA does not provide a true measure of the mineral SA available for these associations, only the surfaces of aggregates. This may explain why SA_{bulk} was not a good predictor. Here, I went a step further by removing OM to expose the surfaces where organo-mineral interactions could potentially occur and a significant increase in SA was measured. This increase is explained by the breaking up of OM-mineral aggregates and opening of sites on minerals (i.e., for quantification by gas adsorption). Strong positive correlations between SA_{min} and pyrophosphate-extracted metals suggest that these metals make up much of the mineral SA available to interact with OM. As expected, SA_{min} was a better predictor, describing about half of its variance (R^2 = 0.48 and 0.52 for % C and % N, respectively), confirming that OM is largely found in association with mineral surfaces. The positive relationships among SA_{min} and %C and %N were best observed in the mid latitude region because of the exceptionally high within-region variability, with an explained variance of 0.78 and 0.87, respectively (Figure 2.6). This is also true for OMC relationships with % C and % N that are driven strongly by the mid-region. Assuming climate and the DOM flux are relatively consistent within this region, the large range in % C and % N here must be explained by variations in soil properties. Highly variable geological parent types in the mid- region, that include some of the most- (ophiolites, carbonates) and least- (quartz dominant siliciclastic) weatherable rock types (Table 2.1), suggest that parent material plays a significant role in OM sequestration as it can strongly influence the soil matrix and weathering products (Gartzia-Bengoetxea et al., 2020).

2.4.2 Strong association between SOM and Al, relative to Fe complexes, indicates important role of redox in these shallow upland forest soils

While both metals were major components of the best models, those containing Al_{pp} performed better than Fe_{pp}, likely due to the redox sensitivity of Fe, such that Fe^{2+} is significantly more soluble than its oxidized counterpart whereas Al solubility is not impacted by soil redox change (Nierop et al., 2002; Jansen et al., 2003; Knorr, 2013). This greater association of Al OMC with %C has been identified in wetlands, seasonally flooded soils, and even poorly drained podzols (Banik et al., 2014; Lacroix et al., 2019), but was not expected in well-drained upland podzols. In flooded low-oxygen soils, reducing environments allow for precipitation of Al OMC, while reduced Fe^{2+} OMC remains soluble and is lost from the soil. But what conditions reduce the role of Fe relative to Al in these well-drained upland soils is less clear.

The abundance of OMCs and their control on SOM is a balance of precipitation and loss. Formation of soluble OMCs in the DOM solution is dependent on the primary mineral weathering rate as determined broadly by the water flux and contribution of elements from parent materials (Slessarev et al., 2021). Precipitation of these products in the mineral horizon is a function of the Al to C ratio of the solution and an increase in pH at depth that decreases their solubility. Remobilization, or loss, of OMCs can result from further interactions with new acidic DOM (Lundstrom et al., 2000), or development of reducing conditions that impact Fe stability only (Nierop et al., 2002). Here, I propose that seasonally driven changes in hydrology likely impact the formation and loss of Fe and Al

OMCs and their controls on mineral horizon SOM in these upland mesic forest soils (Figure 2.7).

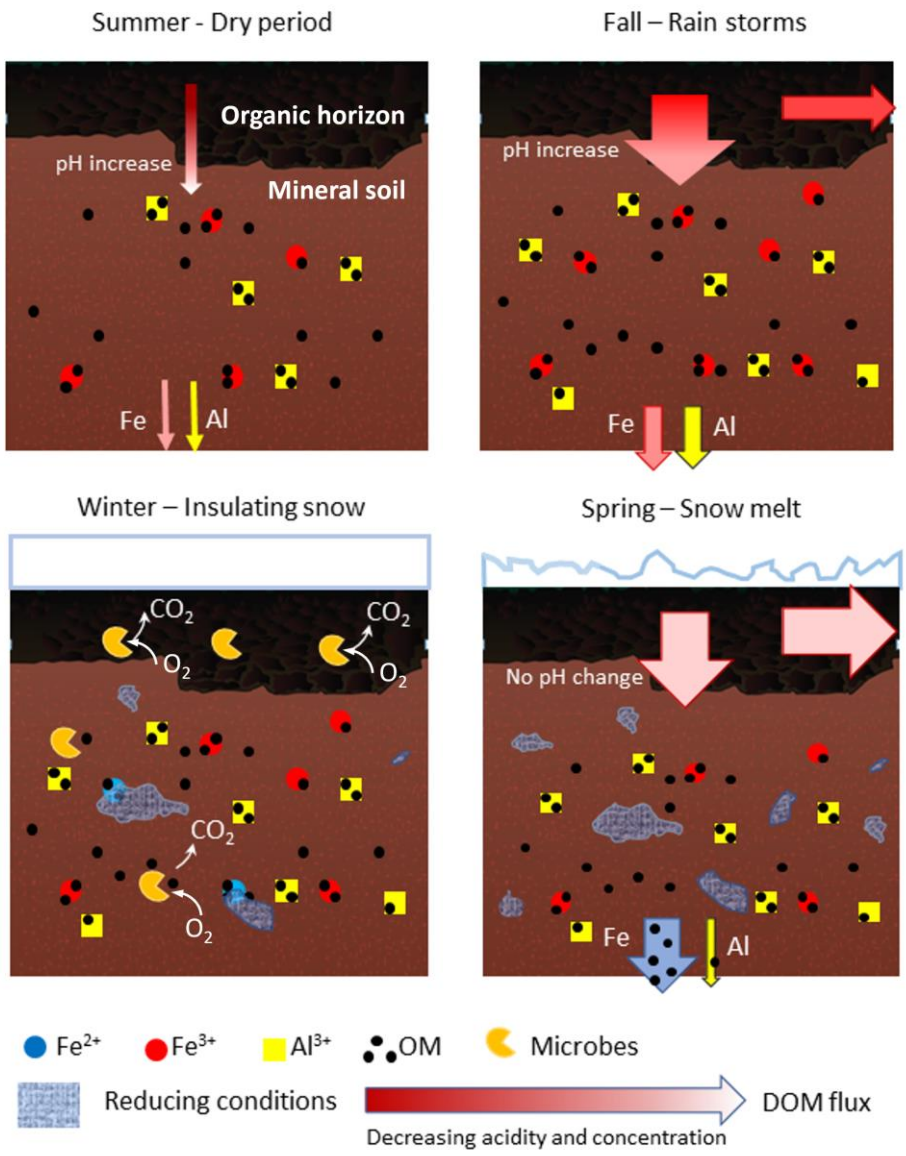

Figure 2.7.

Schematic diagram of impact of seasonal hydrology on the production and loss of organo-metal complexes (OMCs) leading to increased C association with Al complexes. Arrows indicate dissolved organic matter direction (downward percolation or lateral), relative volume (size of arrow), concentration (colour) and change in pH as it flows from the organic to mineral soil horizon (change in colour). Both Fe and Al-OMCs precipitate in the mineral soil with increased pH in lower soil horizons. Reducing conditions formed under

the snowpack and in saturated soils of the spring melt reduce and mobilize Fe-OMCs but leave Al-OMCs unaffected.

During the dry summer months, DOM from the overlying organic horizon is more concentrated and acidic (Bowering et al., 2020). The increase in pH as it percolates down to the oxic mineral horizon promotes the precipitation of both Fe and Al OMCs. Fall rainstorms bring a higher flux of relatively less concentrated but acidic DOM, further precipitating both OMCs with increasing pH conditions. Inputs are greatly reduced during the winter when a thick snowpack insulates the soil in these forests (Bowering et al., 2022). Microsites of reducing conditions likely form beneath the snowpack as oxygen is depleted, or during the spring melt when the higher water flux saturates the soil over a period of several weeks, as has been observed by others even in well-drained soils (e.g., Wang and Bettany, 1995; Bjork et al., 2008; Yin et al., 2019). The higher pH of a more dilute DOM delivered during the spring melt likely results in the formation of relatively less OMCs than the summer and fall seasons, and the locally reducing conditions promote the reduction and removal by dissolution of more Fe OMC relative to Al OMC which remains unaffected by the redox changes. These seasonal dynamics, over time, likely cause Al OMCs to accumulate relative to Fe and suggest that seasonal changes in hydrology play an important role in regulating soil conditions that control SOM sequestration.

I expect that OMCs are also a main control on SOC in deeper horizons, varying as a function of weathering rates, hydrology, and C input. As such, a lower flux of DOM at depth likely forms less OMCs, therefore stabilizing less SOC. However, the extent of Fe OMC solubilization may be reduced in deeper horizons relative to shallow soils as the

saturated soils and microbial activity that promote anoxic conditions are likely more limited at depth in well drained soils (Keiluweit et al., 2016 and 2017). However, redox conditions and impacts on Fe OMC solubilization is likely dependent upon hillslope hydrology and thus a function of soil characteristics and consequential hydrologic flow paths and soil water residence times.

2.4.3 Results suggest that shifts in form and timing of precipitation with climate change will impact mineral SOM stores in these forests

The results of this study suggest that mineralogically-controlled mechanisms are a first-order control on mineral soil C and N content in this boreal forest region. This explains the observed relative constancy of SOC stocks despite increased inputs across the transect and high within-region variability. However, the stability of OMCs that bind to SOM are controlled by pH and redox conditions of the soil, of which, snow dynamics play an important role. Therefore, climate change induced shifts in hydrology may affect SOM in these forests.

An increase in temperature and precipitation is expected for this region with climate change, accompanied by changes in snow dynamics and seasonal hydrology. Such changes include reductions in snowpack duration, shifts in the timing and volume of the delivery of water to the soil, and consequently, the increased mobilization of DOM from the organic horizon (Bowering et al., 2022). The snowpack provides insulation and protection from frost so that SOM degradation continues throughout the winter, and also holds a large volume of water that is released rapidly in the spring. This results in the

mobilization of a large volume of relatively more dilute solution of degraded DOM from the organic horizon and a short soil water residence time for potential interactions with weathering products as water saturated conditions for lateral flow initiation are reached during this period of rapid infiltration (Bowering et al. 2020). Thus, when the snowpack is reduced, as observed during warmer winters, more DOM is mobilized from the organic horizon on an annual basis (Bowering et al., 2022). This suggests that higher DOM mobilization will accompany climate change with implications for mineral soil C and N stores.

These shifts in snowpack dynamics and their associated impact on DOM mobilization with climate change can impact OMC production and stability through changes in DOM concentration and pH, weathering rate, flow paths, and redox conditions. Under current conditions, Al OMCs are more clearly associated with SOM in these shallow soils, likely as a result of the loss of some solubilized Fe complexes under reducing conditions occurring during winter and spring seasons (Figure 2.7). A reduced snowpack season and lower melt volume may result in less solubilization of Fe OMCs in shallow soils. The role of both Al and Fe OMCs could be further enhanced if the predicted increase in precipitation also enhances weathering rates that promote their production (Slessarev et al., 2021). Further, a greater proportion of precipitation in the form of rain and more frequent and smaller winter melts may result in greater infiltration of DOM potentially into deeper mineral soils that have higher OM sequestration potential (Patrick et al., unpublished results). However, the overall understanding of the potential outcome of these shifts in precipitation and snowpack with climate change are dependent upon

understanding the forest soil hydrology, and thus emphasizes the importance of understanding indirect hydrologic impacts of climate change on mineral soil OM stores. Understanding how these hydrological shifts may impact SOM stores is key for predictive models.

2.5 Conclusions

This study investigated factors controlling soil organic C and N in boreal forest mineral soils within a region where SOC is considered vulnerable due to the high effective moisture that could result in changes in proportion of SOC associated with reactive minerals (Kramer and Chadwick, 2018). Although Fe and Al weathering products are often considered together, this study evaluated their roles separately and in doing so identified potentially important drivers associated with climate change in these vulnerable boreal forest regions. Specifically, evidence here indicates (1) mineralogically-controlled mechanisms dominate over climate and some climate-controlled ecosystem parameters (e.g., soil inputs as litterfall and DOC) in regulating SOC of surface mineral soils; and consequently, (2) soil redox and pH conditions likely regulate the dynamics of SOC. These results suggest that the climate change driven shifts in precipitation form and timing and soil DOM inputs predicted for the next century in these boreal forests can illicit significant change in mineral SOC dynamics. This underscores our need to understand forest hydrology, specifically the hydrologic controls on mineral soil adsorption and desorption

of C to enhance our understanding of how this large dynamic C reservoir will respond to climate change.

2.6 References

Anderson, D.R., Burnham, K.P. and Thompson, W.L., 2000. Null hypothesis testing: problems, prevalence, and an alternative. J. of Wildlife Management. 64(4), 912-923.

Arnarson, T. S., Keil, R. G., 2000. Mechanisms of pore water organic matter adsorption to montmorillonite. Marine Chem. 71(3-4), 309-320.

Arnold, T. W., 2010. Uninformative parameters and model selection using Akaike's Information Criterion. J. of Wildlife Management 74(6), 1175-1178.

Baldock, J. A., Skjemstad, J. O., 2000. Role of the soil matrix and minerals in protecting natural organic materials against biological attack. Org. Geochem. 31(7), 697-710.

Banik, C., Harris, W. G., Ellis, R., Hurt, W., Balboa, S., 2014. Relations of iron, aluminum, and carbon along transitions from Udults to Aquods. Geoderma 226, 332-339.

Barré, P., Durand, H., Chenu, C., Meunier, P., Montagne, D., Castel, G., et al., 2017. Geological control of soil organic carbon and nitrogen stocks at the landscape scale. Geoderma, 285, 50–56.

Barrett, E. P., Joyner, L. G., Halenda, P. P., 1951. The determination of pore volume and area distributions in porous substances. I. Computations from nitrogen isotherms. J. of the Am. Chem. Soc. 73(1), 373-380.

Björk, R.G., Björkman, M.P., Andersson, M.X., Klemedtsson, L., 2008. Temporal variation in soil microbial communities in Alpine tundra. Soil Biology and Biochemistry, 40(1), 266-268.

Bowering, K.L., Edwards, K.A., Prestegaard, K., Zhu, X. and Ziegler, S.E., 2020. Dissolved organic carbon mobilized from organic horizons of mature and harvested black spruce plots in a mesic boreal region. Biogeosciences, 17(3), 581-595.

Bowering, K.L., Edwards, K.A., Wiersma, Y.F., Billings, S.A., Warren, J., Skinner, A. and Ziegler, S.E., 2022. Dissolved Organic Carbon Mobilization Across a Climate Transect of Mesic Boreal Forests Is Explained by Air Temperature and Snowpack Duration. Ecosystems, 1-17. https://doi.org/10.1007/s10021-022-00741-0.

Brookes, I. A., 1977.Geomorphology and Quaternary geology of Codroy Lowland and adjacent plateaus, southwest Newfoundland. Can. J. of Earth Sci. 14(9), 2101-2120.

Brunauer, S., Emmet, P.H., Teller, E., 1938. Adsorption of gases in multimolecular layers. J. of the Am. Chem. Soc. 60, 309.

Burnham, K. P. & D. R. Anderson, 1998. Model selection and interference: a practical information theoretical approach. Springer, New York.

Burnham, K. P., D. R. Anderson, 2002. Model selection and multimodel inference: a practical-theoretic approach. Springer-Verlag.

Colman-Sadd, S.P., Hayes, J.P., Knight, I., 2000. Geology of the Island of Newfoundland (Digital version of Map 90-01 with minor revisions). Newfoundland Department of Mines and Energy, Geological Survey, Map 2000-30, scale 1:1 000 000.

Courchesne, F., Turmel, M. C., 2008. Extractable Al, Fe, Mn, and Si. In 'Soil sampling and methods of analysis'. (Eds MC Carter, EG Gregorich) 307–315.

Doetterl, S., Stevens, A., Six, J., Merckx, R., Van Oost, K., Pinto, M. C., Boeckx, P., 2015. Soil carbon storage controlled by interactions between geochemistry and climate. Nature Geosci. 8(10), 780-783.

Eusterhues, K., Rumpel, C., Kögel-Knabner, I., 2005. Organo-mineral associations in sandy acid forest soils: importance of specific surface area, iron oxides and micropores. Euro. J. of Soil Sci. 56(6), 753-763.

Feng, Xiaojuan, André J. Simpson, Myrna J. Simpson, 2005. Chemical and mineralogical controls on humic acid sorption to clay mineral surfaces. Org. Geochem. 36 (11), 1553-1566.

Friedlingstein, P., Meinshausen, M., Arora, V.K., Jones, C.D., Anav, A., Liddicoat, S.K. and Knutti, R., 2014. Uncertainties in CMIP5 climate projections due to carbon cycle feedbacks. Journal of Climate, 27(2), 511-526.

Gartzia-Bengoetxea, N., Virto, I., Arias-González, A., Enrique, A., Fernández-Ugalde, O. and Barré, P., 2020. Mineral control of organic carbon storage in acid temperate forest soils in the Basque Country. Geoderma, 358, 113998.

Geng, J., Fang, H., Cheng, S. and Pei, J., 2021. Effects of N deposition on the quality and quantity of soil organic matter in a boreal forest: Contrasting roles of ammonium and nitrate. Catena, 198, 104996.

Gillman, G. P., E. A. Sumpter, 1986. Modification to the compulsive exchange method for measuring exchange characteristics of soils. Soil Research 24(1), 61-66.

Gower, C. F., 1998. Geology of the upper Eagle River map region, Grenville Province, southeast Labrador. Current Research (1998) Newfoundland Department of Mines and Energy, Geological Survey, 98-1.

Hassink, J., 1997. The capacity of soils to preserve organic C and N by their association with clay and silt particles. Plant Soil 191, 77–87.

Heckman, K., Lawrence, C.R. and Harden, J.W., 2018. A sequential selective dissolution method to quantify storage and stability of organic carbon associated with Al and Fe hydroxide phases. Geoderma, 312, 24-35.

IPCC, Climate Change 2013: The Physical Science Basis. Contribution of 31 Working Group I to the Fifth Assessment Report of the Intergovernmental Panel on Climate Change. Stocker, T.F., D. Qin, G.-K. Plattner, M. Tignor, S.K. Allen, J. Boschung,

A. Nauels, Y. Xia, V. Bex and P.M. Midgley (eds.). Cambridge University Press, Cambridge, United Kingdom and New York, NY, USA, 1535 pp. 2013.

Jansen, B., Nierop, K. G., Verstraten, J. M., 2003. Mobility of Fe (II), Fe (III) and Al in acidic forest soils mediated by dissolved organic matter: influence of solution pH and metal/organic carbon ratios. Geoderma, 113(3-4), 323-340.

Jobbágy, E. G., Jackson, R. B., 2000. The vertical distribution of soil organic carbon and its relation to climate and vegetation. Ecol. App. 10(2), 423-436.

Kaiser, K., and Guggenberger, G. 2003. Mineral surfaces and soil organic matter. Euro. J. of Soil Sci. 54(2), 219-236.

Keiluweit, M., Nico, P.S., Kleber, M. and Fendorf, S., 2016. Are oxygen limitations under recognized regulators of organic carbon turnover in upland soils?. Biogeochem., 127(2), 157-171.

Keiluweit, M., Wanzek, T., Kleber, M., Nico, P. and Fendorf, S., 2017. Anaerobic microsites have an unaccounted role in soil carbon stabilization. Nature comm., 8(1), 1-10.

King, G. A., 1985. A standard method for evaluating radiocarbon dates of local deglaciation: Application to the deglaciation history of southern Labrador and adjacent Québec. Géographie physique et Quaternaire 39(2), 163-182.

Kleber, M., Eusterhues, K., Keiluweit, M., Mikutta, C., Mikutta, R., Nico, P. S., 2015. Mineral–organic associations: formation, properties, and relevance in soil environments. Adv. in Agronomy 130, 1-140

Knorr, K. H., 2013. DOC dynamics in a small headwater catchment as driven by redox fluctuations and hydrological flow paths - are DOC exports mediated by iron reduction/oxidation cycles? Biogeosciences 10, 891–904.

Kramer, M. G., and Chadwick, O. A., 2018. Climate-driven thresholds in reactive mineral retention of soil carbon at the global scale. Nature Climate Change 8(12), 1104.

LaCroix, R. E., Tfaily, M. K., McCreight, M., Jones, M. E., Spokas, L., Keiluweit, M., 2019. Shifting mineral and redox controls on carbon cycling in seasonally flooded mineral soils. Biogeosciences 16, 2573–2589.

Lawrence, C.R., Harden, J.W., Xu, X., Schulz, M.S. and Trumbore, S.E., 2015. Long-term controls on soil organic carbon with depth and time: A case study from the Cowlitz River Chronosequence, WA USA. Geoderma 247, 73-87.

Lundström, U. S., van Breemen, N., Bain, D., 2000. The podzolization process. A review. Geoderma 94(2-4), 91-107.

Maaroufi, N.I., Nordin, A., Hasselquist, N.J., Bach, L.H., Palmqvist, K. and Gundale, M.J., 2015. Anthropogenic nitrogen deposition enhances carbon sequestration in boreal soils. Global change biol. 21(8), 3169-3180.

Mäkipää, R., Karjalainen, T., Pussinen, A. and Kellomäki, S., 1999. Effects of climate change and nitrogen deposition on the carbon sequestration of a forest ecosystem in the boreal zone. Can. J. of Forest Research 29(10), 1490-1501.

Marschner, B., Kalbitz, K., 2003. Controls of bioavailability and biodegradability of dissolved organic matter in soils. Geoderma 113(3-4), 211-235.

Marty, C., Houle, D., Gagnon, C., 2015. Effect of the Relative Abundance of Conifers Versus Hardwoods on Soil δ 13 C Enrichment with Soil Depth in Eastern Canadian forests. Ecosystems 18(4), 629-642.

Masiello, C. A., Chadwick, O. A., Southon, J., Torn, M. S., Harden, J. W., 2004. Weathering controls on mechanisms of carbon storage in grassland soils. Global Biogeochem. Cycles 18(4), GB4023.

McGuire, A.D., Wirth, C., Apps, M., Beringer, J., Clein, J., Epstein, H., Kicklighter, D.W., Bhatti, J., Chapin III, F.S., De Groot, B. and Efremov, D., 2002. Environmental variation, vegetation distribution, carbon dynamics and water/energy exchange at high latitudes. J. of Vegetation Sci. 13(3), 301-314.

McCuaig, S. J., 2002. Quaternary geology of the Alexis River area, and the Blanc-Sablon to Mary's Harbour road corridor, southern Labrador. Current Research. Newfoundland Dept. of Mines and Energy, Geol. Survey Branch, Report, 02-1.

McCullagh, P. and Nelder, J.A., 1989. Binary data. In Generalized linear models (pp. 98-148). Springer US.

McKeague, J. A., J. E. Brydon, N. M. Miles, 1971. Differentiation of forms of extractable iron and aluminum in soils. Soil Sci. Society of Am. J. 35, 33– 38.

Mikutta, C., Mikutta, R., Bonneville, S., Wagner, F., Voegelin, A., Christ, I., Kretzschmar, R., 2008. Synthetic coprecipitates of exopolysaccharides and ferrihydrite. Part I: Characterization. Geochimica et Cosmochimica Acta 72(4), 1111-1127.

Nierop, K. G., Jansen, B., Verstraten, J. M., 2002. Dissolved organic matter, aluminum and iron interactions: precipitation induced by metal/carbon ratio, pH and competition. Sci. of the Total Env. 300(1-3), 201-211.

Oades, J. M., 1988. The retention of organic-matter in soils. Biogeochem. 5(1), 35–70.

Olsson, M. T., Erlandsson, M., Lundin, L., Nilsson, T., Nilsson, Å., Stendahl, J., 2009. Organic carbon stocks in Swedish Podzol soils in relation to soil hydrology and other site characteristics. Silva Fennica 43(2), 209-222.

Oren, R., Ellsworth, D.S., Johnsen, K.H., Phillips, N., Ewers, B.E., Maier, C., Schäfer, K.V., McCarthy, H., Hendrey, G., McNulty, S.G., Katul, G.G., 2001. Soil fertility limits carbon sequestration by forest ecosystems in a CO 2-enriched atmosphere. Nature 411(6836), 469.

Pan, Y., Birdsey, R.A., Fang, J., Houghton, R., Kauppi, P.E., Kurz, W.A., Phillips, O.L., Shvidenko, A., Lewis, S.L., Canadell, J.G., Ciais, P., 2011. A large and persistent carbon sink in the world's forests. Science 333(6045), 988-993.

Philben, M., Ziegler, S.E., Edwards, K.A., Kahler, R. and Benner, R., 2016. Soil organic nitrogen cycling increases with temperature and precipitation along a boreal forest latitudinal transect. Biogeochem. 127(2-3), 397-410.

Porras, R.C., Pries, C.E.H., McFarlane, K.J., Hanson, P.J. and Torn, M.S., 2017. Association with pedogenic iron and aluminum: effects on soil organic carbon storage and stability in four temperate forest soils. Biogeochem. 133(3), 333-345.

Putt, M. M., Bell, T., Batterson, M. J., Smith, J. S., 2010. Late Wisconsinan ice-flow history on the tip of the Northern Peninsula, Northwestern Newfoundland. Current Research (2010), Newfoundland and Labrador Department of Natural Resources, Geol. Survey, Report 10, 1, 171-182.

Rasmussen, C., Heckman, K., Wieder, W.R., Keiluweit, M., Lawrence, C.R., Berhe, A.A., Blankinship, J.C., Crow, S.E., Druhan, J.L., Pries, C.E.H., Marin-Spiotta, E. 2018. Beyond clay: towards an improved set of variables for predicting soil organic matter content. Biogeochem. 137(3), 297-306.

Ricketts, M.J., 2001. Granular aggregate mapping in NTS map areas 1N/2, 1N/11, 110/14 and 110/15. Current Research, Newfoundland Department of Mines and Energy, Geol. Survey Report 2001-1, 279-291.

Ricketts, M. J., Vatcher, S. V., 1996. Granular aggregate-resource mapping in the Roddickton-Main Brook area, Great Northern Peninsula, Newfoundland. Current Research. Newfoundland Department of Natural Resources, Geological Survey, Report, 96-1.

Scharlemann, J. P., Tanner, E. V., Hiederer, R., Kapos, V., 2014. Global soil carbon: understanding and managing the largest terrestrial carbon pool. Carbon Management 5(1), 81-91.

Schenk, H.J., Jackson, R.B., 2002. The global biogeography of roots Ecological monographs, 72(3), 311-328.

Schweizer, S.A., Mueller, C.W., Höschen, C., Ivanov, P. and Kögel-Knabner, I., 2021. The role of clay content and mineral surface area for soil organic carbon storage in an arable toposequence. Biogeochemistry, 156(3), 401-420.

Siregar, A., Kleber, M., Mikutta, R., Jahn, R., 2005. Sodium hypochlorite oxidation reduces soil organic matter concentrations without affecting inorganic soil constituents. Euro. J. of Soil Sci. 56(4), 481-490.

Slessarev, E.W., Chadwick, O.A., Sokol, N.W., Nuccio, E.E. and Pett-Ridge, J., 2022. Rock weathering controls the potential for soil carbon storage at a continental scale. Biogeochem. 157(1), 1-13.

Soukup, D.A, Buck, B.J., Harris, W., 2008 Preparing soils for mineralogical analyses. Methods of Soil Analysis Part 5—Mineralogical Methods, SSSA Book Series 5.5: 13-31.

Stumm, W., 1992. Chemistry of the Solid-Water Interface, John Wiley, Hoboken, N. J.

Tamm, C.O., 2012. Nitrogen in terrestrial ecosystems: questions of productivity, vegetational changes, and ecosystem stability (Vol. 81). Springer Science & Business Media.

Torn, M. S., Trumbore, S. E., Chadwick, O. A., Vitousek, P. M., Hendricks, D. M., 1997. Mineral control of soil organic carbon storage and turnover. Nature 389(6647), 170-173.

Wagai, R., Mayer, L. M., Kitayama, K., 2009. Extent and nature of organic coverage of soil mineral surfaces assessed by a gas sorption approach. Geoderma 149(1-2), 152-160.

Wang, F.L., Bettany, J.R., 1995. Methane emission from a usually well-drained prairie soil after snowmelt and precipitation. Canadian Journal of Soil Science, 75(2), 239-241.

Welham, S.J., Gezan, S.A., Clark, S.J. and Mead, A., 2014. Statistical methods in biology: design and analysis of experiments and regression. CRC Press.

Wieder, W.R., Grandy, A.S., Kallenbach, C.M., Taylor, P.G, Bonan, G.B., 2015. Representing life in the Earth system with soil microbial functional traits in the MIMICS model. Geosci. Model Development 8(6), 1789–1808.

Wiesmeier, M., Urbanski, L., Hobley, E., Lang, B., von Lützow, M., Marin-Spiotta, E., van Wesemael, B., Rabot, E., Ließ, M., Garcia-Franco, N. and Wollschläger, U., 2019. Soil organic carbon storage as a key function of soils-A review of drivers and indicators at various scales. Geoderma, 333,149-162.

Yin, M., Gao, X., Tenuta, M., Gui, D., Zeng, F., 2019. Presence of spring-thaw N2O emissions are not linked to functional gene abundance in a drip-fertigated cropped soil in arid northwestern China. Science of The Total Environment, 695, 133670.

Yu, W., Weintraub, S.R., Hall, S.J., 2021. Climatic and geochemical controls on soil carbon at the continental scale: interactions and thresholds. Global Biogeochem. Cycles 35(3), 2020GB006781.

Zhou, X., Liu, D., Bu, H., Deng, L., Liu, H., Yuan, P., Du, P., Song, H., 2018. XRD-based quantitative analysis of clay minerals using reference intensity ratios, mineral intensity factors, Rietveld, and full pattern summation methods: A critical review. Solid Earth Sci. 3(1), 16-29.

Ziegler, S. E., Benner, R., Billings, S. A., Edwards, K. A., Philben, M., Zhu, X., Laganière, J., 2017. Climate warming can accelerate carbon fluxes without changing soil carbon stocks. Frontiers in Earth Sci. 5, 2.

Zuur, A.F., Ieno, E.N. and Smith, G.M., 2007. Analysing ecological data (Vol. 680). New York: Springer.

Chapter 3: The influence of hillslope hydrology on soil carbon content: implications for climate impacts on boreal forest mineral soil stocks

Abstract

Boreal forests store ~ 30% of forest soil organic carbon (SOC) globally and expect enhanced precipitation in a changing climate. Dissolved organic matter (DOM) facilitates weathering to form organo-metal complexes (OMCs), which control SOC stability in these landscapes. Variations in hillslope hydrology alter DOM delivery, impacting SOC stabilization. Here, I investigate controls on SOC stabilization experimentally using soil columns built from boreal forest mineral horizon soils collected from upslope and footslope positions. A lower bulk density and a well-developed Ae horizon with OMC- and SOC-enriched horizons beneath support greater infiltration in the gently-sloped upslope position. Soil organic layer derived DOM was applied to the soil columns at rates representative of an extreme precipitation event for the region (150 mm day^{-1}). Changes in particulate and dissolved organic carbon (POC and DOC, respectively) were considered within the context of hillslope hydrology. Stabilization of DOC was dependent on OMC saturation with SOC in the soil (ratio of C to Al in OMCs), where relatively undersaturated deep horizons adsorbed significant DOC yet surface soils exhibited little net change. Surface soils were

further vulnerable to DOC desorption in response to rewetting after a dry period. Footslope soils were more vulnerable to POC loss despite having less SOC. Our results suggest that greater infiltration and longer soil water residence times supported by lower relief, upslope soil properties, will likely lead to enhanced capacity for SOC accrual at depth with climate change. In contrast, greater lateral flow in the footslope will reduce the capacity for deep SOC accrual and enhanced POC mobilization may lead to net losses. This work points to the need to incorporate hydrology and soil property interactions at hillslope scales to improve our predictive understanding of SOC in boreal forest landscapes.

3.1 Introduction

Boreal forests contain about 30% of the global forest soil organic carbon (SOC) stock (Pan et al., 2011; Scharlemann et al., 2014). These high latitude regions are expected to experience significant increases in temperature and precipitation (Lee et al. 2021). However, how this large C reservoir will be altered in response to climate change is poorly understood and contributes to the large uncertainty in our ability to predict C storage and release through atmosphere-land C exchange at global scales (Friedlingstein et al., 2014).

Soil forming processes link C dynamics and chemical weathering. In moist, acidic soils like boreal podzols, organic acids percolate downward as dissolved organic matter (DOM) to facilitate chemical weathering by chelating metals to form dissolved organo-metal complexes (OMCs; Kalbitz et al., 2000). These can precipitate as solid OMCs to stabilize organic matter (OM) in the underlying mineral horizon via increasing pH and metal to carbon ratio of the solution (Nierop et al., 2002). Thus, OMCs, particularly Al

OMCs, are a main control on shallow mineral horizon SOC content in boreal forests because they remain stable under changing redox conditions, unlike Fe OMCs (Patrick et al. 2022; Nierop et al. 2002).

At the continental scale, weathering rates control the abundance of OMCs, and SOC is greatest in regions with both excess water and Al-rich parent material (Slessarev et al., 2022). At the hillslope scale, however, spatial variations in hydrological processes and soil properties influence DOM delivery and soil water residence times relevant for OMC formation (Bachmair and Weiler, 2012; Hopp and McDonnell, 2009). Hydrology also controls particle redistribution, influencing hillslope particulate OM distribution and soil hydraulic properties that impact water flow and residence times (Holz and Augustin, 2021; Hu et al., 2016; Zhu et al., 2021).

The fate of dissolved organic carbon (DOC) and its contribution to SOC stores is regulated by soil water flow paths and residence time. Dissolved OMC formation is likely greatest during high DOM flux events such as the spring melt and autumn storm hydrological periods. Vertical infiltration tends to be greatest during these events (Schaetzl et al. 2015; Schaetzl and Rothstein 2016), providing deeper mineral soils with a C source. Yet, observations of stream DOC also indicate significant runoff from shallow organic and mineral horizons with snow melt (Ågren et al., 2010) and large autumn precipitation events (Roebuck et al. submitted). This suggests that much of the dissolved OMCs formed during such events are lost with shallow runoff. Here, short soil water residence times likely limit their coprecipitation in shallow soils as the soil solution does not have sufficient time for weathering to reach the requisite metal concentrations (Nierop et al., 2002). Further, most

subsurface erosion occurs during rapid soil infiltration events, redistributing particulate carbon (Wei et al., 2017). As such, hillslope hydrological processes provide C to the mineral soil (as DOM), but also regulate the mechanisms of C stabilization and redistribution. Therefore, spatial and temporal variations in hillslope hydrology likely contribute to spatial variability in SOC content at the hillslope scale.

The timing and amount of water delivered to the mineral horizon in boreal regions will likely be impacted by climate change with a diminishing spring melt water flux, increasing summer evapotranspiration rates and extent of soil drying, and increasing frequency and precipitation intensity of autumn storms, including formation of atmospheric rivers (Finnis and Daraio 2018; Laudon et al. 2013; Helbig et al. 2020; Hsu and Chen 2020; Wang et al. 2021). Enhanced mobilization of DOC from organic horizons may occur with warmer winters with shorter snowpack seasons, producing higher DOC inputs to the mineral soil in moist boreal forests (Bowering et al. 2022). Mineral horizon DOC uptake has been experimentally measured under conditions of low water fluxes, low volumes, and long soil water residence times (e.g., Jansen et al. 2005; Kothawala et al. 2009, 2012; Nierop et al. 2002; Zolovkina et al. 2018). However, DOC uptake (or loss) under rapid infiltration conditions associated with increasing fall event size and atmospheric rivers has not yet been evaluated (Gimeno et al. 2014; Hsu and Chen 2020). Further, DOC uptake likely varies spatially in the hillslope with soil characteristics and may depend on how saturated Al OMCs are with C in the soil as space for interactions with OM is limited (Masiello et al. 2004). Thus, hillslope scale studies are needed to understand the role of hydrology on mechanisms of C stabilization and redistribution as they relate to SOC

content for our predictive understanding of how boreal forest SOC may respond to climate change.

I employ a combination of observations and experimentation using two hillslope positions within the Pynn's Brook Experimental Watershed Area in eastern Canada to address the following broad questions: (1) How do SOC and soil characteristics related to SOC stability vary by hillslope position where hydrologic controls likely differ? (2) What soil characteristics and conditions controlled at the event scale (event factors; e.g., soil moisture, soil solution composition) likely control SOC response to extreme precipitation events? (3) How may SOC response to the extreme precipitation events vary by hillslope position? To begin to address these questions, I first evaluated SOC and soil characteristics within the context of interpreted hydrological differences by hillslope position. Next, I experimentally investigated controls on SOC response to high intensity precipitation conditions by measuring C uptake and loss as DOM was percolated through the constructed soil columns. Using replicated soil columns, the net change in soil C was related to soil characteristics and spatial position to provide insight on potential mechanisms that contribute to SOC content and how such mechanisms may be impacted by changing hydrology. Event factors were further manipulated to evaluate ephemeral controls related to event or seasonal timescale (e.g., event timing and associated antecedent soil moisture). These controls were considered in the context of the impact of short-term climate change on hydrology to interpret SOC fate in these wet boreal soils. I hypothesize that stabilization of added soil DOC is controlled by the degree of saturation of OMC with C in the soil with greater DOC uptake into SOC at depth where DOC inputs are limited. I further anticipate

greater OMC and SOC content to have developed in upslope shallow relief soils experiencing longer soil water residence times and more vertical infiltration relative to footslope soils in the hillslope studied. The results will aid in our predictive understanding of boreal forest SOC by providing new hypotheses regarding the mechanisms that control SOC response to local shifts in hydrology with climate change.

3.2 Materials and methods

3.2.1 Study area

The Pynn's Brook Experimental Watershed Area, located near Deer Lake in western Newfoundland and Labrador (Canada), experiences a mean annual temperature of 3.6 °C and receives approximately 1095 mm of precipitation annually (Environment Canada Climate Normals, Deer Lake Airport 1981 – 2010). This mesic boreal forest is underlain by humo-ferric podzolic soils and is dominated by black spruce (*Picea mariana*) (Moroni et al. 2009).

The spring melt is currently the largest hydrological event of the year in this region, delivering a large volume of relatively dilute DOM to the mineral soil (~20 – 30 mg C L^{-1}; Bowering et al., 2020). While the autumn season receives a similar total volume of water, it is dispersed among multiple rain events, but DOC concentrations are about twice as high, producing a larger flux of soil DOC (~40 – 70 mg C L^{-1}; Bowering et al. 2020). Dry soil periods are frequent during the summer with the mineral soil receiving

about half the water flux of the autumn or spring seasons but at the highest DOC concentration. During the winter, water flux and DOC concentration are lowest due to snowpack insulation that prevents flow through soil organic horizons (Bowering et al. 2020) and promotes net loss via decomposition (Bowering et al. 2023).

The study region was completely glaciated during the Quaternary, with ice retreating at ~ 13000 YBP and soils restarted pedogenesis from fresh glacial till deposits (Batterson & Catto 2001). Deposits are generally less than 3 m thick, poorly sorted, with clasts of granites, porphyry, sandstone and siltstone (Batterson and Catto, 2001). X-ray diffraction of till collected in the study area indicate that quartz is the most abundant mineral, followed by plagioclase, muscovite, chlorite, K-feldspar and biotite (Table S3.1a; average major oxides in Table S3.1b).

The study site was divided into eight roughly 50 × 50 m plots. In this study, I employ two neighboring plots of mature black spruce forest oriented parallel to the slope. The upslope plot is gently sloped at 6° and well-drained, while the footslope is moderately sloped at 12° and situated just upslope from wetlands, resulting in a relatively higher water table (Figure 3.1). The organic horizon is approximately 12 cm thick, and the Ae horizon is relatively-well developed in the upslope but discontinuous and thin, or non-existent in the footslope (Gates et al., in revision). Below the Ae horizon, in descending order, are Bf, Bfj, BC mineral horizons, all of similar thickness across the hillslope (Gates et al., in revision). A Bf horizon exhibits > 0.6% pyrophosphate-extractable Fe + Al and 0.5 – 5% SOC, the Bfj exhibits < 0.6% pyrophosphate-extractable Fe + Al, and the BC is a transitional mineral horizon that displays some characteristics of the compacted rock C

horizon (Canadian System of Soil Classification; Gates, Masters Thesis, 2022). The Bf and Bfj have a significantly higher soil density (soil per volume of soil filled spaces only) and sand proportion in the footslope depositional zone (Gates, Masters Thesis, 2022). Upslope SOC content is enriched in the Bf and Bfj horizons relative to the Ae and deeper horizons (Figure S3.1a in Appendix). The footslope has relatively less SOC than the upslope in all horizons (1.75 ± 2.0 kg C m^{-2} versus 2.25 ± 0.7 kg C m^{-2}) and does not exhibit a shallow enrichment (Gates, Masters Thesis, 2022).

3.2.2 Experimental design

Soils were collected during the 2019 field season. Six 1 × 1 m^2 soil pits were carefully excavated, three at each slope position (Figure 3.1). Three replicates from each of the Bf and BC horizons were sampled from the wall face in each soil pit using clean trowels (n = 36). Samples were stored in sealed plastic bags and kept at 5°C until they were gently sieved at field soil moisture to 2 mm, weighed and set to air dry. Once dry, the three replicate soils were pooled by weight (n = 12) and homogenized. Soils were sub-sampled for the experimental columns and a portion was ground to a fine powder using a mortar and pestle for mineral soil characteristic analyses.

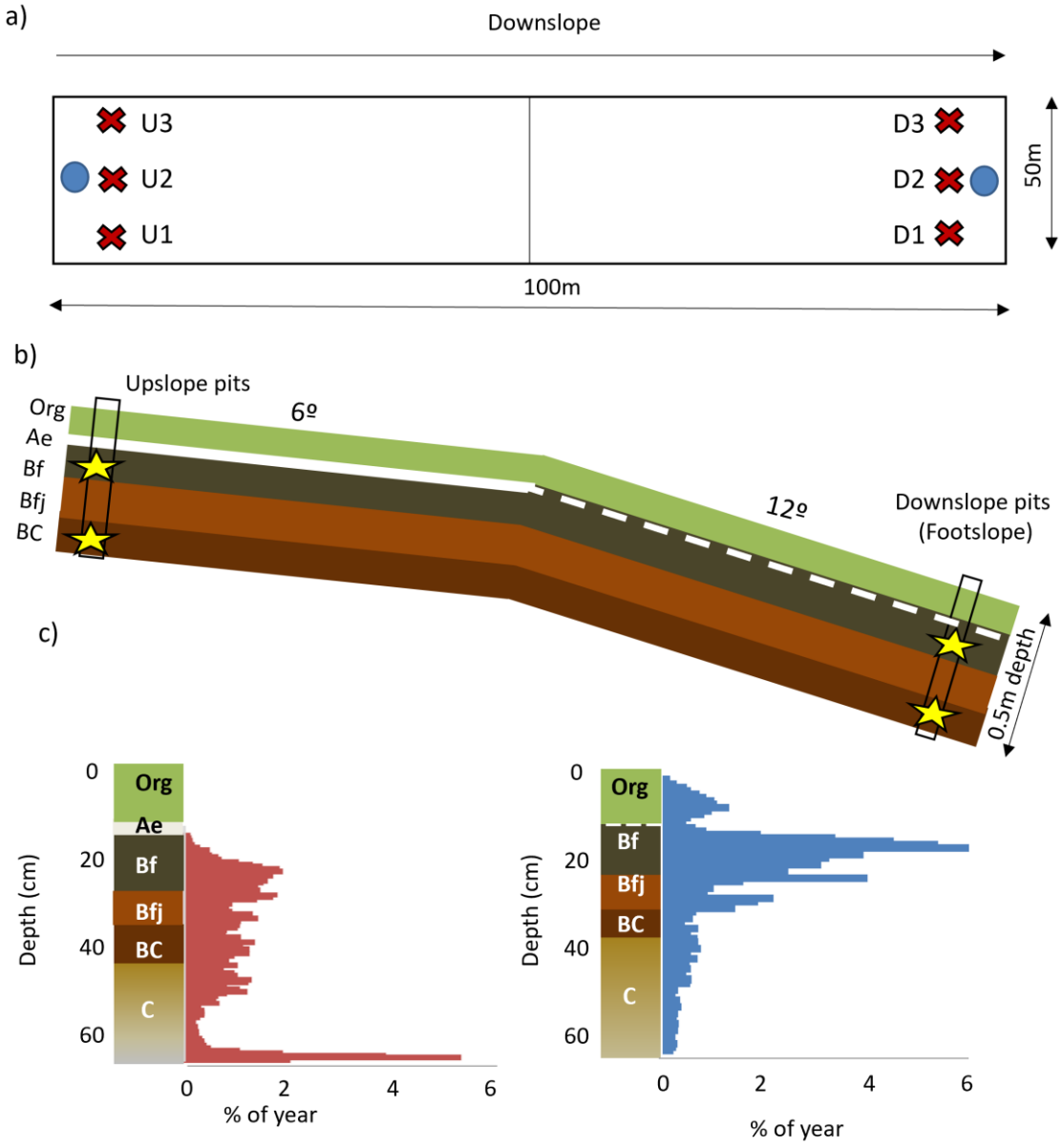

Figure 3.1.

Sample collection locations at the Pynn's Brook experimental watershed showing (a) top view of approximate location of soil pits (red crosses) and piezometers (blue circles); and (b) the cross-section side view of horizon collection points (yellow stars). U and D indicate upslope and downslope soil pits. Horizon designations based on the Canadian Soil Classification System, Org = organic layer, Ae = eluvial horizon, B = mineral horizon. (c) Annual frequency distribution of water depth for the upslope (red) and downslope (blue) locations derived from water level data collected in piezometers at 30 min intervals (January to November 2018). All frequency of depths below 65 cm were grouped into 65 cm increment in the upslope water level dataset.

Soil solution, providing DOM for the experimental additions, was collected from passive pan lysimeters distributed throughout the entire hillslope area of the forested plots (refer to Bowering et al. (2020) for details of the lysimeter design and installation). The soil water was pumped out three times during the late summer to autumn period of 2020 (early September to November). Once collected, it was filtered to 0.1 µm regularly and stored in the dark at 5 ˚C until needed (2 – 8 weeks).

Acrylic open-ended cylinders of 12 cm in height and 5 cm in diameter were used as soil columns. Polypropylene mesh screening was secured over the bottom and the column was supported on the opening of a clean (acid washed and combusted) glass jar for filtrate collection. Columns were filled with soil to 10 cm height with a soil density of 0.9 g cm^{-3}, and a rock volume of 20 or 38 cm^{-3} for the Bf and BC horizons, respectively (Table S3.2). These values of soil density and rock volume represent the average of each by horizon across all 6 soil pits sampled. A preliminary experiment determined that rock inclusion similar to field conditions significantly reduced soil compaction and retained near *in situ* soil bulk density following DOM solution application.

Soils were gently mixed with lysimeter water, adding the water slowly with a dropper, to 60 % of it's water holding capacity on clean aluminum foil prior to column packing. Because of high biological activity upon rewetting (Barnard et al., 2020), the soil columns were left to rest at 4°C in the dark for three weeks in loosely sealed mason jars prior to experiment execution.

The initial soil solution was filtered to 0.1µm before its application to the soil column (Figure 3.2). An aliquot of the initial filtered solution was collected each day for an initial measurement as the lysimeter water had been collected three times during the fall season and a range in solution characteristics was expected (Table 3.1). Three experimental replicate soil columns were prepared to produce 36 soil columns (three replications of 12 soils; from two horizons collected from 6 soil pits). Each of the 3 replicate soil columns received a different initial soil solution to compare how similar soils responded to soil solutions with different pH, and DOC and Al concentrations. Each column received three subsequent applications of the same solution to investigate differences in how soils responded to episodic wetting after a dry period (analogous to first autumn storm after dry summer) versus a second or third storm (Figure 3.2). Soil columns of the same replication (i.e. 1, 2 or 3) and application (i.e. 1, 2 or 3) were run simultaneously each week so that the same initial soil solution was applied to all within the same replication and application. See Table 3.1 for characteristics of the 9 initial soil solutions used to evaluate their influence on soil responses.

Individual applications were used as a proxy for individual storm events with their sequence from the initial application meant to represent the first event after the summer dry period with subsequent events occurring on soil with wetter antecedent conditions more similar to later fall conditions. For each application, 300 ml was added to each column in 20 ml intervals throughout the day. Each 20 ml application is approximately equal to a 10 mm rain event, for a total of a 150 mm storm event. This high infiltration rate is comparable to *in situ* stormflow conditions, maximizing particulate mobilization with the total

application of 150 mm within the range of recent extreme events in Newfoundland (e.g. 196 mm on Nov. 24, 2021, Port aux Basques (Station 73026) , and 200 mm on Sept. 11 2022, St. John's West (Station 71250) from Environment Climate Change Canada).

Table 3.1.

Characteristics of the initial soil solution collected from passive pan lysimeters under the organic horizons at the study site and applied to the column. The replicate column and application pairings are given here to clarify the initial solution characteristics provided in each case including dissolved organic carbon (DOC) concentration, aluminum (Al) concentration, molar Al:C and pH.

Replication	Application	DOC (mgC/L)	Al (ppb)	Molar Al:C	pH
1	1	68.79	931	0.00602	3.95
1	2	50.52	702	0.00619	4.27
1	3	45.79	698	0.00678	4.26
2	1	38.64	589	0.00679	4.46
2	2	69.34	469	0.00301	4.09
2	3	69.54	647	0.00414	4.24
3	1	59.43	960	0.00719	4.12
3	2	42.57	674	0.00704	4.31
3	3	72.14	1204	0.00743	4.38

Column leachate was immediately stirred, a 50 ml aliquot was then transferred to a beaker for pH measurement, and a measured volume was filtered through pre-combusted 25 mm Whatman GF/F filter (0.45µm) for particulate C and N analysis. The remaining solution was centrifuged, and the supernatant was sequentially filtered through pre-combusted Whatman GF/C and GF/F (nominal pore sizes of 0.90 µm and 0.45µm, respectively). Aliquots of the filtrate were then partitioned into 15 ml clean polyethylene tubes with 2 % nitric acid (by volume) for metal analyses, and 24 ml pre-combusted glass vials followed by addition of 20% phosphoric acid (HPLC Grade) to obtain pH ~ 2 for DOC analyses. The difference in the initial soil solution and collected leachate was used to

determine net stabilization or loss of DOC (ΔDOC), and the POC collected on filters from the leachate provided an estimate of POC mobilization during the experiment.

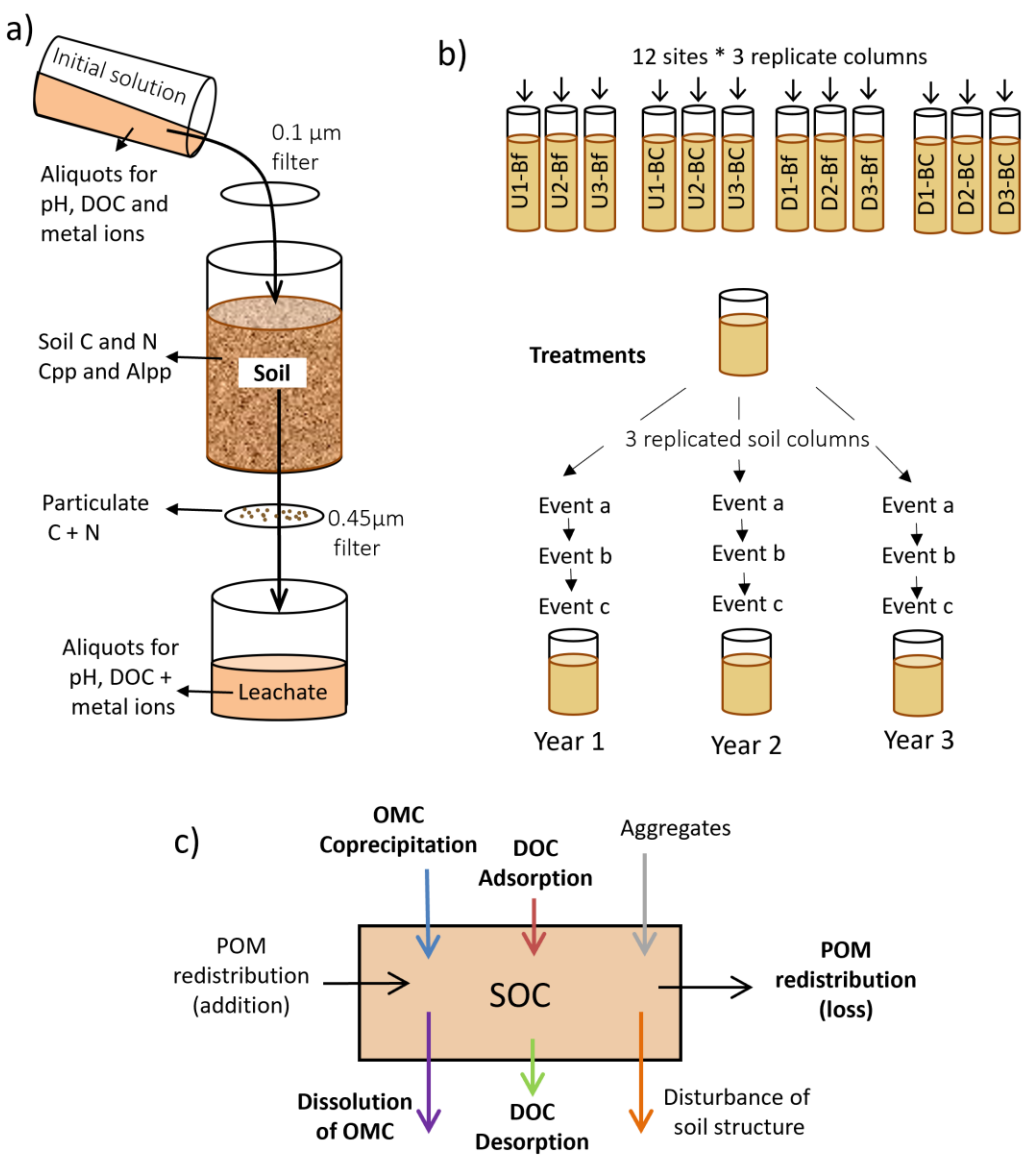

Figure 3.2.

Experimental design showing (a) application of soil solution to soil column and sample collection for analysis and (b) column set up and experimental treatments. Three replicate soil columns were built from each

homogenized soil sample, each column received three applications of initial dissolved organic matter solution to represent sequential events, see Table 3.1 for different initial solutions. (c) Mechanisms that contribute to soil organic carbon (SOC), those in bold were considered directly in the experiment. DOC = Dissolved organic carbon; Rep = replicate; Alpp and Cpp = Al and DOC in pyrophosphate extracted solution from soil; OMC = organo-metal complexes. The labels on each soil column refer to upslope (U) and footslope (D) soil pit location followed by the soil horizon (Bf or BC; e.g., U1-Bf refers to the soil sample collected from Bf horizon in the first soil pit in the upslope).

3.2.3 Site data: water table levels, soil characteristics and analyses

Instrumented piezometers were constructed with 4" diameter PVC pipe with 4 mm holes below 15 cm depth from the top of the mineral soil horizon. The porous section of the pipe was covered with polyethylene screening to reduce sedimentation. These were installed well into the C horizon using a drill auger of similar diameter during the summer of 2017 just above and downslope from the upslope and footslope soil collection sites, respectively (Figure 3.1). Water pressure and conductivity data was recorded every 30 minutes with continuous data loggers (HOBO Water Level and Conductivity Loggers U20-001-04 and U24-001, Onset Inc., Bourne, MA, USA; HOBO, 2002) installed via line to a cap at the top of the piezometer such that each logger was held at the base of the piezometer, with sensors located 0.661m and 0.842m below ground, in the footslope and upslope, respectively. The water table height was determined by processing the difference between the recorded water pressure and local barometric pressure measured onsite (HOBO Water Level Data Logger U20L-04, Onset Inc., Bourne, MA, USA) and using HOBOware software 3.7.23.

To determine the water holding capacity at atmospheric pressure, water was slowly added to approximately 100 grams of < 2 mm mineral soil in a funnel with a filter

until it began to drip. Soils were dried at 105 °C and the water weight was divided by the dry soil weight to provide the water holding capacity (Laganière et al., 2015). To obtain the fine fraction proportion, consisting of clay and silt combined, soils were sieved to 53 µm and their weight was divided by the total initial dry weight of the soil.

Soil density was measured by hammering standardized sheet metal plates into the wall of the soil pit and excavating the entire contents and measuring the final volume (various sized plates were used to accommodate the rocky soils but typically resulted in volumes of approximately 2000 cm^3). This was repeated three times across each horizon (typically one location in each of three faces of the soil pit). The soil was dried, divided into soil, rocks and roots, and soil density was evaluated by excluding the rock volume to only calculate the density within soil filled spaces. For more details on this approach refer to Gates (Masters Thesis, 2022).

Pyrophosphate extracted metals (Al_{pp} and Fe_{pp}) and C (C_{pp}) are proxies for the abundance of soil OMCs and associated C (McKeague, 1967). For this extraction, approximately 0.300 g of < 2mm ground soil was weighed into 50mL polyethylene tubes with 30 mL of 44.6 g/L sodium pyrophosphate solution and shaken for 16 hours in the dark. The solution was centrifuged until clear, and the supernatant was filtered through a pre-combusted Whatman GF/F filter. A proxy for the degree of C saturation of Al OMCs (C_{pp}:Al_{pp}), or the sum Fe and Al OMCs (C_{pp}:M_{pp}), was calculated using molar ratios of pyrophosphate extracted C, Al and Fe.

For soil elemental analysis, ground soil samples were weighed into tin cups with an equal weight of WO_5. For particulate material collected on Whatman GF/F filters, the entire filter was pressed into a pellet for analysis. These were analyzed with a Vario EL Cube elemental analyzer (Elementar) and included filter blanks in the case of the particulate samples. The C and N content of acetanilide was measured three to four times over the course of a run to make a daily correction (typically 1.03 – 0.97) to the calibration curves for C and N detection by the thermal conductivity detector which had a limit of quantification of 20 μg and 5 μg, respectively. A low organic soil reference material (B2153: 1.61 ± 0.09 %C; 0.133 ± 0.023 %N) and a high organic sediment (B2151: 7.45 ± 0.14 % C; 0.52 ± 0.02 % N), both acquired from Elemental Microanalysis, were run as quality control samples and were within the accepted ranges (B2153: 1.56 %C and 0.132 %N; B2151 7.33 %C and 0.51 %N).

To determine the dissolved metal concentrations of the pyrophosphate extractions and experimental initial soil solutions and leachates, the solution was diluted 50x, acidified with 2 % nitric acid by weight, and analysed on a Thermo Fisher Scientific iCAP 6500 Inductively Coupled Plasma Emission Spectrometer (Al and Fe limit of detection of 15 and 3 ppb).

The DOC content of the initial solution, soil experiment filtrate and pyrophosphate-extracted solution was analysed with a Shimadzu TOC-VCSH Total Organic Carbon Analyzer. Pyrophosphate-extracted solutions (to determine C_{pp} of the soil) and sodium pyrophosphate blanks were diluted 10 – 50x, while the experimental initial and leachate solutions were run undiluted. Samples, blanks and standards were acidified with

21.5 % HPLC grade phosphoric acid to pH of 2. A calibration curve was generated from solutions of potassium hydrogen phthalate (KHP) and glutamic acid (GA) standards. In the case of the soil extracts, these standards were prepared in the same sodium pyrophosphate extraction solution. Samples were analysed at 720°C in replicates of 3 or 4, and the best 3 were averaged with sample precision 5% or less. All samples were well above the 2.36 mg/L limit of detection.

3.2.4 Study and statistical design

This study combines the evaluation of in situ soil properties for two contrasting hillslope positions and experimentation with soils from those positions to develop hypotheses regarding controls on SOC and its response to predicted climate change via contribution to three research questions (Table 3.2). This work was designed to: (1) evaluate variations in soil characteristics, SOC content and SOC stability mechanisms by slope position in order to assess potential variation in any in situ hydrologic controls (e.g. infiltration relative to lateral flow, degree of saturation, relative soil water residence time) and their association with SOC, (2) evaluate the controls on SOC response to soil solution additions used here as a proxy for extreme precipitation events with the order of addition providing a proxy for antecedent conditions of dry late summer through wet fall, and (3) given predicted increases in late summer or fall event sizes, use these combined observations to generate hypotheses regarding hillslope SOC responses to this important aspect of climate change in this boreal region.

To understand how slope position relates to SOC content and SOC stability mechanisms, soil characteristics related to SOC storage mechanisms were measured, evaluated for spatial differences and considered within the context of hillslope hydrology to inform on potential hydrological controls (Table 3.2). Differences in hydrology by slope position were interpreted using current water table data, and soil characteristics that inform on the history of hydrology at each slope position (e.g. well-developed Ae suggests vertical infiltration) or theoretically should influence soil water residence time or infiltration (e.g. water holding capacity, bulk density). These characteristics assessed at the two hydrogeomorphic positions provided a means to evaluate *in situ* hillslope hydrologic factors in relationship to soil characteristics that may impact SOC and its response to the proxy precipitation events used in the experimental portion of this study. The gently sloped upslope position exhibited evidence of relatively greater vertical infiltration, while the steeper downslope position was a footslope with evidence of greater lateral flow and seasonally saturated soils. Two horizons were employed at each slope position to create four spatial positions: Upslope-Bf, Upslope-BC, Downslope-Bf and Downslope-BC.

Table 3.2.

Study design combining investigation of samples to understand how soil organic carbon relates to hillslope position and soil characteristics and their use within experimental soil solution additions, and how they are expected to contribute to knowledge informing four large scale research questions. Soil characteristics include water holding capacity (WHC); bulk density (BD); soil water residence time (SWRT) ; soil organic carbon (SOC); Al and Al + Fe extracts from pyrophosphate (Alpp and Mpp, respectively); C saturation of Al organometal complexes (C:Alpp); dissolved organic carbon (DOC) of the soil solution and leachate.

Research question	Spatial or temporal scales		Methods	Data scale
How does hydrology vary with hillslope position and does that evidence relate to SOC and factors controlling SOC?	Hillslope position + long term history	Hydrology	Ae continuity informs vertical infiltration	Hillslope
			WHC, BD and size fractions inform SWRT and hydraulic conductivity	Site
			Site observations: moisture and pyrite crystals	Hillslope
			Pieziometers informs seasonal water table and saturation	Hillslope
		Soil characteristics	SOC content informs long term SOC accumulation	Site
			Alpp, C:Alpp, C:Mpp informs on SOC stability mechanisms	Site
			Spatial variation compared with evidence for hydrology	Hillslope
What controls SOC response to extreme events?	Event factors	Experiment: measure DOC change	Event order (Application #) informs impact of antecedent moisture and event timing	Event-seasonal
			Year (Replicate) informs on 3 event season	Event-seasonal
			Solution DOC conc, pH or Al:C impact	Event-Seasonal
			High water flux emulates extreme precipitation (constant across all)	Event
	Fixed factors		Spatial variation informs on response to flow paths	Hillslope position
			Soil characteristic controls informs SOC stability mechanism	Site
How may SOC be impacted by climate change?	Hillslope position + short-term climate change		Climate projections informs extreme event frequency	Event -Short-term
			Consider hillslope hydrology and SOC response to climate projections for spatial positions	Short-term

To evaluate the potential response of SOC to extreme precipitation events, an experiment was used to measure changes in DOC with percolation through the soil at a high-water flux similar to those expected in these boreal landscapes. Here, event factors were manipulated in treatments to evaluate the roles of ephemeral factors associated with events and seasons (e.g. antecedent soil moisture is often associated with season). Further, soil uptake or loss of DOC was evaluated for spatial differences and thus against factors that are fixed at the event scale (i.e. soil characteristics) to understand potential mechanisms controlling SOC stability during extreme events.

Treatments were designed to evaluate different questions related to events and seasons (Figure 3.2 and Tables 3.2 and S3.3). Each site soil was replicated into three columns, each column received three applications (events) representing a three-event season. The net sum of DOC uptake of all three applications to a single column represents a three-event autumn season (ΔDOC_{SUM}; n = 36) in a fully crossed experimental design. The "Year" term in these models evaluates natural variability that might be expected among years due to variation in the soil solution composition of each event (Table 3.1).

The average of DOC uptake by application across the three soil column replicates was used to evaluate event timing associated with antecedent moisture impact (ΔDOC_{APP}; n = 36). This fully crossed experimental design uses repeated measures, however, a random block was not employed as the ordering of events was of interest. The models use the "Event" factor to evaluate the impact of the sequence of events.

Finally, the entire unaveraged experimental dataset was employed to further evaluate the initial solution influence on SOC response (ΔDOC_{ALL}; n = 108). A range of initial soils varying in composition were used to evaluate the effects of DOC concentration, pH and solution Al:C ratios on soil DOC uptake so that predictions can be made based on anticipated climate change impacts on the soil solution (Table 3.2). Here, the initial solutions were evaluated in models nested within Event as the initial solution is unique to each event, or soil solution addition, as not every soil column experiences each solution.

The relationship of SOC content on POM mobilization was tested as a one-way ANOVA. Many footslope samples from the first application were lost due to filter as the sample size was too large to be compressed in the filter. Therefore, only particulate loss from the first application was included in the tests evaluating POM, rather than the sum of all applications.

Spatial variations in soil characteristics, DOC and POC net change were evaluated with paired T-tests performed in Microsoft Excel 2017. General linear models were used to evaluate the roles of mineral characteristics and spatial positions on DOC change (uptake or loss relative to the soil). ANOVAs were performed in RStudio version 4.2.3. Model residuals were confirmed to be homogeneous, independent, and normally distributed with residual versus fit, lag and quantile-quantile plots, respectively. All tests were conducted using $\alpha = 0.05$ but with a Bonferroni correction for multiple t-tests. Several columns collapsed after the first or second application. Therefore, data from these soil pits were averaged from two soil cores instead of three. The expected number of samples (n) is

provided in Table S3.3 (Appendix), but the actual number of recovered samples is reflected in the calculation for the degrees of freedom in Table S3.4 (Appendix).

3.3 Results

3.3.1 Site and mineral soil characteristics

Shallow Bf horizons in both slope positions exhibited greater SOC content than at depth in the BC horizons. The upslope Bf position exhibited the greatest enrichment, ranging from 3–5% compared with ~1 % for other spatial positions (Figure 3.3a; Figure S3.1a in Appendix). The C:N ratio was also highest in the upslope Bf horizon, followed by the upslope BC soils, and no difference was observed between the footslope horizons where the lowest values were observed (Figure 3.3b).

Piezometers installed adjacent to soil pits at both slope locations indicate that the water table is consistently higher in the footslope position at all times of the year (Figure 3.1c). The water table height is variable but is most frequently in the C horizon upslope and in the Bf or Bfj horizons in the footslope forest position. The soil density was higher in the footslope versus upslope Bf horizon while variability in the deeper BC horizons masked any possible differences in soil density between those and the Bf horizons (Figure 3.3c). The fine size fraction (clay and silt; > 53 μm) was generally greater in the upslope Bf horizon, while no discernable difference was observed in the BC horizon among slope positions (Figure 3.3d). The water holding capacity of the upslope soils was higher than in the footslope, particularly in the Bf horizon (Figure 3.3e).

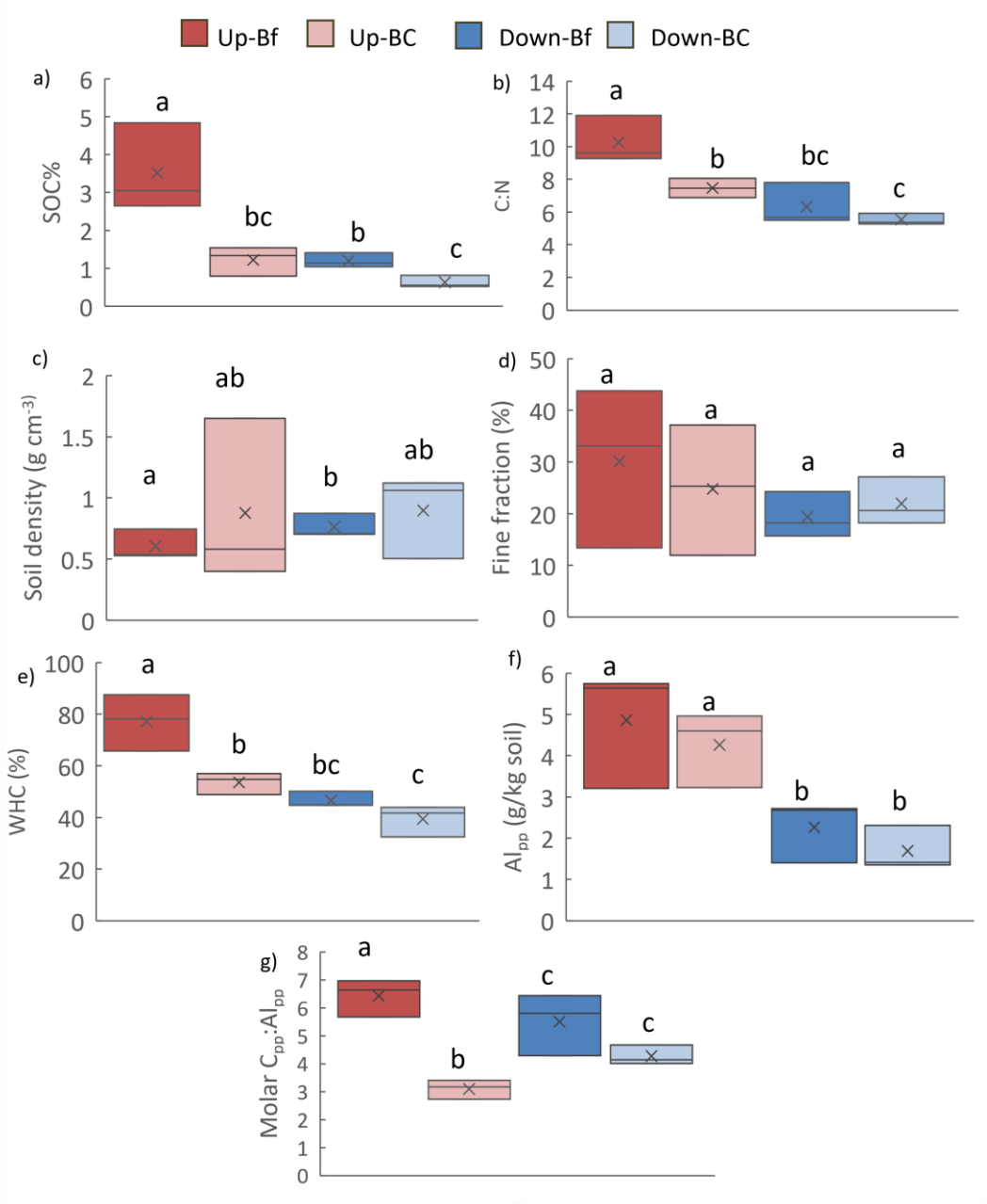

Figure 3.3.

Mineral soil characteristics by spatial position and soil horizon given as upslope (Up) and footslope (Down) position and Bf and BC horizon: (a) SOC (%) (b) molar C:N (c) soil density (d) fine fraction (silt + clay%) (e) water holding capacity (WHC; f) pyrophosphate extracted Al (g) C saturation of Al OMCs. Line in box is the median, x is the mean. Differences among values are given by different letters with t-tests with Bonferroni correction (a = 0.05/6).

Pyrophosphate extracted Al (Al_{pp}) and the sum of Fe and Al (M_{pp}), proxies for OMC metals, were higher in the upslope soils with no significant differences with depth at either slope position (Figure 3.3f). The ratio of pyrophosphate extracted C to Al (C_{pp}:Al_{pp}) and the sum of Fe and Al (C_{pp}:M_{pp}), proxies for the saturation of OMC with C, were higher in the Bf horizon than at depth, and lowest in the upslope BC soils (Figure 3.3g – h). I found that Al_{pp} was positively correlated with SOC content and C_{pp}, describing 51 and 70 % of their variance, respectively (Figure 3.S1b).

3.3.2 Experimental results: net changes in aluminum, dissolved and particulate organic carbon with application of soil solution to mineral soil columns

The same initial soil solution, collected from the passive pan lysimeters, was applied to all soil sample columns within the same replicate and application pairing providing a proxy for different years and sequential precipitation events, respectively (Fig. 2b and Table S3.3 in Appendix). The initial solutions exhibited a range in pH, and DOC and metal content (Table 3.1). Initial soil solution DOC concentrations (DOC_{int}) ranged from 39 – 72 mg C L^{-1}, similar to the observed range across the summer to autumn in this forest hillslope (Bowering et al. 2020). Al ranged from 469 – 1204 ppb and pH from 3.95 –4.46. Each daily 300 ml application was equivalent to 5.6 – 10.7 g C m^{-2} day^{-1}, which is about an order of magnitude larger than the average DOC flux per day in autumn and similar to an extreme event (Bowering et al., 2020).

The pH of the leachate increased relative to the initial soil solution in all samples, with a greater increase observed in the BC horizon soils (Figure S3.2 in Appendix). Depicting net changes from the perspective of the mineral soil, negative and positive ΔDOC values indicate a loss of DOC from the soil and uptake of DOC into the soil, respectively. The ΔDOC results were summarized in three ways: (a) as a net sum of all three applications to the column (ΔDOC_{SUM}; n = 36), (b) as an average by application order (ΔDOC_{APP}; first, second or third; n = 36), and (3) the entire dataset of DOC uptake (ΔDOC_{ALL}; n = 108).

In all models, when the saturation of Al and Fe was considered (C_{pp}:M_{pp} where M_{pp} is the sum of Fe_{pp} and Al_{pp}), there was a reduction in explanatory power relative to models with C_{pp}:Al_{pp} alone (Table S3.4; e.g. R^2 of 0.752 for C_{pp}:Al_{pp} versus 0.584 using C_{pp}:M_{pp}). This suggests the greater importance of Al OMCs in SOC stabilization, consistent with Patrick et al. (2022).

Model results indicate ΔDOC_{SUM} trends with hillslope position. Soils from the Bf horizon exhibited variable $\Delta DOC_{SUM,}$ but BC horizon soils exhibited consistent uptake (Figure 3.4a). About 30% of the applied DOC was taken up by the upslope BC horizon, and a ~1% increase in SOC (Figure S3.3). As hypothesized, ΔDOC_{SUM} was negatively correlated with the molar ratio of pyrophosphate extracted C to Al (C_{pp}:Al_{pp}), a proxy for the degree of C saturation of Al OMCs, alone describing 75% of the variance (Figure 3.4b; Table S3.4 in Appendix). While C_{pp}:M_{pp} was significant, the explained variance was lower than for Al_{pp} alone. The Year term was not significant indicating low variability among years in the response to variations in the soil solution.

There were clear differences in ΔDOC_{APP} with event order and spatial position (Table S3.4 in Appendix). On average, BC horizon soils did not exhibit any difference in ΔDOC_{APP} by application. On the other hand, Bf horizon soils exhibited DOC loss (negative ΔDOC_{APP}) during the first application but net uptake with further applications (Figure 3.4c). As expected, ΔDOC_{APP} varied as a function of C_{pp}:Al_{pp} and application where more C saturated soils experienced relatively greater DOC loss from the soil during the first application (Figure 3.4d). Together, C_{pp}:Al_{pp} and application described 82 % of ΔDOC_{APP} variance (Table S3.4 in Appendix). Since the soil moisture increases with each event, this suggests the importance of extreme event timing as events on dry summer soils would be subject to more loss than later events on wet soils.

Finally, the role of initial soil solution (Table 3.1) on DOC uptake was considered using the full dataset (ΔDOC_{ALL}; n = 108). Again, the hillslope position and C_{pp}:Al_{pp} were significant predictors, as was DOC_{int} which was nested within Event (Table S3.4 in Appendix). Higher DOC uptake (or less loss) is exhibited by columns receiving an initial soil solution with the highest DOC_{int} with few exceptions from the first application (Figure 3.5). The pH, Al concentration and molar Al:C ratio of the initial DOM did not provide further explanation of ΔDOC variation. This suggests again that event timing is important as the concentration of DOC in the soil solution delivered to mineral soils can vary with season (Bowering et al. 2023).

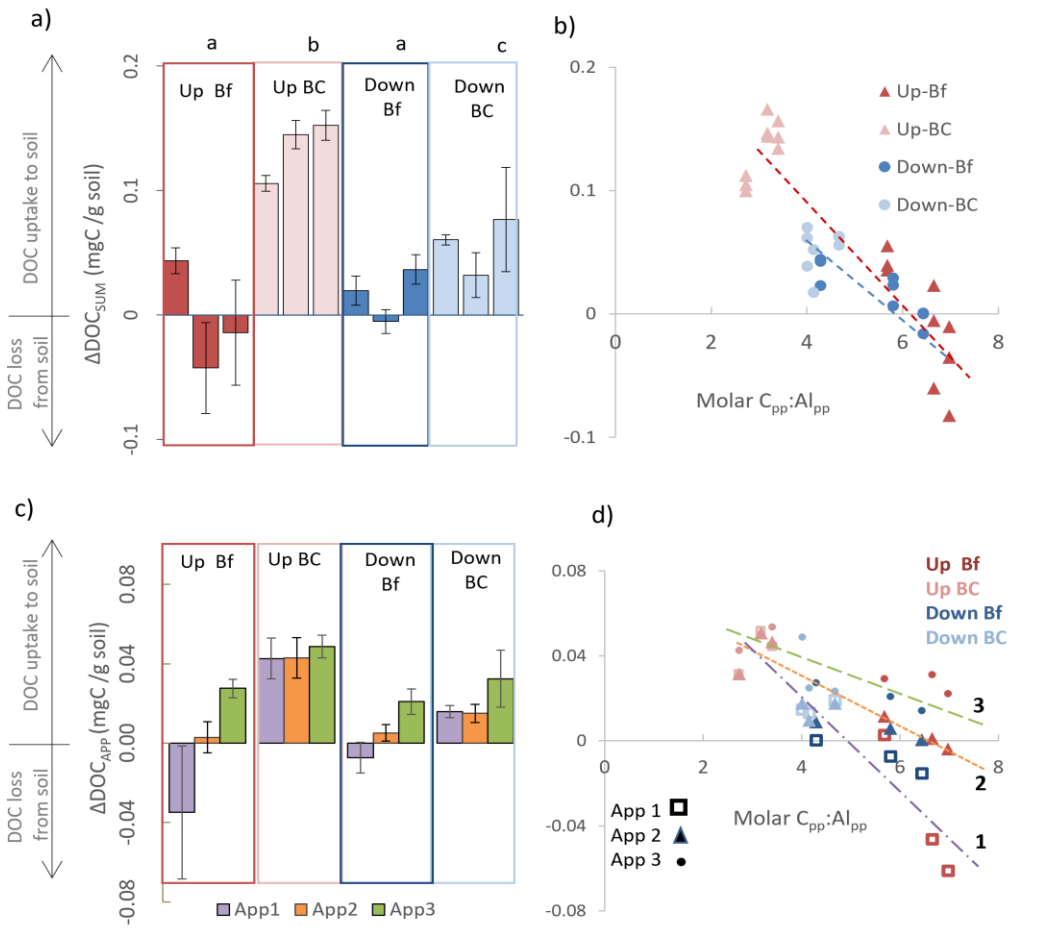

Figure 3.4.

a) Change in dissolved organic carbon (DOC = Initial - Final) as sum of all applications normalized to grams dry weight soil (ΔDOC_{SUM}); uptake to the soil is indicated by positive numbers. Three soil pits per spatial position (3 bars); variance among 3 replications per soil sampling pit indicated with error bars in the histogram. Significant differences among spatial groups are indicated with lowercase letter above larger boxes given for the Upslope Bf horizons (Up Bf), Upslope BC horizon (Up BC), Footslope Bf (Down Bf), and Footslope BC (Down BC). (b) Scatter plot shows relationship between ΔDOC_{SUM} and saturation of Al organo-metal complexes with C extracted in a pyrophosphate solution (molar C_{pp}:Al_{pp}). (c-d) Change in dissolved organic carbon averaged by individual application (ΔDOC_{APP}) is provided in a histogram depicting the average for each spatial position across all soil pits and replications. Scatter plot shows relationship of ΔDOC_{APP} to molar C_{pp}:Al_{pp}.

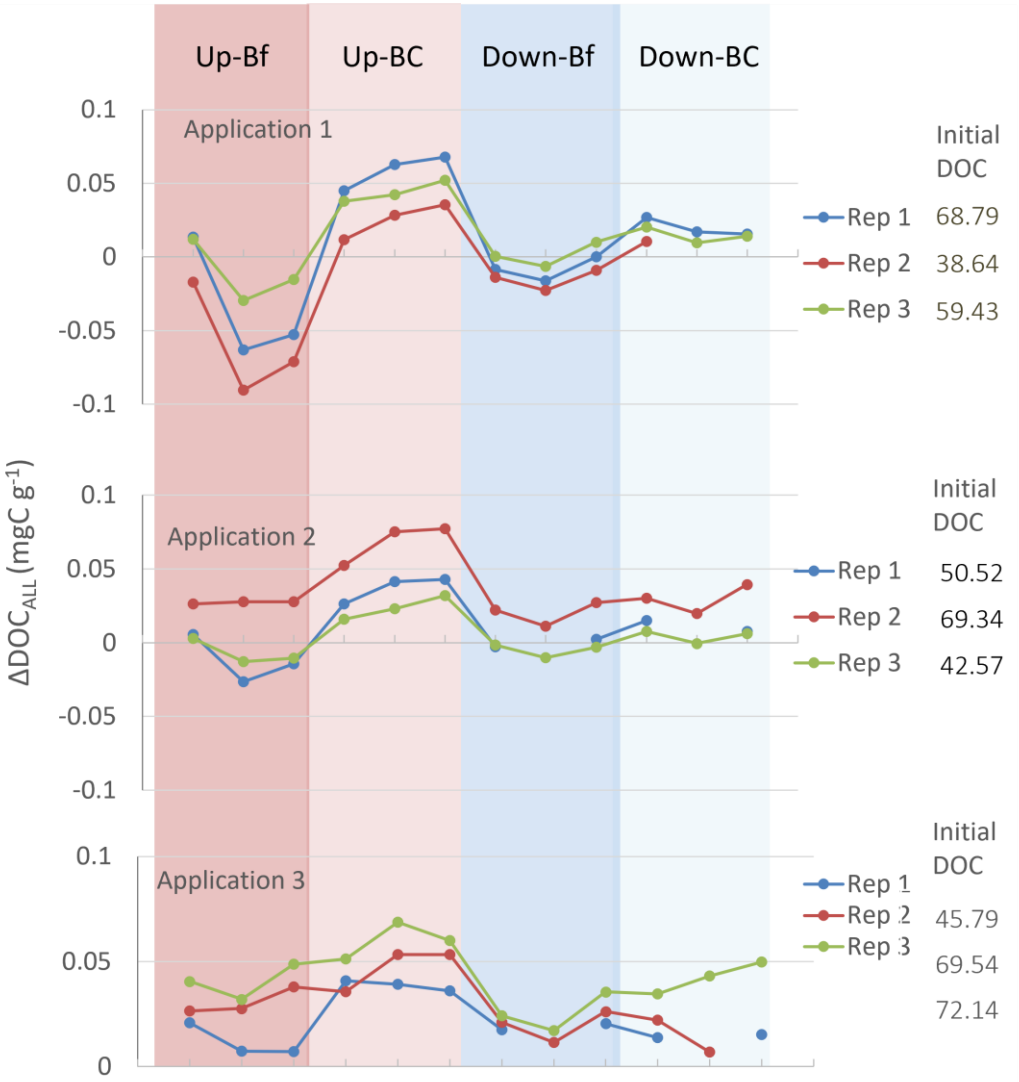

Figure 3.5.

Change in dissolved organic carbon (ΔDOC_{ALL} = Initial - Final) of leachate for all replications (reps 1-3) and applications (1-3). Positive value indicates uptake of DOC into the soil. Initial DOC of the soil solution measured as mg C L^{-1}. Upslope Bf horizons (Up Bf), Upslope BC horizon (Up BC), Footslope Bf (Down Bf), and Footslope BC (Down BC).

Aluminum was released consistently across all soils in the range of 1 – 4 µg Al per gram dry weight soil. Upslope BC soils released the least Al (Figure S3.4a in Appendix). The concentrations of Al and DOC in the leachate were positively correlated

(Figure S3.4b in Appendix), and the molar ratio of Al to DOC of the leachate increased relative to the initial soil solution applied across all samples and ranged from less than 0.007 in the initial solution to 0.01 – 0.02 in the leachate.

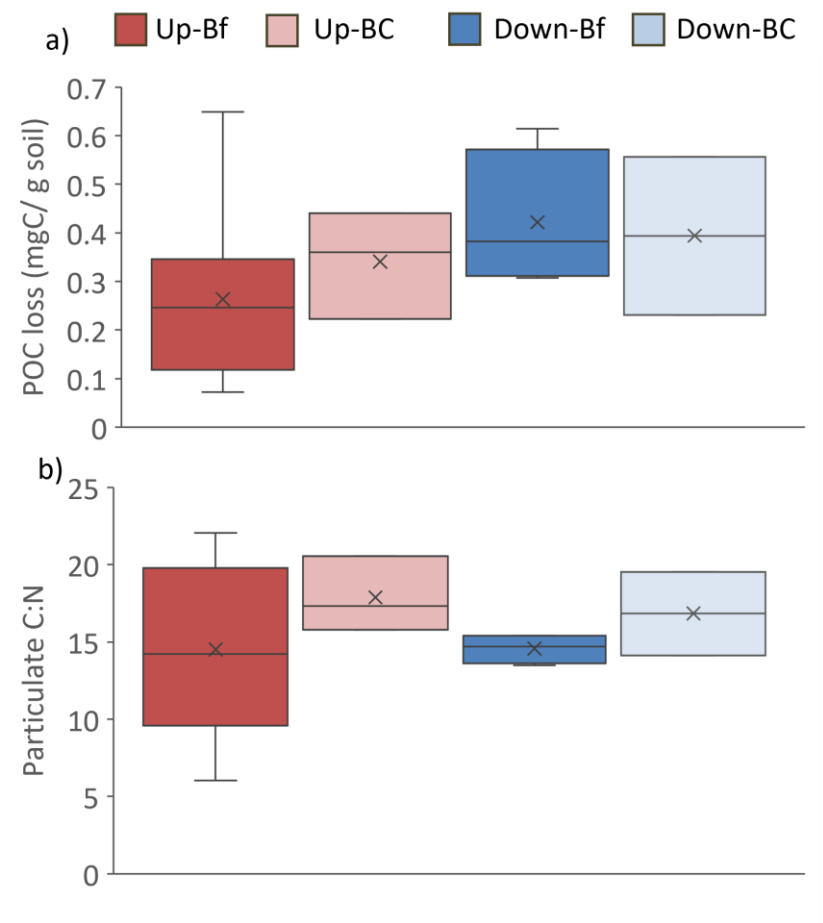

Figure 3.6.

a) Particulate organic carbon (POC) loss (> 0.45µm) per gram soil at each position for soil solution application 1 only. b) The molar carbon to nitrogen ration (C:N) of lost particulate organic matter of application 1.

Losses of POC per gram dry weight soil were higher in the footslope soils, whereas upslope Bf soils experienced on average the least POC loss (Figure 3.6a).

Comparing POC to SOC content, upslope Bf soils lost less than 1% of SOC as POC, while footslope BC soils were most vulnerable losing at least 8% of SOC content (Figure S3.5a in Appendix). POC loss was negatively correlated with SOC, describing 53 % of the variance in POC loss in the first application (Figure S3.5b in Appendix). The average C:N of mobilized particulate ranged from 14 to 18 and did not vary among horizons or positions (Figure 3.6b).

3.4 Discussion

I employed a combination of observations and experimentation using two hillslope positions within an experimental boreal forest site to evaluate SOC and soil characteristics within the context of interpreted hydrological differences by hillslope position. Using soils from these hillslope positions, I experimentally investigated the response of mineral soils to infiltration of surface soil DOM to understand controls on C uptake and loss that may contribute to SOC content at the hillslope scale in this boreal forest site. The solution of DOM was applied rapidly to experimental soil columns, built from mineral soils collected from different horizons and hillslope positions, to provide insight on how SOC content may respond to increases in rainfall intensity with climate warming predicted for this region (Finnis and Daraio 2018). I observed a range in soil C responses that varied with hillslope position and the soil characteristics and properties signifying differences in hydrology associated with geomorphic position. Our results reveal differences in C stabilization and redistribution mechanisms attributed to variations in

hillslope hydrology and associated soil characteristics that lead to relevant variation in SOC content. I use this information to generate hypotheses for how contrasting hydrology and soil characteristics by hillslope position and season impact these processes leading to the observed spatial variation in SOC content and its response to predicted increases in precipitation event sizes in a future warmer and wetter climate.

3.4.1 Soil organic carbon content is the net result of mechanisms of C stabilization, desorption, and redistribution

Aluminum OMCs control SOC content and their degree of undersaturation controls soil DOC adsorption and new storage potential

Consistent with shallow boreal forest minerals soils (Patrick et al. 2022), the positive correlation between SOC and Al OMC (Figure S3.1b in Appendix) indicates that Al OMCs are also an important control on SOC in deeper soils. The stabilization of SOC by OMCs is generally considered to occur through coprecipitation of DOM and reactive metals (Fuss et al., 2011; Nierop et al., 2002; Sauer et al., 2007). However, coprecipitation likely does not explain the experimental uptake of DOC into the soil, as the leachate was well below the threshold Al:C for coprecipitation (Nierop et al., 2002). Mobilized Al suggests dissolved OMCs were formed but did not precipitate, since uncomplexed "free" inorganic Al would decrease with increased pH (Jansen et al., 2003). Instead, the strong negative correlation of C_{pp}:Al_{pp} with DOC uptake to the soil suggests adsorption onto the

surfaces of formerly coprecipitated undersaturated OMCs (low molar C_{pp}:Al_{pp}) is the dominant uptake mechanism during high water flux events (Figure 3.4). This is similar to absorption onto the surfaces poorly crystalline inorganic minerals, as has been described by others, which may also contribute to the observed DOC uptake (Dahlgren and Marrett, 1991; Kothawala et al., 2009).

Therefore, DOC can be stabilized by OMCs in two ways: (1) coprecipitation, which also defines the Al OMC abundance, and (2) through additional DOC adsorption onto their surfaces. The initial coprecipitation of OMCs requires a longer soil water residence time for weathering to achieve the Al:C threshold, and vertical infiltration for increasing pH (Nierop et al., 2002). As such, SOC accrual through coprecipitation is likely highest in shallow soils during the summer via a highly concentrated DOM at low flux rates (Bowering et al. 2020). However, adsorption likely occurs year-round at all water flux rates, but would likely be greatest during seasons with a more concentrated solution (i.e. summer and fall) based on the observed positive relationship with initial DOC concentration (Figure 3.5).

As the DOM flux decreases with depth, greater adsorption in shallow soils likely leads to higher C_{pp}:Al_{pp} (more saturated) and SOC content. Yet, DOC inputs to deeper soil horizons are limited to major, but infrequent hydrological events, like snowmelt and autumn storms (Schaetzl et al. 2015). Therefore, deep OMCs are less saturated (low C_{pp}:Al_{pp}). If deep SOC is limited by DOM transport, there is potential for new SOC storage at depth in these soils.

DOC desorption and POC losses are major mechanisms of SOC mobilization across the hillslope

Our results indicate that summer drying followed by increasing soil moisture in the fall will likely lead to mobilization of DOC largely via desorption from shallow soils, but also microbial lysis. Loss of DOC from the soil was exhibited only in soils with the highest C_{pp}:Al_{pp} during the first, and occasionally second, application (Figure 3.4d). This is likely a result of mobilization of OM that has been desorbed from mineral surfaces during drying as has been documented by others (Kaiser et al., 2015; Bailey et al., 2019; Patel et al., 2021). This would support greater DOC mobilization from soils exhibiting a higher C_{pp}:Al_{pp} via more available OM to desorb. Lysing of bacterial cells during drying providing a source of soluble OM upon further rewetting (Blazewicz et al., 2014) is also plausible but limited to shallow soils with high microbial biomass. Microbial lysis should enhance DOC loss from the soil independent of C_{pp}:Al_{pp}. However, the negative correlation of ΔDOC (DOC of initial soil solution applied minus final soil leachate DOC) with C_{pp}:Al_{pp} was maintained across all applications (Figure 3.4d). The remobilization of OMCs from a fresh supply of acidic DOM could also explain DOC loss (Buurman and Jongmans, 2005). However, this is unlikely as the pH was not low enough to remobilize Al OMCs (Ferro-Vázquez et al., 2014; Kalbitz et al., 2000). Finally, DOC loss could be explained by DOC desorption from solid OMCs to buffer the soil solution. However, this is also unlikely as this mechanism is limited to soils with very high C_{pp}:Al_{pp} (usually eluvial Ae horizons) and soil solutions with very high Al:C (Jansen et al., 2004).

As expected, experimental POC loss was at least two times greater than DOC adsorption (-0.1 – 0.6 mg POC g^{-1} versus 0 – 0.08 mg DOC g^{-1}), because most erosion occurs during high intensity infiltration events (Wei et al., 2017). Therefore, POC remobilization is likely highest during the spring melt and large fall storms. Consequently, small accruals of SOC are likely occurring throughout the year from OMC precipitation and adsorption with loss via desorption limited to shallow soils and periods following dry conditions, while losses due to remobilization of POM may be larger in magnitude but occur less frequently during the largest events. Finally, disturbance of the soil structure during collection, sieving to 2 mm, and column building likely enhanced POC loss. Therefore, such loss measurements are likely overstated but also provide insight into the effects of anthropogenic soil disturbance on SOC loss via POC mobilization.

3.4.2 Longer water residence times and greater vertical infiltration upslope enhance SOC content and storage potential while shorter residence times and lateral flow in the footslope enhance POC mobilization

Hydrology varies as a function of hillslope position and the variations in soil properties that influence water infiltration, lateral flow and soil water residence times. These hydrological variations affect mechanisms of C stabilization, C loss, and spatial variations in SOC in this forest site (Figure 3.7). Soil water flow paths deliver DOC to mineral horizons and redistribute particulates with soil water residence times controlling concentrations and contact time for weathering reactions and precipitation of OMCs.

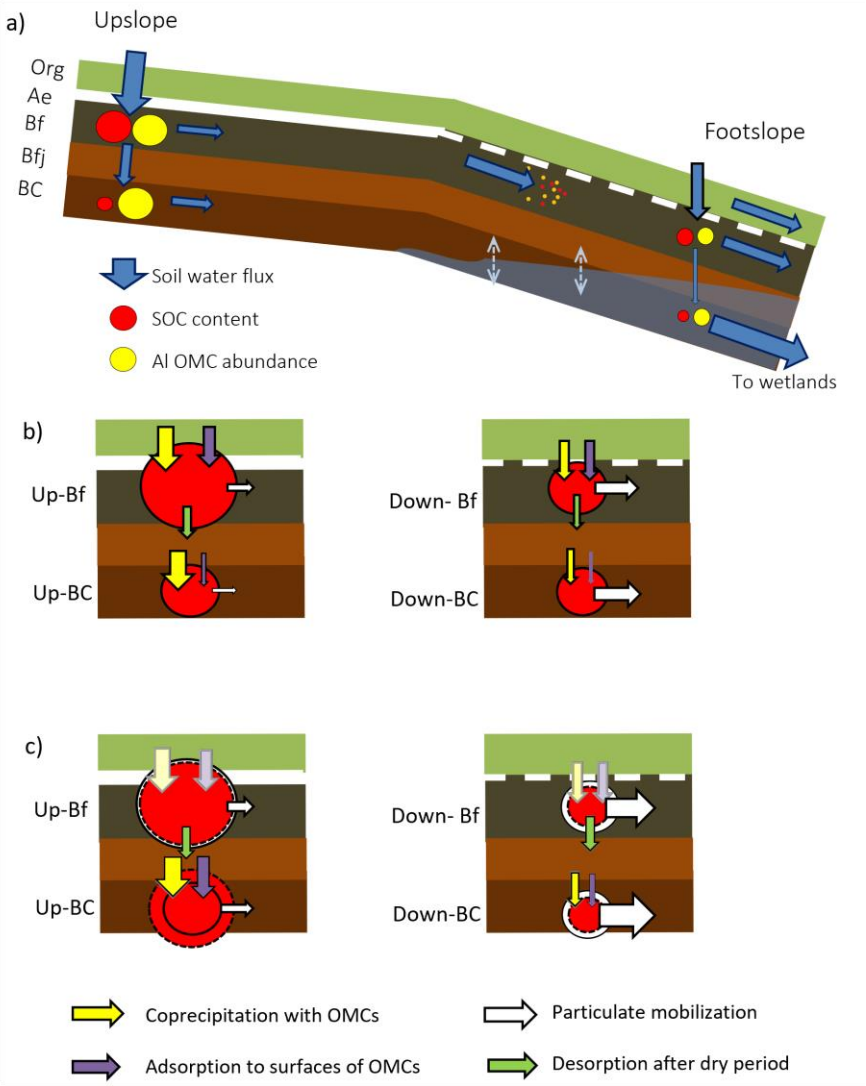

Figure 3.7.

a) Schematic diagram showing the relative abundance of bulk SOC (red circles) and Al organo-mineral complexes (Al OMC; yellow circles), and relative size and direction of soil water flux (blue arrows), by spatial position across the hillslope (See Figure 3.1 for soil horizon identifiers given on left side). b) Relative magnitude of the mechanisms contributing to the current SOC content and (c) predictions of how the mechanisms and inventory will be impacted by climate change. Solid red circle size indicates current relative SOC inventories, dotted circle shows predicted SOC. Arrows pointed into the circle indicate mechanisms that stabilize SOC, arrows pointing out contribute to SOC loss. Greyed out arrows in the predictions panel (c) indicate no predicted change in magnitude of the mechanism. Only mechanisms that were informed by the study results are included here, this does not consider formation of aggregates, POM deposition, OMC dissolution, structure disturbance, etc.

The higher water holding capacity of the upslope soils (Figure 3.3e) promotes longer water residence times, while the lower soil density allows for greater hydraulic conductivity to depth, promoting vertical infiltration. The long water residence times and vertical infiltration are conducive to OMC coprecipitation and have likely contributed to the greater OMC abundance upslope (Figure 3.7b). A well-developed Ae horizon, with OMC and SOC accumulation below the Ae also supports an enhanced role of vertical infiltration and podzolization in SOC stabilization in the upslope relative to footslope hillslope positions. Adsorption of DOC to OMCs has led to more saturated OMCs in shallow soils overall owing to a greater DOM input while particles in the upslope Bf may be relatively more resistant to mobilization as a result of higher aggregation. The higher bulk soil C:N ratio in the upslope-Bf suggests that a considerable portion of the SOC likely occurs in less degraded aggregates (Figure 3.3; Holz & Augustin, 2021; Lavallee et al., 2020). The C:N ratio of mobilized particles is lower than that of the bulk soil, consistent with mineral associated OM, which suggests preferential retention of aggregates (Figure 3.6b).

Particles and DOM are transported downslope during rapid infiltration events that reach lower hydraulic conductivity layers to promote lateral flow via preferential flow through connected macropores (Anderson et al., 2009; Bouma, 1981; Kienzler & Naef, 2008). This is supported by evidence from a study conducted at this site (Roebuck et al, in review). The poorly developed or absent Ae horizon at downslope sites (Gates et al, in revision) is further evidence of greater lateral flow and less vertical flow compared to the upslope position. Additionally, particle deposition has led to a relatively higher soil density,

higher sand content and a significantly lower water holding capacity (Figure 3.3e) likely promoting shorter soil water residence times in the footslope. Higher mobilization of POC in the footslope may be explained by the dynamic environment where suspended particles pass through, and some are deposited. These particles may be more easily remobilized during the next major precipitation event as many of the clay- and silt-sized particles are simply passing through when the flow energy is high enough to mobilize them.

The footslope proximity to wetlands leads to a higher water table (i.e. saturated soils) than the upslope position at all times of the year (Figure 3.1c), and wetter antecedent conditions, one of the strongest controls on the initiation of flow following any precipitation event (Bachmair and Weiler, 2012; Redding and Devito, 2008). The shorter water residence time and reduced vertical infiltration may contribute to the lower OMC abundance and suggests less potential for new C storage through OMC coprecipitation. Further, downslope OMCs may not all be the result of *in situ* coprecipitation, some may have been transported from upslope and deposited there, this deposition would not contribute to an overall increase in hillslope SOC. Field identification of pyrite in the BC horizon also indicates anoxic conditions as a result of seasonal saturation. Despite observations by others of SOC accumulation under anoxic conditions in water saturated soils because of slowed decomposition (Bernal and Mitsch, 2012; Nahlik and Fennessy, 2016), high POM mobilization under these higher lateral flow conditions likely prevents accumulation in the footslope BC horizon regardless of evidence of anoxia and seasonally saturated soil.

Our results suggest greater potential for storage at depth in the upslope soils as these soils exhibited greater uptake at the same C_{pp}:Al_{pp} (Figure 3.4b). Greater DOC uptake by Fe OMCs in the upslope could potentially explain this as the reducing footslope conditions at depth suggest limited Fe OMC content (Nierop et al., 2002; Patrick et al. 2022). However, the explained variance in DOC uptake decreases when the C saturation of the sum of Al and Fe OMCs is employed (C_{pp}:Al_{pp} + Fe_{pp}), suggesting that greater upslope DOC uptake is simply a result of a greater upslope abundance of Al OMC allowing for relatively more DOC uptake at the same C_{pp}:Al_{pp}. As such, the abundance of Al OMC as well as the C_{pp}:Al_{pp} influence DOC adsorption. Therefore, upslope, well-drained soils have an advantage for SOC storage because of higher OMC formation with lower C_{pp}:Al_{pp} as a result of longer soil water residence times. In contrast, the higher particulate loss from the footslope may further contribute to reduced DOC uptake by potentially mobilizing solid Al OMCs that could have adsorbed DOC. This is also supported by our results as the explained variance increases describing DOC change by almost 10 % (to 84 %) when POC loss is accounted for in addition to C_{pp}:Al_{pp}.

3.4.3 Seasonal variation in hydrological controls on SOC content suggest hillslope specific trajectories in SOC response to regional climate change

Carbon stabilization and loss mechanisms controlling SOC content will be impacted by shifts in seasonal hydrology in response to climate change, but these impacts will likely differ along the hillslope (Figure 3.7bc). Total annual precipitation is expected

to increase in this region, along with shorter duration snowpacks, more frequent smaller melt events, and more frequent high intensity autumn precipitation events (Finnis and Daraio 2018). These changes are expected to increase organic layer DOC mobilization (Bowering et al. 2022) via soil solutions that are more acidic and concentrated in DOC in these forest landscapes (Bowering et al., 2020).

Reduced moisture and deeper drying as a result of increased evapotranspiration from increasing temperature (Helbig et al., 2020; Wang et al., 2021) may enhance the extent of desorption in shallow soils in the summer. Further, the rooting depth may increase in the upslope as trees adjust to reduced moisture, enhancing hydraulic conductivity to promote greater infiltration depths (Brantley et al., 2017).

Increasing intensity of autumn storms could enhance deep upslope SOC inventories via a greater and more concentrated DOC source relative to a dilute snowmelt solution, as our experimental results suggest that the *in-situ* C storage potential of deep soils is likely limited by a DOC source. Intense storms, however, also increases POC mobilization, thereby offsetting reductions in POC mobilization expected with a smaller spring melt. POC mobilization will likely be greater in the vulnerable downslope soils.

I suggest that greater DOC infiltration coupled with a greater potential storage capacity will likely lead to enhanced capacity for SOC accrual in the deeper undersaturated mineral soils of the upslope forest hillslope via enhanced adsorption and coprecipitation (Figure 3.7bc). In contrast, the higher lateral flow rates, lower water holding capacity, and higher POM mobility suggest that the deeper soil horizons of the foot slope will likely not

have the capacity to accrue SOC and may experience net losses attributed to enhanced mobilization.

3.5 Implications and conclusions

Combining hillslope soil observations with experimentation I find evidence for hydrologic processes and soil properties that impact change in DOC and POC, providing clues to how current SOC stocks formed, and their fate with increased evapotranspiration and precipitation intensity underway with climate change. Given the results of this study I hypothesize that deeper mineral SOC stores will exhibit different trajectories of change in response to a changing climate, increasing upslope SOC and decreasing in the footslope position. Furthermore, low to moderate relief shallow boreal mineral soils will likely decrease or exhibit little change with climate change as a result of their saturated organo-metal complexes. However, upland lower relief soils will likely accrue SOC at depth via greater vertical infiltration while footslope deposition zones will exhibit net decreases in SOC inventories as a result of their greater vulnerability to POC loss. Testing these hypotheses through future work designed to incorporate greater hillslope monitoring and modelling aimed at incorporating slope position, hydrology, and soil property at hillslope scales will improve our predictive understanding of SOC in boreal forest landscapes.

3.6 References

Ågren, A., Haei, M., Köhler, S.J., Bishop, K., Laudon, H., 2010. Regulation of stream water dissolved organic carbon (DOC) concentrations during snowmelt; The role of discharge, winter climate and memory effects. Biogeosciences 7, 2901–2913. https://doi.org/10.5194/bg-7-2901-2010

Anderson, A.E., Weiler, M., Alila, Y., Hudson, R.O., 2009. Dye staining and excavation of a lateral preferential flow network. Hydrol Earth Syst Sci 13. https://doi.org/10.5194/hess-13-935-2009

Bachmair, S., Weiler, M., 2012. Hillslope characteristics as controls of subsurface flow variability. Hydrol Earth Syst Sci 16, 3699–3715. https://doi.org/10.5194/hess-16-3699-2012

Bailey, V.L., Pries, C.H., Lajtha, K., 2019. What do we know about soil carbon destabilization? Environmental Research Letters. https://doi.org/10.1088/1748-9326/ab2c11

Barnard, R.L., Blazewicz, S.J., Firestone, M.K., 2020. Rewetting of soil: Revisiting the origin of soil CO2 emissions. Soil Biol Biochem. https://doi.org/10.1016/j.soilbio.2020.107819

Batterson, M.J., Catto, N.R., 2001. Topographically-controlled deglacial history of the Humber River basin, western Newfoundland. Geographie Physique et Quaternaire 55, 213–228. https://doi.org/10.7202/006851ar

Bernal, B., Mitsch, W.J., 2012. Comparing carbon sequestration in temperate freshwater wetland communities. Glob Chang Biol 18. https://doi.org/10.1111/j.1365-2486.2011.02619.x

Blazewicz, S.J., Schwartz, E., Firestone, M.K., 2014. Growth and death of bacteria and fungi underlie rainfall-induced carbon dioxide pulses from seasonally dried soil, Ecology.

Bouma, J., 1981. Soil morphology and preferential flow along macropores. Agric Water Manag 3. https://doi.org/10.1016/0378-3774(81)90009-3

Bowering, K.L., Edwards, K.A., Prestegaard, K., Zhu, X., Ziegler, S.E., 2020. Dissolved organic carbon mobilized from organic horizons of mature and harvested black spruce plots in a mesic boreal region. Biogeosciences 17, 581–595. https://doi.org/10.5194/bg-17-581-2020

Bowering, K.L., Edwards, K.A., Wiersma, Y.F., Billings, S.A., Warren, J., Skinner, A., Ziegler, S.E., n.d. Dissolved Organic Carbon Mobilization Across a Climate Transect of Mesic Boreal Forests Is Explained by Air Temperature and Snowpack Duration. https://doi.org/10.1007/s10021-022-0074

Bowering, K. L., Edwards, K. A., and Ziegler, S. E.: Seasonal controls override forest harvesting effects on the composition of dissolved organic matter mobilized from boreal forest soil organic horizons, Biogeosciences, 20, 2189–2206, https://doi.org/10.5194/bg-20-2189-2023, 2023.

Brantley, S.L., Eissenstat, D.M., Marshall, J.A., Godsey, S.E., Balogh-Brunstad, Z., Karwan, D.L., Papuga, S.A., Roering, J., Dawson, T.E., Evaristo, J., Chadwick, O., McDonnell, J.J., Weathers, K.C., 2017. Reviews and syntheses: On the roles trees play in building and plumbing the critical zone. Biogeosciences 14, 5115–5142. https://doi.org/10.5194/bg-14-5115-2017

Buurman, P., Jongmans, A.G., 2005. Podzolisation and soil organic matter dynamics. Geoderma 125, 71–83. https://doi.org/10.1016/j.geoderma.2004.07.006

Cotrufo, M.F., Ranalli, M.G., Haddix, M.L., Six, J., Lugato, E., 2019. Soil carbon storage informed by particulate and mineral-associated organic matter. Nat Geosci 12, 989–994. https://doi.org/10.1038/s41561-019-0484-6

Dahlgren, R.A., Marrett, D.J., 1991. Organic Carbon Sorption in Arctic and Subalpine Spodosol B Horizons. Soil Science Society of America Journal 55. https://doi.org/10.2136/sssaj1991.03615995005500050030x

Ferro-Vázquez, C., Nóvoa-Muñoz, J.C., Costa-Casais, M., Klaminder, J., Martínez-Cortizas, A., 2014. Metal and organic matter immobilization in temperate podzols: A high resolution study. Geoderma 217–218, 225–234. https://doi.org/10.1016/j.geoderma.2013.10.006

Friedlingstein, P., Meinshausen, M., Arora, V.K., Jones, C.D., Anav, A., Liddicoat, S.K., Knutti, R., 2014. Uncertainties in CMIP5 climate projections due to carbon cycle feedbacks. J Clim 27, 511–526. https://doi.org/10.1175/JCLI-D-12-00579.1

Fuss, C.B., Driscoll, C.T., Johnson, C.E., Petras, R.J., Fahey, T.J., 2011. Dynamics of oxidized and reduced iron in a northern hardwood forest. Biogeochemistry 104. https://doi.org/10.1007/s10533-010-9490-x

Gates Z. (2023) Optimized ground penetrating radar methods can account for landscape variance in properties informing soil carbon distribution in boreal forest hillslopes. Masters Thesis. 188 pages.

Gimeno, L., Nieto, R., Vázquez, M., Lavers, D.A., 2014. Atmospheric rivers: A mini-review. Front Earth Sci (Lausanne). https://doi.org/10.3389/feart.2014.00002

Helbig, M., Waddington, J.M., Alekseychik, P., Amiro, B.D., Aurela, M., Barr, A.G., Black, T.A., Blanken, P.D., Carey, S.K., Chen, J., Chi, J., Desai, A.R., Dunn, A., Euskirchen, E.S., Flanagan, L.B., Forbrich, I., Friborg, T., Grelle, A., Harder, S., Heliasz, M., Humphreys, E.R., Ikawa, H., Isabelle, P.E., Iwata, H., Jassal, R., Korkiakoski, M., Kurbatova, J., Kutzbach, L., Lindroth, A., Löfvenius, M.O., Lohila, A., Mammarella, I., Marsh, P., Maximov, T., Melton, J.R., Moore, P.A., Nadeau, D.F., Nicholls, E.M., Nilsson, M.B., Ohta, T., Peichl, M., Petrone, R.M., Petrov, R., Prokushkin, A., Quinton, W.L., Reed, D.E., Roulet, N.T., Runkle, B.R.K., Sonnentag, O., Strachan, I.B., Taillardat, P., Tuittila, E.S., Tuovinen, J.P., Turner, J., Ueyama, M., Varlagin, A., Wilmking, M., Wofsy, S.C., Zyrianov, V., 2020. Increasing contribution of peatlands to boreal evapotranspiration in a warming climate. Nat Clim Chang 10. https://doi.org/10.1038/s41558-020-0763-7

Holz, M., Augustin, J., 2021. Erosion effects on soil carbon and nitrogen dynamics on cultivated slopes: A meta-analysis. Geoderma 397. https://doi.org/10.1016/j.geoderma.2021.115045

Hopp, L., McDonnell, J.J., 2009. Connectivity at the hillslope scale: Identifying interactions between storm size, bedrock permeability, slope angle and soil depth. J Hydrol (Amst) 376. https://doi.org/10.1016/j.jhydrol.2009.07.047

Hsu, H.-H., Chen, Y.-T., 2020. Simulation and Projection of Circulations Associated with Atmospheric Rivers along the North American Northeast Coast. J Clim 33, 5673–5695. https://doi.org/10.1175/jcli-d-19-0104.1

Hu, Y., Berhe, A.A., Fogel, M.L., Heckrath, G.J., Kuhn, N.J., 2016. Transport-distance specific SOC distribution: Does it skew erosion induced C fluxes? Biogeochemistry 128, 339–351. https://doi.org/10.1007/s10533-016-0211-y

Jansen, B., Nierop, K.G.J., Verstraten, J.M., 2005. Mechanisms controlling the mobility of dissolved organic matter, aluminium and iron in podzol B horizons. Eur J Soil Sci 56, 537–550. https://doi.org/10.1111/j.1365-2389.2004.00686.x

Jansen, B., Nierop, K.G.J., Verstraten, J.M., 2004. Mobilization of dissolved organic matter, aluminium and iron in podzol eluvial horizons as affected by formation of metal-organic complexes and interactions with solid soil material. Eur J Soil Sci 55. https://doi.org/10.1111/j.1365-2389.2004.00598.x

Jansen, B., Nierop, K.G.J., Verstraten, J.M., 2003. Mobility of Fe(II), Fe(III) and Al in acidic forest soils mediated by dissolved organic matter: Influence of solution pH and metal/organic carbon ratios, in: Geoderma. Elsevier, pp. 323–340. https://doi.org/10.1016/S0016-7061(02)00368-3

Kalbitz, K., Solinger, S., Park, J.H., Michalzik, B., Matzner, E., 2000. Controls on the dynamics dissolved organic matter in soils: A review. Soil Sci 165. https://doi.org/10.1097/00010694-200004000-00001

Kienzler, P.M., Naef, F., 2008. Subsurface storm flow formation at different hillslopes and implications for the "old water paradox." Hydrol Process 22, 104–116. https://doi.org/10.1002/hyp.6687

Kothawala, D.N., Moore, T.R., Hendershot, W.H., 2009. Soil Properties Controlling the Adsorption of Dissolved Organic Carbon to Mineral Soils. Soil Science Society of America Journal 73, 1831–1842. https://doi.org/10.2136/sssaj2008.0254

Kothawala, D.N., Roehm, C., Blodau, C., Moore, T.R., 2012. Selective adsorption of dissolved organic matter to mineral soils. Geoderma 189–190, 334–342. https://doi.org/10.1016/j.geoderma.2012.07.001

Laganière, J., Podrebarac, F., Billings, S.A., Edwards, K.A., Ziegler, S.E., 2015. A warmer climate reduces the bioreactivity of isolated boreal forest soil horizons without increasing the temperature sensitivity of respiratory CO2 loss. Soil Biol Biochem 84, 177–188. https://doi.org/10.1016/j.soilbio.2015.02.025

Laudon, H., Tetzlaff, D., Soulsby, C., Carey, S., Seibert, J., Buttle, J., Shanley, J., Mcdonnell, J.J., Mcguire, K., 2013. Change in winter climate will affect dissolved organic carbon and water fluxes in mid-to-high latitude catchments. Hydrol Process 27. https://doi.org/10.1002/hyp.9686

Lavallee, J.M., Soong, J.L., Cotrufo, M.F., 2020. Conceptualizing soil organic matter into particulate and mineral-associated forms to address global change in the 21st century. Glob Chang Biol 26, 261–273. https://doi.org/10.1111/gcb.14859

Lee, J.-Y., Marotzke, Jochem, Bala, Govindasamy, Milinski, S., Yun, K.-S., Ribes, A., Ruane, A.C., Kumar Kanikicharla Qatar, K., Kattsov, V., Kimoto, M., Marotzke, J, Bala, G, Cao, L., Corti, S., Dunne, J., Engelbrecht, F., Fischer, E., Fyfe, J., Jones, C., Maycock, A., Mutemi, J., Ndiaye, O., Panickal, S., Zhou, T., Pirani, A., Connors, S., Péan, C., Berger, S., Caud, N., Chen, Y., Goldfarb, L., Gomis, M., Huang, M., Leitzell, K., Lonnoy, E., Matthews, J., Maycock, T., Waterfield, T., Yelekçi, O., Yu, R., Zhou, B., n.d. Chapter 4: Future Global Climate: Scenario-based Projections and Near-term Information 553–672. https://doi.org/10.1017/9781009157896.006

McKeague, J.A., 1967. AN EVALUATION OF 0.1 M PYROPHOSPHATE AND PYROPHOSPHATE-DITHIONITE IN COMPARISON WITH OXALATE AS EXTRACTANTS OF THE ACCUMULATION PRODUCTS IN PODZOLS AND SOME OTHER SOILS . Can J Soil Sci 47. https://doi.org/10.4141/cjss67-017

Moroni, M.T., Carter, P.Q., J Ryan, D.A., T, M.M., n.d. Harvesting and slash piling affect soil respiration, soil temperature, and soil moisture regimes in Newfoundland boreal forests.

Nahlik, A.M., Fennessy, M.S., 2016. Carbon storage in US wetlands. Nat Commun 7. https://doi.org/10.1038/ncomms13835

Nierop, K.G.J., Jansen, B., Verstraten, J.M., 2002. Dissolved organic matter, aluminium and iron interactions: precipitation induced by metalycarbon ratio, pH and competition, The Science of the Total Environment.

Pan, Y., Birdsey, R.A., Fang, J., Houghton, R., Kauppi, P.E., Kurz, W.A., Phillips, O.L., Shvidenko, A., Lewis, S.L., Canadell, J.G., Ciais, P., Jackson, R.B., Pacala, S.W., McGuire, A.D., Piao, S., Rautiainen, A., Sitch, S., Hayes, D., 2011. A large and persistent carbon sink in the world's forests. Science (1979) 333, 988–993. https://doi.org/10.1126/science.1201609

Patel, K.F., Myers-Pigg, A., Bond-Lamberty, B., Fansler, S.J., Norris, C.G., McKever, S.A., Zheng, J., Rod, K.A., Bailey, V.L., 2021. Soil carbon dynamics during drying vs. rewetting: Importance of antecedent moisture conditions. Soil Biol Biochem 156. https://doi.org/10.1016/j.soilbio.2021.108165

Redding, T.E., Devito, K.J., 2008. Lateral flow thresholds for aspen forested hillslopes on the Western Boreal Plain, Alberta, Canada. Hydrol Process 22, 4287–4300. https://doi.org/10.1002/hyp.7038

Sauer, D., Sponagel, H., Sommer, M., Giani, L., Jahn, R., Stahr, K., 2007. Podzol: Soil of the year 2007. A review on its genesis, occurrence, and functions. Journal of Plant Nutrition and Soil Science. https://doi.org/10.1002/jpln.200700135

Schaetzl, R.J., Luehmann, M.D., Rothstein, D., 2015. Pulses of Podzolization: The Relative Importance of Spring Snowmelt, Summer Storms, and Fall Rains on Spodosol Development. Soil Science Society of America Journal 79, 117–131. https://doi.org/10.2136/sssaj2014.06.0239

Schaetzl, R.J., Rothstein, D.E., 2016. Temporal variation in the strength of podzolization as indicated by lysimeter data. Geoderma 282, 26–36. https://doi.org/10.1016/j.geoderma.2016.07.005

Scharlemann, J.P.W., Tanner, E.V.J., Hiederer, R., Kapos, V., 2014. Global soil carbon: Understanding and managing the largest terrestrial carbon pool. Carbon Manag. https://doi.org/10.4155/cmt.13.77

Slessarev, E.W., Chadwick, O.A., Sokol, N.W., Nuccio, E.E., Pett-Ridge, J., 2022. Rock weathering controls the potential for soil carbon storage at a continental scale. Biogeochemistry 157. https://doi.org/10.1007/s10533-021-00859-8

Wang, T., Zhang, H., Zhao, J., Guo, X., Xiong, T., Wu, R., 2021. Shifting Contribution of Climatic Constraints on Evapotranspiration in the Boreal Forest. Earths Future 9. https://doi.org/10.1029/2021EF002104

Wei, S., Zhang, X., McLaughlin, N.B., Chen, X., Jia, S., Liang, A., 2017. Impact of soil water erosion processes on catchment export of soil aggregates and associated SOC. Geoderma 294, 63–69. https://doi.org/10.1016/j.geoderma.2017.01.021

Zhu, Y., Wang, D., Wang, X., Li, W., Shi, P., 2021. Aggregate-associated soil organic carbon dynamics as affected by erosion and deposition along contrasting hillslopes in the Chinese Corn Belt. Catena (Amst) 199. https://doi.org/10.1016/j.catena.2020.105106

Zolovkina, D.F., Karavanova, E.I., Stepanov, A.A., 2018. Sorption of Water-Soluble Organic Substances by Mineral Horizons of Podzol. Eurasian Soil Science 51, 1154–1163. https://doi.org/10.1134/S1064229318100162

Chapter 4: Event timing controls mineral soil carbon response to extreme precipitation in moist boreal forests

Abstract

Moist boreal forests host significant soil organic carbon (SOC) and are experiencing enhanced evapotranspiration and extreme precipitation events. Dissolved organic carbon (DOC) can chelate Al and co-precipitate as organo-metal complexes (Al_{OMC}) with increasing Al concentration to sequester mineral horizon SOC. Yet, extreme precipitation should limit Al_{OMC} co-precipitation and the impact of soil drying on boreal forest SOC is unclear. I experimentally measured the uptake and loss of DOC at a high-water flux in boreal climate transect soils with varying regional parent material. Antecedent moisture was evaluated through sequential applications emulating extreme events on dry summer to wet late autumn soils. I found that the degree of saturation of Al_{OMC} with C and antecedent soil moisture control SOC response regardless of climate or parent material. I present a simple predictive model demonstrating shallow SOC loss in dry soils and shallowing transition depth to DOC uptake with increasing soil moisture. This indicates extreme events occurring on dry summer soils are more vulnerable to SOC loss versus later wet autumn

soils. Therefore, event timing and infiltration depth are key to enhancing our ability to predict SOC response to climate change in moist boreal forests.

4.1 Introduction

Boreal forests contain about 30% of the global forest soil organic carbon (SOC) stock (Pan et al., 2011; Scharlemann et al., 2014). These high latitude regions are expected to experience enhanced soil drying via rising temperatures and increases in the size and frequency of extreme precipitation events (Lee et al., 2021). However, how this large C reservoir will respond to climate change is poorly understood and contributes to the large uncertainty in our ability to predict C storage and release through atmosphere-land C exchange at global scales (Friedlingstein et al., 2014).

In moist, acidic, boreal podzols, dissolved organic matter (DOM) facilitates chemical weathering by forming dissolved complexes with metals (Lundstrom et al., 2000). With increasing metal concentrations in the soil solution, these complexes can coprecipitate as organo-metal complexes (OMCs) to stabilize organic matter (OM) in the mineral horizon (Nierop et al., 2002). Thus, OMCs are a main control on SOC content and stability in boreal soils, but particularly Al OMCs, which are stable under changing redox conditions unlike Fe OMCs (Nierop et al. 2002; Patrick et al. 2022).

Climate and geological parent material influence Al OMC formation via DOM and Al availability (Slessarev et al., 2022). Geomorphology further influences their

formation by controlling DOM delivery via hillslope flow paths. However, OMC formation should be limited during extreme precipitation events as short soil water residence times do not support metal concentrations for their coprecipitation. Instead, experimental evidence from a previous hillslope-scale experiment in (Chapter 3) suggests exchange of DOC with surfaces of extant OMCs in the soil is controlled by the degree of saturation of Al OMC with C in the soil (C_{pp}:Al_{pp}). In this previous study, the deep undersaturated mineral horizon soils exhibited DOC uptake despite a short soil water residence time suggesting surficial absorption to OMCs. However, the shallow soils in this study exhibited a variable response from uptake to loss. Since shallow mineral soils experience the greatest DOM flux (C input), and often support the greatest SOC content, these soils deserve more focus.

This new research expands on the previous experiment by extending the range of saturation of Al OMCs to soils with greater saturation. It focuses on shallow mineral soils to explore the variability of SOC response exhibited in the former experiment. It further evaluates the impact of climate and parent material history on SOC response by employing three climate regions of the Newfoundland and Labrador Boreal Ecosystem Latitudinal Transect (NL-BELT), a boreal climate transect with varying parent material. This transect falls within the zone of high sensitivity to changing moisture, suggesting that climate change may have a significant impact on the proportion of SOC associated with reactive metal weathering products (Kramer and Chadwick, 2018).

Enhanced soil drying with climate change may further selectively desorb DOC into the soil solution, leading to net SOC reductions (Helbig et al., 2020; Wang et al., 2021). Therefore, event timing may be important in SOC response as an event occurring on dry

late summer soils may exhibit greater loss than wetter late autumn soils. As such, despite an anticipated increase in DOM flux from the organic horizon with climate change in moist boreal regions (Bowering et al., 2022), the storage of this enhanced C source in the underlying mineral horizon may be influenced by the regional parent material, infiltration depth, timing and hydrology.

Here, I evaluate SOC response to projected short-term climate change by focusing on the following questions: (1) does SOC response to extreme events vary by climate region? (2) what soil characteristics control SOC response at high water flux in shallow soils? (3) how do antecedent soil conditions associated with event timing impact SOC response and does this vary with depth? To answer these questions, I experimentally measured controls on DOC uptake and loss by boreal forest shallow mineral soils under high water flux conditions.

Soil columns were built from soils collected from three climate regions of the NL-BELT. Soil solution (DOM) collected from passive pan lysimeters installed beneath the organic horizon was percolated through the soil columns. The change in DOC was evaluated in terms of fixed controls like soil characteristics and regional characteristics, and further by event factors using experimental treatments of sequential additions of DOC. Results were used to develop a model for predicting SOC response to extreme precipitation over depth for a range of antecedent moisture analogous to late summer to late autumn. These model results were utilized to understand the impact of event timing on the fate of SOC. I hypothesize that these more saturated soils will exhibit net losses of DOC as controlled by C_{pp}:Al_{pp} with greater losses associated with drier antecedent conditions. The

results of this research will aid in our predictive understanding of SOC response to climate change in moist boreal forests.

4.2 Methods

4.2.1 Study area

The Newfoundland and Labrador Boreal Ecosystem Latitudinal Transect (NL-BELT) is a climate transect of study sites spanning 5.5º latitude along the eastern coast of Labrador and western coast of the island of Newfoundland. The transect spans a 5 ºC gradient in mean annual temperature and a range of 1073 to 1505 mm in mean annual precipitation (Environment and Climate Change Canada 30-year normal for 1980 – 2010). The NL-BELT exhibits a water availability (mean annual precipitation subtract potential evapotranspiration) of 641 – 832 mm, which falls within the zone of high sensitivity to changing moisture (Kramer and Chadwick, 2018). This work focuses on three of the four established regions, Eagle River (ER; 53° latitude), Salmon River (SR; 51° latitude) and Grand Codroy (GC; 48° latitude) which I will refer to as North, Mid, and South latitude regions, respectively (Figure 4.1). Within each region are three established forest stand sites approximately 80 m x 80 m. All sites are dominated by mature stands of balsam fir (*Abies balsamea*), with mesic, well-drained humo-ferric podzolic soils classified as Bf horizon soils (> 0.6% pyrophosphate-extractable Fe + Al and 0.5 – 5% SOC; Canadian System of Soil Classification). Soils are of young to intermediate maturity, formed in a post-glacial area from till that varies in depth and composition between regions (Figure

4.1). Data from a previous experiment conducted in the Pynn's Brook Experimental Watershed Area (PBEWA) are combined with those of this work to develop models for predicting SOC response in soils across a range of C_{pp}:Al_{pp}. Details of this fourth region of the NL-BELT are found in Chapter 3.

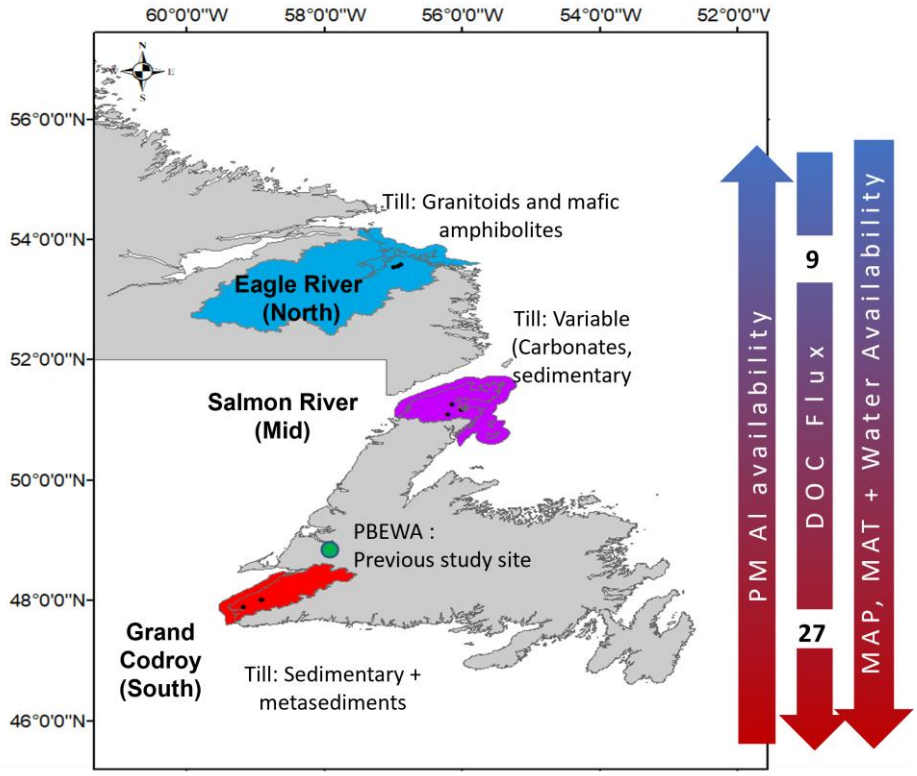

Figure 4.1.

Map of Newfoundland and Labrador Boreal Ecosystem Latitudinal Transect (NL-BELT) with regions and collection sites used in this study. This experiment utilizes the North (ER), Mid (SR) and South (GC) regions, in addition results from a previous hillslope scale experiment conducted in the the Pynn's Brook Experimental Watershed Area (PBEWA). The geological parent material, or till, composition is given for each region as established from regional sampling conducted closest to study sites (Patrick et al. 2022). Mean regional annual precipitation (MAP; mm); and temperature (MAT; ˚C); and annual dissolved organic carbon flux in gC m^{-2} yr^{-1} (DOC) are provided in the arrows on the right side.

The Laurentide Ice Sheet covered the entire research area during the Late Wisconsinan Glacial Maxima. Presumably all developed soil was removed during its

retreat, leaving rock to restart pedogenesis. Glacial retreat began in the south around 14 ka, with retreat, re-advance, and a final retreat at 12.6 ka (Brookes, 1977), while the mid and high latitude regions were ice-free by 11.5 ka and 10 ka, respectively (Ricketts and Vatcher, 1996; Putt et al. 2010; King, 1985). This places an upper limit on the age of the soil in each region.

The higher latitude region is underlain by early Proterozoic bedrock of the Grenville Province (Gower, 1998) including granite, quartzofeldspathic and mafic amphibolites and gneisses. The local till is largely composed of gneissic or granitic clasts, potentially locally derived and is generally less than 50 cm thick, with sub-angular to very angular granule to boulder size clasts making up, on average, 35 % of the (McCuaig, 2002). The mid-latitude region is underlain by early Ordovician limestone and dolostone bedrock of the Humber Zone (Colman-Sadd et al., 2000). Bedrock found nearby includes granite, gneiss, ultramafics, and fine siliciclastic sedimentary rocks. The till is highly variable across the region, composed of fresh and weathered granite, slightly-to-moderately weathered sandstone, and fresh limestone, shale and phyllite (Ricketts and Vatcher, 1996). The lower latitude region is underlain by siliciclastic non-marine sedimentary bedrock of the Carboniferous and Devonian Codroy and Anguille Groups (Coleman-Sadd et al., 2000). Here, till is largely composed of micaceous sandstone and siltstone and granite (Ricketts, 2001).

Litterfall, soil respiration, and DOC fluxes from the organic layer increase along the transect with decreasing latitude (Ziegler et al., 2017) with DOC fluxes increasing as a function of increased winter temperature and reduced snowpack (Bowering et al. 2022).

Similarly, organic horizon % C and % N increase with decreasing latitude. Average surface mineral SOC content is similar among regions and exhibits high within-region variation occurring as a function of Al OMCs (Patrick et al., 2022).

4.2.2 Sample collection and preparation

Experimental soil samples were collected during the 2019 field season. At each plot, a 10 × 10 cm^2 area was measured and the organic horizon was removed. If the Ae horizon was present, it was scraped away with a trowel, and the Bf mineral horizon was carefully excavated to 10 cm depth. Samples were collected at three plots within each site, except for the SR-TM site for which three replicate samples were collected within each of two plots in an effort to capture the heterogeneity observed in previous studies (Patrick et al., 2022). Samples were stored in sealed plastic bags and kept at 5 °C until they were gentle sieved at field soil moisture to 2 mm, weighed and set to air dry. Once dry, the soils collected within each site were pooled by weight and gently homogenized at the site level except SR-TM which was homogenized at plot scale in an attempt to capture the heterogeneity of the site (Patrick et al. 2022). Homogenized soil samples were sub-sampled for the experimental columns, and a separate subsample was ground to a fine powder using a mortar and pestle for mineral soil characteristic analyses.

Mineral soil samples were collected across full depth of the mineral profile from soil pits excavated at two sites from each of the North and South regions in the summer of 2014. The characteristics measured from these profiles were used for predicting DOC uptake to or loss from the soil based on the equations fit to the experimental results. Soils

were carefully scraped from the wall face by genetic horizon. Thick horizons (> 15 cm) were divided into two or more sections. These were sieved to 2 mm, dried and sub-sampled for analysis of SOC and pyrophosphate extractions.

Soil solution, providing DOM for the experimental additions, was collected from passive pan lysimeters distributed throughout the hillslope area of Pynn's Brook Experimental Watershed Area, an intermediate region of the NL-BELT near Deer Lake in western Newfoundland (refer to Bowering et al. (2020) for details of the lysimeter design and installation). The soil water was pumped out three times during the late summer to fall period of 2020 (early September to November). Once collected, it was filtered to 0.1 μm regularly and stored in the dark at 5 ˚C until needed.

4.2.3 Experimental design

Soil columns were built in 12 cm tall and 5 cm in diameter acrylic open-ended cylinders. Polypropylene mesh screening was secured over the bottom with plastic cable ties, and the column was supported on the opening of a clean (acid washed and precombusted) glass jar for filtrate collection (Figure 4.2). Columns were filled with soil to 10 cm height based on the measured soil density of each site and a rock volume averaged among all sites (Table S4.1 in Appendix). A preliminary experiment determined that rock inclusion similar to field conditions significantly reduced soil compaction and retained near *in situ* soil conditions following DOM solution application (Patrick et al., 2022).

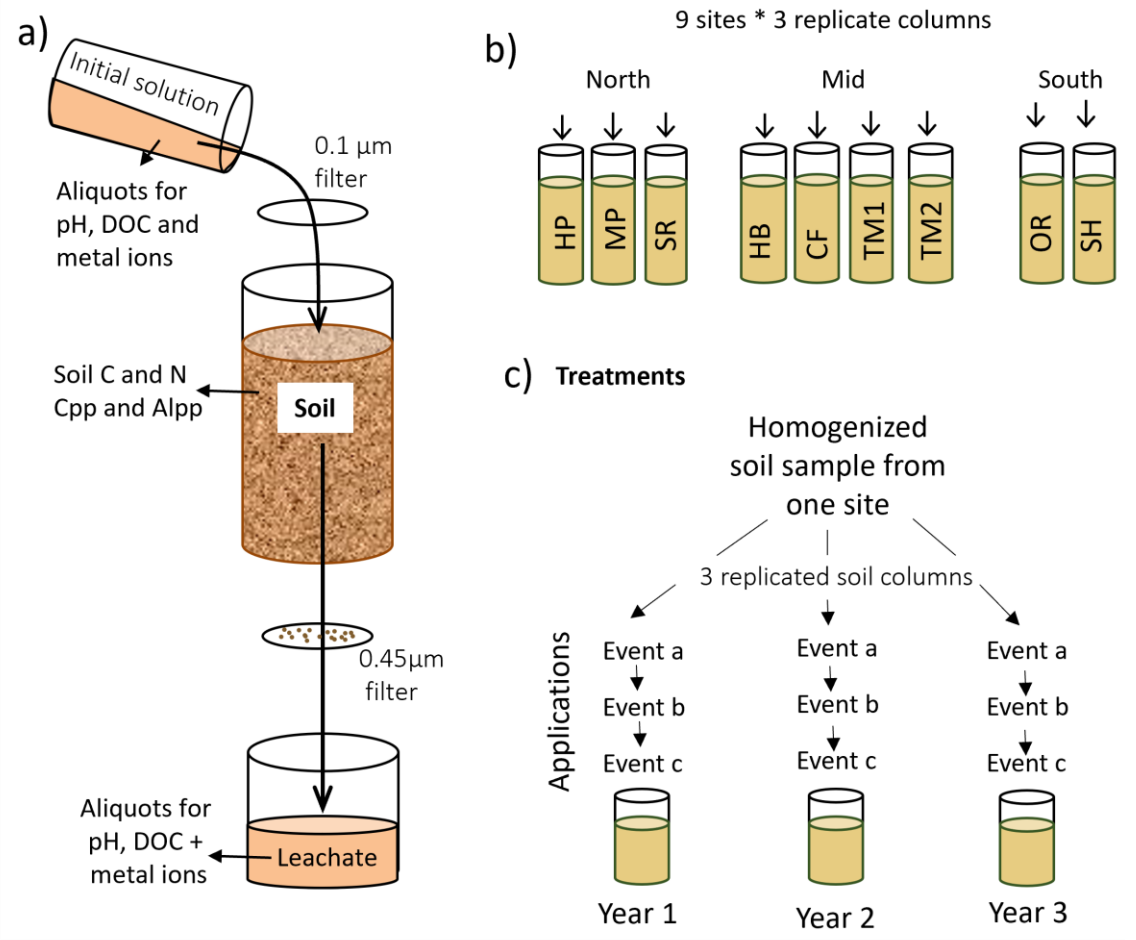

Figure 4.2.

Experiment set up. (a) Samples of the initial and leachate soil solutions were analyzed for dissolved organic carbon (DOC), pH and metals, and experimental columns for soil C and N, and pyrophosphate extractions of C and Al (Cpp and Alpp). (b) Soil columns were established from soils collected at three plots within each site from three regions (North, Mid, South) and homogenized by weight. Three replicate columns were prepared from each homogenized soil for each site except for SR-TM site where three samples were collected, homogenized and replicated at the plot level for two plots due to site heterogeneity. (c) Experimental treatments were established and illustrated here using one soil sample example. Three replicate columns were built from each homogenized soil sample, with each replicate having received three applications of initial soil dissolved organic matter solution (see Table 4.1 characteristics of the initial solutions).

Soils were gently mixed with lysimeter water to 60% of the soil water holding capacity on clean foil prior to column packing. Because of high biological activity upon rewetting (Barnard et al., 2020), the soil columns were left to rest at 4 °C in the dark for

three weeks in loosely sealed mason jars prior to experiment execution. This approach was meant to represent conditions similar to those experienced following late summer and early fall after peak evapotranspiration when soils are slowly rewetted.

The initial soil solution was filtered to 0.1μm before its application to the soil column (Figure 4.2). An aliquot of the initial solution was collected prior to each application for an initial measurement of DOM properties (Table S4.2 in Appendix). Three experimental replicate columns were prepared of each sample to produce 27 soil columns (three replications of soils from 9 forest sites).

Each column received three applications of the initial solution to investigate differences in how a soil may respond to the first event after a dry period (analogous to first autumn event after dry summer) versus a second or third precipitation event (Figure 4.2 and Table 4.1). Soil columns of the same replication (i.e. 1, 2 or 3) and application (i.e. a, b or c) were run simultaneously each week so that the same initial soil solution was applied to all within the same replication (see Table S4.2 in Appendix for initial soil solution characteristics).

Table 4.1.

Experimental design for soil column leaching experiment to evaluate SOC response to extreme precipitation via change in dissolved organic carbon (DOC). Nine sites from three regions were replicated into three soil columns where each replicate represents a different year. Each column received three sequential applications representing events (3 events/year). The sum of net DOC change across three applications (DOMsum) to a single column represents a three-event season, while net DOC change among applications averaged over three replicates (DOMapp) evaluates difference in event sequence related to increasing moisture

Column set up

Region (3)	North				Mid			South	
Site (9) * 3 column reps	ER-HP	ER-MP	ER-SR	SR-CF	SR-HB	SR-TM1	SR-TM2	GC-OR	GC-SH

Treatments

	Year (Column rep)		
Event (Application)	1	2	3
a	1a	2a	3a
b	1b	2b	3b
c	1c	2c	3c

DOC_{sum}: Sum of all applications for each column

Region (3)	North				Mid			South	
Site (9) * 3 column reps	ER-HP	ER-MP	ER-SR	SR-CF	SR-HB	SR-TM1	SR-TM2	GC-OR	GC-SH
Treatment (36): Year 1-3	1	1	1	1	1	1	1	1	1
	2	2	2	2	2	2	2	2	2
	3	3	3	3	3	3	3	3	3

DOC_{app}: Average DOC change for each application for each site

Region (3)	North				Mid			South	
Site (9) * 3 column reps	ER-HP	ER-MP	ER-SR	SR-CF	SR-HB	SR-TM1	SR-TM2	GC-OR	GC-SH
Treatment (36): Event	a	a	a	a	a	a	a	a	a
	b	b	b	b	b	b	b	b	b
	c	c	c	c	c	c	c	c	c

For each storm event (each application), 300 ml was added to each column in 20 ml intervals throughout the day. Each 20 ml application is approximately equal to a 10 mm rain event, for a total of a 150 mm storm event. This high infiltration rate is comparable to *in situ* stormflow conditions, maximizing particulate mobilization with the total application of 150 mm within the range of recent extreme events in Newfoundland (e.g. 196 mm on Nov. 24 2021, Port aux Basques (Station 73026) , and 200 mm on Sept. 11 2022, St. John's West (Station 71250) from Environment Climate Change Canada) and regional trends of increasing frequency of large late summer or early fall rain events (Finnis and Daraio, 2018).

The collected soil leachate was centrifuged, and the supernatant was sequentially filtered through pre-combusted Whatman GF/C and GF/F (nominal pore sizes of 0.90 μm and 0.45 μm, respectively). Aliquots of the filtrate were then partitioned into 24 ml precombusted glass vials followed by addition of 20 % phosphoric acid (HPLC Grade) for DOC analyses. The difference in the initial soil solution and collected leachate was used to determine net stabilization or loss of DOC (ΔDOC).

4.2.4 Analysis of soil characteristics and experiment data

To determine the water holding capacity at atmospheric pressure, water was slowly added to approximately 100 grams dry weight of < 2 mm mineral soil in a Buchner funnel with a Whatman GF/C filter until it began to drip. After dripping stopped, soils were transferred to tin cups and dried at 105°C and the water weight was divided by the dry soil weight to provide the water holding capacity (Laganière et al., 2015).

Pyrophosphate extracted metals (Al_{pp} and Fe_{pp}) and C (C_{pp}) are proxies for the abundance of soil OMCs and associated C (McKeague, 1967). For this extraction, approximately 0.300 g of < 2 mm ground soil was weighed into 50 mL polyethylene tubes with 30 mL of 44.6 g/L sodium pyrophosphate solution and shaken for 16 hours in the dark. The solution was centrifuged until clear, and the supernatant was filtered through a precombusted Whatman GF/F filter. To determine the metal concentrations of the pyrophosphate extractions the solution was diluted 50x, acidified with 2 % nitric acid by weight, and analysed on a Thermo Fisher Scientific iCAP 6500 Inductively Coupled Plasma Emission Spectrometer (Al and Fe limit of detection of 15 and 3 ppb). A proxy for the degree of saturation of Al OMCs with C (C_{pp}:Al_{pp}) was calculated using molar ratios of pyrophosphate extracted C and Al.

For soil C analysis, ground soil samples were weighed into tin cups with an equal weight of WO_5. These were analyzed with a Vario EL Cube elemental analyzer (Elementar). The C and N content of acetanilide was measured three to four times over the course of a run to make a daily correction (typically 1.03 – 0.97) to the calibration curves for C and N of the thermal conductivity detector. These have a limit of quantification of 20 μg and 5 μg, respectively. A low organic soil reference material (B2153: 1.61 ± 0.09 % C; 0.133 ± 0.023 % N) and a high organic sediment (B2151: 7.45 ± 0.14 % C; 0.52 ± 0.02 % N), both acquired from Elemental Microanalysis, were run as quality control samples and were within the accepted ranges (B2153: 1.56 % C and 0.132 % N; B2151 7.33 % C and 0.51 % N).

Dissolved organic carbon of the initial DOM solution, experiment filtrate and pyrophosphate-extracted solution was analysed with a Shimadzu TOC-VCSH Total Organic Carbon Analyzer paired with a Shimadzu TNM-1 Total Nitrogen Measuring Unit. Pyrophosphate-extracted solutions and sodium pyrophosphate blanks were diluted 10 –50 x, while the experimental solutions were undiluted. Samples, blanks and standards were acidified with 21.5 % HPLC grade phosphoric acid to pH of 2. In the case of the pyrophosphate extractions, standards of potassium hydrogen pthalate (KHP) and glutamic acid (GA) were prepared in the same extraction solution and used to generate calibration curve. Samples were analysed at 720 °C in replicates of 3 or 4, and the best 3 were averaged with sample precision 5 % or less. All samples were well above the 2.36 mg/L limit of detection.

To determine the net soil uptake or loss of DOC (ΔDOC), the DOC content of the leachate was subtracted from the initial soil solution content and normalized to grams of dry weight soil in the experimental soil column (n = 81; 3 replications of 3 applications to 9 soils). Depicting net changes from the perspective of the mineral soil, negative and positive ΔDOC values indicate a loss of DOC from the soil and uptake of DOC into the soil, respectively.

4.2.5 Design and Statistics

This work aimed to understand how increasing evapotranspiration and precipitation intensity predicted for boreal regions may impact shallow mineral horizon SOC content by evaluating controls on experimentally measured DOC uptake or loss in

soils. Here, event factors were manipulated in treatments to evaluate the roles of ephemeral factors associated with events and seasons (e.g. antecedent soil moisture is often associated with season). Further, DOC change was evaluated for spatial differences and against factors that are fixed at the event scale (i.e. soil characteristics) to understand the mechanisms controlling SOC stability during extreme events. Comparing results for the soils collected from three climate regions with contrasting parent material enabled evaluation of any regional impact on SOC response. The range of C_{pp}:Al_{pp} across these sites include more saturated Al OMCs (higher C_{pp}:Al_{pp}) in shallow soils where the DOM flux is the largest and therefore could have the greatest impact. The results of this study were then combined with the former experiment to evaluate the impact of the full range of C_{pp}:$Al_{pp.}$ Here, only C_{pp}:Al_{pp} and soil moisture predictors were utilized across the two experiments because of their significant relationships with DOC change and the lack of regional controls.

Treatments were designed to evaluate differences among years and event timing (Figure 4.2 and Table 4.1). Each site soil was replicated into three columns, each column received three applications or events. The sum of net DOC change for the three applications to a single column represents the net result of a three-event autumn season (ΔDOC_{SUM}; n = 27) in a fully crossed experimental design. Models 1 and 2 evaluate the controls on ΔDOC_{SUM} using the results from the soils collect across the climate transect. The "Year" term in these models evaluates natural variability in the character of soil DOM mobilized among years related to variation in soil solution processes of events.

Model 3 evaluates ΔDOC_{SUM} data from both the climate transect and forest hillslope experiments. A "Horizon" term was included here to evaluate depth in addition to C_{pp}:Al_{pp} controls.

$$DOC_{SUM} \sim Region + Year + Region*Year \quad \text{(Model 1)}$$

$$DOC_{SUM} \sim C_{pp}:Al_{pp} + Year + C_{pp}:Al_{pp} *Year \quad \text{(Model 2)}$$

$$DOC_{SUM} \sim C_{pp}:Al_{pp} + Horizon + C_{pp}:Al_{pp} *Horizon \quad \text{(Model 3)}$$

The average of DOC uptake by application across the three soil column replicates was used to evaluate event timing associated with antecedent moisture (ΔDOC_{APP}; 3 applications; n = 27). This fully crossed experimental design essentially uses repeated measures, however, a random block was not employed as the ordering of events was of interest (Figure 4.2 and Table 4.1). Model 4 uses the application number, included here as the "Event" factor, to represent and evaluate the impact of the sequence of precipitation events from late summer through the wet fall using data from both experiments.

$$DOC_{APP} \sim C_{pp}:Al_{pp} + Event + C_{pp}:Al_{pp}*Event \quad \text{(Model 4)}$$

General linear models were used to evaluate the roles of C_{pp}:Al_{pp}, region and event factors on DOC change. ANOVAs were evaluated in RStudio version 4.2.3. All tests were conducted using $\alpha = 0.05$. Model residuals were checked to be homogeneous, independent, and normally distributed with residual versus fit, lag and quantile-quantile plots, respectively. Where models did not meet these criteria, log-transformed data was a better

fit. The data for several columns could not be used in these tests as they collapsed or were compacted after the first or second application and thus omitted from some analyses.

To apply experimental results to forest soils, simple models were developed using the results to make predictions of SOC response over depth to the three moisture levels representing the event timing. Equations were fit to the SOC response relationship with C_{pp}:Al_{pp} for each event using ΔDOC_{APP}. These models were used with the measured C_{pp}:Al_{pp} depth profiles from four of the climate transect sites to determine the depth ranges across which DOC uptake and loss occurs in dry, moist and wet soils. The depth at which DOC loss transitions to uptake (uptake threshold) for each moisture level was used to predict SOC response to events in different seasons.

4.3 Results and Discussion

4.3.1 Soil organic carbon response to extreme precipitation is controlled by C saturation of organo-metal complexes and antecedent soil moisture

The shallow mineral soils largely exhibited DOC loss during the experimental addition of soil solution (Figure 4.3a). The variation in DOC loss was best explained by a negative relationship with C_{pp}:Al_{pp}, where soils with more carbon saturated Al OMCs (greater C_{pp}:Al_{pp}) experienced greater carbon loss (Figure 4.3b; Table 4.2 for model results). This is consistent with the DOC uptake relationship with lower C_{pp}:Al_{pp} exhibited by soils in the previous hillslope experimental study (Chapter 3). Combining the results

from the climate transect sites with those previous findings provided a wide range of C_{pp}:Al_{pp} informing the natural log relationship explaining net DOC change from uptake to loss scenarios (Figure 4.4a).

Table 4.2.

Model results from ANOVA tables evaluating controls on experimental net change in dissolved organic carbon (DOC) as sum of all applications to a single column (DOC_{SUM}) or among applications averaged across replicates (DOC_{APP}). Each application represents an 'Event' (treatment) where each column receives three applications representing a three-event season. The 'Year' (treatment) evaluates the natural variability among years (three column replicates). Pyrophosphate-extracted ratio of C to Al used as a proxy for the degree of C saturation of organometal complexes (CAl_{pp}) is the main soil characteristic of interest. Models are evaluated using explained variance adjusted for number of predictor variables (R^2) and the p-value (P). Degrees of freedom are indicated with Df. Predictors or interactions determined to have a significant influence on the dependent variable are given in black as opposed to grey which are not significant.

Dataset	Model	Predictor	Df	Adjusted R^2	P
Transect	DOC_{SUM}~ Region + Year + Region*Year	Region	2	0.236	0.086
		Year	2	0.044	0.594
		Region*Year	4	0.062	0.821
		Residuals	16	0.657	
		Total		0.014	0.446
	DOC_{SUM}~ CAl_{pp} + Year + CAlpp*Year	CAl_{pp}	1	0.636	6.11E-06
		Year	2	0.048	0.264
		CAl_{pp}*Year	2	0.001	0.972
		Residuals	19	0.316	
		Total		0.601	0.000282
Transect + Hillslope	DOC_{SUM}~ logCAl_{pp} + Horizon + logCAlpp*Horizon	CAl_{pp}	1	0.761	2.20E-16
		Horizon	1	0.018	0.026
		CAl_{pp}*Horizon	1	0.023	0.012
		Residuals	58	0.198	
		Total		0.791	2.20E-16
	log(DOC_{APP}+1)~ CAl_{pp} + Event + CAlpp*Event	CAl_{pp}	1	0.553	4.23E-13
		Event	2	0.116	0.0003
		CAl_{pp}*Event	2	0.000	0.989
		Residuals	54	0.331	
		Total		0.6379	7.10E-12

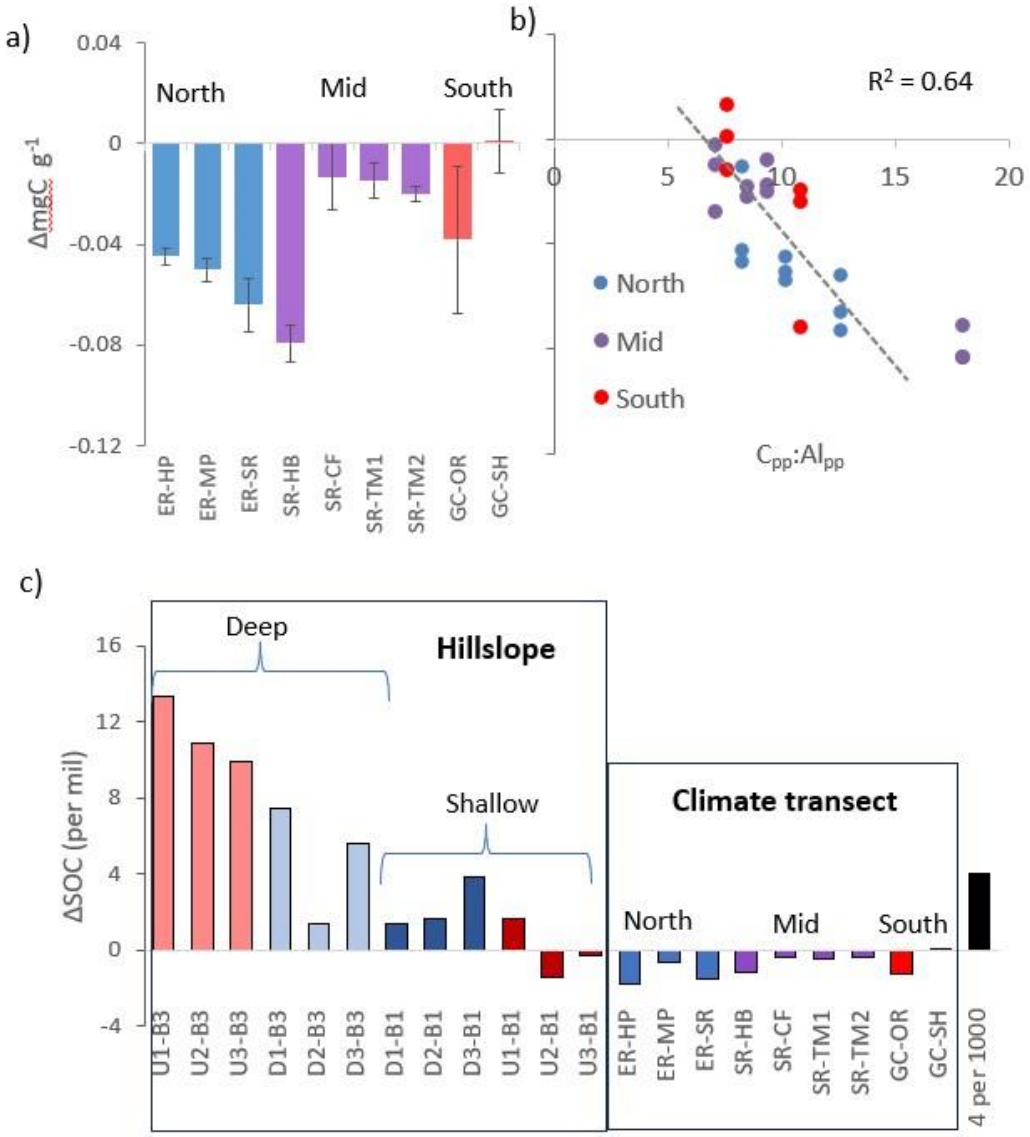

Figure 4.3.

a) Experiment results for surface mineral soils sites collected from three regions of a boreal forest climate transect (North, Mid, South). The sum of dissolved organic carbon uptake (+) or loss (-) into or from the soil across three experimental applications (ΔDOC_{SUM}) normalized to gram dry weight soil for each site. Error bars indicate standard deviation of the three replications per site. b) the relationship between ΔDOC_{SUM} and the saturation of Al organo-metal complexes with C via pyrophosphate extraction (molar C_{pp}:Al_{pp}). (c) Change in soil organic carbon (SOC) per mil summed across all applications and averaged among plots. See Chapter 3 for details on Hillslope experiment. Four per mil indicated for comparison to climate mitigation goals.

Surprisingly, there was no difference in DOC loss among regions despite regional variations in climate and parent material which control and contribute to variation in Al OMC abundance (Table 4.3 for soil characteristics). The absence of parent material controls may be explained by the short water residence times limiting OMC coprecipitation as the requisite Al concentrations could not be realized here no matter the availability of parent material Al. Therefore, with minimal DOC adsorption via OMC coprecipitation, it is likely that the experimentally measured net change is predominantly surficial exchange of DOM. The relationship of DOC change with C_{pp}:Al_{pp} suggests this exchange is largely with extant OMCs but does not rule out surface exchange with poorly crystalline reactive metals at depth.

Table 4.3.

Mineral soil characteristics of each site which was homogenized by weight from three collections. These include soil organic carbon (SOC), concentration of carbon and Al from pyrophosphate extractions (Cpp and Alpp), molar ratio of C to Al in the pyrophosphate extracts (Cpp:Alpp), and water holding capacity (WHC).

Site	Region	SOC (%)	C_{pp} (%)	Al_{pp} (g kg^{-1})	C_{pp}:Al_{pp}	Soil Density (g cm^{-3})	WHC (%)
ER-HP	North	2.53	0.50	1.36	8.27	0.98	95.3
ER-MP		7.49	1.52	3.36	10.14	0.93	79.0
ER-SR		4.23	0.90	1.60	12.63	0.81	72.9
SR-HB	Mid	6.94	0.90	1.14	17.89	0.80	74.1
SR-CF		3.35	2.61	8.29	7.06	0.92	88.9
SR-TM1		3.18	1.19	2.86	9.37	0.52	56.3
SR-TM2		5.61	2.24	5.94	8.45	0.53	56.3
GC-OR	South	3.08	1.13	2.37	10.74	0.65	97.7
GC-SH		3.50	1.05	3.10	7.61	0.81	83.7

The relationship of DOC change with C_{pp}:Al_{pp} was further evaluated in terms of the sequence of events. Events on soils that most recently experienced dry conditions, analogous to the first late summer event, consistently exhibited greater DOC loss at high C_{pp}:Al_{pp} and less uptake at low C_{pp}:Al_{pp} than wetter soils (Figure 4.4b and S4.2). Importantly, the C_{pp}:Al_{pp} threshold at which the transition from DOC loss to uptake occurs increases with wetter antecedent conditions as evidenced by the increase in x-axis intercept of the application trendlines. Enhanced DOC loss with events on recently dry soils may be explained by desorbed DOM from mineral surfaces during drying that are later mobilized as has been observed by others (Kaiser et al., 2015; Bailey et al., 2019; Patel et al., 2021). Therefore, these results suggest that the soil metric C_{pp}:Al_{pp} and antecedent soil moisture conditions control SOC response during extreme events regardless of the soils regional parent material or climate history.

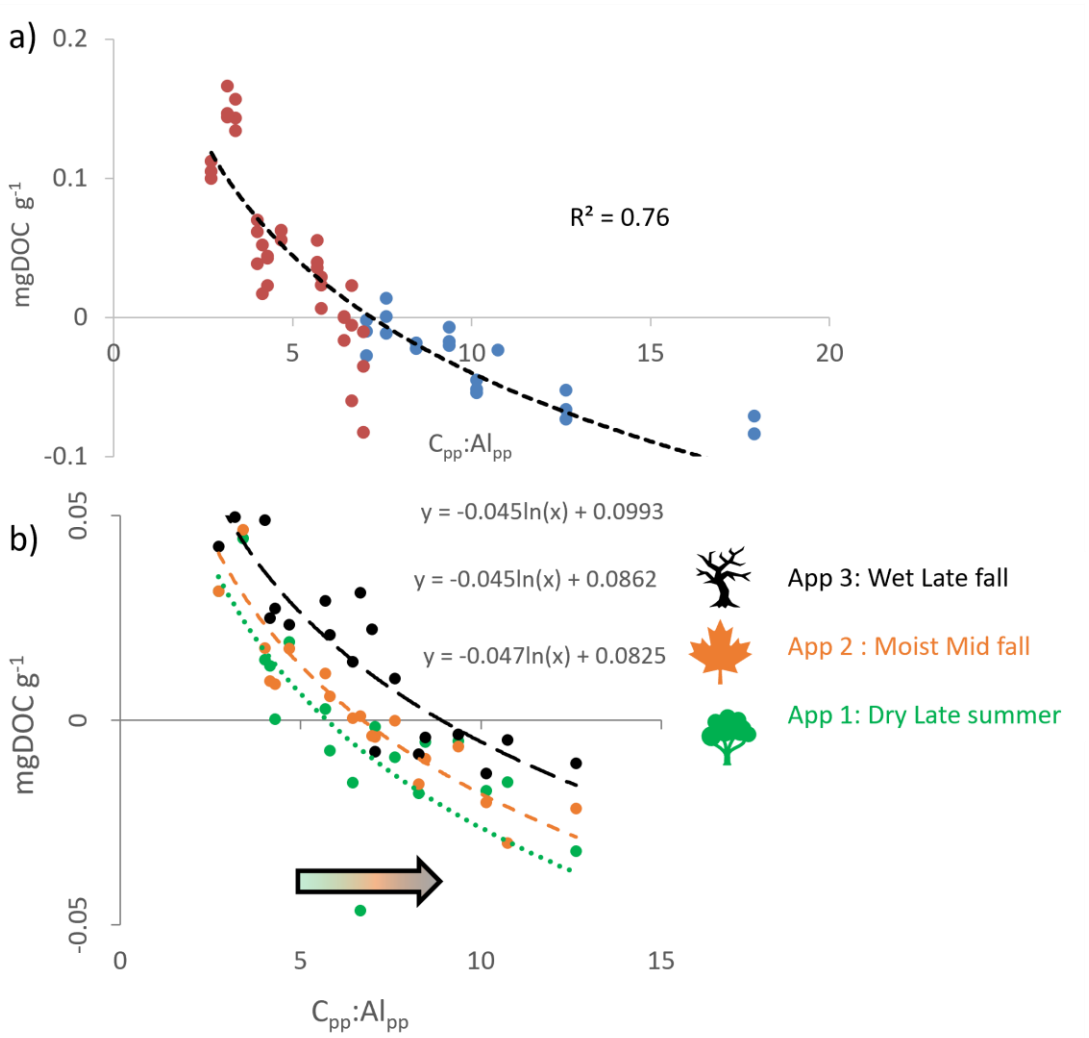

Figure 4.4.

a) Net change in dissolved organic carbon (DOC) as sum of three applications to soil column (ΔDOC_{SUM}) as a function of the saturation of Al organo-metal complexes with C as determined from pyrophosphate extraction (molar C_{pp}:Al_{pp}). Uptake of C into the soil is given as a positive value while loss from soil is negative. Data from across the climate transect sites are given in blue while those from the previous hillslope study by Patrick et al. (Chapter 3) are in red (b) Net change in DOC per application averaged among three column replicates per site, and the relationship with C_{pp}:Al_{pp} is given separately below where the arrow indicates the change in threshold value of C_{pp}:Al_{pp} depicting the transition from C loss to uptake that occurs increasing with soil moisture.

4.3.2 Soil drying increases depth over which carbon loss occurs with extreme precipitation

By fitting an equation to the net DOC change relationship with C_{pp}:Al_{pp} for each application using data from both experiments, SOC response to events and varying soil moisture was predicted with depth in soils with known C_{pp}:Al_{pp} (Figure 4.5). Employing four soil profiles for this purpose, two from each of the North and South regions, I was able to make predictions of the depth ranges of DOC uptake or loss and interpret the response of SOC to different event scenarios (Figure S4.1 in Appendix).

Despite contrasting parent material and climate history, the C_{pp}:Al_{pp} profiles were depth-dependent but did not exhibit regional differences (Figure S4.1 in Appendix). Shallow soils were very C saturated (greater C_{pp}:Al_{pp}) and exhibited a rapid decrease at ~10 – 30 cm. As such, net DOC loss was predicted in shallow soils, transitioning to net uptake at variable depths (~10 – 35cm; Figure 4.5). Within an individual profile, the depth of this threshold to net uptake was deeper in dry soils, and dry soils exhibited greater DOC loss. In one profile, ER-MP, loss is predicted to a depth of 20 cm with antecedent dry conditions, while uptake is predicted across the entire profile in wetter conditions.

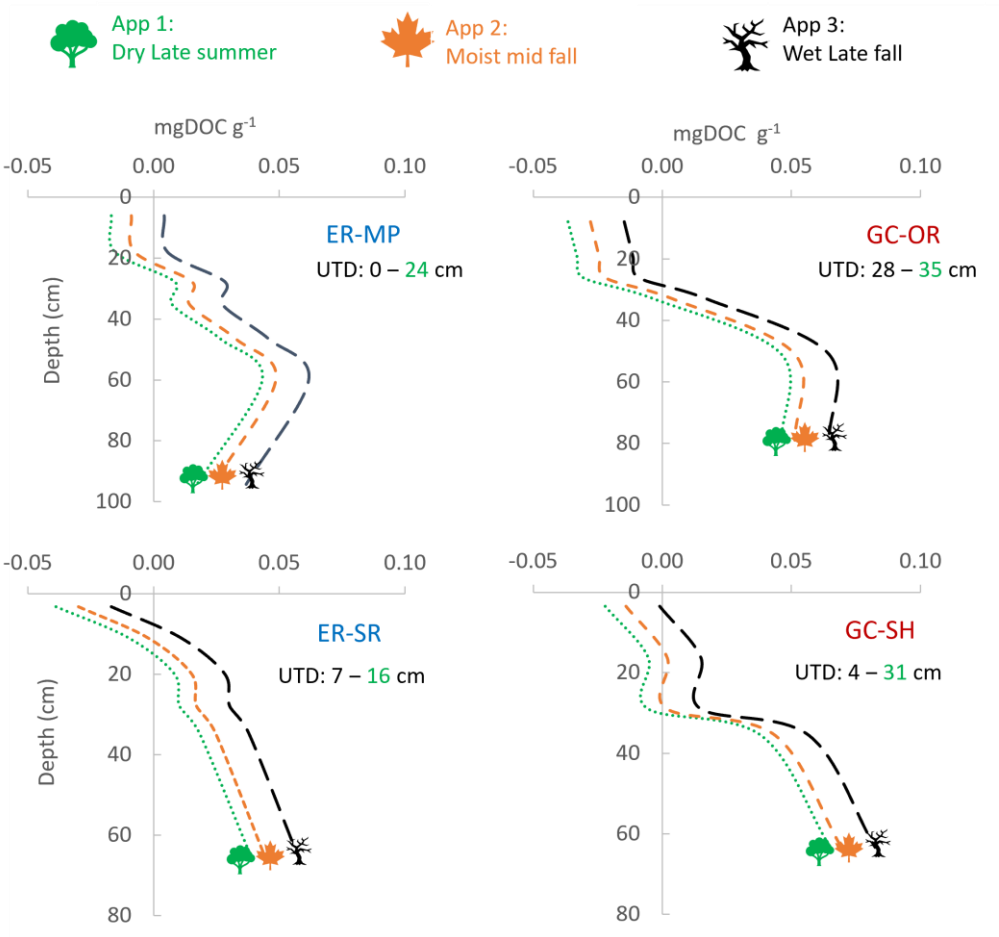

Figure 4.5.

Predicted net dissolved organic carbon (DOC) change over depth per gram dry weight soil in response to high intensity precipitation events using equations fitted to applications of experiment representing antecedent soil moisture conditions associated with time of year (see Figure 4.4). Negative net DOC change indicates loss from soil, and positive, uptake to the soil. Depth at which line crosses y-axis is the location where the threshold exists between net loss and net uptake of DOC. Range of uptake threshold depth (UTD) indicated below site name. ER-MP and ER-SR are sites from the North (blue), and GC-OR and GC-SH are from the South (red).

This suggests that in drier conditions, SOC is more vulnerable to loss during extreme precipitation events and the soil solution would have to infiltrate deeper to reach the threshold of uptake conditions. It is important to note that while deeper soils exhibit significant capacity for C uptake and storage via undersaturated OMCs, this is dependent

on the impact of climate change on hydrology. Shallow preferential flow paths are common as hydraulic conductivity generally decreases with depth. Thus, deeper SOC is likely limited by a C source. Gentle slopes should have greater potential for deep SOC accrual as infiltration is generally greater than in steeper landscapes (Kamel et al, in prep.; Chapter 3).

4.3.3 Event timing determines shallow SOC response to climate change

Evapotranspiration will likely be enhanced via increasing summer temperatures, inducing deeper and more extensive soil drying (Helbig et al., 2020; Wang et al., 2021). Since dry soils are more vulnerable, events on dry soils could lead to shallow SOC reductions in wet boreal mineral soils with climate change. Therefore, the timing of such events is particularly important.

Our results suggest that a 'worst-case' scenario for DOC loss is a late summer to early autumn event occurring directly on dry soils (Figure 4.6). Here, the threshold for uptake is deeper meaning greater infiltration is required before net DOC uptake is exhibited. This suggests that late summer events may exhibit shallow DOC loss from the soil and rapid transport to the stream or downstream environment (e.g., wetland) via preferential or lateral flow paths.

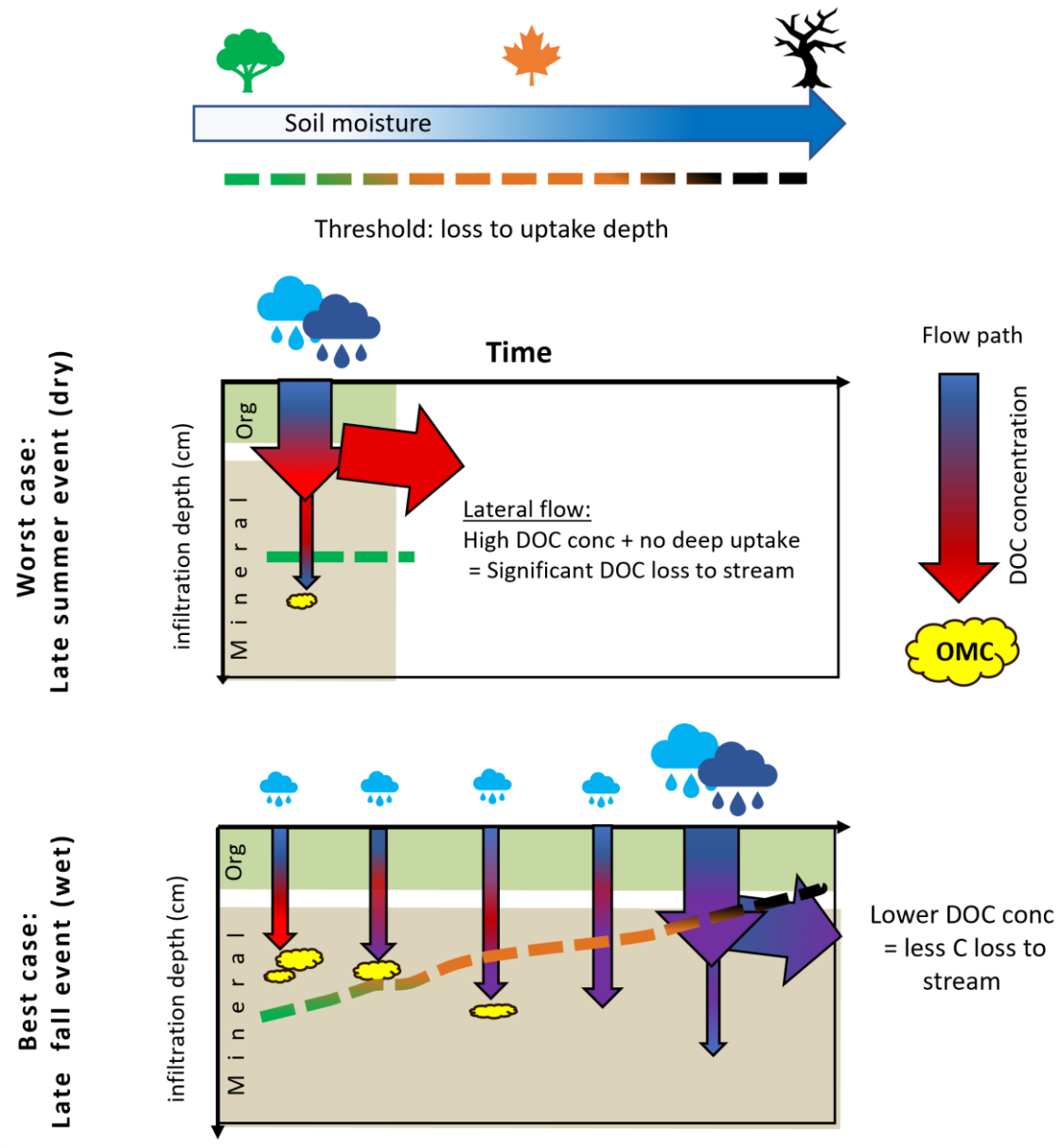

Figure 4.6.

Impact of event timing on mineral soil organic carbon response illustrating the proposed worst- and best-case scenarios as informed by this study. Size of rain cloud indicates relative size of precipitation event. The soil moisture gradient increases from late summer (green) to mid fall (orange) and then late fall (black). Soil moisture in turn impacts the threshold, defined by the ratio of carbon to Al in the organometal complexes (OMC), which controls the depth at which the transition from dissolved organic carbon (DOC) loss to uptake occurs in the soil.

In a contrasting scenario, a slow increase in soil moisture after a dry summer through multiple small events would likely not transport any desorbed DOC a significant distance. Much desorbed DOC would likely be reabsorbed or coprecipitated into OMCs as a result of the longer water residence times. A subsequent large event on late autumn wet soils would result in negligible SOC loss or slight uptake because of the shallow uptake threshold.

The experimentally measured cumulative SOC loss via DOC in the soils of the climate transect suggests a potential ~0.5 – 2 ‰ SOC reduction in shallow wet boreal soils during a single fall season with three events (Figure 4.3c and Table S4.3 in Appendix). This is a significant loss considering that this horizon is often the most SOC-enriched horizon in boreal forests and receives the greatest water flux. Further, a few seasons with this kind of SOC loss, particularly those with initial largest events happening in late summer or start of fall, would be detrimental to the working progress towards a 4 ‰ increase in SOC storage globally in the short term for climate change mitigation (Minasny et al., 2017). In contrast, the deeper soils from the hillslope study exhibited up to a 13 ‰ increase in SOC, indicating significant storage potential at depth (Figure 4.3c).

Finally, I expect historically wetter boreal biomes to be most impacted by shallow SOC loss via enhanced summer drying. Relatively drier boreal biomes with historically lower mean annual precipitation support less SOC and relatively reduced C_{pp}:Al_{pp} suggesting shallow DOC uptake is likely even under dry conditions based on our model.

4.4 Conclusions

In this study, I measured net DOC change in response to high infiltration rates representative of extreme rain events in shallow mineral soils across a boreal forest climate transect. I found that the soil characteristic C_{pp}:Al_{pp} and antecedent soil moisture control SOC response to extreme rain events regardless of the regional parent material and climate. By looking at a wide range in C_{pp}:Al_{pp}, I was able to uncover the essential role of pre-event soil moisture in controlling the C_{pp}:Al_{pp} threshold that ultimately dictates the capacity of these forest soils to take up or lose C during these precipitation events. I find that pre-event soil moisture shifts the negative relationship of net DOC change and C_{pp}:Al_{pp} towards greater loss or less uptake in dry soils. This highlights the importance of extreme event timing as SOC is more vulnerable to loss in dry conditions like late summer relative to late fall soils which may experience uptake. Models of SOC response with depth like those presented in this study can be combined soil moisture and infiltration depths to make predictions of the fate of boreal SOC. Therefore, future efforts should be focused on enhancing our predictive understanding of soil hydrology given predicted changes in evapotranspiration and precipitation regimes to allow incorporation of SOC response into Earth System Models.

4.5 References

Bailey, V.L., Pries, C.H., Lajtha, K., 2019. What do we know about soil carbon destabilization? Environmental Research Letters. https://doi.org/10.1088/1748-9326/ab2c11

Barnard, R.L., Blazewicz, S.J., Firestone, M.K., 2020. Rewetting of soil: Revisiting the origin of soil CO2 emissions. Soil Biol Biochem. https://doi.org/10.1016/j.soilbio.2020.107819

Bowering, K.L., Edwards, K.A., Prestegaard, K., Zhu, X., Ziegler, S.E., 2020. Dissolved organic carbon mobilized from organic horizons of mature and harvested black spruce plots in a mesic boreal region. Biogeosciences 17, 581–595. https://doi.org/10.5194/bg-17-581-2020

Bowering, K.L., Edwards, K.A., Wiersma, Y.F., Billings, S.A., Warren, J., Skinner, A., Ziegler, S.E., n.d. Dissolved Organic Carbon Mobilization Across a Climate Transect of Mesic Boreal Forests Is Explained by Air Temperature and Snowpack Duration. https://doi.org/10.1007/s10021-022-0074

Brookes, I.A., 1977. Geomorphology and Quaternary geology of Codroy Lowland and adjacent plateaus, southwest Newfoundland, Can. J. Earth Sci. 2101–2120.

Colman-Sadd, S.P., Hayes, J.P., Knight, I., 2000. Geology of the Island of Newfoundland (Digital version of Map 90-01 with minor revisions). Newfoundland Department of Mines and Energy, Geological Survey, Map 2000-30, scale 1:1 000 000.

Finnis J, and Daraio, J, (2018) Projected Impacts of Climate Change for the Province of Newfoundland & Labrador: 2018 Update. Memorial University of Newfoundland, St. John's, NL.

Gower, C. F., 1998. Geology of the upper Eagle River map region, Grenville Province, southeast Labrador. Current Research (1998) Newfoundland Department of Mines and Energy, Geological Survey, 98-1.

Helbig, M., Waddington, J.M., Alekseychik, P., Amiro, B.D., Aurela, M., Barr, A.G., Black, T.A., Blanken, P.D., Carey, S.K., Chen, J., Chi, J., Desai, A.R., Dunn, A., Euskirchen, E.S., Flanagan, L.B., Forbrich, I., Friborg, T., Grelle, A., Harder, S., Heliasz, M., Humphreys, E.R., Ikawa, H., Isabelle, P.E., Iwata, H., Jassal, R., Korkiakoski, M., Kurbatova, J., Kutzbach, L., Lindroth, A., Löfvenius, M.O., Lohila, A., Mammarella, I., Marsh, P., Maximov, T., Melton, J.R., Moore, P.A., Nadeau, D.F., Nicholls, E.M., Nilsson, M.B., Ohta, T., Peichl, M., Petrone, R.M., Petrov, R., Prokushkin, A., Quinton, W.L., Reed, D.E., Roulet, N.T., Runkle, B.R.K., Sonnentag, O., Strachan, I.B., Taillardat, P., Tuittila, E.S., Tuovinen, J.P., Turner, J., Ueyama, M., Varlagin, A., Wilmking, M., Wofsy, S.C., Zyrianov, V., 2020. Increasing contribution of peatlands to boreal evapotranspiration in a warming climate. Nat Clim Chang 10. https://doi.org/10.1038/s41558-020-0763-7

King, G. A., 1985. A standard method for evaluating radiocarbon dates of local deglaciation: Application to the deglaciation history of southern Labrador and adjacent Québec. Géographie physique et Quaternaire 39(2), 163-182.

Laganière, J., Podrebarac, F., Billings, S.A., Edwards, K.A., Ziegler, S.E., 2015. A warmer climate reduces the bioreactivity of isolated boreal forest soil horizons without

increasing the temperature sensitivity of respiratory CO2 loss. Soil Biol Biochem 84, 177–188. https://doi.org/10.1016/j.soilbio.2015.02.025

Lee, J.-Y., Marotzke, Jochem, Bala, Govindasamy, Milinski, S., Yun, K.-S., Ribes, A., Ruane, A.C., Kumar Kanikicharla Qatar, K., Kattsov, V., Kimoto, M., Marotzke, J, Bala, G, Cao, L., Corti, S., Dunne, J., Engelbrecht, F., Fischer, E., Fyfe, J., Jones, C., Maycock, A., Mutemi, J., Ndiaye, O., Panickal, S., Zhou, T., Pirani, A., Connors, S., Péan, C., Berger, S., Caud, N., Chen, Y., Goldfarb, L., Gomis, M., Huang, M., Leitzell, K., Lonnoy, E., Matthews, J., Maycock, T., Waterfield, T., Yelekçi, O., Yu, R., Zhou, B., n.d. Chapter 4: Future Global Climate: Scenario-based Projections and Near-term Information 553–672. https://doi.org/10.1017/9781009157896.006

Lundstrom, U.S., van Breemen, N., Bain, D., 2000. The podzolization process. A review, Geoderma. https://doi.org/10.1016/S0016-7061(99)00036-1

McCuaig, S. J., 2002. Quaternary geology of the Alexis River area, and the Blanc-Sablon to Mary's Harbour road corridor, southern Labrador. Current Research. Newfoundland Dept. of Mines and Energy, Geol. Survey Branch, Report, 02-1.

McKeague, J. A., 1967. An evaluation of 0.1 m pyrophosphate and pyrophosphate-dithionite in comparison with oxalate as extractants of the accumulation products in podzols and some other soils , Can J Soil Sci, 47, https://doi.org/10.4141/cjss67-017.

Minasny, B., Malone, B.P., McBratney, A.B., Angers, D.A., Arrouays, D., Chambers, A., Chaplot, V., Chen, Z.S., Cheng, K., Das, B.S., Field, D.J., Gimona, A., Hedley, C.B., Hong, S.Y., Mandal, B., Marchant, B.P., Martin, M., McConkey, B.G., Mulder, V.L.,

O'Rourke, S., Richer-de-Forges, A.C., Odeh, I., Padarian, J., Paustian, K., Pan, G., Poggio, L., Savin, I., Stolbovoy, V., Stockmann, U., Sulaeman, Y., Tsui, C.C., Vågen, T.G., van Wesemael, B., Winowiecki, L., 2017. Soil carbon 4 per mille. Geoderma. https://doi.org/10.1016/j.geoderma.2017.01.002

Nierop KGJ, Jansen B, Verstraten JM (2002) Dissolved organic matter, aluminium and iron interactions: precipitation induced by metalycarbon ratio, pH and competition. Sci. of the Total Env. 300:201-211, https://doi.org/10.1016/S0048-9697(02)00254-1

Pan, Y., Birdsey, R.A., Fang, J., Houghton, R., Kauppi, P.E., Kurz, W.A., Phillips, O.L., Shvidenko, A., Lewis, S.L., Canadell, J.G., Ciais, P., Jackson, R.B., Pacala, S.W., McGuire, A.D., Piao, S., Rautiainen, A., Sitch, S., Hayes, D., 2011. A large and persistent carbon sink in the world's forests. Science (1979) 333, 988–993. https://doi.org/10.1126/science.1201609

Patel, K.F., Myers-Pigg, A., Bond-Lamberty, B., Fansler, S.J., Norris, C.G., McKever, S.A., Zheng, J., Rod, K.A., Bailey, V.L., 2021. Soil carbon dynamics during drying vs. rewetting: Importance of antecedent moisture conditions. Soil Biol Biochem 156. https://doi.org/10.1016/j.soilbio.2021.108165

Patrick, M.E., Young, C.T., Zimmerman, A.R., Ziegler, S.E., 2022. Mineralogic controls are harbingers of hydrological controls on soil organic matter content in warmer boreal forests. Geoderma 425. https://doi.org/10.1016/j.geoderma.2022.116059

Putt, M.M., Bell, T., Batterson, M.J., Smith, J.S., 2010. Late wisconsinan ice-flow history on the tip of the northern peninsula, northwestern newfoundland, Current Research.

Ricketts and vatcher (1996) granuler aggregate resource mapping in the roddickton-main brook area, great northern peninsula, newfoundland.

Ricketts, M. J.: 2001.Granular aggregate mapping in nts map areas 1n/2, 1n/11, 11o/14 and 11o/15, Current Research, 279–291.

Schaetzl, R.J., Luehmann, M.D., Rothstein, D., 2015. Pulses of Podzolization: The Relative Importance of Spring Snowmelt, Summer Storms, and Fall Rains on Spodosol Development. Soil Science Society of America Journal 79, 117–131. https://doi.org/10.2136/sssaj2014.06.0239

Scharlemann, J.P.W., Tanner, E.V.J., Hiederer, R., Kapos, V., 2014. Global soil carbon: Understanding and managing the largest terrestrial carbon pool. Carbon Manag. https://doi.org/10.4155/cmt.13.77

Slessarev, E.W., Chadwick, O.A., Sokol, N.W., Nuccio, E.E., Pett-Ridge, J., 2022. Rock weathering controls the potential for soil carbon storage at a continental scale. Biogeochemistry 157. https://doi.org/10.1007/s10533-021-00859-8

Wang, T., Zhang, H., Zhao, J., Guo, X., Xiong, T., Wu, R., 2021. Shifting Contribution of Climatic Constraints on Evapotranspiration in the Boreal Forest. Earths Future 9. https://doi.org/10.1029/2021EF002104

Ziegler, S. E., Benner, R., Billings, S. A., Edwards, K. A., Philben, M., Zhu, X., Laganière, J., 2017. Climate warming can accelerate carbon fluxes without changing soil carbon stocks. Frontiers in Earth Sci. 5, 2.

Chapter 5: Parent material can set the threshold for mineral soil organic carbon response to short-term climate change in wet boreal forests

Abstract

Boreal forests store significant soil organic carbon (SOC) in regions vulnerable to climate change. Dissolved organic matter (DOM) facilitates weathering to form Al organo-metal complexes (Al OMC) which precipitation with increasing Al to stabilize mineral horizon SOC. An enhanced DOM source to the mineral horizon is expected with climate change but a concomitant increase in water flux via annual precipitation may limit Al OMC precipitation. A boreal climate transect is employed to investigate water, DOM and parent material controls on SOC content and its response to short-term climate change. The south region has an Al-poor parent material and a 3-fold higher DOM input, while the north region has greater SOC and a weatherable Al-rich parent material. Soil characteristics recording weathering and SOC stability were evaluated for spatial trends to inform on their controls. I found that SOC was best predicted with Al OMC and its interaction with soil characteristics controlled by biome-scale water balance.

Mass transfer (Tau) Al weathering profiles coupled with SOC depth-trends indicated significant retention of DOM and weathered Al in OMC in the northern sites, while the depleted Tau Al profiles indicated substantial Al loss in the south. This suggested that the Al-rich north region frequently met the requisite soil solution C:Al for Al OMC precipitation. Therefore, the northern region can likely accrue SOC via OMC precipitation to a greater DOM flux (threshold) and increased SOC is expected with climate change despite a concomitant enhanced water flux. However, the southern region may exhibit SOC losses as the low-Al availability suggests a lower threshold of DOM flux that may already be surpassed. Therefore, parent material can set the threshold DOM flux for SOC accrual with climate change within this climate transect, suggesting greater SOC accumulation in wet boreal soils formed from Al-rich parent material.

5.1 Introduction

Boreal forests contain about 30 % of the global forest soil organic carbon (SOC) stock (Pan et al., 2011; Scharlemann et al., 2014). It is estimated that approximately half the boreal forest SOC stock is stored in the subsoil (Scharlemann et al. 2014) but there is large uncertainty in these estimates as studies are rare. These high latitude regions are expected to experience significant increases in temperature and changes in precipitation volume, form, and intensity (Lee et al. 2021). However, our predictive understanding of this large C reservoir is poor and likely contributes significantly to the large uncertainty in Earth system models of atmosphere-land C exchange (Friedlingstein et al., 2014).

Global-scale water balance determines the mechanisms of SOC storage, where the proportion of SOC stored in total metal weathering products increases with available soil moisture in water replete biomes to a maximum threshold of ~65 % (Kramer and Chadwick, 2018). At the continental scale, parent material and climate govern the formation of these weathering products through weathering rates. As such, SOC is greatest in "enhanced weathering zones" where regions with young parent material with significant Al-bearing primary minerals and excess water occur together (Slessarev et al., 2022). Water-replete boreal biomes should fall within the enhanced weathering zone as young soils in recently deglaciated regions often still contain ample weatherable primary minerals. Comparisons of model predictions and observed SOC suggest climate factors are overemphasized in models at the biome scale, while geological parent material may be of greater relative importance (Georgiou et al., 2021). Therefore, regional studies within a biome are best suited to evaluate SOC content predictors as this spatial scale isolates specific SOC stabilization mechanisms relevant to the biome and captures variations in regional parent material. Further, regional climate transect studies within a biome are most relevant for short-term climate change (20 – 100 years) as shifts in climate can be observed across space while the biomes features remain generally fixed (e.g. not experiencing dominant vegetation shifts).

In moist, acidic soils like boreal podzols, Al organo-metal complexes (OMCs) are the dominant mechanism of SOC storage in shallow mineral horizon SOC (Patrick et al., 2022). These sequester SOC in two steps: (1) first, dissolved organic matter (DOM) facilitates chemical weathering by chelating metals to form dissolved OMCs, and next, (2)

these may coprecipitate as solid OMCs via increasing pH and Al weathering to surpass a requisite solution C to Al ratio to stabilize DOM in the mineral horizon as SOC (Nierop et al., 2002). Therefore, the availability of Al for weathering, and therefore geological parent material contributions, should play an important role in reaching the threshold Al concentration for OMC precipitation for SOC storage.

However, short water residence times associated with anticipated high water flux events should limit Al OMC precipitation and therefore, SOC accrual. This is consistent with experimental studies that suggest exchange of DOM with extant Al OMCs surfaces is dominant during high intensity precipitation events, with little to no OMC precipitation (Chapter 3 and 4). This exchange is dependent upon the degree of C saturation of extant Al OMC and antecedent moisture conditions, where shallow soils with more saturated Al OMCs exhibit SOC loss under dry conditions, but less loss or minimal change in wet soils. However, deeper soils consistently exhibited uptake of DOM even at high water flux, highlighting the importance of infiltration depth on SOC accrual. Therefore, the impact of a changing climate on the hydrology of the soil, including infiltration depths, should also be considered in short-term SOC predictions.

An enhanced DOM flux is expected with warming in moist boreal forests (Bowering et al., 2022). While this will increase the mineral horizon C source and weathering rates, the concomitant reduction in soil water residence times may reduce Al OMC precipitation. Therefore, SOC response to climate change in these forests requires understanding the trade off between increasing C source and decreasing storage

mechanisms. This would be informed through better understanding of the role of parent material Al availability during chemical weathering and Al OMCs precipitation.

This work aims to: (1) develop better predictors of boreal forest subsoil SOC content, and (2) evaluate the roles of climate and parent material on SOC content and its response to short-term climate change in wet boreal forests. To address these to goals, I employ two to four climate regions of a wet boreal climate transect with parent material of contrasting Al availability. The Newfoundland and Labrador Boreal Ecosystem Latitudinal Transect (NL-BELT) exhibits a water availability (mean annual precipitation subtract potential evapotranspiration) of 641 – 832 mm (Kramer and Chadwick, 2018). This places the transect in the high-sensitivity zone to changes in precipitation and suggests that ~60% of mineral SOC is associated with metal weathering products.

First, I evaluated SOC content and soil characteristics related to weathering and mechanisms of SOC storage and stability (Table 5.1). The characteristics were also evaluated for spatial trends to inform on their controls and scales of operation (i.e. depth-, region-, or biome-dependent). A model was developed using for predicting SOC content using soil characteristics that were major controls across four regions. The relative roles of regional parent material and climate variables on the dominant mechanisms of SOC storage were considered through the history recorded in soil characteristics and weathering profiles. The response of SOC to short-term climate change was considered through the regional history and SOC response to precipitation events in the context of expected climate change. Given the similar water availability across the two regions, but the far richer weatherable parent material source of Al expected in the northern forests, I

hypothesize a greater Al availability and thus SOC storage via OMC precipitation in the northern forest soils.

5.2 Methods

5.2.1 Study area

The Newfoundland and Labrador Boreal Ecosystem Latitudinal Transect (NL-BELT) is a climate transect spanning 5.5º latitude along the eastern coast of Labrador and western coast of the island of Newfoundland. The transect spans a 5 ºC gradient in mean annual temperature and a range of 1073 to 1340 mm in mean annual precipitation (Environment and Climate Change Canada 30-year normal for 1980 – 2010). This work focuses on two of four established regions, Eagle River (ER; 53 ° latitude) and Grand Codroy (GC; 48 ° latitude) which I will refer to as the north and south regions, respectively (Figure 5.1). The other two intermediate regions, Salmon River and Pynn's Brook, were used for developing the SOC multiple linear regression model only (Details on these regions can be found in Patrick et al., 2022; Bowering et al., 2020). Within each region are three established forest stand sites approximately 80 m x 80 m. All sites are dominated by mature stands of balsam fir (*Abies balsamea*), with mesic, well-drained humo-ferric podzolic soils. Soils are of young to intermediate maturity, formed in a post-glacial area from till that varies in composition among regions (Figure S5.1; Table S5.1 in Appendix).

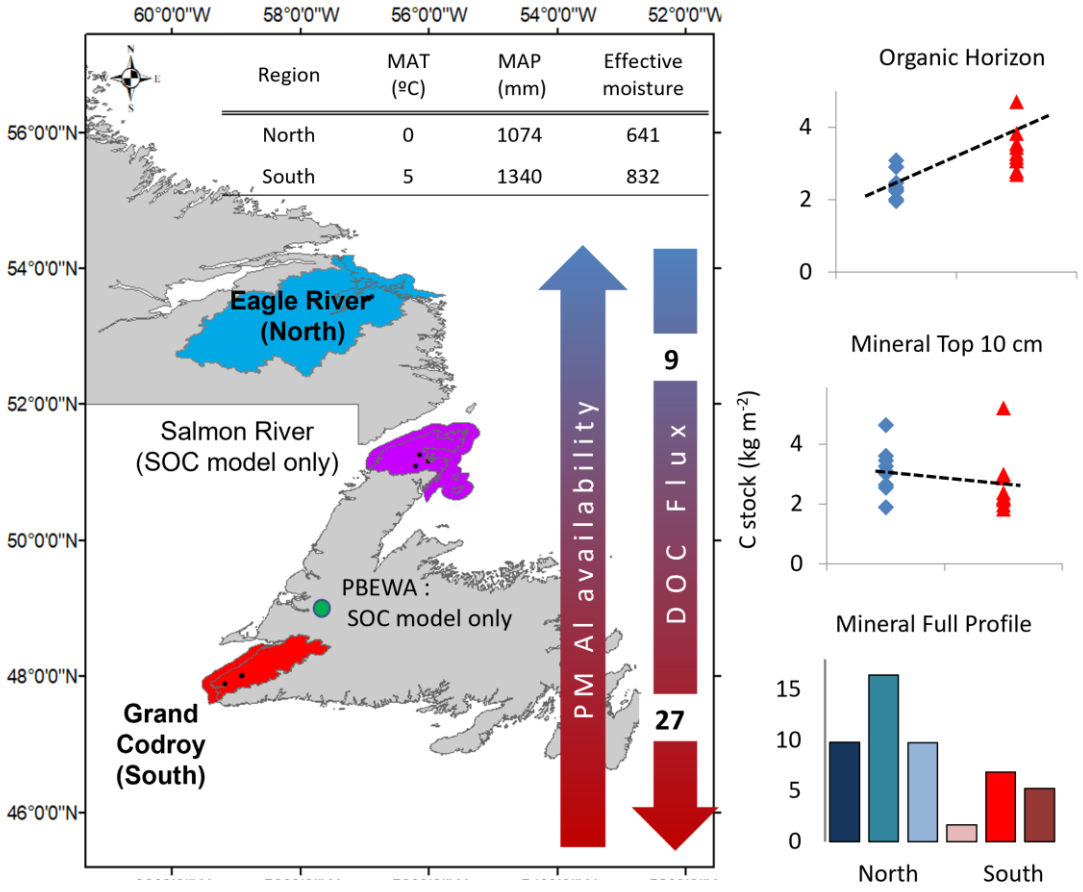

Figure 5.1.

Newfoundland and Labrador Boreal Latitudinal Ecosystem Transect map with regions, site locations, climate and parent material information, and trends of C stocks of the organic horizon, shallow mineral horizon (top 10 cm) and full mineral profile for the north and south regions. This study employs the north and south regions of the transect, but data from Salmon River and the Pynns Brook Experimental Watershed Area (PBEWA) are used for developing the SOC model only. Mean annual temperature (MAT), precipitation (MAP) and potential evapotranspiration (PET) are based on Environment Climate Change Canada climate normals for 1981 – 2010 from the Cartwright, Plum Point and Stephenville weather stations. Effective moisture is calculated as the difference of MAP and PET. Mean annual dissolved organic carbon flux in g C m^{-2} yr^{-1} (DOC) and parent material (PM). Effective moisture is the difference of MAP and potential evapotranspiration. Organic and shallow mineral stocks from Ziegler et al (2017). Range of blue (North) and Red (South) for the C stock of the mineral full profile represent the three study sites per region.

The Laurentide Ice Sheet covered the entire research area during the Late Wisconsinan Glacial Maxima. Presumably all developed soil was removed during its

retreat, leaving deposited glacial sediment to restart pedogenesis. Glacial retreat began in the south around 14 ka, with retreat, re-advance, and a final retreat at 12.6 ka (Brookes, 1977), while the northern region was ice-free by 10 ka (King, 1985). This places an upper limit on the age of the soil in each region.

The northern region is underlain by Proterozoic bedrock of the Grenville Province (Gower, 1998) with bedrock including granite, quartzofeldspathic and mafic amphibolites and gneisses. The local till is largely composed of gneissic or granitic clasts, potentially locally derived and is generally less than 50 cm thick, with sub-angular to very angular granule to boulder size clasts making up, on average, 35 % of the till (McCuaig, 2002). The southern region is underlain by siliciclastic non-marine sedimentary bedrock of the Carboniferous and Devonian Codroy and Anguille Groups (Coleman-Sadd et al., 2000). Here, till is largely composed of micaceous sandstone and siltstone, granite, with lesser dolomite, diorite, gabbro, gneiss and quartz pebbles (Ricketts, 2001).

Litterfall, soil respiration, and DOM fluxes from the organic layer increase along the transect with decreasing latitude (Ziegler et al., 2017) with DOM fluxes increasing as a function of increased winter temperature and reduced snowpack (Bowering et al., 2022). Similarly, organic horizon C and N stocks, as well as % C and % N, increase with decreasing latitude. Average surface mineral SOC content is similar among regions despite high within-region variation which varies as a function of Al OMCs (Patrick et al., 2022).

5.2.2 Sample collection

Till samples were collected in 2017 after selecting study sites based on roadside outcrop geology within the study area. Shovels were used to dig and remove outer debris to expose till to about 0.3 m depth to avoid surface overprinting. Sample volumes of approximately two litres were collected into plastic rock sample bags. Four to five samples were collected from each region. Till was ground into a fine powder with a rock a crusher and then pulverizer.

Soil samples were collected during the 2014 field season. One pit from each of three sites per region was dug to the C horizon, for a total of 6 soil pits. Horizons were identified using the Canadian System of Soil Classification. Soil was scraped from the wall face with a clean trowel across the full horizon or subdivisions of thicker horizons. Metal cores with a radius of 2.54 cm were hammered into the wall face for the collection of soil for bulk density. Samples were stored in plastic soil sample bags in coolers at 5 °C until returned to lab, weighed, and set to air dry. Dry soils were sieved to 2 mm and a subsample was ground using a mortar and pestle.

Three soil pits were employed for C and N content, isotopes, and mass transfer coefficients of weathering. Two soil pits from each region were chosen to evaluate C radiocarbon ages and other soil characteristics. Selection was based on soil profiles that had ample sample size at every depth in the profile for the analyses. The pit with the smallest C stock from the south was not employed, yet the largest C stock was eliminated in the northern region.

5.2.3 Analyses

Till mineral proportions

X-ray diffraction (XRD) on a Rigaku Ultima-IV system with a Cu source was used to identify and quantify minerals of ground till samples. Jade software (MDI, California) was used for mineral identification by matching peak locations using the International Centre for Diffraction Database (ICDD). Mineral proportions were quantified using reference intensity ratios as a proportion of the peak height of minerals with known proportions within the database (Zhou et al., 2018).

Till and soil major element analysis

Major elements of the till and soil were analysed on a Thermo Fisher Scientific iCAP 6500 Inductively Coupled Plasma Emission Spectrometer (Cambridge) after fusion using the methods of Cremer and Schlocker (1976). Powdered samples were brought into solution by fusion in a high-purity graphite crucible at 1000 °C for 30 min using a flux consisting of a combination of lithium metaborate ($LiBO_2$) and lithium tetraborate ($Li_2B_4O_7$) in a ratio of 0.06 g sample to 1 g of flux. The molten bead was transferred to a 100 mL polypropylene tubes containing 80 mL of 10 % distilled nitric acid and stirred on a magnetic stir plate until dissolved and diluted to a final volume of 100 mL. Values were reported as major oxides and normalized to remove the amount lost to ignition.

C and N elemental and isotopic analysis

For C and N elemental and isotopic analysis, ground subsamples were weighed into tin cups and analyzed with a Vario EL Cube elemental analyzer (Elementar) coupled to a Delta V Plus isotope ratio mass spectrometer (Thermo Scientific) via a ConFlo IV interface. As per the manufacturer's instructions, the combustion reactor (CuO) was held at 950 ºC, while the reduction reactor (Cu) was at 600 ºC.

For elemental analysis, the C and N content of acetanilide was measured three to four times over the course of a run to make a daily correction (typically 1.03 – 0.97) to the built-in calibration curves for C and N of the thermal conductivity detector. A low organic soil reference material (B2153: 1.61 ± 0.09 % C; 0.133 ± 0.023 % N) and a high organic sediment (B2151: 7.45 ± 0.14 % C; 0.52 ± 0.02 % N), both acquired from Elemental Microanalysis, were run as quality control samples. These have a limit of quantification of 20 μg and 5 μg, respectively.

For isotopic analysis, scale calibration was performed daily with EDTA #2 (δ^{13}C = -40.38 ± 0.01 ‰; δ^{15}N = -0.83 ± 0.04 ‰) and caffeine #2 (δ^{13}C = -14.79 ± 0.04 ‰; δ^{15}N = 20.17 ± 0.06 ‰) standards, both from Indiana University. The same quality control samples as for elemental analysis were used as isotopic quality controls (B2153: δ^{13}C = -26.71 ± 0.24 ‰; δ^{15}N = 7.00 ± 0.13 ‰; B2151: δ^{13}C = -28.90 ± 0.10 ‰; δ^{15}N = 4.35 ± 0.20 ‰). The limit of quantification for δ^{13}C and δ^{15}N was 80 mg C and 25 mg of N.

Pyrophosphate extracted metals and carbon

Pyrophosphate extracted metals (Al_{pp} and Fe_{pp}) and C (C_{pp}) are proxies for the abundance of soil OMCs and associated C (McKeague, 1967). For this extraction, approximately 0.300 g of < 2 mm pulverized soil was weighed into centrifuge tubes with 30 mL of 44.6 g/L sodium pyrophosphate solution and shaken for 16 hrs in the dark. The solution was centrifuged until clear, and the supernatant was filtered through a Whatman GF/F filter to 0.45 μm. A proxy for the degree of saturation of Al OMCs with C (C_{pp}:Al_{pp}) was calculated using molar ratios of pyrophosphate extracted C and Al.

To determine the metal concentrations of the pyrophosphate extractions, the extracted solution was diluted 50 x, acidified to 2 % nitric acid by weight, and analysed on a Thermo Fisher Scientific iCAP 6500 Inductively Coupled Plasma Emission Spectrometer (USA).

Pyrophosphate-extracted dissolved organic carbon (C_{pp}) was analysed with a Shimadzu TOC-VCSH Total Organic Carbon Analyzer (Kyoto). Pyrophosphate-extracted solutions and sodium pyrophosphate blanks were diluted 10–50x and acidified to a pH of 2 with 21.5 % HPLC grade phosphoric acid. Standards of potassium hydrogen pthalate (KHP) and glutamic acid (GA) were prepared and used to generate calibration curves. Samples were analysed at 720 °C in replicates of 4 and the best 3 were averaged with a sample precision of <5 %.

Bulk density and C and Al stocks

The bulk density of each soil horizon was measured by hammering a metal core (2.54 cm radius) into the soil pit face and excavating the entire contents. The soil was dried, divided into soil, roots and rocks, and soil bulk density was evaluated by the weight of dry soil divided by the full volume of the core.

The C stock of the entire soil profile was determined by multiplying the bulk density of each soil horizon by C content and the horizon depth (cm) to get the horizon C stock and summing the result of each horizon. Similarly, the total profile Al stock contributed by OMCs was calculated as the sum of each horizon stock, where the bulk density was multiplied by the horizon depth and Al_{pp} (g/kg).

Radiocarbon ages

Two soil pits were selected from each region for radiocarbon dating across depth. Further, nine samples per region were collected from the top 10 cm of the mineral horizon, pooled by site, and separated into coarse and fine fractions (> 53 μm and < 53 μm). To remove inorganic carbon, samples were prepared by fumigating twice with 12 M HCl for 24 hrs and dried at 40 °C (Komada et al., 2008; Walthert et al., 2010). Inorganic carbon removal was confirmed on a subsample by measuring CO_2 production after HCl addition. Sample $^{14}C/^{13}C$ ratios were measured via radiocarbon accelerator mass spectrometry at the Center for Applied Isotope Studies (University of Georgia) with a 500 kV NEC 1.5SDH-1 pelletron (CAMS) accelerator equipped with a 134-cathode MC-SNICS negative ion source. We report $\Delta^{14}C$ and mean radiocarbon age by correcting for isotope fractionation with the $\delta^{13}C$ of each sample (Prasad et al. 2019).

Mass transfer coefficients and total profile Al weathering loss

Gains or losses of elements in the mineral soil over depth with respect to the deepest soil collected (freshest least-weathered parent material) were calculated with mass transfer coefficients, or tau (τ) values:

$$\tau_i = ((C_{j,w} \times C_{i,p})/(C_{i,w} \times C_{j,p})) - 1$$

where *i* and *j* indicate the concentrations of immobile and mobile elements, and *p* and *w* are the least weathered parent and weathered material, respectively (Chadwick et al. 1990). Our till sampling results indicate the till is too variable to be used as the parent material, so the deepest collected soil sample (top of C horizon) was used as the least weathered material. Therefore, tau values are not comparable among soil plots within a region and are used to interpret each soil profile individually. Consistent with the work of others in podzols, Ti was used as the immobile element (Dixon et al., 2016). This was confirmed with consistent ratios of immobile elements over depth.

Total loss of Al from each profile was determined as the difference of the present-day profile total Al inventory and that of the profile prior to weathering using the methods of Taylor & Blum (1995). The unweathered Al inventory was estimated by assuming that the full soil profile would have the same composition as the least weathered material (i.e. deepest collected sample).

5.2.4 Study design and statistics

Table 5.1. Study Design

Study design providing (a) the approach to evaluate soil organic carbon (SOC) response to short-term climate change via SOC variable controls across a range of timescales, and (b) the descriptions of the soil characteristics evaluated here as predictors including Al and C extracted with pyrophosphate (Al_{pp} and C_{pp}) as proxies for organometal complexes (OMC), mean SOC radiocarbon age (Age), C saturation of OMCs (C_{pp}:Al_{pp}), proportion of SOC in OMC (C_{pp}:SOC), stable carbon isotope composition ($d^{13}C$), and the carbon to nitrogen ratio of soil organic matter (C:N).

Table 1a. Response Variable

SOC Variable	Timescale	Approach	Reference(s)
SOC content	100-1000s yrs	Observational: Soil characteristic insights on dominant mechanisms and SOC content controls	This study and Patrick et al. in prep. (Ch.2 and 3)
Short-term climate change response	20-100 yrs	Interpreted via SOC content and event response with anticipated climate change impacts on hydrology	This study
Seasonal Response	Months	Experimental: Impact of soil moisture and soil solution composition on DOC uptake or loss	Patrick et al. in prep. (Ch.2 and 3)
Event response: High water flux	Hours - Day(s)	Experimental: Controls on DOC uptake/loss	Patrick et al. in prep. (Ch.2 and 3)
Event response: normal precipitation	Hours - Day(s)	Experimental: Controls on Al OMC coprecipitation	Nierop et al. (2002)

Table 1b. Explanatory Variable (Soil characteristics)

Variable	Description	Hypothesis
Al_{pp}	Al OMCs	Greater in Northern region where Al availability is higher
Age	SOC age	Increase with depth and younger in South where warmer weather increases microbial activity and SOC turnover
C_{pp}:Al_{pp}	C saturation of OMCs	Decrease saturation with depth where infiltration is more limited
C_{pp}:SOC	Proportion of SOC in OMCs	Increase with depth as vulnerable SOC is lost
TauAl	Al weathering degree	Greater Al loss in South where lower Al availability limits Al OMC coprecipitation
$\delta^{13}C$	OM degradation proxy	Increase more with depth in South where warmer
C:N	OM degradation proxy	Decrease with depth more in South where warmer

The goal of this study was to enhance our predictive understanding of subsoil SOC and its response to short-term climate change. This was possible by considering SOC response to precipitation events (experimental) relative to the history of SOC stability mechanisms recorded in soil characteristics (e.g. observations of SOC content and mean age, Al OMCs and weathered Al, etc.) within the context of expected climate change impacts (Table 5.1a).

First, I evaluated if subsoil SOC stocks exhibited the same increasing trend across the transect with warming as surficial soils using a T-test. This was a first order evaluation of the relative roles of parent material and climate controls on SOC with depth.

Second, I determined key soil characteristics that inform on mechanisms of SOC accumulation or loss (e.g. storage with Al OMCs or τ_{Ti} weathering indicators, see hypotheses for each in Table 5.1b). Spatial controls on soil characteristics were evaluated using 3-way ANOVA tests (Soil characteristic ~ Depth + Region + Depth*Region) to determine the spatial scales at which the characteristics are relevant and operating. Where necessary, the response and depth variables were pre-transformed to logarithm, cube root, or square root to fit the normal distribution and homogeneous requirements of a general linear model.

Weathering depth profiles using tau mass transfer coefficients were interpreted in the context of long-term parent material Al availability and water flux controls on Al OMC formation. Weathering trends of Al relative to SOC with depth provides insights as to the formation and fate of dissolved Al OMCs (e.g. depletion-enrichment trend of Al and SOC

suggests formation and coprecipitation of Al). Current total profile Al stocks in OMCs only inform on the long-term accumulation of Al OMCs. Since Al is generally considered an immobile element during weathering, I assume that the total weathered Al stock is largely weathered via complexation with DOM and transported via OMCs (Price and Velbel, 2003). These findings are further used in our interpretation of the relative regional response of Al OMC and associated SOC to short-term climate change.

A multiple linear regression model for predicting mineral horizon SOC content was developed to: (1) enhance our predictive ability of deep SOC content to gain better resolution estimates across boreal forests, and (2) understand the controls contributing to long-term accumulation of SOC and thus informing the potential SOC response to short-term climate change. Data from this study and previous work in regions of the NL-BELT were used to make a more robust model and include a wide range of SOC content (Data from Chapters 3 and 4). The model was designed around Al_{pp} (predictor variable as proxy for Al OMC) and other soil characteristics related to weathering that vary with depth as informed by previous work (Patrick et al, 2022; Chapter 3 and 4). Predictors and all interactions were evaluated in general linear models using ANOVA tests. Factors that were not significant were eliminated to identify the best multiple linear regression model for predicting SOC content. From here, the model was simplified by identifying the factors that could be estimated with depth so that only Al_{pp} and depth are needed to predict SOC.

To understand SOC response to short-term climate change, it was necessary to evaluate how each region contributed to SOC storage via OMC precipitation historically based on their Al, C and water availability, and how such factors may be impacted with

climate change. Therefore, a threshold for OMC precipitation was inferred for each region based on experimental event-scale controls on DOM storage and the history of SOC and weathering from soil characteristics.

Using the experiment of Nierop et al. (2002), which increases the soil solution Al concentration to determine Al OMC precipitation, the response of a high or low Al soil to increasing water and DOM flux was inferred. This suggested an event threshold for Al OMC precipitation in each region, where a greater water flux would limit precipitation and SOC storage. The total profile Al OMC stocks, Al loss and weathering profiles were used to estimate the frequency that this threshold was met for Al OMC precipitation in the past and suggest the potential for meeting the threshold with short-term climate change.

The ANOVA tests were performed in RStudio version 4.2.3. All tests were conducted using $\alpha = 0.05$. Model residuals were checked to be homogeneous, independent, and normally distributed with residual versus fit, lag and quantile-quantile plots, respectively (McCullagh and Nelder, 1989; Zuur et al., 2007; Welham et al., 2007). Microsoft Excel 2017 was used to run T-tests and construct scatter plots and bar graphs.

5.3 Results

5.3.1 Parent material composition

Felsic igneous intrusive rocks and mafic amphibolites were dominant components of the northern till based on visual analysis of clasts. Plagioclase was the most abundant

mineral (36 ± 4.3 %), followed by quartz, K-feldspar, amphibole, chlorite, biotite, and muscovite (Figure S5.1 in Appendix). In the south, sedimentary and metasedimentary rocks were most abundant – quartz was the main constituent (63 ± 2.8 %) with lesser chlorite, K-feldspar, plagioclase and muscovite. The northern till had greater Al_2O_3, Fe_2O_3, CaO, Na_2O and P_2O_5 relative to the southern till (Table S5.1 in Appendix). The latter chemical and mineralogical characteristics, specifically the greater abundance of clay minerals relative to precursor silicate minerals, are also reflected in the greater chemical index of alteration (CIA) value of the southern till (74) relative to the northern till (61) (Nesbitt & Young, 1984).

5.3.2 Soil organic carbon content and mineral soil characteristics

Total profile mineral horizon C stocks were greater in the north, ranging from 9 – 17 kg C m^{-2} compared with 2 – 8 kg C m^{-2} in the south (Figure 5.1b). Northern SOC % exhibited Ae horizon depletion to shallow-mineral horizon enrichment (depletion-enrichment) trends with depth: a reduced Ae horizon with 1 – 2.5 %, enrichment of SOC in the B1 or B2 mineral horizons (3 – 4 % at 20 – 35 cm), and lesser SOC accumulation in the deeper B3-B4 horizons (0.5 – 2 %; Figure 5.2a). In the south, one soil profile had a SOC depletion-enrichment profile with 2.5 % in the enriched B1 horizon, yet the other two profiles were most enriched in the Ae horizon (1 – 2 %) and decreased to <0.5 % at depth (Figure 5.2b).

Southern soils had, on average, more than twice as much weight percent soil within the >2 mm size fraction relative the north (33.7 % compared with 14.2 %; Table S5.2). Northern soils had a higher sand component (0.63 μm – 2mm) and both regions had similar average weight percent in the fine size fraction of silt and clay (<0.63 μm; 28–29 %). Bulk density was variable across depth and among sites given the varied rock content but was on average greater in the northern soils (Table S5.3).

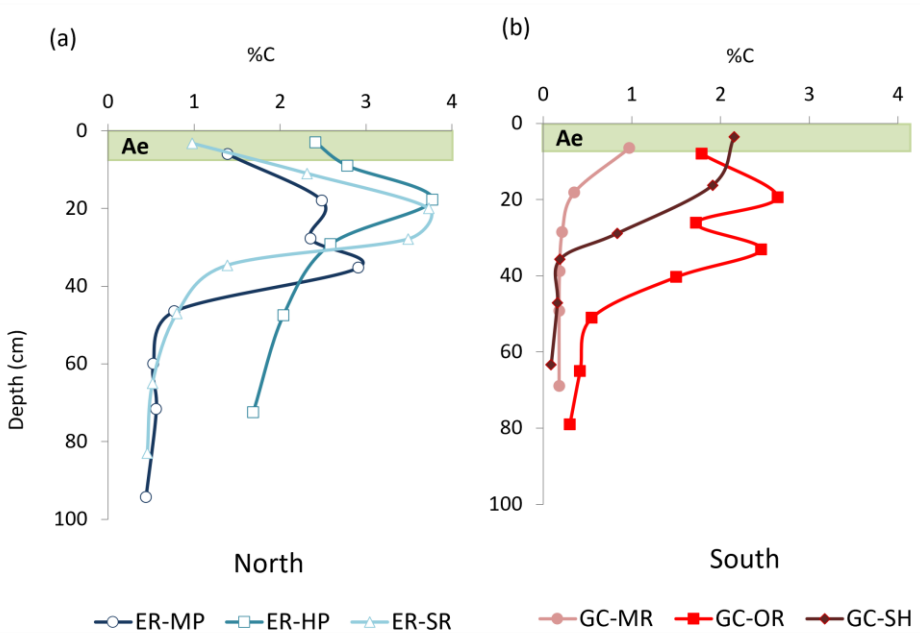

Figure 5.2.

Soil depth profiles showing soil organic carbon content (%) for three sites in the (a) north and (b) south regions.

In all profiles, Al_{pp} exhibited a depletion-enrichment distribution with depth. The Ae horizon were consistently depleted; however, the enriched horizons were more pronounced in the north, up to 7 – 8 g Al kg^{-1} compared with 3 – 5 g Al kg^{-1} (Figure 5.3a). Depletion-enrichment trends were also exhibited in C_{pp}, with an enriched horizon of 1.0 –

1.8 % at 15 – 35 cm depth (Figure S5.2 in Appendix). This measure made up 20 – 40 % of SOC content in the Ae horizon and consistently ~60 % of SOC in soils below 20 – 30 cm in all (Figure 5.3b). All profiles exhibited a decreasing molar C_{pp}:Al_{pp} with depth: 8 – 13 in the Ae horizon decreasing to 2 – 3 by 50 cm depth (Figure 5.3c). C_{pp}:Al_{pp} and C_{pp}:SOC were not regionally different.

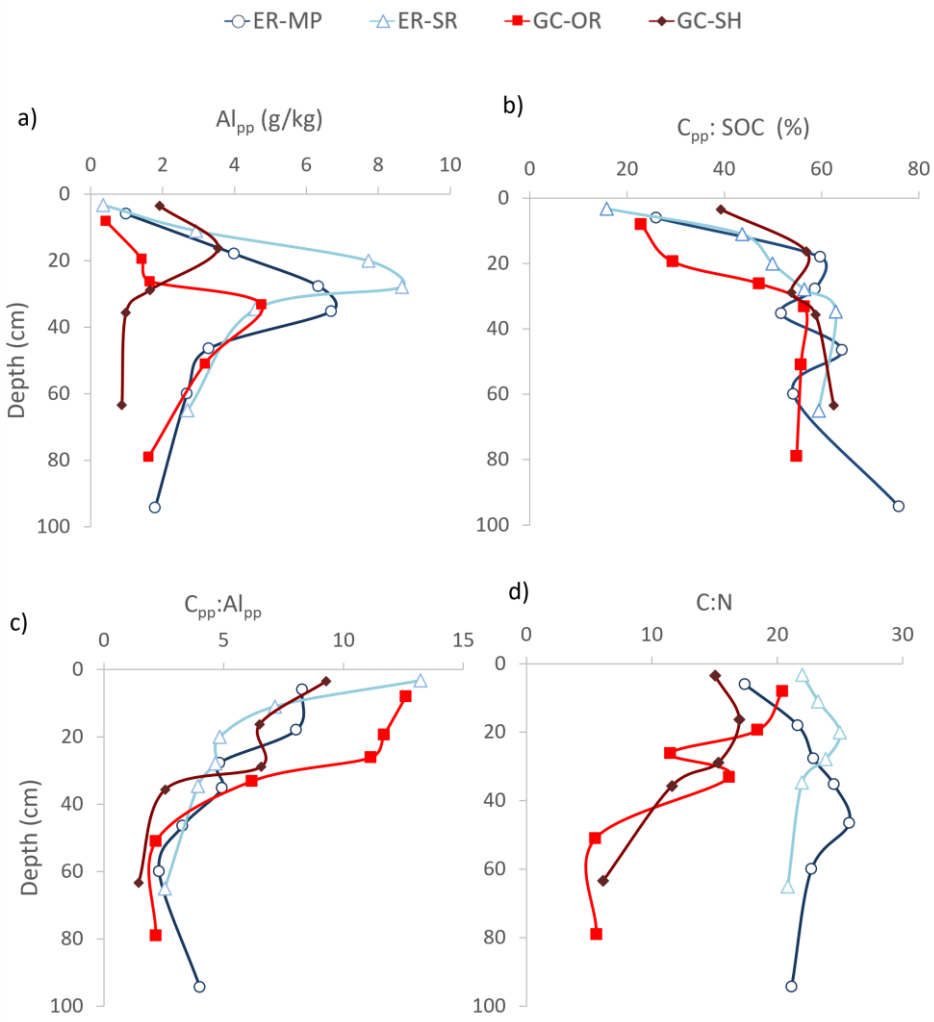

Figure 5.3.

Mineral soil characteristics of two profiles per region: (a) pyrophosphate extracted Al (Al_{pp}), a proxy for Al organo-metal complexes (OMCs); (b) proportion of pyrophosphate extracted carbon (C_{pp}; OMC proxy) in

soil organic carbon (C_{pp}:SOC) ; (c) carbon saturation of Al OMCs (C_{pp}:Al_{pp}); (d) carbon to nitrogen ratio as a proxy for organic matter degradation (C:N).

The C:N decreased from 15 – 20 in the Ae to 5 – 8 with depth in the south. The C:N was consistently higher in the north within the range of 20 – 25 with small enrichments at mid depths (Figure 5.3d). This trend suggests a greater degree of microbial degradation over depth in the south. Both regions exhibited increases in $\delta^{13}C$ with depth, from -27 – -26 in the Ae horizon to -25 – -24 in the deepest horizon (Figure S5.2b in Appendix). Both regions exhibited $\delta^{15}N$ in the range of 4 – 6, with a slight increase with depth.

Higher resolution sampling (n = 9 per region and pooled by site) of the top 10 cm of the mineral horizon resulted in generally younger average aged SOC in the southern forest sites, consistent with a previous study (Ziegler et al., 2017). The coarse fraction exhibited modern ages across all samples in the south, with fine fraction ages from 100 – 200 ybp. In the north, the coarse and fine fractions exhibited SOC ages of modern to 450 ybp, and 200 – 600 ybp, respectively (Figure S5.3 in Appendix). These differences were not discernable in the full depth profiles that were used to focus on depth distribution. The radiocarbon content of the bulk soil decreased with depth in all profiles but did not exhibit any regional differences (Figure 5.4a). All shallow soils exhibited mean ages of <1000 ybp with a sharp increase at about 30 cm reaching 2500 – 4000 ybp in the deepest horizon. Two modern ages at 5 and 20 cm depth were exhibited by one northern site (ER-SR). Mean SOC age is strongly correlated with C_{pp}:Al_{pp}, regardless of depth or region. The relationship and threshold C_{pp}:Al_{pp} defining the rapid change in mean SOC age with depth

is similar to that explaining surficial exchange of DOC with extant OMCs suggesting a similar control.

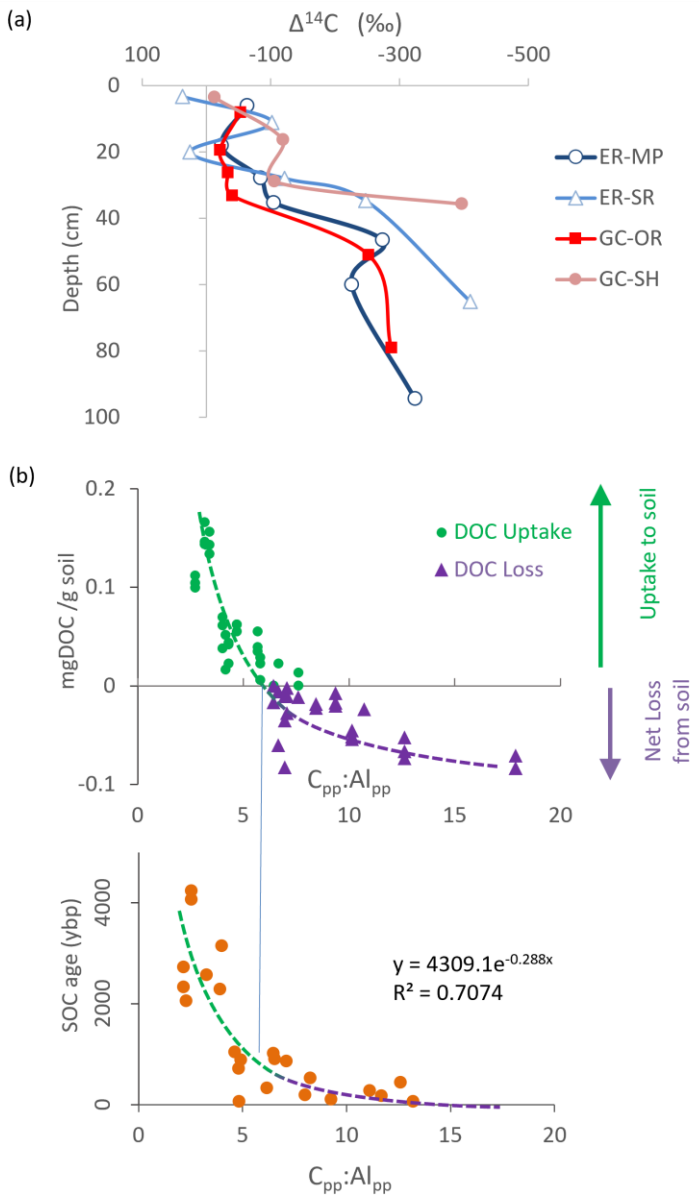

Figure 5.4.

a) Radiocarbon content ($\Delta^{14}C$ ‰) of bulk soil (<2mm) by depth for two soil profiles in the north (blue) and south (red) regions. b) The threshold observed for C saturation of Al OMCs (C_{pp}:Al_{pp}), where uptake of dissolved organic carbon (DOC) through the surficial exchange of (DOC) with organo metal complexes (OMC) changes to net loss of DOC (top), also defines the threshold of mean soil organic carbon (SOC) age

relationship with C_{pp}:Al_{pp} (bottom). Experimental data from top figure in b from Patrick (Chapter 5) which includes data from four regions within the NL-BELT.

5.3.3 Weathering profiles and Al loss

Mass transfer values were used to show the distribution of major elements over depth as a proxy for understanding weathering. These weathering profiles were constructed using mass transfer coefficients (Tau_{Ti}) relative to the deepest collected sample show different weathering trends among regions (Figures 5.5 and S5.4). All elements follow a depletion-enrichment trend in the north, where elements are depleted in the Ae, enriched in the shallow mineral horizon, and minimally weathered at depth. While the relative enrichment magnitude varied among elements, all were depleted and enriched at the same depths and coupled with SOC enrichments. This is with one exception in ER-SR where P and Fe do not follow the same distribution as others (Figure S5.4 in Appendix). In all profiles, P and Fe had the sharpest relative enrichments, while Si, Na, K and Al were impacted least.

The weathering profiles in the south were variable among sites, elements did not all follow similar distributions within a profile and were decoupled from SOC enrichments (Figures 5.5 and S5.4). Site GC-SH exhibited smooth weathering profiles of varying degrees of largely depleted (Mg, Al, and K) to largely depletion-enrichment (Fe, P and Ca) distributions. The depth of enrichment also varied: (1) SOC content was most enriched in the Ae horizon, (2) Fe and P displayed shallow mineral horizon enrichment at 20 cm, (3) Mg, Al, and K at 30 cm, and (4) Na, Si, and Ca at 40 cm. In GC-OR, all elements were

sharply depleted to 30 cm depth, then displayed varying degrees of depletion (Mg) to depletion-enrichment distributions (P, Ca and Si). Similar to GC-SH, elements were enriched at different depths. Elements were least depleted in GC-MR, exhibiting a surface enrichment of P that coincided with SOC (uplift distribution), and minimal difference over depth for all others.

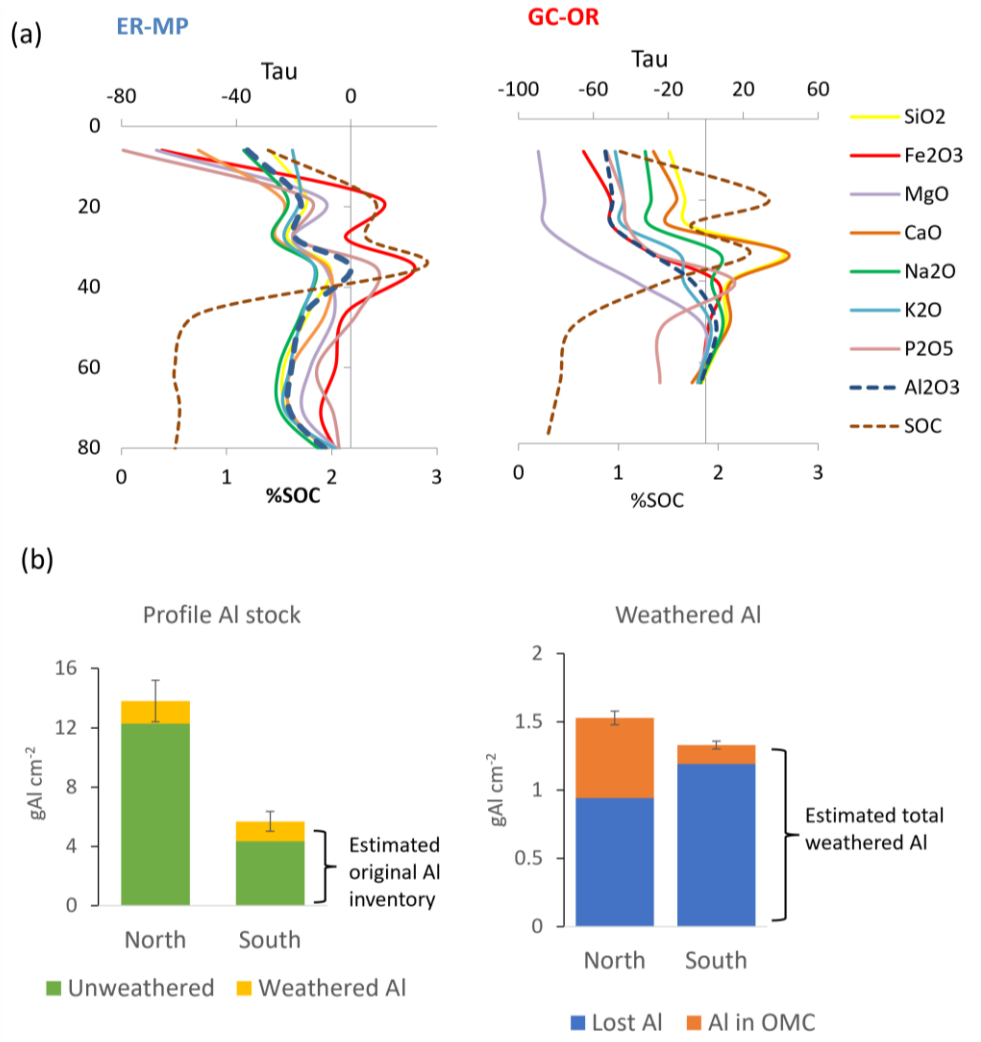

Figure 5.5.

a) One representative weathering depth profile per region: north (ER-MP: blue, left panel) and south (GC-OR: red, right panel). Mass transfer coefficients (Tau) of major elements were calculated using Ti as the

immobile element and were relative to the top of the C horizon (least weathered material). Soil organic carbon content (SOC) distribution over depth is shown on the bottom x-axis. See figure S5.4 for other two sites in these regions. b) Estimated original total profile Al stocks prior to weathering and proportion of weathered Al lost or precipitated in Al organo-metal complexes (OMC) for north (three sites) and south regions (two sites). Estimations of Al lost from profile are determined by reintegrating Al to match the least weathered parent material. Error bars indicate standard deviation.

A total profile inventory of Al of the soil prior to weathering was estimated by assuming the entire profile started with the same composition as the deepest horizon which represented a least weathered parent material. The Al inventory prior to weathering was significantly higher in the north, 13.8 g cm^{-2} compared with 5.1 g cm^{-2} in the south (Figure 5.5). Total Al weathering was relatively similar in the two regions, 1.53 g cm^{-2} and 1.33 g cm^{-2} in the north and south, respectively. However, significantly more Al was lost from the profile as the current inventory of Al OMCs is more than three times higher in the north, 0.59 g cm^{-2} compared with 0.14 g cm^{-2} in the south.

5.3.4 Model results

The mean SOC age, C_{pp}:Al_{pp}, and C_{pp}:SOC exhibit logarithmic relationships with depth with no regional differences (Figure 5.6 and Table S5.4). Similarly, $\delta^{13}C$ is depth-dependent with no regional differences, however, the relationship is linear with depth. As expected, Al_{pp} is regionally dependent because of contrasting parent material composition, and C:N varies with region and depth.

Soil organic carbon was best predicted with Al_{pp} and its interactions with C_{pp}:Al_{pp} and C_{pp}:SOC in a multiple linear regression model (Figure 5.7 and Table S5.5). Observed

SOC from four climate regions with varying parent material, a range of depths and slope angles, was predicted with 0.96 explained variance.

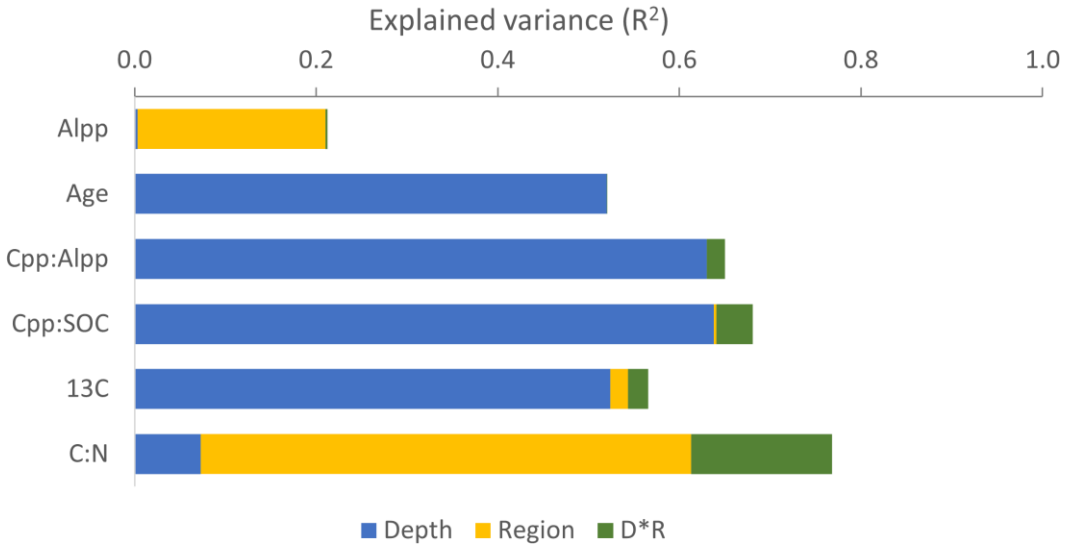

Figure 5.6.

Explained variance for models evaluating spatial controls of depth and region on soil characteristics Al and C extracted with pyrophosphate as proxies for OMCs (Al_{pp} and C_{pp}), mean radiocarbon-based age of the soil organic carbon (SOC; age); C saturation of organometal complexes (OMC; C_{pp}:Al_{pp}), proportion of SOC in OMC (C_{pp}:SOC), the stable carbon isotope composition ($d^{13}C$), and the carbon to nitrogen ratio of the soil organic matter (C:N). D*R is the interaction of depth and region.

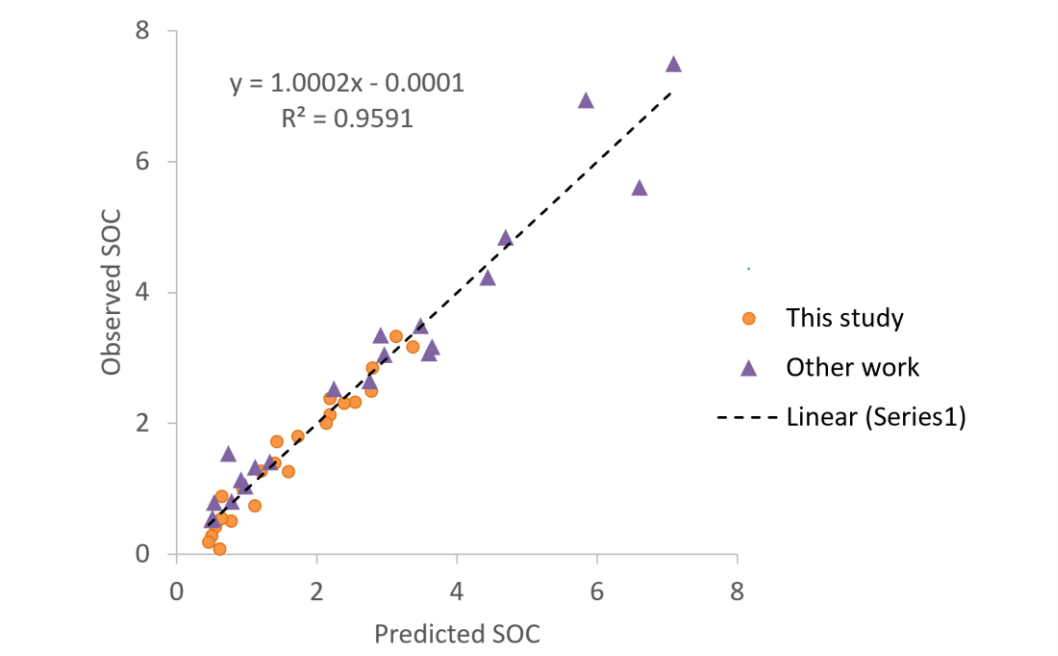

$$SOC \sim Al_{pp} + Al_{pp} * C_{pp}:Al_{pp} + Al_{pp} * C_{pp}:SOC + C_{pp}: SOC * C_{pp}:Al_{pp} + Al_{pp} * C_{pp}: SOC * C_{pp}:Al_{pp}$$

Figure 5.7.

Predicted soil organic carbon (SOC) content using the multiple linear regression model developed in this study compared with observed SOC. Model was created with data from this study (north and south regions and depth) and previous work from the Newfoundland and Labrador Boreal Ecosystem Latitudinal Transect including shallow mineral horizon soils from four regions, and hillslope scale collections at two inclines and depth (Patrick, Chapters 2 and 3 in this Thesis). Predictors include Al extracted by pyrophosphate as proxy for organo-metal complexes (Alpp) and their saturation with C (Cpp:Alpp) and the proportion of SOC that is in organo-metal complexes (Cpp:SOC). Coefficients for model are in Table S5b.

5.4 Discussion

Our ability to predict soil organic carbon relies on understanding factors controlling Al organometal complex precipitation

Despite larger organic horizon SOC stocks and a 3-fold greater C source of DOM in the warmer south region, subsoil SOC stocks are lower than the Al-rich north region.

This suggests a difference in the mechanism of SOC storage at depth among regions. The evidence uncovered in this study indicates a greater role of parent material composition than C source in SOC accrual via OMC coprecipitation in at depths below ~30 cm.

Congruent with surface mineral horizons (Patrick et al. 2022), Al OMCs are the main mechanism controlling subsoil SOC, consistently making up ~60 % of SOC (C_{pp}:SOC) below 30 cm. The predictive multiple linear regression model for SOC included Al_{pp} and its interactions with C_{pp}:Al_{pp} and C_{pp}:SOC. Despite inclusion of soils from sites across four climate regions and a range of parent material for this model, these factors explained 96% of SOC variance alone (Figure 5.7 and Table S5.5). This high explanatory descriptive power suggests that regional-scale studies within a biome are ideal for SOC investigations as the dominant SOC stability mechanisms are likely biome-specific.

Both C_{pp}:Al_{pp} and C_{pp}:SOC exhibited depth-dependent trends that were relatively uniform across the climate transect. Consistent with Kramer and Chadwick (2018) observations of biome water balance controls on the proportion of SOC in metal weathering products, the lack of regional differences in C_{pp}:Al_{pp} and C_{pp}:SOC are also likely a result of relatively consistent water balance across the biome. The logarithmic trends with depth exhibited by both ratios could be linked to infiltration depth frequency, as the soil solution providing the C source for these weathering mechanisms becomes increasingly limited with depth. Both C_{pp}:Al_{pp} and C_{pp}:SOC are maintained across the transect despite evidence of greater OM degradation in the south, suggesting maintenance of SOC associated with OMCs regardless of microbial activity. The same logarithmic depth trend in SOC age and its relationship with C_{pp}:Al_{pp} further indicates the dominant role of infiltration depth in

mechanisms of SOC stability or turnover. Surficial exchange of DOM with extant OMC is enhanced in shallow soils as controlled by C_{pp}:Al_{pp} (Chapter 3). The threshold of this surficial exchange and increase in SOC age occur at the same C_{pp}:Al_{pp} (and depth), thus suggesting a link between OMC stability and SOC turnover as facilitated by water infiltration frequency (Figure 5.4b).

These results suggest that within this biome: (1) water infiltration controls long-term variations in weathering mechanisms and SOC stability with depth, and (2) the lack of regional differences in C_{pp}:Al_{pp} and C_{pp}:SOC implies that Al_{pp} controls regional variation in SOC content and potential storage. Therefore, for making SOC content predictions in new regions with limited soil data, C_{pp}:Al_{pp} and C_{pp}:SOC can be fit to equations with depth and applied across the biome (coefficients for this application in Table S5.5c). Estimating C_{pp}:Al_{pp} and C_{pp}:SOC would introduce significantly more error to the shallowest soil SOC predictions because of the rapid change with depth. Subsoil SOC predictions, the focus of this study, should be more accurate as C_{pp}:Al_{pp} and C_{pp}:SOC have less variation below 30 cm. However, Al_{pp} cannot be so easily approximated as it is regionally dependent and likely a product of Al availability, and water and DOM fluxes. The role of these factors in Al OMC precipitation for each region are interpreted next with mass transfer coefficients.

Parent material can determine the threshold for SOC storage via soil water residence time controls on Al organo-metal complex precipitation

Precipitation of Al OMCs to support new SOC storage is a function of parent material Al availability, and the fluxes of water and DOM. A requisite soil solution Al:C of 0.03 for OMC coprecipitation initiation was experimentally determined at a constant water and DOM flux (Nierop et al., 2002). This suggests that during a precipitation event, there is a water flux above which the soil water residence time becomes too short for the weathering rate to meet the Al concentration for OMC precipitation (Figure 5.8a). Above this event threshold, only surficial exchange of DOM with OMCs would be expected.

A low water flux would likely allow the soil solution to reach equilibrium. Such event conditions would precipitate the greatest proportion of DOM into Al OMCs, yet the DOM flux is low and therefore supports the smallest C_{pp} yield (SOC associated with OMCs). Increasing the DOM flux enhances the C source, yet the concomitant reduction in soil water residence time decreases the proportion stored until the event threshold is reached. Enhanced Al weathering rates in soils with an Al-rich parent material would support greater Al OMC coprecipitation at the same DOM flux as a soil with lower Al availability and support coprecipitation to a higher event water flux threshold (Figure 5.8a).

Greater Al availability in the northern soils is supported by a parent till material with high Al_2O_3 content in weatherable silicate minerals, amphibole and Ca-plagioclase, which actively convert to kaolinite (potentially via smectites for amphiboles) or halloysite during chemical weathering (e.g., Wilson, 2004), creating reactive Al sites in the process. In contrast, the quartz-dominant sedimentary till in the south contains less Al_2O_3 overall with more of the Al in less weatherable phases such as muscovite, and a greater fraction of coarse material (dominated by quartz) with less reactive surface area.

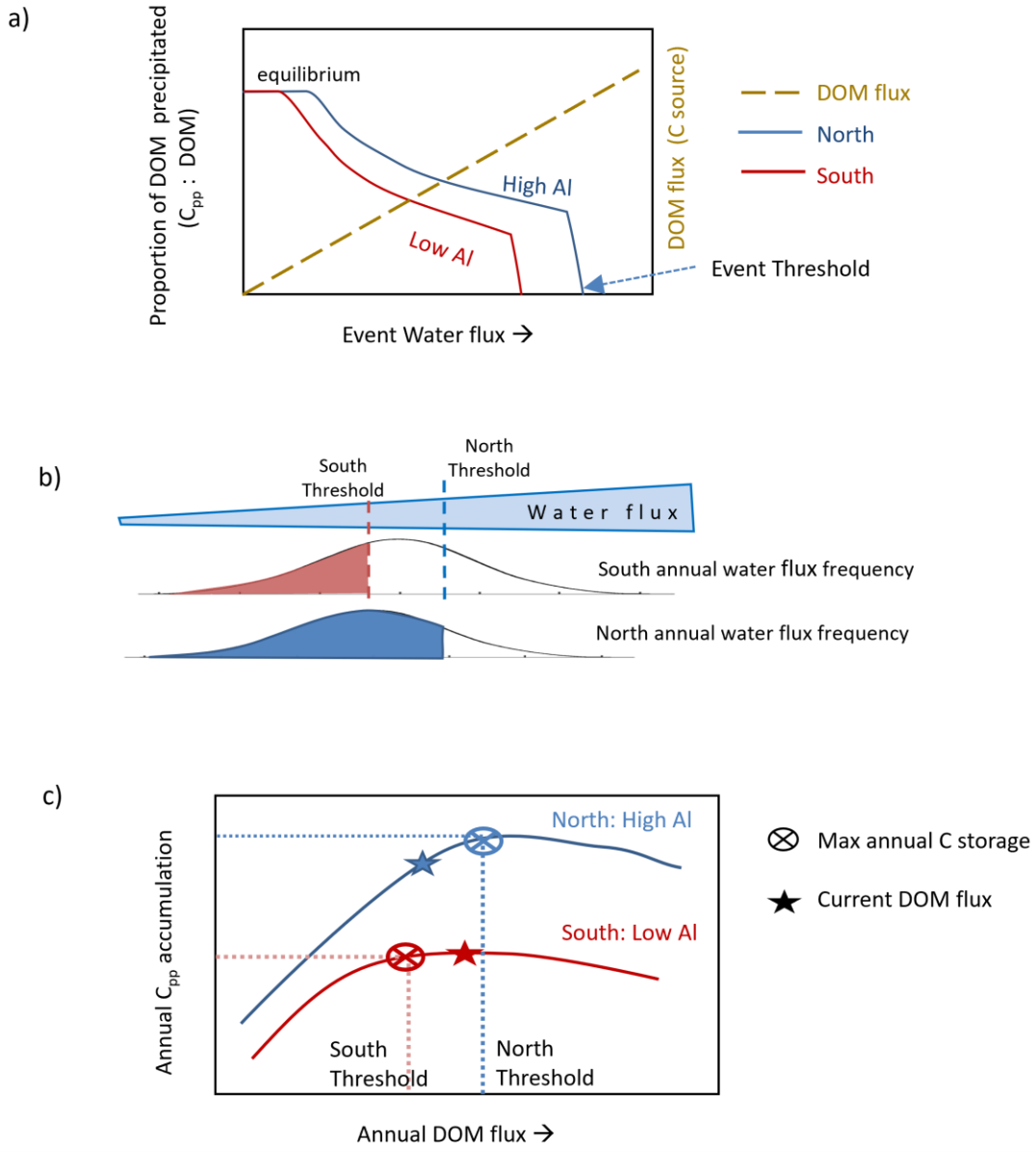

Figure 5.8.

a) Event water and DOM (dissolved organic matter) flux relationship to proportion of DOM precipitated as soil organic carbon in organometal complexes (C_{pp}). The event threshold indicates the greatest water flux that can still support organometal complex precipitation (soil solution >0.03 Al:C). b) Interpreted frequency of annual precipitation events where the threshold for organometal complex precipitation is met in the north and south regions given the greater proportion of weathered Al that is coprecipitated as Al organo-metal complexes. c) Annual increase in C_{pp} accumulation with DOM flux to threshold of maximum annual storage. Relative location of current DOM flux to threshold is indicated with a star and suggests north region likely has SOC storage potential with climate change while forests in the south do not.

The coupled SOC and depletion-enrichment weathering profiles exhibited by soils in the northern forests are consistent with podzolization-dominant retention of SOC in Al OMC weathering products. This suggests soil solution metal concentrations reach precipitation-thresholds in the north region more readily than in the south where depletion-dominant Al weathering profiles that are decoupled from SOC profiles indicate significant Al loss. Greater retention of weathered Al via Al OMC coprecipitation in the north region is further supported by four times greater profile Al OMC stocks despite a similar average estimate of total weathered Al between the two regions. Over time, soils in the north region have experienced enhanced Al OMC and SOC accumulation as these event water flux thresholds for Al OMC precipitation are more frequently met (Figure 5.8b). This explains the greater northern SOC stocks since a significantly greater proportion of the smaller DOM source has been stored.

Soil organic carbon response to short-term climate change depends on threshold of carbon accrual via organometal complex precipitation set by parent material

With short-term climate change (20 – 100 years), this wet boreal biome is expected to experience increases in soil drying and in the DOM flux via increased mean annual temperature and shifts in precipitation form and timing, increasing storm frequency and intensity (Finnis and Daraio, 2018; Bowering et al., 2022). The response of mineral horizon SOC to these climate shifts will be a net result of the impact on all mechanisms of

SOC accrual and loss. Since SOC is dominantly stored in Al OMC, the threshold for their precipitation is key to understanding the SOC trajectory of change.

Thus, the impact of short-term climate change is expected to be a trade-off between an increasing DOM flux to the mineral horizon (C source) and a diminishing storage mechanism via soil water residence time reductions that occur concomitantly with the enhanced soil DOM flux. Therefore, each individual region should exhibit a maximum annual accrual of C_{pp} as a net result of this trade-off and the frequency of events that have met the event water flux threshold for Al OMC precipitation annually (Figure 5.8b–c). The maximum annual C_{pp} accrual is expected to occur at a greater annual DOM flux (greater threshold) in Al-rich soil substrates such as those in the northern soils (Figure 5.8c).

As such, I expect SOC storage via OMC coprecipitation to increase in climate regions where the C_{pp} threshold has not yet been met. Considering the Al depletion profiles, decoupling of metal and SOC profiles, and limited SOC content relative to DOM flux, the southern region is likely past the threshold. Contrastingly, Al OMC and SOC retention suggests the current DOM flux in the northern region is likely below the maximum annual C_{pp} threshold. This suggests that the north region should experience increased OMC precipitation with enhanced water and DOM fluxes expected with climate change, while coprecipitation in the south region will likely remain constant or decrease (Figure 5.8c and 9).

Increasing temperature and precipitation intensity should further enhance shallow soil microbial mineralization and DOM desorption in shallow soils, stimulating SOC

turnover others (Kaiser et al., 2015; Bailey et al., 2019; Patel et al., 2021). However, a biome-fixed C_{pp}:Al_{pp} profile suggests that enhanced adsorption may replace such losses, therefore future SOC may be younger and more degraded, but Al OMC abundance would still control SOC content in these forests. Enhanced coprecipitation in shallow northern soils will increase total SOC content. However, if Al OMC coprecipitation cannot maintain Al OMC as soil profile Al evolves into poorly crystalline oxy-hydroxides or is mobilized with fresh acidic DOM, southern shallow soils may exhibit net SOC loss (Figure 5.9). The fate of deeper soils, which exhibit significant SOC storage potential, will depend on soil water infiltration depths and dissolved organic C concentration as deep soils are currently limited by a C source (Chapter 3).

5.5 Conclusion

This work suggests that parent material composition is key to predicting subsoil SOC content and its response to climate change in wet boreal biomes. The capacity of the soil to accrue SOC in response to an increasing DOM flux with climate change is defined by a Al OMC precipitation threshold, where soils on Al-rich parent material support greater precipitation to a higher threshold DOM flux. Regions already above the threshold would likely not exhibit shallow SOC accrual with an enhanced DOM flux despite the increased C source. Thus, evaluating these thresholds will increase our predictive understanding of SOC response to climate change in boreal forest landscapes. Future work should focus on defining these thresholds through modeling efforts and further evaluating SOC response to

various scenarios of enhanced DOM flux via a range of ratios of increased dissolved organic C concentration and water flux.

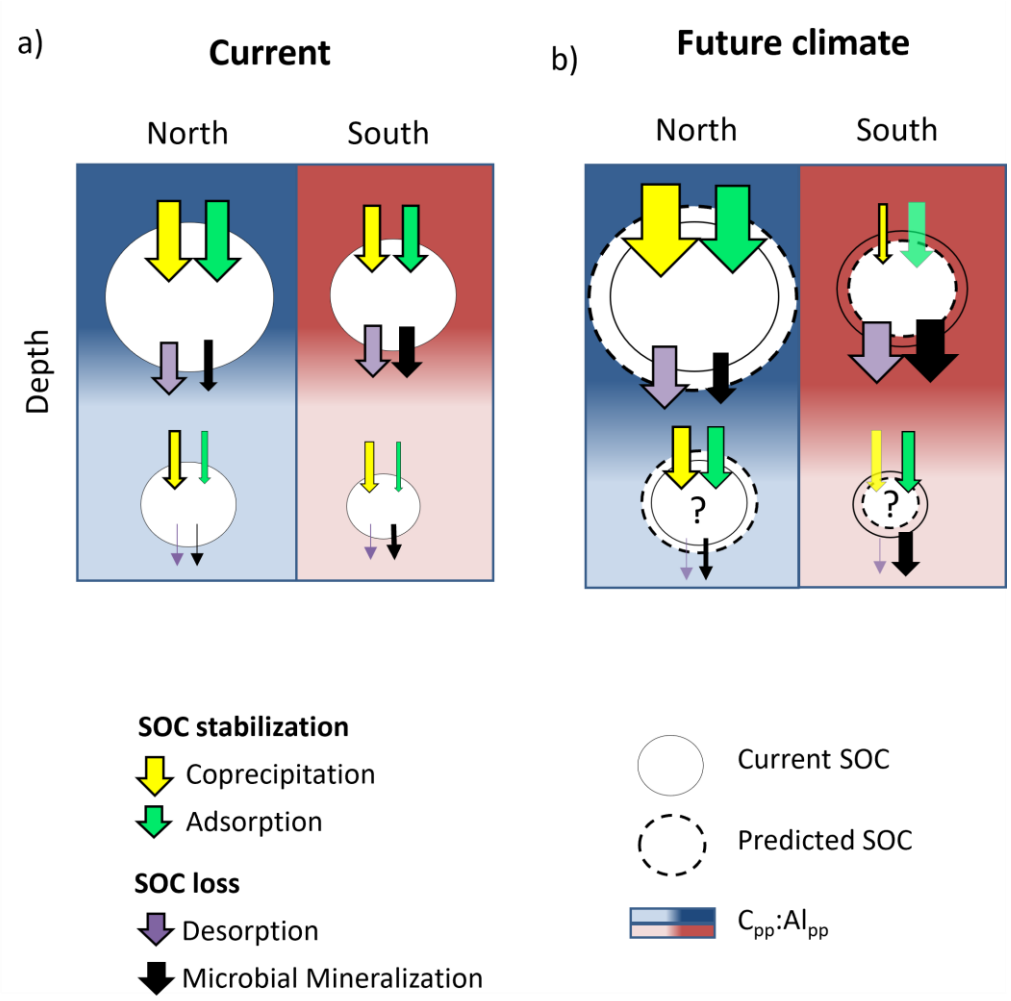

Figure 5.9.

Mechanisms contributing to the soil organic carbon SOC stocks (SOC) in the north (blue) and south (red) regions (a) in the present and (b) as predicted with short-term future climate given mechanisms uncovered in this study. Relative change in SOC and mechanisms are exaggerated to show difference. Transparent arrows in panel (b) indicate no change in flux from current day. Background intensity indicates Al organometal complex (OMC) saturation with carbon (C_{pp}:Al_{pp}). Question mark indicates the uncertainty in deep SOC stocks which remain dependent on future infiltration depths.

5.6 References

Bowering, K. L., Edwards, K. A., Prestegaard, K., Zhu, X., and Ziegler, S. E., 2020. Dissolved organic carbon mobilized from organic horizons of mature and harvested black spruce plots in a mesic boreal region, Biogeosciences, 17, 581–595, https://doi.org/10.5194/bg-17-581-2020.

Bowering, K. L., Edwards, K. A., Wiersma, Y. F., Billings, S. A., Warren, J., Skinner, A., and Ziegler, S. E., 2022. Dissolved Organic Carbon Mobilization Across a Climate Transect of Mesic Boreal Forests Is Explained by Air Temperature and Snowpack Duration. Ecosystems, 1-17. https://doi.org/10.1007/s10021-022-00741-0.

Brookes, I. A., 1977. Geomorphology and Quaternary geology of Codroy Lowland and adjacent plateaus, southwest Newfoundland, Can. J. Earth Sci, 2101–2120.

Chadwick, O. A., Brimhall, G.H. and Hendricks, D.M., 1990. From a black to a gray box—A mass balance interpretation of pedogenesis, Geomorphology, 3(3–4), 369–390.

Colman-Sadd, S.P., Hayes, J.P., Knight, I., 2000. Geology of the Island of Newfoundland (Digital version of Map 90-01 with minor revisions). Newfoundland Department of Mines and Energy, Geological Survey, Map 2000-30, scale 1:1 000 000.

Cremer, M. and Schlocker, J., 1976. Lithium borate decomposition of rocks, minerals, and ores. American Mineralogist, 61(3-4), 318-321.

Dixon, J. L., Chadwick, O. A., and Vitousek, P. M., 2016. Climate-driven thresholds for chemical weathering in postglacial soils of New Zealand, J Geophys Res Earth Surf, 121, 1619–1634, https://doi.org/10.1002/2016JF003864.

Friedlingstein, P., Meinshausen, M., Arora, V. K., Jones, C. D., Anav, A., Liddicoat, S. K., and Knutti, R.: Uncertainties in CMIP5 climate projections due to carbon cycle feedbacks, J Clim, 27, 511–526, https://doi.org/10.1175/JCLI-D-12-00579.1, 2014.

Finnis J, and Daraio, J, 2018. Projected Impacts of Climate Change for the Province of Newfoundland & Labrador: 2018 Update. Memorial University of Newfoundland, St. John's, NL. 2018.

Georgiou, K., Malhotra, A., Wieder, W. R., Ennis, J. H., Hartman, M. D., Sulman, B. N., Berhe, A. A., Grandy, A. S., Kyker-Snowman, E., Lajtha, K., Moore, J. A. M., Pierson, D., and Jackson, R. B. 2021. Divergent controls of soil organic carbon between observations and process-based models, Biogeochemistry, 156, 5–17, https://doi.org/10.1007/s10533-021-00819-2.

Gower, C. F., 1998. Geology of the upper Eagle River map region, Grenville Province, southeast Labrador. Current Research (1998) Newfoundland Department of Mines and Energy, Geological Survey, 98-1.

King, G. A., 1985. A standard method for evaluating radiocarbon dates of local deglaciation: Application to the deglaciation history of southern Labrador and adjacent Québec. Géographie physique et Quaternaire 39(2), 163-182.

Komada, T., Anderson, M.R. and Dorfmeier, C.L., 2008. Carbonate removal from coastal sediments for the determination of organic carbon and its isotopic signatures, δ13C and Δ14C: comparison of fumigation and direct acidification by hydrochloric acid. Limnology and Oceanography: Methods, 6(6), 254-262.

Kramer, M. G. and Chadwick, O. A., 2018. Climate-driven thresholds in reactive mineral retention of soil carbon at the global scale, Nat Clim Chang, 8, 1104–1108, https://doi.org/10.1038/s41558-018-0341-4.

Lee, J.-Y., Marotzke, J., Bala, G., Milinski, S., Yun, K.-S., Ribes, A., Ruane, A. C., Kumar Kanikicharla Qatar, K., Kattsov, V., Kimoto, M., Marotzke, J., Bala, G., Cao, L., Corti, S., Dunne, J., Engelbrecht, F., Fischer, E., Fyfe, J., Jones, C., Maycock, A., Mutemi, J., Ndiaye, O., Panickal, S., Zhou, T., Pirani, A., Connors, S., Péan, C., Berger, S., Caud, N., Chen, Y., Goldfarb, L., Gomis, M., Huang, M., Leitzell, K., Lonnoy, E., Matthews, J., Maycock, T., Waterfield, T., Yelekçi, O., Yu, R., and Zhou, B., 2022. Chapter 4: Future Global Climate: Scenario-based Projections and Near-term Information, 553–672, https://doi.org/10.1017/9781009157896.006.

McCuaig, S. J., 2002. Quaternary geology of the Alexis River area, and the Blanc-Sablon to Mary's Harbour road corridor, southern Labrador. Current Research. Newfoundland Dept. of Mines and Energy, Geol. Survey Branch, Report, 02-1.

McCullagh, P. and Nelder, J.A., 1989. Binary data. In Generalized linear models (pp. 98-148). Springer US.

McKeague, J. A., 1967. An evaluation of 0.1 m pyrophosphate and pyrophosphate-dithionite in comparison with oxalate as extractants of the accumulation products in podzols and some other soils , Can J Soil Sci, 47, https://doi.org/10.4141/cjss67-017.

Nesbitt, H. W. and Young, G. M., 1982. Prediction of some weathering trends of plutonic and volcanic rocks based on thermodynamic and kinetic considerations. Nature, 299(5885), 715.

Nierop, K. G. J., Jansen, B., and Verstraten, J. M. 2002. Dissolved organic matter, aluminium and iron interactions: precipitation induced by metalycarbon ratio, pH and competition. Sci. of the Total Env. 300(1-3), 201-211.

Pan, Y., Birdsey, R. A., Fang, J., Houghton, R., Kauppi, P. E., Kurz, W. A., Phillips, O. L., Shvidenko, A., Lewis, S. L., Canadell, J. G., Ciais, P., Jackson, R. B., Pacala, S. W., McGuire, A. D., Piao, S., Rautiainen, A., Sitch, S., and Hayes, D., 2011. A large and persistent carbon sink in the world's forests. Science, 333, 988–993, https://doi.org/10.1126/science.1201609.

Patrick, M. E., Young, C. T., Zimmerman, A. R., and Ziegler, S. E., 2022. Mineralogic controls are harbingers of hydrological controls on soil organic matter content in warmer boreal forests, Geoderma, 425, https://doi.org/10.1016/j.geoderma.2022.116059.

Prasad, G.R., Culp, R. and Cherkinsky, A., 2019. δ13C correction to AMS data: Values derived from AMS vs IRMS values. Nuclear Instruments and Methods in Physics Research Section B: Beam Interactions with Materials and Atoms, 455, 244-249.

Price, J.R. and Velbel, M.A., 2003. Chemical weathering indices applied to weathering profiles developed on heterogeneous felsic metamorphic parent rocks. Chemical geology, 202(3-4), 397-416.

Ricketts, M. J.: 2001.Granular aggregate mapping in nts map areas 1n/2, 1n/11, 11o/14 and 11o/15, Current Research, 279–291.

Scharlemann, J.P.W., Tanner, E.V.J., Hiederer, R., Kapos, V., 2014. Global soil carbon: Understanding and managing the largest terrestrial carbon pool. Carbon Manag. https://doi.org/10.4155/cmt.13.77

Slessarev, E. W., Chadwick, O. A., Sokol, N. W., Nuccio, E. E., and Pett-Ridge, J., 2022. Rock weathering controls the potential for soil carbon storage at a continental scale, Biogeochemistry, 157, https://doi.org/10.1007/s10533-021-00859-8.

Taylor, A. and Blum, J. D., 1995. Relation between soil age and silicate weathering rates determined from the chemical evolution of a glacial chronosequence, Geology, 23(11), 979-982.

Walthert, L., Graf, U., Kammer, A., Luster, J., Pezzotta, D., Zimmermann, S. and Hagedorn, F., 2010. Determination of organic and inorganic carbon, δ13C, and nitrogen in soils containing carbonates after acid fumigation with HCl. Journal of Plant Nutrition and Soil Science, 173(2), 207-216.

Welham, S.J., Gezan, S.A., Clark, S.J. and Mead, A., 2014. Statistical methods in biology: design and analysis of experiments and regression. CRC Press.

Wilson, M.J., 2004. Weathering of the primary rock-forming minerals: processes, products and rates. Clay Minerals, 39(3), 233-266.

Zhou, X., Liu, D., Bu, H., Deng, L., Liu, H., Yuan, P., Du, P., Song, H., 2018. XRD-based quantitative analysis of clay minerals using reference intensity ratios, mineral intensity factors, Rietveld, and full pattern summation methods: A critical review. Solid Earth Sci. 3(1), 16-29.

Ziegler, S. E., Benner, R., Billings, S. A., Edwards, K. A., Philben, M., Zhu, X., Laganière, J., 2017. Climate warming can accelerate carbon fluxes without changing soil carbon stocks. Frontiers in Earth Sci. 5, 2.

Zuur, A.F., Ieno, E.N. and Smith, G.M., 2007. Analysing ecological data (Vol. 680). New York: Springer.

Chapter 6: Summary and Concluding Remarks

In this thesis, I investigated controls on mineral horizon soil organic carbon (SOC) storage and its response to climate change in wet boreal forests. These soils store significant SOC in regions vulnerable to climate change, but have remained poorly understood, particularly in the subsoil. Global and continental scale studies have highlighted water availability and weathering links with SOC storage mechanisms (Kramer and Chadwick, 2018; Slessarev et al., 2022). Here, I considered these factors within the wet boreal biome at the regional scale to evaluate the relative roles of climate and parent material and enhance the resolution of our predictive ability in this key forest region. This spatial scale allowed for focus on SOC stability mechanisms specific to this biome, to evaluate the role of regional parent material, and evaluate SOC responses to short-term climate change expected prior to biome shifts. Further, the role of changes in water flow paths, water balance (annual precipitation minus potential evapotranspiration), and residence times via shifts in precipitation intensity with climate change was evaluated at depth to hillslope scales. Such changes impact the delivery of dissolved organic carbon (DOC) input throughout the soil and influence the timing of storage mechanisms.

The controls on SOC across a range of timescales were evaluated in four chapters (2 – 5) in order to predict the fate of SOC in response to enhanced extreme precipitation and soil dryness with climate change. After Al organo-metal complexes (OMC) were determined to be the main control of SOC content in Chapter 2, the following chapters investigated this mechanism across timescales. I found that the precipitation of Al OMC to

stabilize SOC during an event occurs up to a maximum water flux, determined by Al weathering to concentrate the solution. Enhanced extreme precipitation should place more events above the threshold for Al OMC precipitation. Chapters 3 and 4 investigated SOC response to such high-water flux conditions to find surficial exchange of dissolved organic matter (DOM) with Al OMCs, but no new storage via precipitation. Chapter 5 finds that the water flux threshold is defined by Al availability of the parent material, and that the proportion of events meeting the threshold over time leads to SOC accumulation. Using this understanding of Al OMC precipitation at the event scale and the accumulation of SOC over time, I suggest that there may be SOC accumulation in Al rich soils with climate change where the threshold has not yet been surpassed.

6.1 Soil organic carbon distribution is a function of the spatial variation in factors of Al organo-metal complex formation

I found that Al OMC and weathering mechanisms related to their formation and stability are the main controls on SOC. Approximately 60% of SOC below 15–20 cm in the mineral horizon was associated with OMCs. In multiple linear regression models, Al OMC content and its interaction with the proxies for their saturation with C (C_{pp}:Al_{pp}) and their proportion of SOC content (C_{pp}:SOC) were the best factors for predicting SOC (Figure 6.1). Depth profiles of Al OMC were region-dependent because of regional variation in the main factors of their formation: DOM, water, and Al availability. Further, the horizon of Al OMC enrichment was deeper in soils on gentle slopes, indicating that the

impact of slope on water infiltration depth plays an important role in Al OMC coprecipitation. Both soil characteristics C_{pp}:Al_{pp} and C_{pp}:SOC exhibited logarithmic depth-trends that were consistent across four regions of the transect. This suggested that water infiltration depth was key to the development of these characteristics, whereas variations in water balance (annual precipitation minus potential evapotranspiration) across the climate are not important at this scale, consistent with water balance control at the biome-scale.

Greater SOC storage than loss via Al OMC coprecipitation over 10 – 1000s of years of precipitation events has led to the Al OMC accumulations observed in these forest sites. Enhanced shallow infiltration frequency of DOM has further saturated shallow Al OMCs with C and supported rapid SOC turnover via surface adsorption and exchange with Al OMC. Carbon age increased with depth via a similar logarithmic depth trend as C_{pp}:Al_{pp} and C_{pp}:SOC that did not exhibit regional variation. This suggests the dominant role of infiltration depth on subsoil SOC dynamics via a decreasing DOM supply with depth for surface absorption and overturn. The relative roles of DOM, water and Al availability variations at the event scale were considered in terms of the spatial distribution of those long-term accumulations to assess the fate of SOC with enhanced large precipitation events associated short-term climate change.

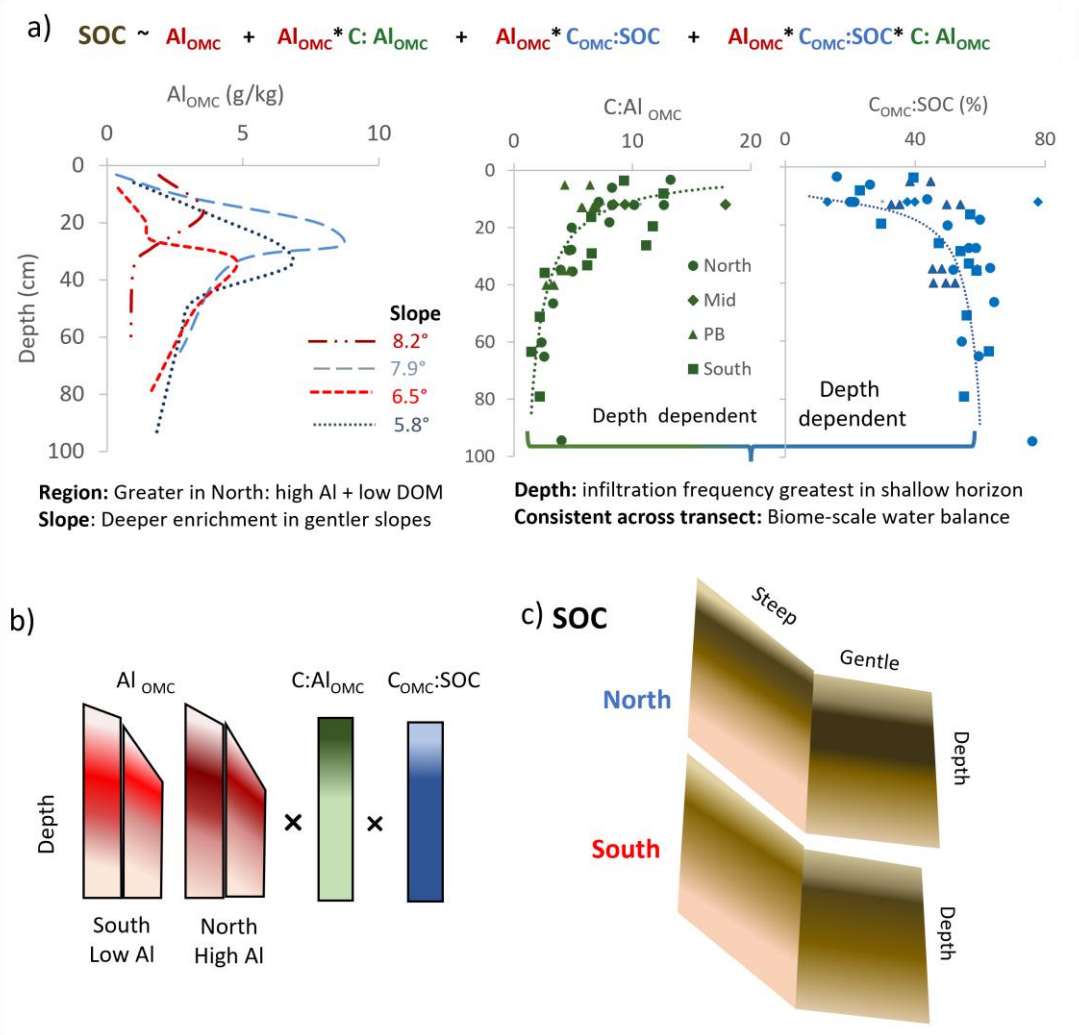

Figure 6.1.

a) Soil characteristics that predict soil organic carbon (SOC). Depth profiles of Al organo-metal complexes (Al_{OMC}) employ four soil profiles from North (blue) and South (red) regions; Al_{OMC} saturation with C (C: Al_{OMC}) and proportion of SOC in Al_{OMC} (C_{OMC}:SOC) use all data points from 4 regions, depth and hillslope. b) SOC predictors and (c) SOC content represented spatially with heat maps.

6.2 Relative roles of factors controlling soil organic carbon storage in Al organo-metal complexes dependent on parent material sources of Al.

The distributions of soil characteristics at regional, depth and hillslope scales suggest variation in water, DOM and Al availability with space and time that aid in our understanding of controls on SOC in these forests (Figure 6.2). The input of each of these governing factors among regions is a function of regional climate (Bowering et al., 2022) and parent material. The distribution of each within a region further varies with depth and incline via geomorphic controls on infiltration depth and flow paths. With time, interactions among these factors contribute to the observed distributions of soil characteristics and SOC, which can further control SOC response at shorter time scales.

Water distributes DOM in the soil solution via flow paths to depth or downslope as governed by geomorphology. The event water residence time controls the interaction time with the soil to influence reactive metal and C concentration and reactions. Variation among individual precipitation events is high but the depth distribution of infiltration over decadal to century timescales (infiltration-depth frequency) is similar among regions. Soil characteristics C_{pp}:$Al_{pp,}$ C_{pp}:SOC, and SOC age are depth-dependent likely from greater shallow infiltration that decreases with depth. Spatial variations in characteristics within the hillslope where parent material and climate inputs are consistent further suggest the importance of hydrology and flow path distribution. Yet, regional differences in water balance do not appear to contribute to soil characteristic variation. This suggests that the

distribution of water within the soil, attributed to geomorphology, is much more important in soil characteristic development than the regional difference in water input across this climate transect representing the decadal to century prediction for total annual precipitation. While annual DOM flux varies among regions with annual temperature (Bowering et al., 2022), the distribution of this C source within the soil still depends on water flow paths. Therefore, DOM inputs should follow similar depth-distribution as water depth frequency.

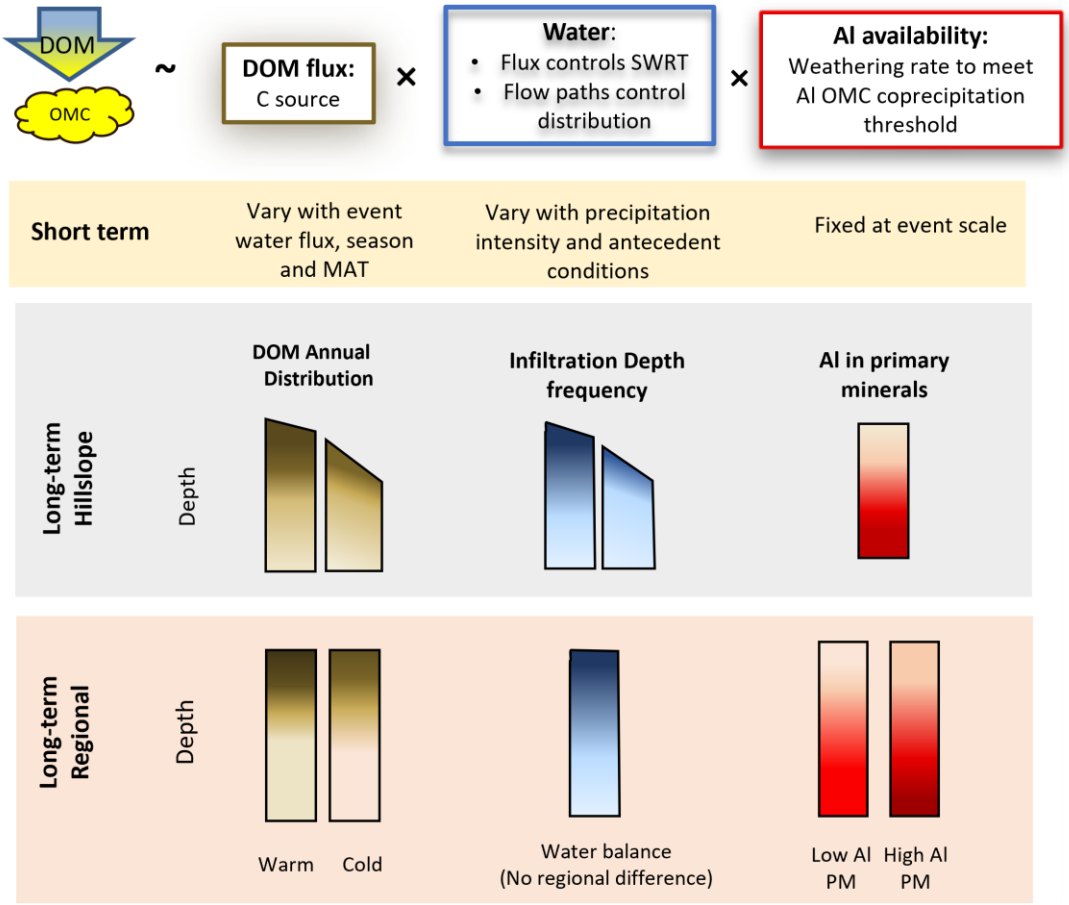

Figure 6.2.

Spatial distribution of the main factors in Al organometal complex (OMC) coprecipitation: availability of Al, dissolved organic matter (DOM) and water. Brown and blue intensity represent the magnitude of the DOM

and water fluxes (or water balance). The availability of Al is indicated by red intensity. Slope is represented by the relative angle at the top of the rectangular bar in the hillslope scale panel; slope angle is not considered in the regional controls panel. Soil water residence time = SWRT; mean annual temperature = MAT.

Parent material controls Al availability regional variation which further increases with depth as shallow soils have experienced greater weathering loss of Al. This is supported via distinct Al weathering profiles indicating enhanced Al weathering ability from the rich Al-mineral parent material of the North and limited weathering loss below ~30 cm. With long-term weathering over 100 – 1000s years, Al availability will diminish further as podzolization deepens. However, at the event scale, Al availability spatial distribution is fixed and therefore the depth of infiltration determines what soils the solution will interact with. Despite a 3 times greater annual DOM source in the warm South region, SOC content is greater in the Al-rich colder region where coupled SOC and weathering profiles suggest greater Al OMC formation. The difference in climate among these regions is equivalent to expected short-term climate change for the region. Thus, the relative roles of these factors in SOC dynamics within each region are important for interpreting the response of SOC to climate change. Their roles in SOC accumulation or loss across timescales are discussed next.

6.3 Potential soil organic carbon response to shifts in precipitation events attributed to short-term climate change

6.3.1 Accumulation of soil organic carbon is a function of frequency of precipitation events meeting physiochemical thresholds for Al organo-metal complex coprecipitation

The best predictors of SOC are Al_{pp} and the interaction of Al_{pp} with C_{pp}:Al_{pp}. This indicates coprecipitation of DOC with Al OMCs and further surface adsorption of DOC onto Al OMC surfaces are the main mechanisms supporting SOC in these soils. Accumulation of SOC begins at the event scale where coprecipitation of DOM and chelated metals from the soil solution is initiated above a requisite Al concentration and increase in pH (Nierop et al., 2002). The water flux defines the time to reach this concentration via the soil water residence time and Al availability controls the weathering rate. Soils with greater Al availability can reach the threshold concentration faster and therefore, coprecipitation is supported to a higher water flux and further, a greater proportion of DOM is stabilized as SOC (Figure 6. 3a). Therefore, the threshold defining the maximum water flux of which there can be coprecipitation is controlled by the Al availability for weathering to reach soil solution > 0.03 Al:C. Above this event threshold, surficial exchange of DOM with OMCs is dominant as this mechanism is not limited by water flux (discussed next section).

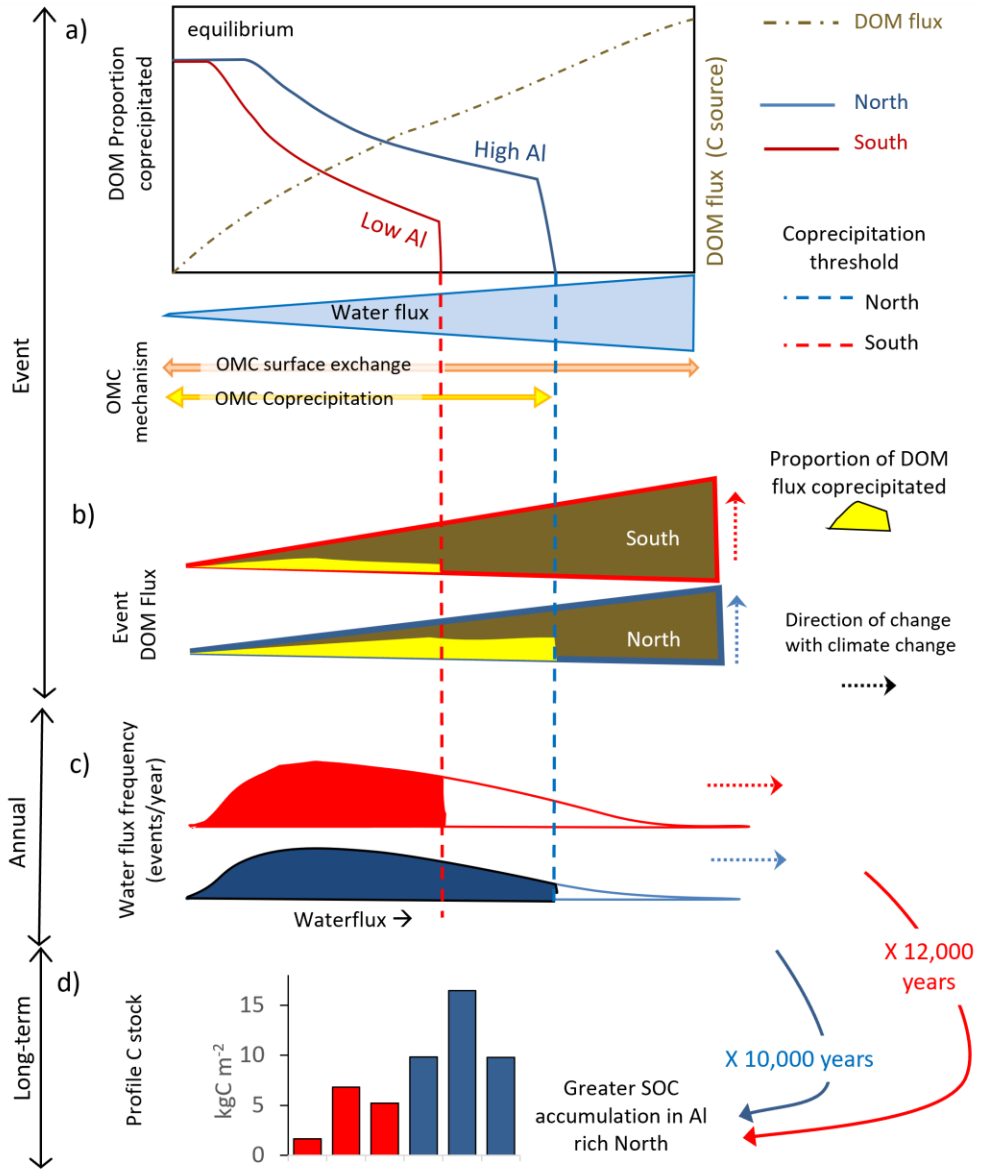

Figure 6.3.

a) Event water and dissolved organic matter (DOM) flux relationship to proportion of DOM precipitated as soil organic carbon in Al organometal complexes (OMC). Threshold indicates the greatest water flux of which there can be OMC coprecipitation (soil solution > 0.03 Al:C). b) Interpreted proportion of event DOM flux (brown) coprecipitated with Al OMC (yellow). c) Estimated water flux frequency distribution (binned average frequency of events with water flux averaged per annuum) shaded to indicate events where the threshold for organometal complex precipitation is met in the North and South regions. (d) Soil organic carbon (SOC) profile stocks after 100-1000s years of accumulation.

Among regions, Al availability is controlled by regional parent material which controls the composition (e.g. Al content and weatherability) and thus degree of weathering within the soil. A greater threshold for the coprecipitation of reactive metals and organic matter in Al-rich soils indicates a higher probability that the threshold will be met for SOC storage during an event (Figure 6.2b–c). Therefore, over 10 – 1000s of years, SOC accrual will be greater in soils formed on Al-rich parent material (Figure 6.2d).

Within a region, where parent material is assumed consistent, the shallowest horizons have experienced the greatest degree of weathering indicating increasing Al availability with depth. This, paired with the concomitant rapid increase in pH with depth, suggests that the potential for coprecipitation during an event increases with infiltration depth (Figure 6.4a). However, shallow infiltration events are more frequent, therefore many events do not support coprecipitation (Figure 6.4b). Instead, long-term Al OMC accumulation is greatest in mid- depth mineral soils where they exhibit a sharp pH and Al increase, and frequent shallow infiltration supports further saturation of shallow Al OMCs with C (Figure 6.4c). This OMC-associated C (C_{pp}) contributes a smaller proportion of SOC content in shallow soils where Al OMC content is low despite high saturation, yet C_{pp} consistently comprises ~60 % of SOC at mid-depth and below (Figure 6.4d).

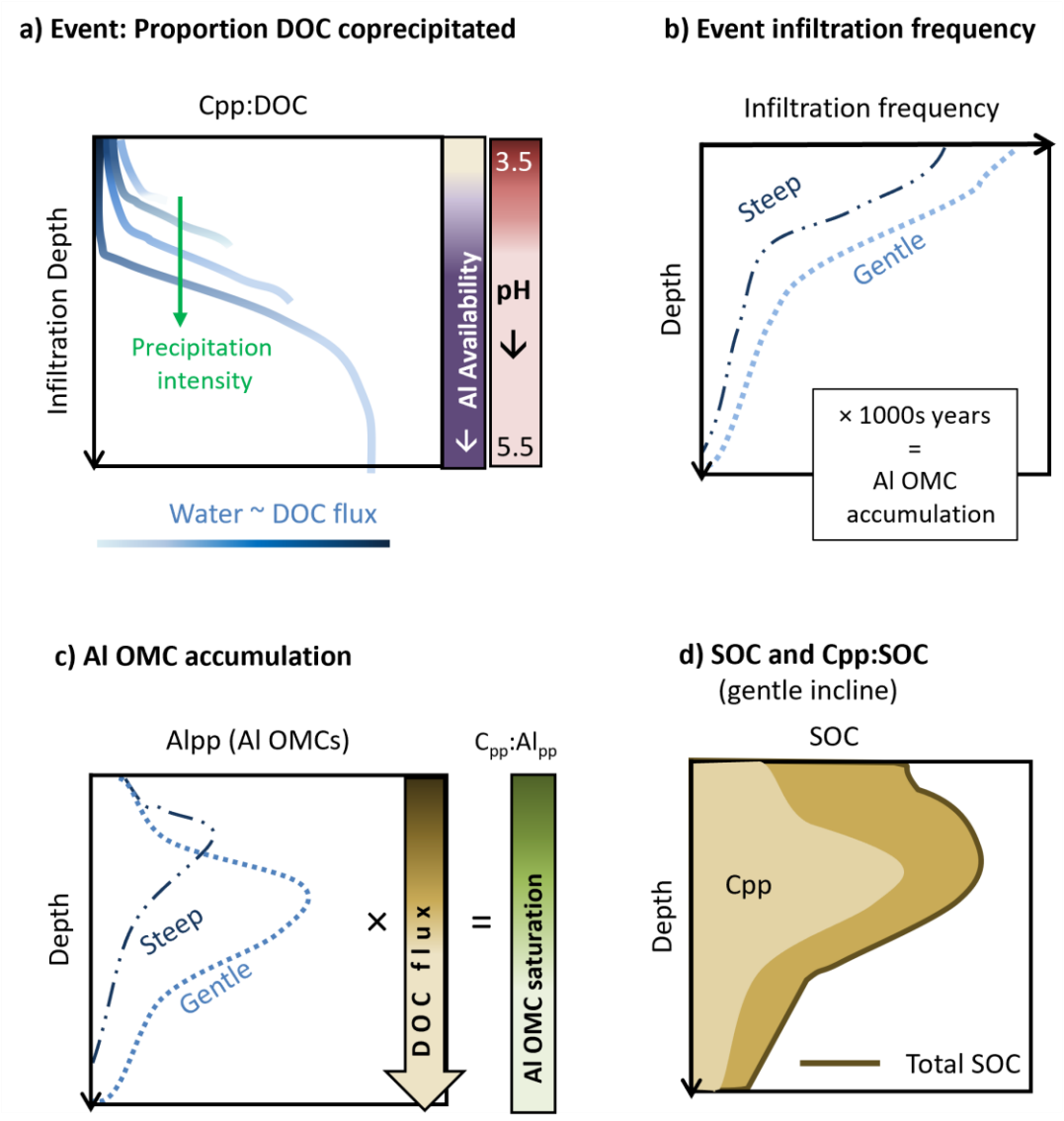

Figure 6.4.

Development soil characteristics and soil organic carbon (SOC) with time over depth. a) Proportion of dissolved organic C (DOC) coprecipitated (Cpp:DOC) with organo-metal complexes (OMCs) with precipitation intensity and infiltration depth. b) Annual infiltration depth frequency of events for shallow and steep incline (6° and 12°). c) Accumulation of Al OMCs (Alpp) in soil and their increasing saturation with depth (C_{pp}:Al_{pp}). d) SOC content and proportion associated with OMCs (Cpp).

Slope incline further impacts the depth distribution of these soil characteristics via infiltration depth frequency. Steep soils likely experience greater shallow lateral flow and

less vertical infiltration than gentle slopes (Figure 6.4b). Therefore, a shallower and smaller enrichment of Al OMC, C_{pp}, and SOC, and a lower C_{pp}:Al_{pp} is expected in soils underlaying steeper portions of the hillslope.

6.3.2 Impact of extreme precipitation events on uptake or loss of carbon via surface exchange with Al OMCs is controlled by infiltration depth and time of year

Beyond coprecipitation, extant Al OMCs within the soil can also interact with the soil solution to adsorb more DOC to their surface or desorb their associated C. This mechanism may occur at any water flux, but SOC accrual may be limited to this mechanism at higher water fluxes that exceed those supporting the OMC coprecipitation threshold (i.e. soil solution >0.03 Al:C).

This DOC exchange is controlled by C_{pp}:Al_{pp}, with loss from shallow saturated soils and adsorption to less saturated soils below a transition threshold depth. The threshold value of C_{pp}:Al_{pp} defines whether C is adsorbed or desorbed from existing OMCs with antecedent moisture. Therefore, since C_{pp}:Al_{pp} is fixed over depth at the event scale, the depth at which the soil solution must infiltrate to, before transition to uptake, is shallower under wetter conditions. This suggests that infiltration depth and event timing of high intensity precipitation events are key in SOC response predictions. This means late summer events on dry soils will promote greater SOC loss from shallow soils than late autumn events on wet soils.

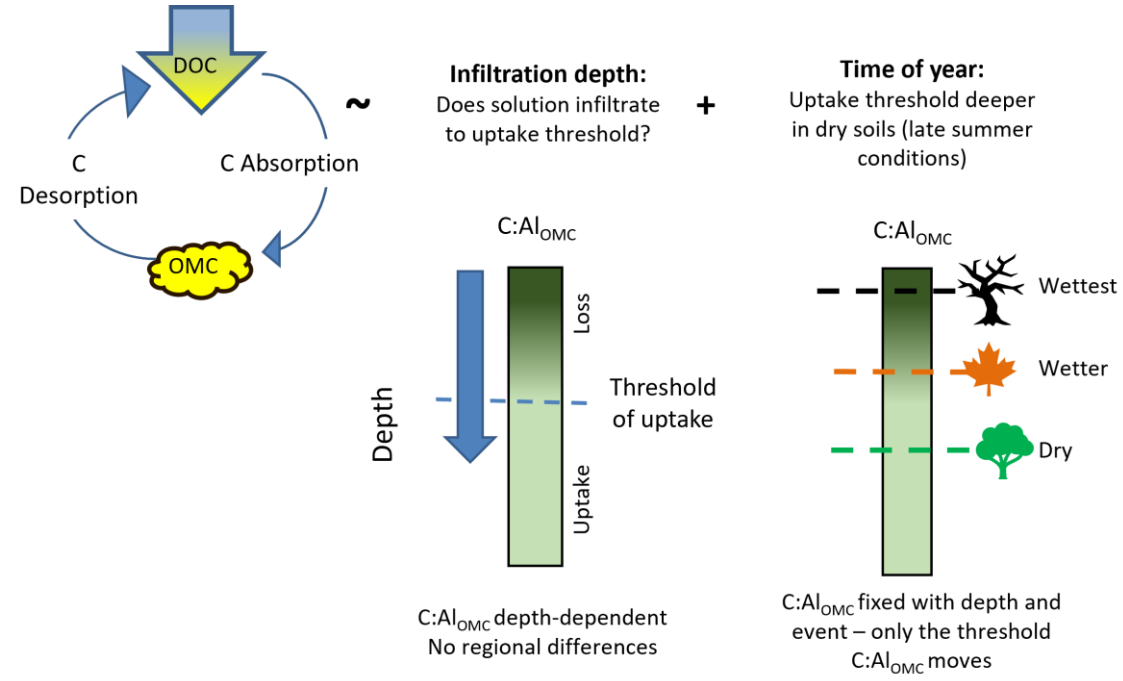

Figure 6.5.

Spatial and temporal controls on surface exchange of dissolved organic carbon (DOC) with Al organo-metal complexes Al_{OMC} during extreme events (but also applicable at lower precipitation intensity as mechanism likely occurs at any water flux). Saturation of Al_{OMC} with C ($C:Al_{OMC}$) controls uptake or loss of DOC with loss in shallow saturated soils but uptake at depth. Depth of uptake threshold, defining the transition from loss to uptake, becomes shallower with increased soil moisture, therefore events in late summer (green dotted line) will lose more DOC than from late autumn wet soils (orange and black dotted lines) due to transition from intense evapotranspiration to little evapotranspiration.

6.4 Implications for climate change predictions, limitations and future work

This thesis investigated mineral horizon SOC dynamics in boreal forest regions that are expected to experience significant increases in temperature and precipitation intensity. I found that Al OMCs were the main control on SOC dynamics, where their

coprecipitation to stabilize SOC varied with time and space as a function of the factors of their formation: water, DOM and Al availability.

At the event scale, Al availability set the threshold water flux for Al OMC coprecipitation to store SOC. Therefore, soils formed from Al-rich parent material should support increases in net SOC content to a greater water and DOM flux. Further, water infiltration-depth frequency within a region was more important than differences in water balance among regions for SOC accumulation, where greater infiltration supports more SOC storage potential. This suggests that shifts in the frequency of events towards higher precipitation intensity with climate change may limit new Al OMC formation in low Al soils but a concurrent increase in DOM flux may support more storage in Al-rich soils. Further, deep soils may experience SOC accrual if enhanced mean annual precipitation and reduced snowpack promote a shift towards a deeper infiltration frequency distribution where Al OMCs storage mechanisms are supported.

By evaluating spatiotemporal variations in Al OMC formation factors, this research has enhanced our predictive understanding of SOC dynamics in boreal forest mineral horizons, particularly in the poorly understood subsoil. Parent material composition is key to our predictive understanding of SOC dynamics at regional scales relevant to short-term climate change within this biome. It has highlighted the need for more regional scale studies including a range of parent material compositions to inform further our predictive understanding of deep mineral SOC stores, including relationships with management strategies aimed at mitigation solutions and informing Earth systems models.

The SOC controls uncovered in this thesis are limited to the regional scale within a moist boreal biome as parent material generally varies locally to regionally and the main mechanisms of SOC storage should differ among biomes via variations in vegetation, temperature and water availability. While common parent material varieties were employed provided a good range in weatherability, more types are needed to fully explore the response of SOC in such landscapes. For example, carbonated dominated regions where Al is limited likely exhibit different mechanisms of SOC storage. Therefore, these findings are expected to be applicable in boreal regions where Al is available for Al OMC formation. A greater number of soil depth profiles per region are also needed as local hydrology can be highly variable based on the geomorphology and could influence SOC content and response.

In future work, I plan to predict SOC content for much of Newfoundland and Labrador with further development of the models presented here with regional climate data and projections, geomorphology interpretated with 5 m digital elevation models, and a large database of parent material compositions provided by the Geological Survey of Newfoundland. Trajectories of SOC response with short-term climate change can also be modeled using the same data inputs paired with a geochemical weathering model to determine the thresholds of Al OMC coprecipitation at regional scales interpreted within the context of expected climate change. Further, extension of these models into other boreal biomes with contrasting water availability may be applicable by verifying model output with observed SOC content or modified with new data obtained through similar studies.

The parent material may also control the SOC accrual threshold at the regional scale in wetter boreal biomes where Al OMC formation via weathering is likely a dominant control on SOC because the mobility of reduced of Fe OMC. In historically drier boreal biomes, these results suggest: (1) less modern SOC content than this moist boreal transect because of limited weathering, (2) enhanced SOC content in OMCs with increasing mean annual precipitation with climate change, and (3) a greater role of Fe OMCs than in wetter biomes. A similar study design could evaluate the relative roles of climate and parent material in such biomes. Furthermore, SOC predictions should consider regional parent material in any biome with positive water availability where weathering products could contribute to significant SOC storage. Finally, parent material should not be important at larger scales where differences in vegetation, water availability and temperature likely have a greater control on SOC storage mechanisms.

6.5 References

Bowering, K.L., Edwards, K.A., Wiersma, Y.F., Billings, S.A., Warren, J., Skinner, A., Ziegler, S.E., 2022. Dissolved Organic Carbon Mobilization Across a Climate Transect of Mesic Boreal Forests Is Explained by Air Temperature and Snowpack Duration. https://doi.org/10.1007/s10021-022-0074

Kramer, M.G., Chadwick, O.A., 2018. Climate-driven thresholds in reactive mineral retention of soil carbon at the global scale. Nat Clim Chang 8, 1104–1108. https://doi.org/10.1038/s41558-018-0341-4

Nierop, K.G.J., Jansen, B., Verstraten, J.M., 2002. Dissolved organic matter, aluminium and iron interactions: precipitation induced by metalycarbon ratio, pH and competition, The Science of the Total Environment.

Slessarev, E.W., Chadwick, O.A., Sokol, N.W., Nuccio, E.E., Pett-Ridge, J., 2022. Rock weathering controls the potential for soil carbon storage at a continental scale. Biogeochemistry 157. https://doi.org/10.1007/s10533-021-00859-8

Appendix

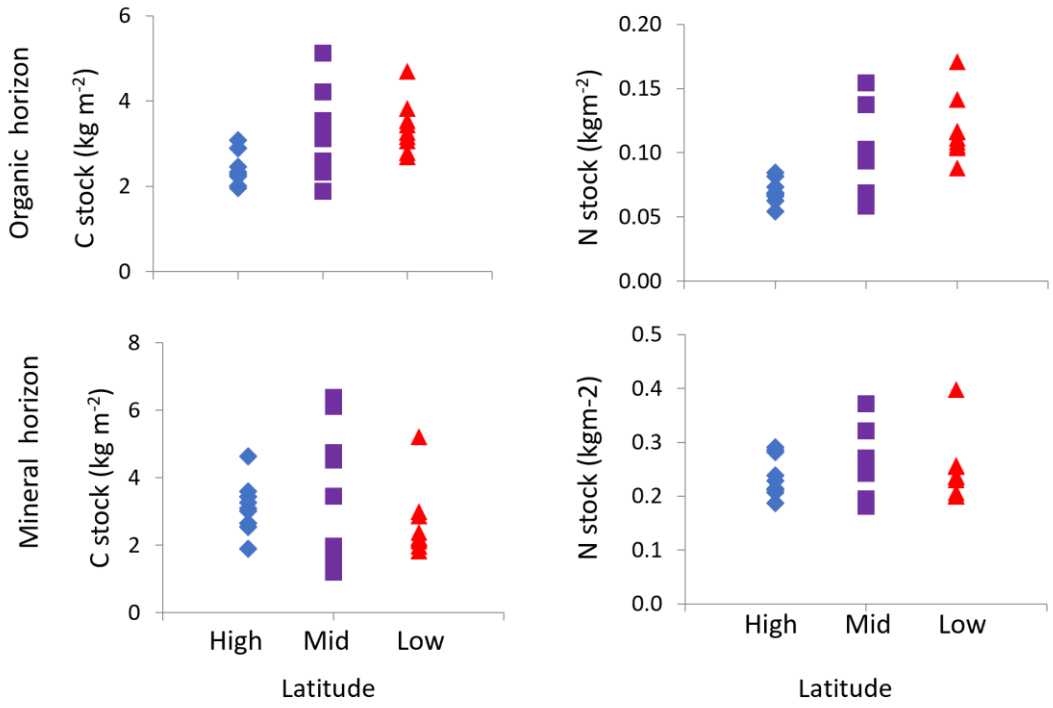

Figure S0.1

NLBELT regional variation in soil C and N stocks from the organic horizon and top 10 cm of the mineral soil.

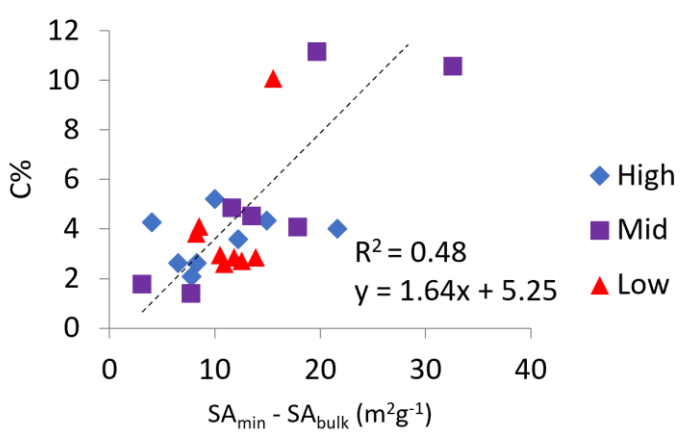

Figure S0.2.

Relationship of %C with surface area after organic matter removal (SA_{min}). SA_{bulk} is the bulk surface area of <2mm mineral soil.

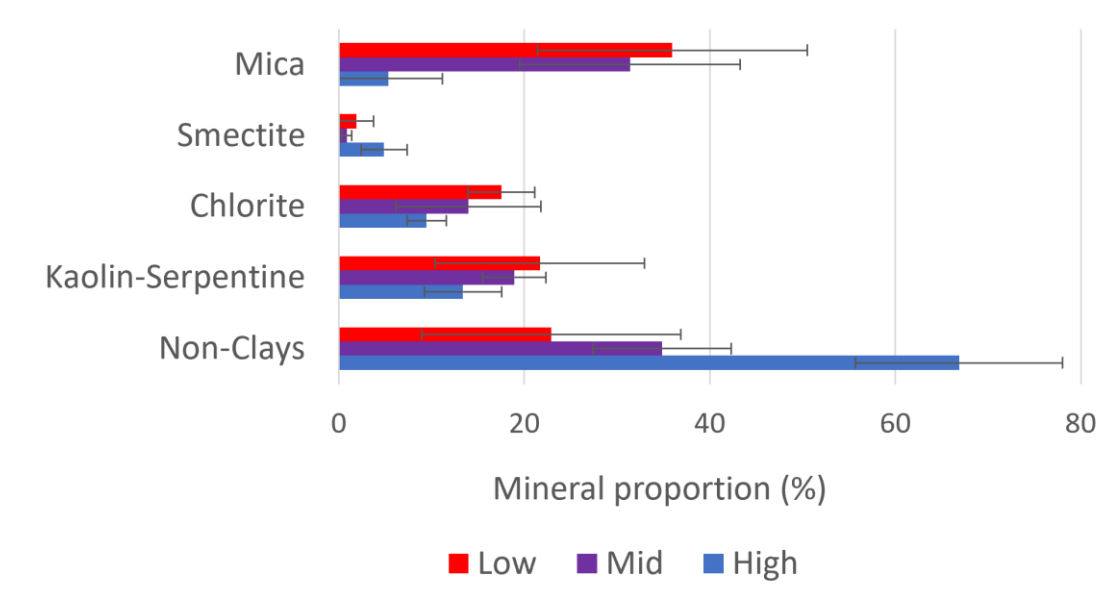

Figure S0.3.

Average clay mineral proportions by region in shallow mineral horizon soils of the NL-BELT.

Table S0.1 Mineral soil characteristics.

Regional averages and standard deviation of mineral soil characteristics of the NL-BELT, including pyrophosphate-extracted Fe and Al (Fe_{pp} and Al_{pp}) as a proxy for organometal complexes, surface area of the bulk <2mm soil and after removal of organic matter (SA_{bulk} and SA_{min}), pore volume (PV), cation exchange capacity (CEC) and the clay size fraction (clay).

	Fe_{pp}	**Al_{pp}**	**SA_{bulk}**	**SA_{min}**	**PV**	**CEC**	**Clay**
	g kg^{-1}	g kg^{-1}	m^2 g^{-1}	m^2 g^{-1}	mm^3 g-1	cmol kg-1	%
High	8.3 ± 2.9	5.4 ± 3.2	3.9 ± 2.1	13.8 ± 7.0	11.5 ± 3.2	7.8 ± 1.4	4.0 ± 1.3
Mid	10.4 ± 5.2	6.3 ± 7.2	11.7 ± 4.8	26.2 ± 13	31 ± 14.5	19.2 ± 9.3	16.3 ± 9.7
Low	14.3 ± 4.6	5.4 ± 2.5	13.9 ± 4.2	25.2 ± 5.2	25 ± 7.9	9.9 ± 1.4	6.3 ± 2.4

Table S0.2 Term correlations.

Pearson correlation coefficient heat map among all variables considered in models to describe C and %N in NL-BELT mineral soils. Terms with low correlations (<0.4, no colour) can be used together within a model, while terms with moderate to strong correlations (light and dark pink) cannot.

	Litterfall	C_{org}	N_{org}	Fe_{pp}	Al_{pp}	SA_{bulk}	SA_{min}	PV	Clay	CEC
Litterfall		0.16	0.31	-0.16	-0.31	0.39	-0.2	0.37	0.14	0.14
C_{org}	0.16			0.05	-0.26	0.34	-0.23	0.4	0.04	0.31
N_{org}	0.31			0.18	-0.27	0.43	-0.16	0.4	-0.08	0.64
Fe_{pp}	-0.02	0.04	0.18		0.58	0.66	0.66	0.47	0.34	0.34
Al_{pp}	-0.31	-0.26	-0.27	0.58		0.31	0.62	0.07	0.64	0.64
SA_{bulk}	0.39	0.34	0.43	0.66	0.31		0.61	0.65	0.36	0.36
SA_{min}	-0.2	-0.23	-0.16	0.66	0.62	0.61		0.62	0.15	0.4
PV	0.37	0.4	0.4	0.47	0.07	0.65	0.62		0.74	0.44
Clay	0.31	0.31	0.25	0	-0.13	0.36	0.15	0.74		0.32
CEC	0.14	0.04	-0.08	0.34	0.64	0.36	0.4	0.44	0.32	

Correlation Coefficient	
0.6-0.8	Strong
0.4-0.6	Moderate
<0.4	Low

Table S0.3. All models tested for %C.

Sub-models tested for each full model listed in Table 2. An AIC modified for small sample size (AIC_c) was employed and is based on the maximum log-likelihood with a penalty for additional terms that do not add additional predictive power. A smaller (more negative) AIC_c indicates a better model. Delta AIC_c (ΔAIC_c) is the difference in AIC_c from the highest ranked model, all models with ΔAIC_c <2 are considered highly plausible. Akaike weights (w_i) indicate the weight of evidence in favour of each model as a decimal percent. Terms in italics are uninformative parameters that add no additional predictive power to the model. Highly plausible models are highlighted in yellow.

Full model	Model	AICc	ΔAICc	weight	loglik
1	Fepp+CEC*Fepp+E	-67.322	0	0.33474	37.248
1	Fepp+CEC*Fepp+LF*Fepp+E	-66.401	0.9204	0.21127	37.814
1	Fepp+E	-66.136	1.18531	0.18506	35.631
1	CEC+Fepp+E	-65.066	2.25574	0.10836	36.12
1	CEC+Fepp+CEC*Fepp+E	-65.27	2.052	0.11998	37.248
1	LF+Fepp+LF*Fepp+E	-62.501	4.8207	0.03005	35.864
1	LF+CEC+Fepp+LF*CEC+LF*Fepp+CEC*Fepp+E	-60.398	6.92358	0.0105	37.91
1	LF+CEC+LF*CEC+E	-46.708	20.6138	1.10E-05	27.968
1	Litter+E	-46.168	21.1531	8.50E-06	25.647
1	CEC+E	-36.868	30.4532	8.20E-08	20.997
2	Fepp+E	-66.136	0	0.47266	35.631
2	Fepp+LF*Fepp+E	-64.554	1.58203	0.2143	35.864
2	LF+Fepp+E	-64.09	2.04635	0.1699	35.632
2	LF+Fepp+LF*Fepp+E	-62.501	3.63539	0.07676	35.864
2	Fepp+Clay+Fepp*Clay+E	-62.068	4.06841	0.06182	35.648
2	LF+Fepp+Clay+LF*Clay+Clay*Fepp+LF*Fepp+E	-56.847	9.28883	0.00454	36.134
2	LF+E	-46.168	19.9678	2.20E-05	25.647
2	Clay+E	-42.23	23.9065	3.00E-06	23.677
2	LF+Clay+LF*Clay+E	-40.456	25.6807	1.30E-06	24.841
3	Alpp+SAbulk*Alpp+E	-67.622	0	0.30653	37.398

3	SAbulk+Alpp+E	-67.568	0.054	0.29837	37.371
3	Alpp+Alpp*LitterNo+E	-67.08	0.54196	0.23377	37.127
3	SAbulk+Alpp+SAbulk*Alpp+E	-65.569	2.05336	0.1098	37.398
3	Alpp+E	-63.909	3.71249	0.0479	34.517
3	SAbulk+Litter+Alpp+SAbulk*LF+SAbulk*Alpp+Alpp*LF+E	-58.401	9.22094	0.00305	36.911
3	SAbulk+E	-53.853	13.769	0.00031	29.489
3	Alpp+LF+Alpp*LF+E	-53.29	14.3317	0.00024	31.259
3	SAbulk+Litter+SAbulk*LF+E	-48.564	19.058	2.20E-05	28.896
3	LF+E	-46.168	21.4534	6.70E-06	25.647
4	Alpp+Alpp*LF+E	-67.08	0	0.49637	37.127
4	Alpp+LF+E	-66.205	0.87506	0.32047	36.689
4	Alpp+E	-63.909	3.17053	0.1017	34.517
4	Alpp+PV*Alpp+E	-62.658	4.42154	0.05441	34.916
4	PV+Alpp+E	-59.532	7.54832	0.01139	33.353
4	PV+Alpp+PV*Alpp+E	-58.822	8.2577	0.00799	34.025
4	PV+LF+Alpp+PV*LF+PV*Alpp+Alpp*LF+E	-58.594	8.48578	0.00713	37.008
4	Alpp+LF+Alpp*LF+E	-53.29	13.7897	0.0005	31.259
4	LF+E	-46.168	20.9115	1.40E-05	25.647
4	PV+E	-45.448	21.6314	1.00E-05	25.287
4	PV+LF+PV*LF+E	-45.415	21.6645	9.80E-06	27.321
5	Alpp+Norg*SAbulk+Norg*Alpp+Alpp*SAbulk+E	-80.469	0	0.35006	45.877
5	Alpp+Norg*Alpp+E	-80.148	0.3208	0.29819	43.661
5	SAbulk+Alpp+Norg*SAbulk+Norg*Alpp+Alpp*SAbulk +E	-78.405	2.06429	0.12471	45.877
5	Norg+Alpp+Norg*SAbulk+Norg*Alpp+Alpp*SA+E	-78.405	2.06429	0.12471	45.877
5	Norg+SAbulk+Alpp+Norg*SAbulk+Norg*Alpp+Alpp*SAbulk+E	-77.149	3.3205	0.06654	46.285
5	Alpp+Norg*Alpp+Alpp*SAbulk+E	-75.53	4.9387	0.02963	42.379
5	Norg+Alpp+E	-72.013	8.45644	0.0051	39.593

5	Norg+Alpp+Norg*Alpp+E	-68.207	12.2617	0.00076	38.717
5	SAbulk+Alpp+SAbulk*Alpp+E	-65.569	14.9005	0.0002	37.398
5	Alpp+E	-63.909	16.5596	8.90E-05	34.517
5	Norg+SAbulk+Norg*SAbulk+E	-56.415	24.054	2.10E-06	33.207
5	SAbulk+E	-53.853	26.6161	5.80E-07	29.489
5	Norg+E	-46.349	34.1205		25.737
6	SAmin+E	-59.026	0	0.38094	32.075
6	SAmin+LitterNo*SAmin+E	-58.883	0.14325	0.3546	33.028
6	Litter+SAmin+E	-56.987	2.03885	0.13744	32.08
6	Litter+SAmin+LitterNo*SAmin+E	-56.829	2.19661	0.12702	33.028
6	Litter+E	-46.168	20.9115	1.40E-05	25.647
7	Norg+SAmin+E	-60.804	0	0.36386	33.989
7	Norg+SAmin+Norg*SAmin+E	-60.638	0.16582	0.33491	34.933
7	SAmin+Norg*SAmin+E	-59.054	1.7499	0.15169	33.114
7	SAmin+E	-59.026	1.77839	0.14954	32.075
7	Norg+E	-46.349	14.4557	0.00026	25.737

Table S0.4. All models tested for %N.

List of all models tested to describe %C in shallow NL-BELT mineral soils. Sub-models tested for each full model listed in Table 2. An AIC modified for small sample size (AIC_c) was employed and is based on the maximum log-likelihood with a penalty for additional terms that do not add additional predictive power. A smaller (more negative) AIC_c indicates a better model. Delta AIC_c (ΔAIC_c) is the difference in AIC_c from the highest ranked model, all models with $\Delta AIC_c < 2$ are considered highly plausible. Akaike weights (w_i) indicate the weight of evidence in favour of each model as a decimal percent. Terms in italics are uninformative parameters that add no additional predictive power to the model. Highly plausible models are highlighted in yellow.

Full model	Model	AICc	ΔAICc	weight	loglik
1	Fepp+CEC*Fepp+E	-67.322	0	0.33474	37.2477
1	Fepp+CEC*Fepp+LF*Fepp+E	-66.401	0.9204	0.21127	37.8142
1	Fepp+E	-66.136	1.18531	0.18506	35.6306
1	CEC+Fepp+E	-65.066	2.25574	0.10836	36.1198
1	CEC+Fepp+CEC*Fepp+E	-65.27	2.052	0.11998	37.2484
1	LF+Fepp+LF*Fepp+E	-62.501	4.8207	0.03005	35.864
1	LF+CEC+Fepp+LF*CEC+LF*Fepp+CEC*Fepp+E	-60.398	6.92358	0.0105	37.9095
1	LF+CEC+LF*CEC+E	-46.708	20.6138	1.10E-05	27.9675
1	Litter+E	-46.168	21.1531	8.50E-06	25.6467
1	CEC+E	-36.868	30.4532	8.20E-08	20.9967
2	Fepp+E	-66.136	0	0.47266	35.6306
2	Fepp+LF*Fepp+E	-64.554	1.58203	0.2143	35.864
2	LF+Fepp+E	-64.09	2.04635	0.1699	35.6319
2	LF+Fepp+LF*Fepp+E	-62.501	3.63539	0.07676	35.864
2	Fepp+Clay+Fepp*Clay+E	-62.068	4.06841	0.06182	35.6475
2	LF+Fepp+Clay+LF*Clay+Clay*Fepp+LF*Fepp+E	-56.847	9.28883	0.00454	36.1342
2	LF+E	-46.168	19.9678	2.20E-05	25.6467
2	Clay+E	-42.23	23.9065	3.00E-06	23.6774

2	LF+Clay+LF*Clay+E	-40.456	25.6807	1.30E-06	24.8414
3	Alpp+SAbulk*Alpp+E	-67.622	0	0.30653	37.3979
3	SAbulk+Alpp+E	-67.568	0.054	0.29837	37.3709
3	Alpp+Alpp*LitterNo+E	-67.08	0.54196	0.23377	37.1269
3	SAbulk+Alpp+SAbulk*Alpp+E	-65.569	2.05336	0.1098	37.3979
3	Alpp+E	-63.909	3.71249	0.0479	34.5172
3	SAbulk+Litter+Alpp+SAbulk*LF+SAbulk*Alpp+Alpp*LF+E	-58.401	9.22094	0.00305	36.911
3	SAbulk+E	-53.853	13.769	0.00031	29.489
3	Alpp+LF+Alpp*LF+E	-53.29	14.3317	0.00024	31.2587
3	SAbulk+Litter+SAbulk*LF+E	-48.564	19.058	2.20E-05	28.8956
3	LF+E	-46.168	21.4534	6.70E-06	25.6467
4	Alpp+Alpp*LF+E	-67.08	0	0.49637	37.1269
4	Alpp+LF+E	-66.205	0.87506	0.32047	36.6894
4	Alpp+E	-63.909	3.17053	0.1017	34.5172
4	Alpp+PV*Alpp+E	-62.658	4.42154	0.05441	34.9162
4	PV+Alpp+E	-59.532	7.54832	0.01139	33.3528
4	PV+Alpp+PV*Alpp+E	-58.822	8.2577	0.00799	34.0248
4	PV+LF+Alpp+PV*LF+PV*Alpp+Alpp*LF+E	-58.594	8.48578	0.00713	37.0076
4	Alpp+LF+Alpp*LF+E	-53.29	13.7897	0.0005	31.2587
4	LF+E	-46.168	20.9115	1.40E-05	25.6467
4	PV+E	-45.448	21.6314	1.00E-05	25.2867
4	PV+LF+PV*LF+E	-45.415	21.6645	9.80E-06	27.3213
5	Alpp+Norg*SAbulk+Norg*Alpp+Alpp*SAbulk+E	-80.469	0	0.35006	45.8774
5	Alpp+Norg*Alpp+E	-80.148	0.3208	0.29819	43.6611
5	SAbulk+Alpp+Norg*SAbulk+Norg*Alpp+Alpp*SAbulk +E	-78.405	2.06429	0.12471	45.8774

5	Norg+Alpp+Norg*SAbulk+Norg*Alpp+Alpp*SA+E	-78.405	2.06429	0.12471	45.8774
5	Norg+SAbulk+Alpp+Norg*SAbulk+Norg*Alpp+Alpp*SAbulk+E	-77.149	3.3205	0.06654	46.2848
5	Alpp+Norg*Alpp+Alpp*SAbulk+E	-75.53	4.9387	0.02963	42.3788
5	Norg+Alpp+E	-72.013	8.45644	0.0051	39.5933
5	Norg+Alpp+Norg*Alpp+E	-68.207	12.2617	0.00076	38.7173
5	SAbulk+Alpp+SAbulk*Alpp+E	-65.569	14.9005	0.0002	37.3979
5	Alpp+E	-63.909	16.5596	8.90E-05	34.5172
5	Norg+SAbulk+Norg*SAbulk+E	-56.415	24.054	2.10E-06	33.2074
5	SAbulk+E	-53.853	26.6161	5.80E-07	29.489
5	Norg+E	-46.349	34.1205		25.7368
6	SAmin+E	-59.026	0	0.38094	32.0754
6	SAmin+LitterNo*SAmin+E	-58.883	0.14325	0.3546	33.0282
6	Litter+SAmin+E	-56.987	2.03885	0.13744	32.0804
6	Litter+SAmin+LitterNo*SAmin+E	-56.829	2.19661	0.12702	33.0282
6	Litter+E	-46.168	20.9115	1.40E-05	25.6467
7	Norg+SAmin+E	-60.804	0	0.36386	33.9891
7	Norg+SAmin+Norg*SAmin+E	-60.638	0.16582	0.33491	34.9328
7	SAmin+Norg*SAmin+E	-59.054	1.7499	0.15169	33.1141
7	SAmin+E	-59.026	1.77839	0.14954	32.0754
7	Norg+E	-46.349	14.4557	0.00026	25.7368

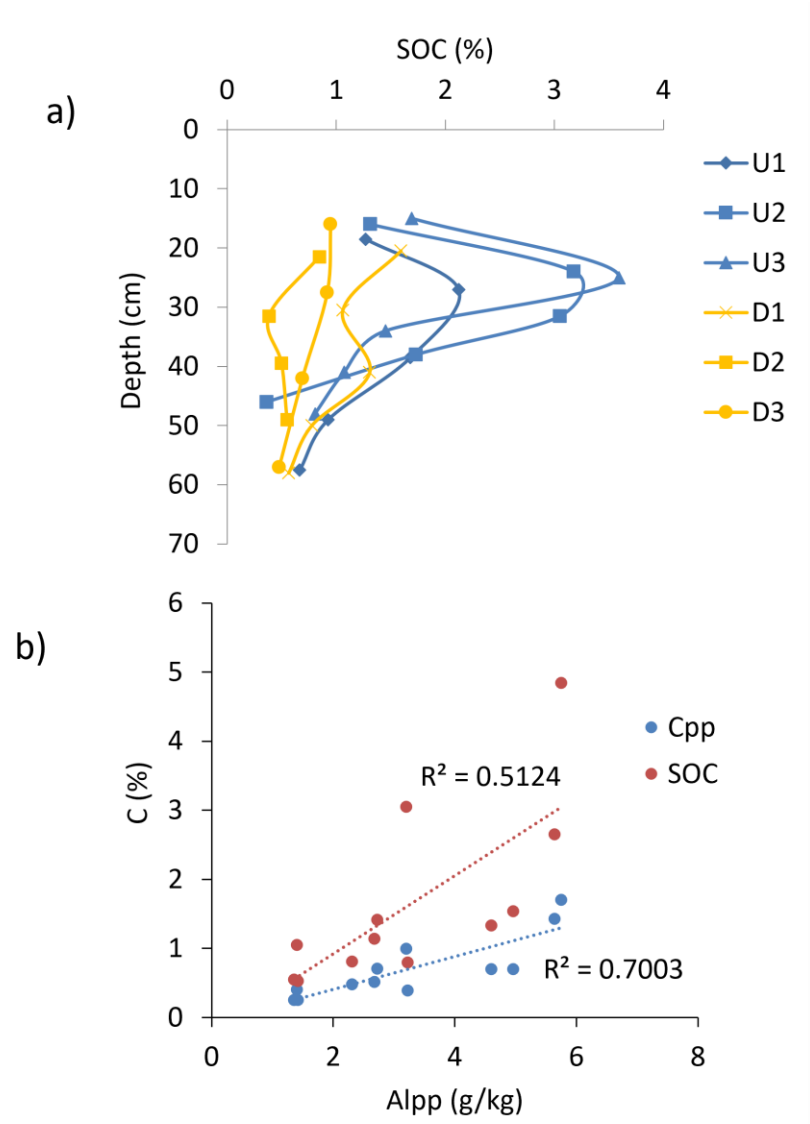

Figure S7.1

a) Soil organic carbon (SOC) for full soil profile. 3 soil pits per slope position. U = upslope; D = downslope. b) Relationship of pyrophosphate-extracted aluminium (Alpp; Al OMC proxy) with SOC and Cpp (pyrophosphate extracted DOC; C in OMCs).

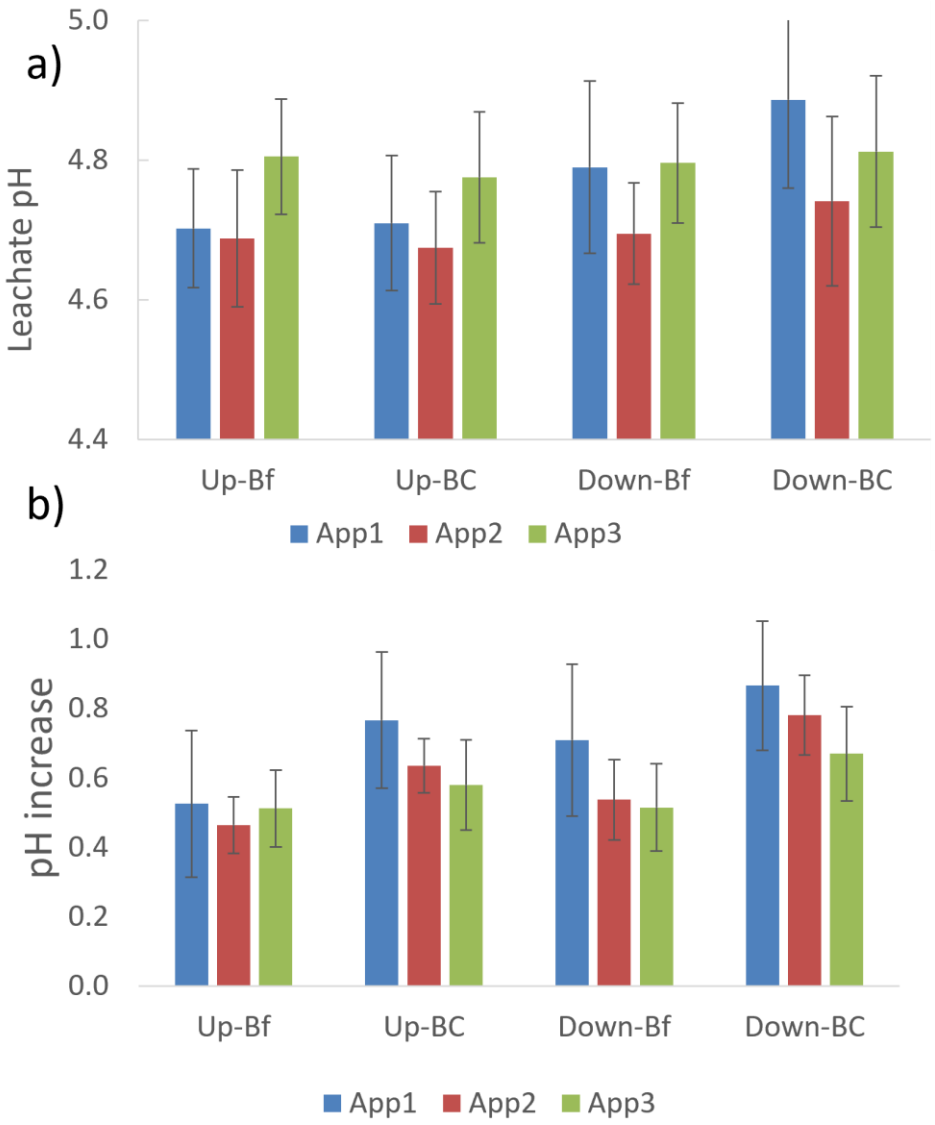

Figure S7.2.

Average (a) leachate pH and (b) pH increase relative to initial soil solution added to the soil column given by spatial position and application.

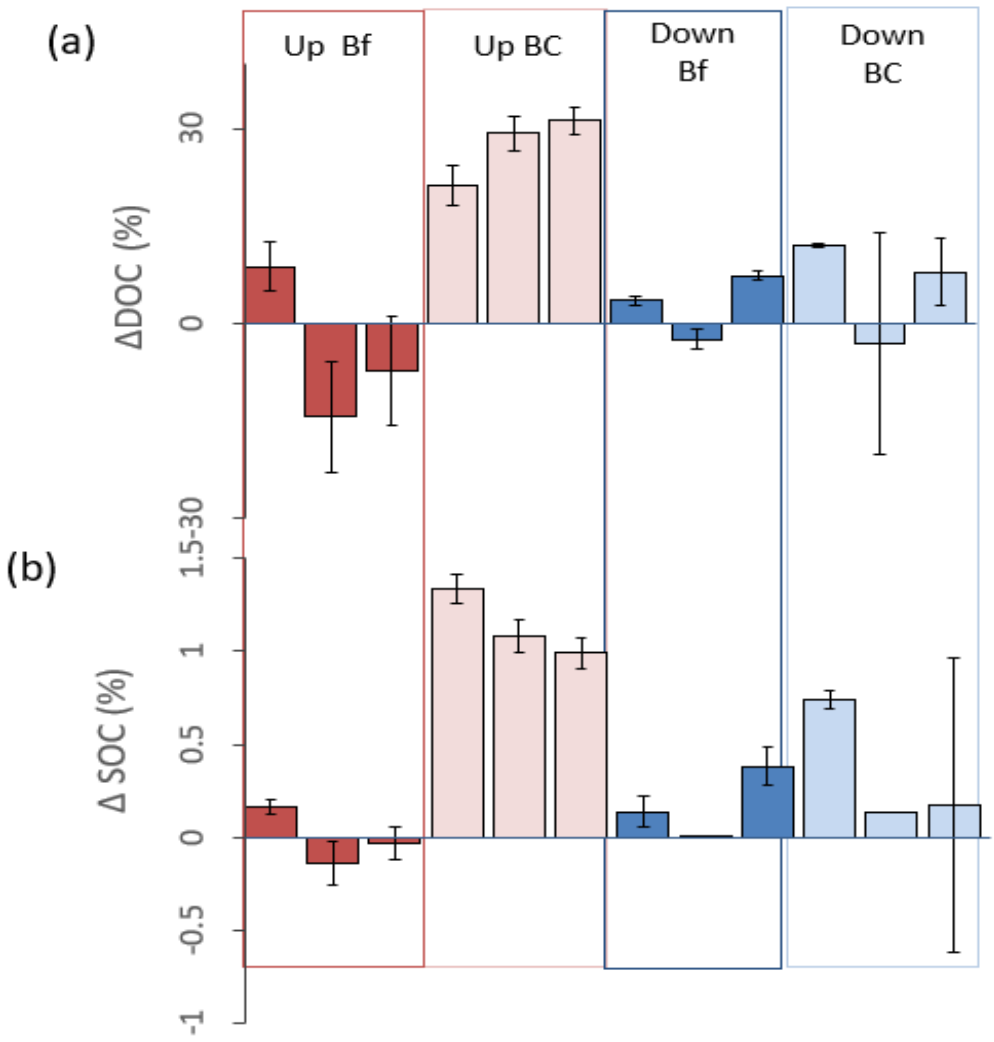

Figure S3.3.

(a) Change in dissolved organic carbon (DOC = Initial - Final) as percent of applied DOC, and (b) change in SOC (%), average of 3 applications to each soil column. Uptake to the soil is indicated by positive numbers. Three soil pits per spatial position (3 bars); variance among 3 replications per soil sampling pit indicated with error bars in the histogram. Upslope Bf horizons (Up Bf), Upslope BC horizon (Up BC), Footslope Bf (Down Bf), and Footslope BC (Down BC). (b) Scatter plot shows relationship between ΔDOC_{SUM} and saturation of Al organo-metal complexes with C extracted in a pyrophosphate solution (molar C_{pp}:Al_{pp}). (c-d) Change in dissolved organic carbon averaged by individual application (ΔDOC_{APP}) is provided in a histogram depicting the average for each spatial position across all soil pits and replications. Scatter plot shows relationship of ΔDOC_{APP} to molar C_{pp}:Al_{pp}.

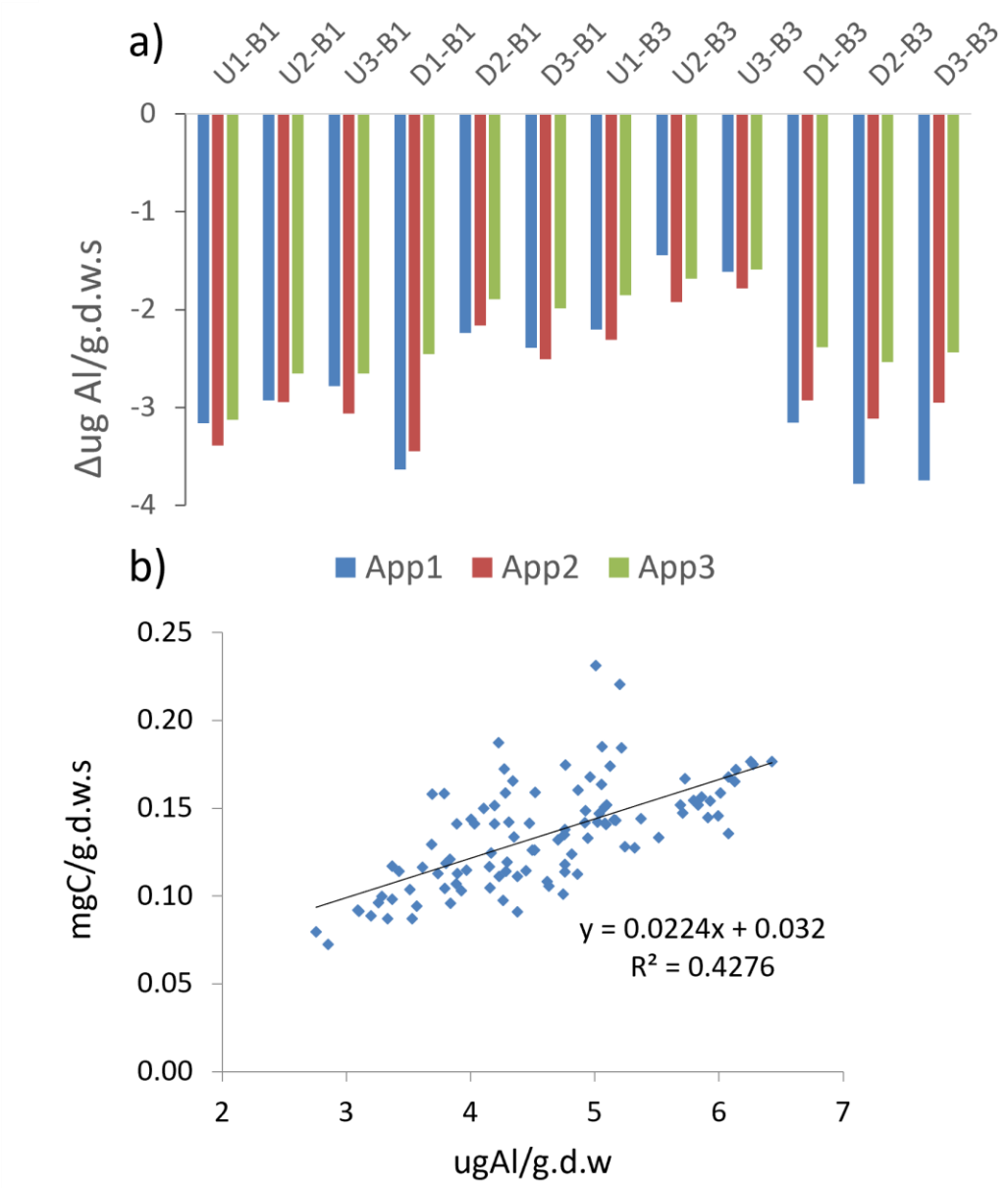

Figure S7.4.

a) Change in Al in leachate by application per gram dry weight soil (g.d.w.s). Negative = Al loss from soil.
b) Relationship among DOC and Al content in the leachate relative to grams of dry weight soil in column.

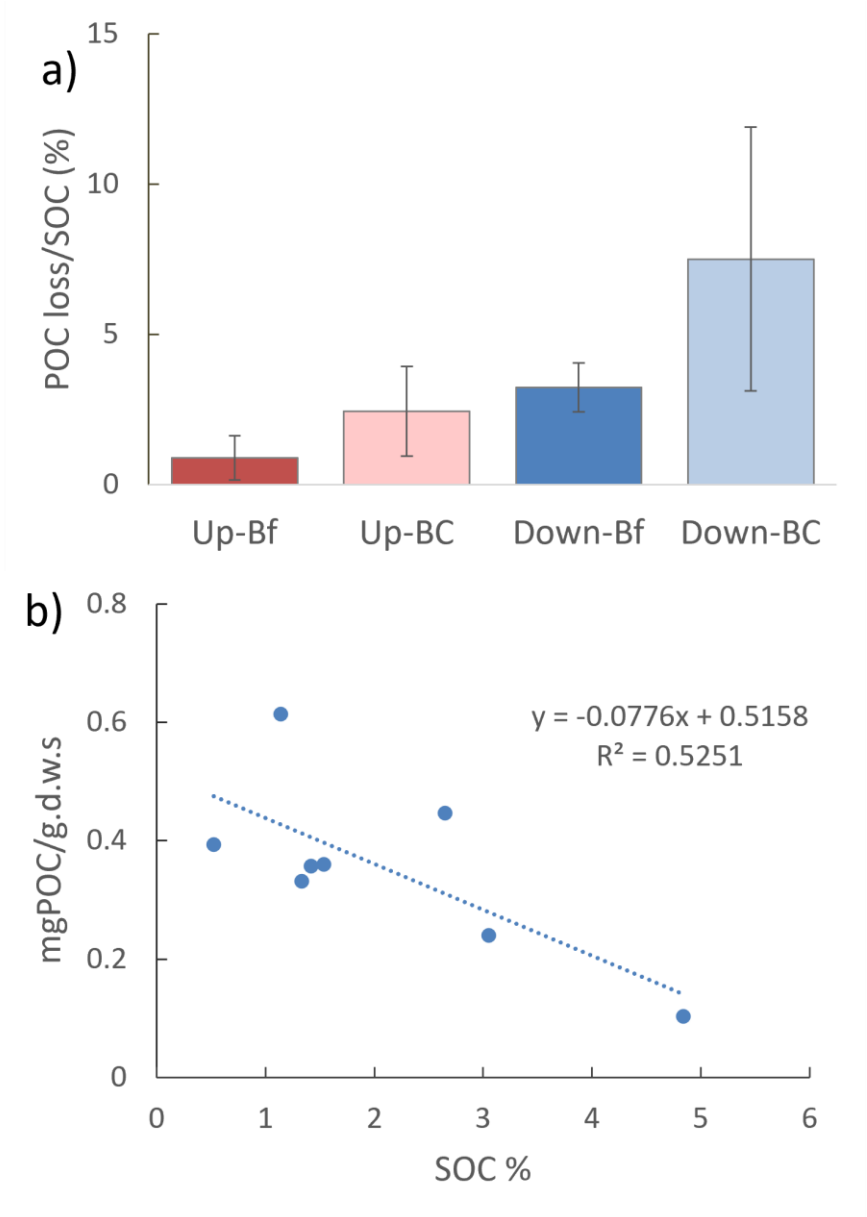

Figure S7.5.

a) Particulate organic carbon (POC) loss as percent of SOC by spatial position. b) Particulate organic carbon loss per gram dry weight soil (g.d.w.s) relationship with SOC content.

Table S7.1. Till composition of Pynn's Brook experimental watershed

a) average major oxide (%) as determined using ICP-OES fusion

	SiO_2	Al_2O_3	Fe_2O_3*	MgO	CaO	Na_2O	K_2O	TiO_2	MnO	P_2O_5
Ave	69.81	14.40	5.27	2.44	1.62	2.82	2.64	0.736	0.118	0.145
St. Dev	4.93	2.25	2.08	1.05	1.17	0.69	0.43	0.190	0.047	0.033

b) average mineral proportions as a percent from X-ray diffraction.

	Quartz	Plagioclase	K-Feldspar	Chlorite	Muscovite	Biotite
Ave	38.2	24.7	5.4	13.5	14.1	4.2
St. Dev	5.1	12.4	1.6	6.0	8.5	1.7

Table S7.2. Soil weight, rock volume and soil water additions used in column building.

WHC = Water holding capacity.

	Dry wt soil (g)	Bulk density (g/cm3)	Rock volume (%)	WHC (%)	Water for 60% WHC (ml)
U1-Bf	122.93	0.9	13	65.82	48.55
U2-Bf	122.93	0.9	13	78.09	57.60
U3-Bf	122.93	0.9	13	87.52	64.55
U1-BC	107.39	0.9	24	48.93	31.53
U2-BC	107.39	0.9	24	56.94	36.69
U3-BC	107.39	0.9	24	54.73	35.27
D1-Bf	122.93	0.9	13	44.88	33.10
D2-Bf	122.93	0.9	13	50.13	36.97
D3-Bf	122.93	0.9	13	44.76	33.02
D1-BC	107.39	0.9	24	41.78	26.92
D2-BC	107.39	0.9	24	32.47	20.92
D3-BC	107.39	0.9	24	43.97	28.33

Table S7.3 Experimental design.

Twelve soil sites (hillslope position, horizon) were replicated into three soil columns. Each replicate soil column (year) received three sequential applications (events). The site names refer to their spatial position as upslope (U) and footslope (D) soil pit location followed by the soil horizon (Bf or BC). For example, U1-Bf refers to the soil sample collected from Bf horizon in the first soil pit located in the upslope position of the experimental forest hillslope.

Column set up

Spatial Position (4)	Up-Bf			Up-BC			Down-BF			Down-BC		
Site name (12) * 3 column reps	U1-BF	U2-Bf	U3-Bf	U1-BC	U2-BC	U3-BC	D1-BF	D2-Bf	D3-Bf	D1-BC	D2-BC	D3-BC

Treatments

	Year (Column rep)		
Event (Application)	1	2	3
A	1A	2A	3A
B	1B	2B	3B
C	1C	2C	3C

DOC_{sum}: Sum of all applications for each column

Spatial Position (4)	Up-Bf			Up-BC			Down-BF			Down-BC		
Site Name (12)	U1-BF	U2-Bf	U3-Bf	U1-BC	U2-BC	U3-BC	D1-BF	D2-Bf	D3-Bf	D1-BC	D2-BC	D3-BC
Treatment (36): Year 1-3	1	1	1	1	1	1	1	1	1	1	1	1
	2	2	2	2	2	2	2	2	2	2	2	2
	3	3	3	3	3	3	3	3	3	3	3	3

DOC_{app} Average DOC change for each application for each site

Spatial Position (4)	Up-Bf			Up-BC			Down-BF			Down-BC		
Site Name (12)	U1-BF	U2-Bf	U3-Bf	U1-BC	U2-BC	U3-BC	D1-BF	D2-Bf	D3-Bf	D1-BC	D2-BC	D3-BC
Treatment (36): Event	a	a	a	a	a	a	a	a	a	a	a	a
	b	b	b	b	b	b	b	b	b	b	b	b
	c	c	c	c	c	c	c	c	c	c	c	c

Table S7.4. Model results.

DOC_{SUM} = Change in dissolved organic carbon (DOC = Initial - Final) as sum of all applications normalized to grams dry weight soil. Change in dissolved organic carbon averaged by individual application (DOC_{APP}). Position = four spatial positions in hillslope; Year (treatment) = 3 event season (years 1-3); Event (treatment) = 3 precipitation events ordered; C saturation of Al or Al+Fe organometal complexes (CAl_{pp} and CM_{pp}); DOC concentration of initial solution (DOC_{int}); Explained variance (R^2); p-value (P); Degrees of freedom (Df). Predictors or interactions determined to have a significant influence on the dependent variable are given in black as opposed to grey.

Model	Predictor	Df	R^2	P
DOMsum~ Position * Year	Position	3	0.783	5.80E-09
	Year	2	0.030	0.1402
	Position*Year	6	0.025	0.7417
	Residuals	23	0.162	
	Total		0.809	1.74E-08
DOM Sum~ CAl_{pp} + Year + CAl_{pp}*Year	CAl_{pp}	1	0.752	2.01E-11
	Year	2	0.034	0.1015
	CAl_{pp}*Year	2	0.017	0.2919
	Residuals	29	0.197	
	Total		0.803	2.00E-09
DOMSum~ CM_{pp} + Year + CM_{pp}*Year	CM_{pp}	1	0.584	1.06E-07
	Year	2	0.021	0.4364
	CM_{pp}*Year	2	0.031	0.2886
	Residuals	30	0.364	
	Total		0.636	6.91E-06
DOCApp~ Position + Event + Position*Event	Position	3	0.495	1.54E-07
	Event	2	0.215	3.55E-05
	Position*Event	6	0.131	0.01673
	Residuals	24	0.159	
	Total		0.841	4.47E-07
DOCApp~ CAl_{pp} + Event + CAl_{pp}*Event	CAl_{pp}	1	0.492	3.68E-10
	Event	2	0.215	6.68E-06
	CAl_{pp}*Event	2	0.117	0.000505
	Residuals	30	0.177	
	Total		0.823	1.98E-10
DOCApp~ CM_{pp} + Event + CM_{pp}*Event	CM_{pp}	1	0.449	9.62E-09
	Event	2	0.215	3.55E-05
	CM_{pp}*Event	2	0.117	0.001601
	Residuals	30	0.219	
	Total		0.781	4.51E-09
DOCall ~ Position + DOC_{int}:Event + Position*DOC_{int}:Event	Position	3	0.395	2.20E-16
	DOC_{Int}:Event	3	0.288	3.07E-16
	Position*DOCInt:Event	9	0.113	1.12E-05
	Residuals	85	0.204	
	Total		0.796	2.20E-16
	CAl_{pp}	1	0.389	2.20E-16

$DOCall \sim CAl_{pp} + DOC_{int}:Event + C:Al_{pp}*DOC_{int}:Event$	DOC_{Int}:Event	3	0.283	1.03E-15
	CAl_{pp}:DOC_{Int}:Event	3	0.089	1.70E-06
	Residuals	93	0.239	
	Total		0.761	2.20E-16
$DOCall \sim CM_{pp} + DOC_{int}:Event + C:M_{pp}*DOC_{Int}:Event$	CM_{pp}	1	0.354	2.20E-16
	DOC_{Int} :Event	3	0.278	4.14E-14
	CM_{pp}:DOC_{Int} :Event	3	0.093	5.33E-06
	Residuals	93	0.275	
	Total		0.725	2.20E-16

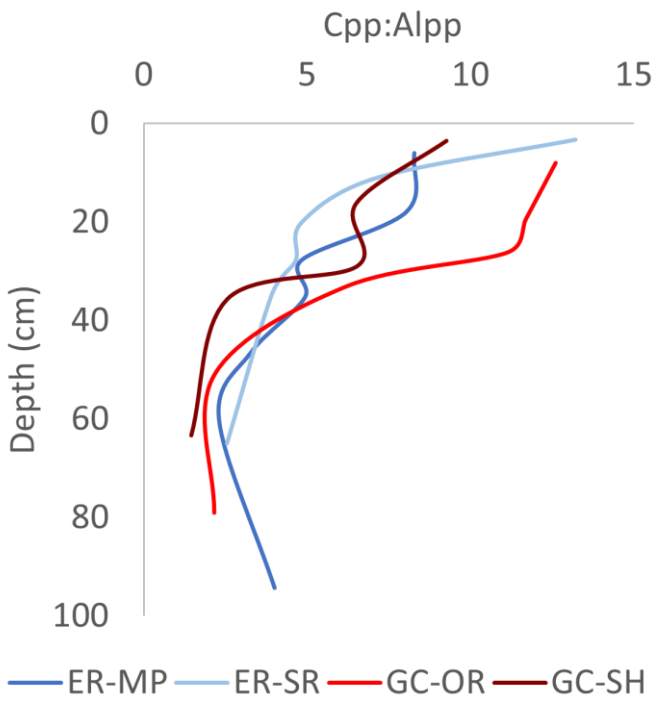

Figure S8.1.

Molar ratio of pyrophosphate extracted C to Al (Cpp:Alpp) is used to assess the carbon saturation of organometal complexes for soil profiles. These results were used for modelling the net change in dissolved organic carbon with depth reported in Figure 4.5. Blue and red lines indicate sites from the North and South regions, respectively.

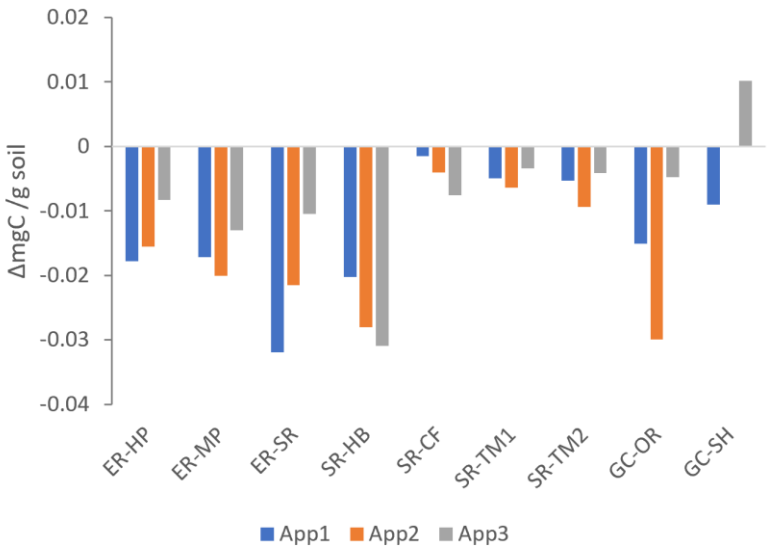

Figure S8.2.

Average change (D) in dissolved organic carbon by application with experimental percolation through mineral soil columns. Each average is derived from 3 replicate columns for each site with values given per gram dry weight soil. Site names beginning with ER are from the North region, SR from the Mid, and GC from the South.

Table S8.1.

Soil weight, rock volume and water additions used in building the experimental soil columns. The water holding capacity (WHC) was evaluated at the site level while rock volume was averaged among all sites.

Site	Dry wt soil (g)	Soil density (g/cm3)	Rock volume (%)	Rock volume Cm3	Cylinder volume	WHC (%)	ml H2O for 60% WHC
ER-HP	143.33	0.982	7	10.99	157	95.26	81.92
ER-MP	135.69	0.929	7	10.99	157	79.00	64.32
ER-SR	118.01	0.808	7	10.99	157	72.89	51.61
SR-HB	116.67	0.799	7	10.99	157	74.08	51.86
SR-CF	134.37	0.920	7	10.99	157	88.93	71.69
SR-TM1	75.79	0.519	7	10.99	157	56.34	25.62
SR-TM2	77.59	0.531	7	10.99	157	56.34	26.23
GC-OR	95.35	0.653	7	10.99	157	97.67	55.88
GC-SH	117.84	0.807	7	10.99	157	83.68	59.16

Table S8.2.

Characteristics of the initial solutions for each soil column replication, including dissolved organic carbon (DOC), total dissolved aluminum, their ratio, and pH. The same solution was used for all applications of a given replication. These are the average of two samples of the initial solution that were collected per day, which were further measured in triplicates of each for DOC.

	DOC (mg/L)	Al (ppb)	Molar Al/C	pH
Rep1	49.1	720	0.00653	4.08
Rep2	49.8	725	0.006474	4.11
Rep3	47.5	720	0.006744	4.41

Table S8.3.

Experimental fraction of SOC lost from soil (% or per mil) for all shallow climate transect soils. Blue, purple and red indicate the North, Mid and South regions.

	Average % of SOC lost	**Average SOC lost per mil**
ER-HP	-0.177	-1.77
ER-MP	-0.067	-0.67
ER-SR	-0.151	-1.51
SR-HB	-0.114	-1.14
SR-CF	-0.039	-0.39
SR-TM1	-0.047	-0.47
SR-TM2	-0.036	-0.36
GC-OR	-0.124	-1.24
GC-SH	0.003	0.03
Average all sites	-0.082 ± 0.066	-0.82 ± 0.66

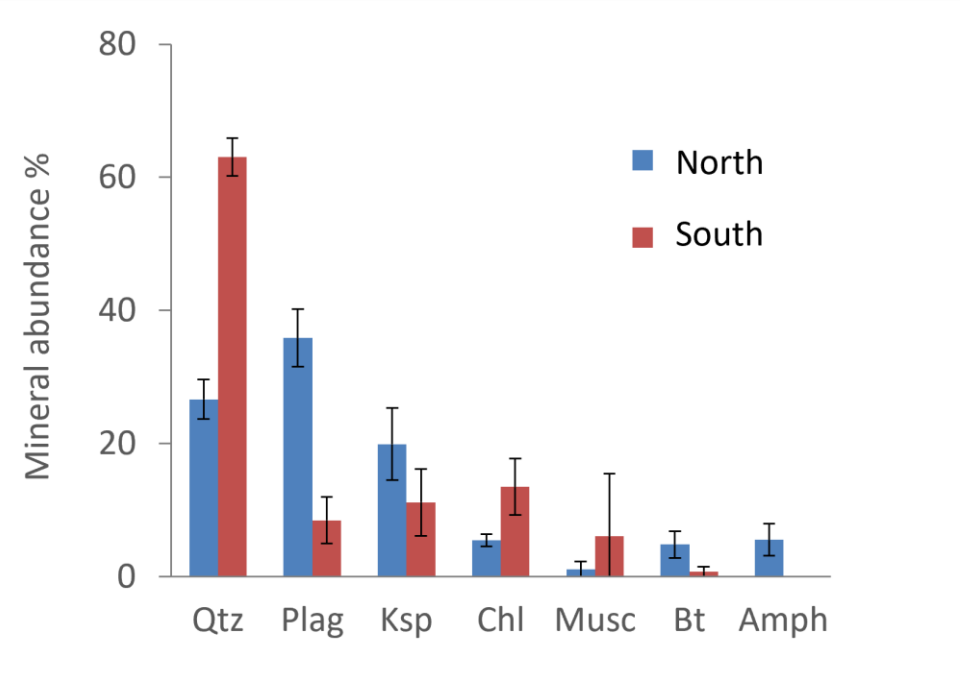

Figure S9.1.

Mineral abundances (%) of dominant minerals of till for each region as interpreted from X-ray diffraction. Quartz (qtz), plagioclase (plag), K-feldspar (ksp), chlorite (chl), muscovite (musc), biotite (bt) and amphibole (amph).

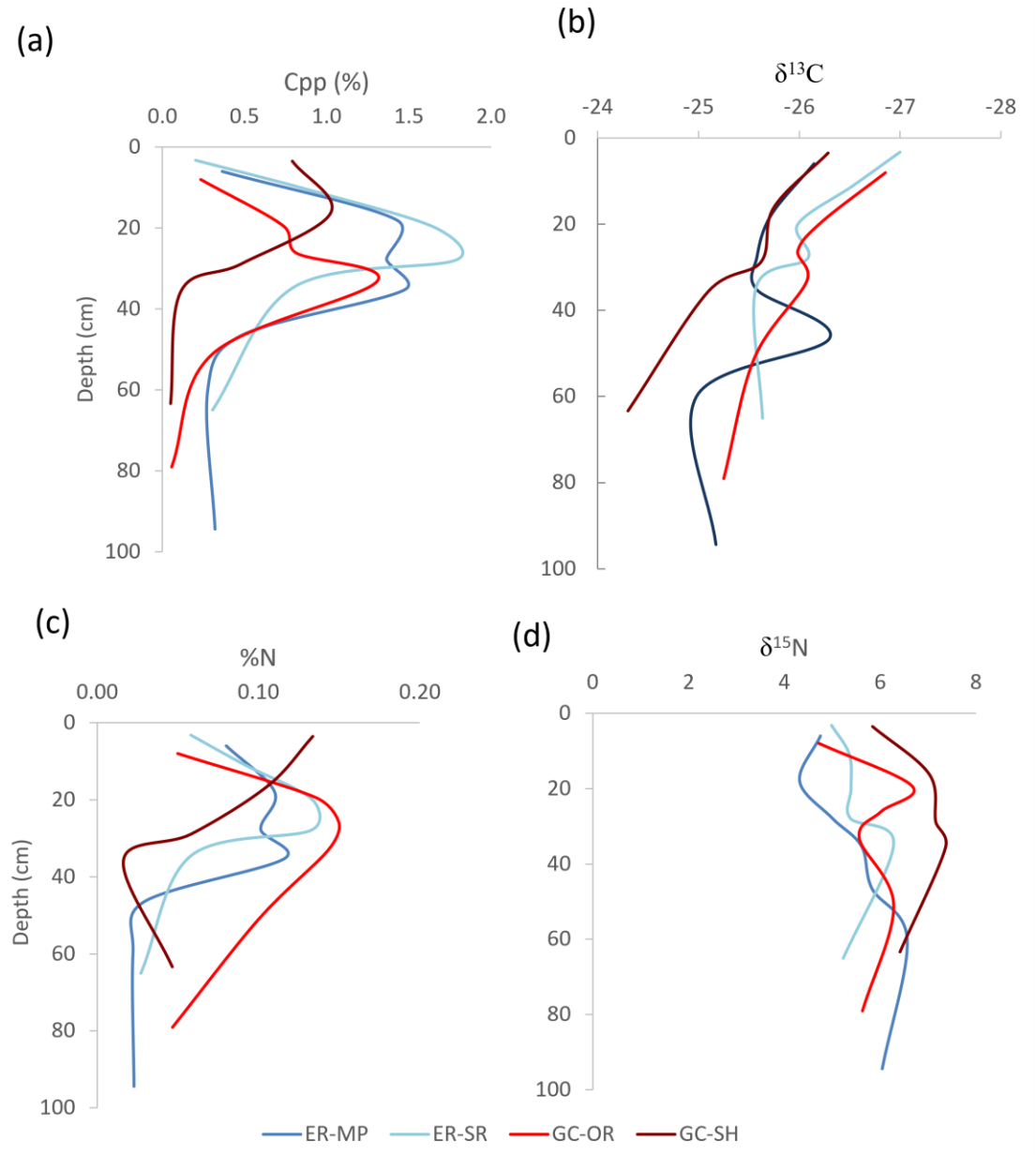

Figure S9.2.

Mineral soil characteristics of two profiles per region: (a) pyrophosphate extracted carbon (C_{pp}) which is a proxy for carbon associated with organo-metal complexes (OMCs), (b) delta 13 C isotopic ratio ($\delta^{13}C$) (c) nitrogen content as percent weight; (d) delta 15 N isotopic ratio ($\delta\ ^{15}N$).

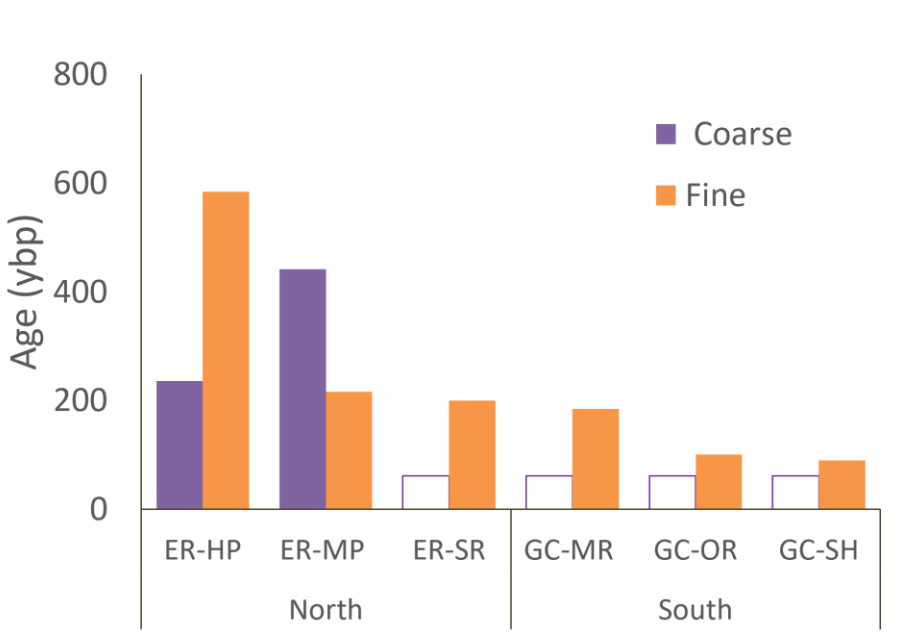

Figure S9.3.

Average bulk radiocarbon ages of top 10 cm mineral horizon soils by size fraction. Coarse > 63 µm; fine <63µm. Average of three plots per site. Unfilled bars indicate modern carbon ages (less than ~60 years).

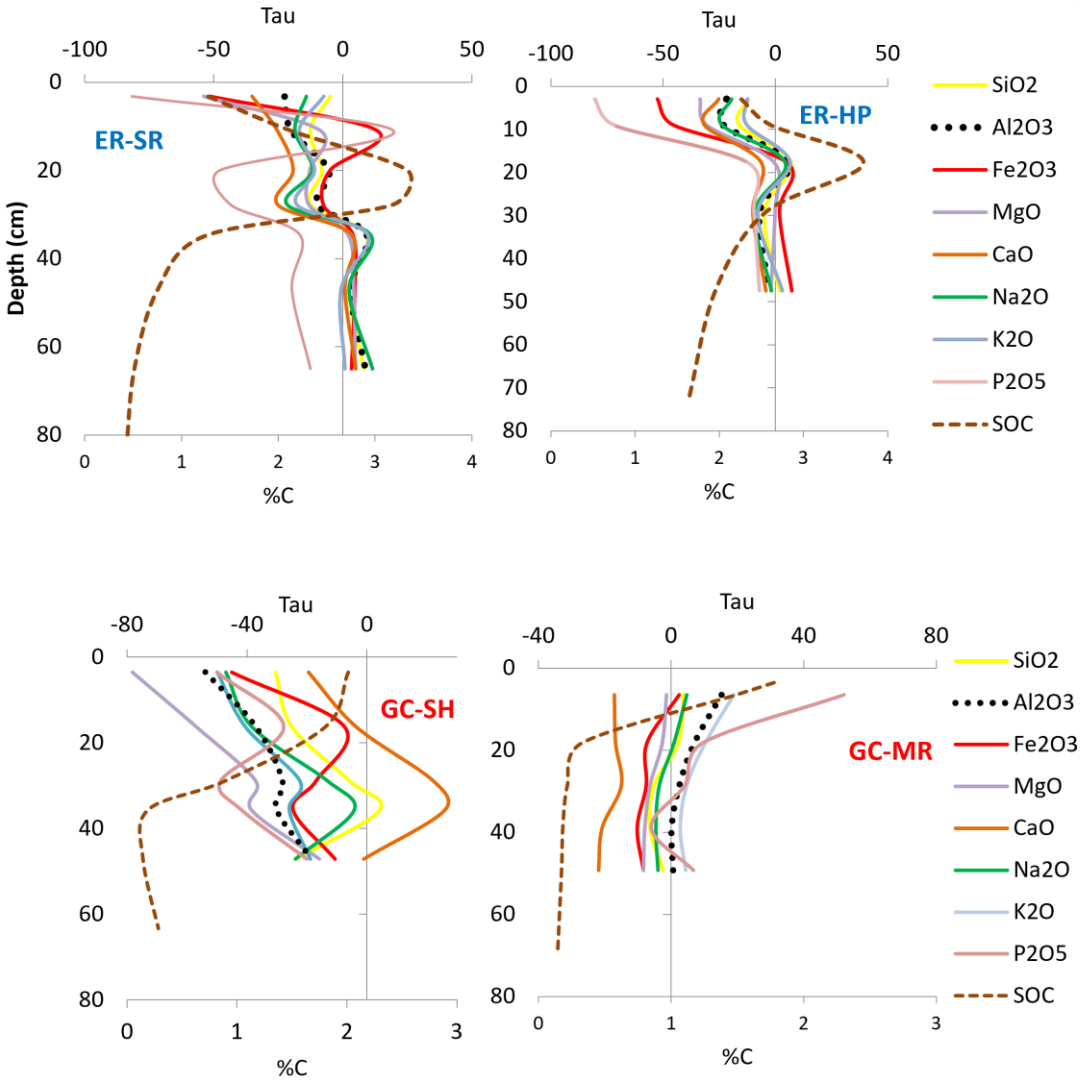

Figure S9.4.

Weathering profiles: Tau elemental distributions (mass transfer coefficients) relative to the top of the C horizon using Ti as the immobile element. Blue = North region, Red = South region. Two weathering depth profile per region (see Figure 5.5 for others): north (blue, top) and south (red, bottom). Mass transfer coefficients (Tau) of major elements were calculated using Ti as the immobile element and were relative to the top of the C horizon (least weathered material). Soil organic carbon content (SOC) distribution over depth is shown in brown on the bottom x-axis. See figure S5.4 for other two sites in these regions.

Table S9.1.

Oxide major element analysis of regional till (%) from inductively coupled plasma optical emission spectroscopy fusion method. Average of 4-6 till samples per region.

	SiO_2	Al_2O_3	Fe_2O_3	MgO	CaO	K_2O	Na_2O	TiO_2	P_2O_5	MnO
North	62.7	16.6	6.6	2.5	3.5	3.8	3.2	0.80	0.22	0.13
South	76.3	11.5	4.4	2.9	0.2	0.7	3.1	0.68	0.08	0.09

Table S9.2. Size fraction weight percent

		North					South		
		Coarse	Sand	Fine			Coarse	Sand	Fine
ER-MP	Ae	14.5	55.1	30.4	GC-MR	B1	52.9	34.2	12.9
	B1	15.2	62.2	22.6		B2	63.9	21.2	14.9
	B2	18.6	64.5	16.9		B3	21.2	30.5	48.3
	B3	11.8	48.0	40.2	GC-OR	Ae	66.4	15.3	18.3
	B4	20.6	44.1	35.2		B1	23.8	47.2	29.0
ER-HP	Ae	1.4	74.9	23.7		B2	34.1	45.7	20.1
	B1	11.4	52.0	36.6		B3	52.2	28.7	19.1
	B2	14.9	53.1	32.0	GC-SH	Ae	18.2	41.9	39.9
ER-SR	Ae	14.8	30.3	54.9		B1	19.4	48.2	32.4
	B1	11.8	65.2	22.9		B2	11.2	57.7	31.1
	B2	16.7	64.4	18.9		B3	7.7	47.3	45.0
	B3	18.7	61.3	20.0					

Table S9.3. Bulk density (g cm^{-3})

	North			South		
Horizon	ER-MP	ER-HP	ER-SR	GC-MR	GC-OR	GC-SH
Ae	1.10	1.12	0.91	N/A	1.14	1.05
B1	0.81	0.88	0.89	0.25	0.93	0.81
B2	0.45	0.76	1.02	1.05	0.73	1.42
B3	1.28		0.53	1.02	0.20	0.06
B4	1.32					

Table S9.4.

a) P-values and (b) explained variance (R^2) of models evaluating the spatial variation of soil characteristics that may control soil organic carbon (SOC) content or SOC dynamics. These include Al extracted by pyrophosphate as proxy for organo-metal complexes (Alpp) and their saturation with C (Cpp:Alpp), the proportion of SOC that is in organo-metal complexes (Cpp:SOC), SOC age (Age), delta 13 C isotopic ratio (^{13}C), and the carbon to nitrogen ratio (C:N).

Table S5.4a. Spatial control best models and P-value results

	Depth	Region	D*R	Best fit model
Al_{pp}	0.77658	0.03293	0.803	Al_{pp} ~ Depth + Region + D*R
Age	2.2E-04	0.946	0.985	logAge ~ Depth + Region + D*R
C_{pp}:Al_{pp}	7.6E-06	0.779	0.32	logC_{pp}:Al_{pp} ~ logDepth+ Region + logD*R
C_{pp}:SOC	3.5E-07	0.669	0.127	logC_{pp}:SOC ~ logDepth+ Region + logD*R
$\delta^{13}C$	8.4E-05	0.356	0.321	^{13}C ~ Depth + Region + D*R
C:N	0.021	1.2E-06	0.0016	$C:N^{1/3}$ ~ logDepth+ Region + logD*R

Table S5.4b. Explained variance (R^2) of spatial models in (a)

	Depth	Region	D*R	Overall
Al_{pp}	0.003	0.207	0.003	0.21
Age	0.520	0.000	0.000	0.52
C_{pp}:Al_{pp}	0.630	0.000	0.020	0.65
C_{pp}:SOC	0.638	0.003	0.040	0.68
$\delta^{13}C$	0.524	0.019	0.023	0.57
C:N	0.073	0.540	0.155	0.77

Table S9.5.

a) The analysis of variance (ANOVA) table and (b) coefficients for soil organic carbon (SOC) predictor model developed in this study. Predictors in this model include Al extracted by pyrophosphate as proxy for Al organo-metal complexes (Alpp) and their saturation with C (Cpp:Alpp), and the proportion of SOC that is in organo-metal complexes (Cpp:SOC). c) Coefficients for models predicting Cpp:Alpp and Cpp:SOC factors with depth. Df = degrees of freedom.

Table S5.5a. SOC prediction model ANOVA

Variable	Df	SumSq	P-value
Al_{pp}	1	15.765	2.27E-13
Al_{pp} * C_{pp}:SOC	1	39.623	2.20E-16
C_{pp}:SOC * C_{pp}:Al_{pp}	1	15.744	2.32E-13
Al_{pp} * C_{pp}:Al_{pp}	1	40.292	2.20E-16
Al_{pp} * C_{pp}:SOC * C_{pp}:Al_{pp}	1	10.328	8.39E-11
Residuals	39	5.201	

Table S5b. SOC model Coefficients

	Estimate	Std. Error	P-value
(Intercept)	0.8235102	0.2754584	0.00482
Al_{pp}	-1.862624	0.2201286	2.32E-10
Al_{pp} * C_{pp}:SOC	0.0298298	0.0044433	5.31E-08
C_{pp}:SOC * C_{pp}:Al_{pp}	-0.0036131	0.0010245	0.00109
Al_{pp} * C_{pp}:Al_{pp}	0.4444954	0.0286474	2.00E-16
Al_{pp} * C_{pp}:SOC * C_{pp}:Al_{pp}	-0.0056544	0.0006425	8.39E-11

Table S5c. Characteristic coefficient

Model	Intercept	Coefficient	R^2	p-value
LogCpp:Alpp ~ LogDepth	3.35141	-0.54137	0.63	3.80E-06
LogCpp:SOC ~ LogDepth	2.82954	0.32484	0.64	2.85E-06